

Luminescent Ionic Liquids

Inaugural-Dissertation
zur Erlangung des Doktorgrades
der Mathematisch-Naturwissenschaftlichen Fakultät
der Universität zu Köln

vorgelegt von

Slawomir Pitula
aus Bydgoszcz (Polen)

Köln 2009

Prüfungsvorsitz: Prof. Dr. U. Deiters
Berichtersteller: Prof. Dr. G. Meyer
Prof. Dr. A.-V. Mudring

Tag der mündlichen Prüfung: 4.2.2010

Die experimentellen Untersuchungen zu dieser Arbeit wurden in der Zeit von August 2007 bis Dezember 2009 am Institut für Anorganische Chemie der Universität zu Köln unter der Anleitung von Frau Prof. Dr. A.-V. Mudring durchgeführt.

Danksagung

Die ersten Worte widme ich meiner verehrten Doktormama Prof. Dr. Anja-Verena Mudring, deren Aufnahme in ihren Arbeitskreis, ihre Unterstützung, ihr Rat und ihre Geduld mir meinen Weg geebnet und mich sehr bereichert hat. Danke für alles. Dem Arbeitskreis Mudring bin ich für die schöne Zeit und deren Hilfe in jeder Lage dankbar.

Gleichauf soll Prof. Dr. Gerd Meyer für seine Bereitschaft, Hilfe und die Aufnahme in seinen Arbeitskreis nicht im geringsten nachstehen. Seinem Arbeitskreis bin ich für die gute Zusammenarbeit und deren Hilfestellungen sehr dankbar, insbesondere Peter Kliesen, Ingrid Müller und Horst Schumacher.

Prof. Dr. Urs Welz-Biermann sei vielmals gedankt für die angenehme Zeit im CHILL in Dalian und die Mitwirkung in seinem Team. Seinem Arbeitskreis bin ich für die Gastfreundschaft und deren Aufnahme in ihren Kreis dankbar. Feng Lu, Liu Quinshan, Dr. Renate Schwiedernoch, Yan Peifang, Jiang Xiao, Zhang Zhida und Dr. Li Changping für ihre Freundschaft und wunderschöne Tage und Abende in Dalian.

Prof. Dr. Axel König sei gedankt für die tolle Zusammenarbeit, interessante Gespräche und seine Nachhilfe in thermischer Verfahrenstechnik.

Ich danke Prof. Dr. Axel Klein für die Benutzung seiner Geräte und seine Unterstützung.

Dr. D. Schaniel und seiner Gruppe danke ich für die Zusammenarbeit, Hilfestellung und Ermöglichung unseres gemeinsamen Projekts.

Die ungezählten Stunden, die Dr. Ronald Alle mir die Thermodynamik und die Cyclovoltammetrie erklärt hat, bleiben unvergessen. Ebenso sei Dr. Wieland Tyrra mit seinen Ratschlägen geehrt.

Dr. Volker von der Gönna sei für die Übernahme der Schriftführung und seine Hilfe herzlich bedankt.

Ein ganz besonderer Dank gilt unseren Glasbläsern, da ohne sie nichts gelaufen wär.

Meinen lieben Kollegen und Freunden aus Bochum Bert, Si-Fu, Kai, Tarek, Agnes, Joanna, Mei, Rosa und Tobij; Marcel, Niko, Sven, Angie; Robert, Andre K., Andre U., Andi, Roland; Svenja, Martin,

Johannes, Vladi und Yarek – einfach danke, dass ihr da wart und seid. Besonders Jenny aus der Physik sei geehrt für die Zusammenarbeit und ihre Hilfe bei unserem gemeinsamen Projekt.

Meine Freunde Jonas, Rosi, Huni, Jacek, Roman, Demian, Max, Yan-Yan, Adam und Kathi – danke, dass ihr alles mitgemacht habt und eure Freundschaft.

Abbreviations

IL	<u>i</u> onic <u>l</u> iquid
RT	<u>r</u> oom <u>t</u> emperature
RTIL	<u>r</u> oom <u>t</u> emperature <u>i</u> onic <u>l</u> iquid
WCA	<u>w</u> eakly <u>c</u> oordinating <u>a</u> nion
DCA	<u>d</u> icyan <u>a</u> mide
FAP	tris(pentafluoroethyl)trifluorophosphate
NTf ₂	<u>b</u> istrifluoromethylsulfonimide
OTf	<u>t</u> riflate
TCB	<u>t</u> etracyanob <u>o</u> rate
C _n	alkyl chain length, $n \in \mathbb{N}$
DODC	3,3'-diethyloxadicyanone iodide
dpph	2,2'- <u>d</u> iphenyl-1- <u>p</u> icryl <u>h</u> ydrazyl
mim	<u>m</u> ethyl <u>i</u> midazolium
mpyr	<u>m</u> ethyl <u>p</u> yrrolidinium
pyrid	<u>p</u> yr <u>i</u> dinium
MTMS	<u>m</u> ethyl <u>t</u> rimethoxy <u>s</u> iloxane
N ₁₄₄₄	tributylmethyl <u>a</u> mmonium
NCS	<u>N</u> - <u>c</u> hloro <u>s</u> uccinimide
P _{666 14}	Trihexyltetradecyl <u>p</u> hosponium
Rh6G	<u>R</u> hodamine <u>6</u> <u>G</u>
TMOS	<u>t</u> etramethoxy <u>s</u> iloxane
s	<u>s</u> inglet

d	<u>d</u> ublet
t	<u>t</u> riplet
q	<u>q</u> uartet
quin	<u>q</u> uintet
hex	<u>h</u> extet
m	<u>m</u> ultiplet
a. u.	<u>a</u> rbitrary <u>u</u> nit
al	<u>a</u> ll <u>l</u> ine; whole emission spectrum of a light source
cw	<u>c</u> ontinuous <u>w</u> ave
DPSS	<u>d</u> iode <u>p</u> umped <u>s</u> olid state
HOMO	<u>h</u> ighest <u>o</u> ccupied <u>m</u> olecular <u>o</u> rbital
IC	<u>i</u> nternal <u>c</u> onversion
ISC	<u>i</u> nter <u>s</u> ystem <u>c</u> rossing
IC	<u>i</u> on <u>c</u> hromatography
DSC	<u>d</u> ifferential <u>s</u> canning <u>c</u> alorimetry
EA	<u>e</u> lemental <u>a</u> nalysis
EPR	<u>e</u> lectron <u>p</u> aramagnetic <u>r</u> esonance
EXAFS	<u>e</u> xtended <u>x</u> -ray <u>a</u> bsorption <u>f</u> ine <u>s</u> tructure
FIR	<u>f</u> ar <u>i</u> nfra- <u>r</u> ed
IR	<u>i</u> nfra- <u>r</u> ed
NIR	<u>n</u> ear <u>i</u> nfra- <u>r</u> ed
NMR	<u>n</u> ucleo <u>m</u> agnetic <u>r</u> esonance
UV	<u>u</u> ltraviolet
Vis	<u>v</u> isual

Summary

In the present thesis the interaction of solutes with ionic liquids (ILs) as solvents are investigated by means of their optical properties and their electrochemical behaviour. Several ILs were prepared as ionic liquid matrices for the introduction of different d- and f-element salts and of several organic dyes. The absence of high frequent oscillating groups in the WCAs of the ILs provides systematic studies on luminescent properties of the d- and f-element ions and organic dyes. Spectroscopic techniques like photoluminescence, EPR, absorption, IR/Raman spectroscopy and also DSC were applied to determine the coordination and luminescent properties of these compounds and their thermal behaviour.

Several Mn^{2+} containing ILs were synthesized and characterized concerning their structural and optical properties. Depending on the ligand and its coordination to the Mn^{2+} center reddish (octahedrally coordinated) or greenish (tetrahedrally coordinated) photoemission was obtained. It turned out that WCAs, i. e. the NTf_2 anion, are suitable for the stabilization of excited states which is observed in the longest – so far known – emission decay lifetime of the ${}^4\text{T}_1(\text{G}) \rightarrow {}^6\text{A}_1$ transition of Mn^{2+} .

The photostability of organic dyes could be extended by orders of magnitudes by dissolution into ILs compared to common used alcoholic solutions without any loss of their superior luminescent properties. In several combined studies the main decomposition pathway of the photodegradation of dyes was determined to be the arbitrary oxidation by oxygen.

The examination of optical spectra of transition metal ion doped ILs offered the determination of their electron donation power, e. g. the acid-base properties of the ILs. Herein, a novel approach close to the concept of optical basicity – initially developed by DUFFY – was successfully transferred from solid oxide hosts to ILs by characterization of the ${}^6\text{A}_1 \rightarrow {}^4\text{A}, {}^4\text{E}(\text{D})$ transition and calculation of the nephelauxetic parameters of the IL. However, the basicity of ILs is dominated by the very weak basic anion nature.

Since about the coordination number of lanthanide ions in ILs is little known, EXAFS spectroscopy was applied to obtain information about the coordination numbers of Eu^{3+} and Yb^{3+} ions dissolved in different ILs. Atomic distances of the dissolved ions in ILs are in good agreement with the respective lanthanide WCA salts and with recent literature data. The electrochemistry of Eu^{3+} in ILs was studied by cyclic voltammetry and shows irreversible one-electron transfers in all cases. The half step potentials depend predominantly only slightly on the applied scan rate and the viscosity of the IL.

Zusammenfassung

In der vorliegenden Arbeit wurde die Solvens-Solvat-Interaktion mit ionischen Flüssigkeiten (ILs) als Lösungsmittel im Hinblick auf ihre optischen Eigenschaften und ihr elektrochemisches Verhalten untersucht. In einer Reihe synthetisierter ILs wurden hierzu verschiedene d- und f-Metallsalze sowie organische Farbstoffe eingeführt. Durch die Abwesenheit hochfrequenter Oszillatoren in den WCAs der ILs konnte eine systematische Untersuchung der lumineszenten Eigenschaften der d- und f-Metallionen und der Farbstoffe durchgeführt werden. Mit Hilfe von Photolumineszenz-, ESR-, UV/Vis- und IR/Ramanspektroskopie sowie der DSC wurden die Koordinationsmodi, die physikooptischen Eigenschaften sowie das thermische Verhalten dieser Verbindungen aufgeklärt.

Zur Untersuchung ihres strukturellen Aufbaus und ihrer physikooptischen Eigenschaften wurden verschiedene Mn^{2+} -haltige ILs synthetisiert. Je nach Koordination des Mn^{2+} wird rote (oktaedrisch) oder grüne (tetraedrisch) Photoemission beobachtet. WCAs, insbesondere das NTf_2 Anion, sind in der Lage elektronisch angeregte Zustände stabilisieren zu können. Dies konnte anhand der – bisher längsten beobachteten – Lebensdauer des ${}^4\text{T}_1(\text{G}) \rightarrow {}^6\text{A}_1$ Übergangs gezeigt werden.

Die Photostabilität organischer Farbstoffe wurde durch deren Einbettung in ILs – im Vergleich zu konventionellen Farbstofflösungen – um einige Größenordnungen erhöht. Als Hauptursache für die Photodegradation konnte die Oxidation der Farbstoffe mit Sauerstoff identifiziert werden.

Aus Absorptionsmessungen von Übergangsmetallionen-dotierten ILs wurde die Elektronendonorfähigkeit bzw. die Säure/Basenstärke von ILs ermittelt. Basierend auf dem Konzept der optischen Basizität von DUFFY konnte ein überarbeitetes Konzept auf ILs übertragen werden. Für verschiedene Mn^{2+} -dotierte ILs wurde der ${}^6\text{A}_1 \rightarrow {}^4\text{A}$, ${}^4\text{E}(\text{D})$ Übergang ausgewertet und zur Bestimmung des nephelauxetischen Parameters der IL benutzt. Die Basizität der ILs wird dabei durch die sehr schwach basische Natur des Anions bestimmt.

Die Aufklärung der – noch unbekanntenen – Koordination von Seltenerdionen, wie Eu^{3+} und Yb^{3+} in ILs wurde mittels EXAFS-Spektroskopie durchgeführt. In Lösung konnten ähnliche Kern-Kern-Abstände für die Seltenerdionen gefunden werden wie in ihren WCA-Salzen und im Einklang mit Literaturdaten. Die Elektrochemie des Eu^{3+} in ILs wird durch irreversible Einelektronenprozesse bestimmt, wobei das Halbstufenpotential des Redoxpaares $\text{Eu}^{3+}/\text{Eu}^{2+}$ in den meisten Fällen unabhängig von der Vorschubgeschwindigkeit und der Viskosität der IL ist.

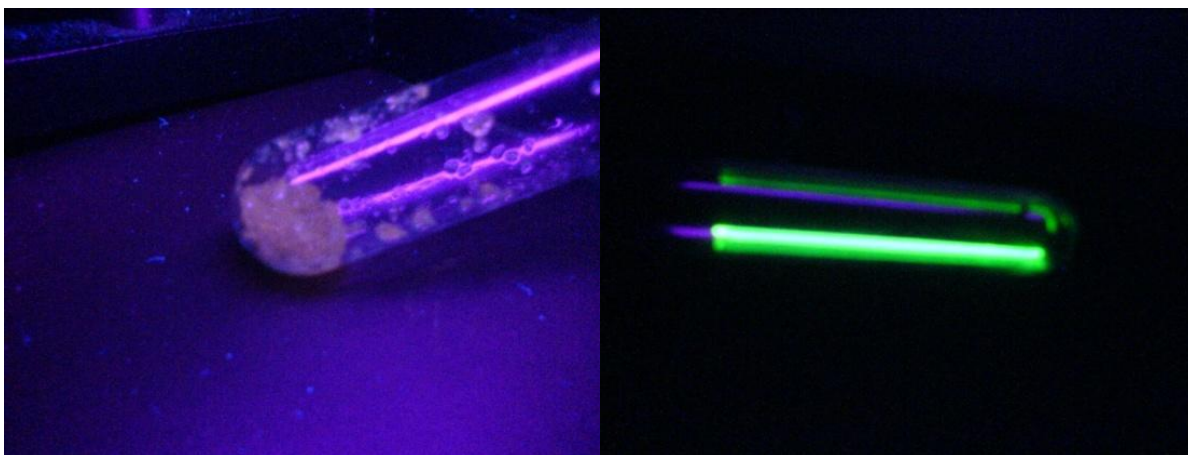
Table of content

1	SYNTHESIS, STRUCTURAL AND PHYSIC-OPTICAL PROPERTIES OF MANGANATE(II) BASED IONIC LIQUIDS	1
1.1	ABSTRACT.....	1
1.2	INTRODUCTION	2
1.3	RESULTS AND DISCUSSION	3
1.3.1	Thermal Analysis	3
1.3.2	Infrared and Raman Spectroscopy.....	5
1.3.3	Optical spectroscopy – general aspects	7
1.3.4	UV/Vis.....	8
1.3.5	Luminescence spectroscopy.....	10
1.3.6	Emission decay studies.....	13
1.3.7	Triboluminescence	15
1.3.8	Electroluminescence	15
1.4	EXPERIMENTAL SECTION	16
1.4.1	Synthesis of MnCl ₂	16
1.4.2	Synthesis of Mn(NTf ₂) ₂	16
1.4.3	Synthesis of bistrifluoromethansulfonic acid.....	16
1.4.4	General procedure for the synthesis of 1- <i>n</i> -alkyl-3-methylimidazolium chlorides and bromides	17
1.4.5	General procedure for the synthesis of 1- <i>n</i> -alkyl-3-methylimidazolium bis(trifluoromethane)sulfonylimides	18
1.4.6	General procedure for the synthesis of the bis(1-alkyl-3-methylimidazolium) tetrahalogenomanganates	18
1.4.7	General procedure for the synthesis of the 1-alkyl-3-methylimidazolium tris(bis(trifluoromethanesulfonyl)imide)manganates(II)	19
1.5	CONCLUSIONS	20
1.6	REFERENCES.....	21
2	OPTICAL BASICITY OF IONIC LIQUIDS	24
2.1	ABSTRACT.....	24
2.2	INTRODUCTION	25
2.3	EXPERIMENTAL	32
2.3.1	Materials	32
2.3.2	Syntheses.....	32
2.3.3	UV/Vis measurements.....	33
2.3.4	General synthesis procedure for nitrile-ILs	33
2.3.5	General synthesis procedure for 1- <i>n</i> -alkyl-3-methylimidazolium chlorides and bromides	33
2.3.6	General synthesis procedure bis(trifluoromethane)sulfonylamide ionic liquids.....	34
2.3.7	General synthesis procedure for trifluoroacetate ionic liquids	35

2.3.8	General synthesis procedure for dicyanamide ionic liquids	36
2.3.9	General synthesis procedure for diethylsulfate ionic liquids	36
2.3.10	General synthesis procedure for nitrate ionic liquids	36
2.3.11	General synthesis procedure for perchlorate ionic liquids	37
2.3.12	General synthesis procedure for tetrahalogenomanganate ionic liquids.....	37
2.3.13	General synthesis procedure for tris(bis(trifluoromethanesulfonyl)amide)manganate(II) ionic liquids.....	38
2.3.14	Synthesis of bistrifluoromethansulfonic acid.....	39
2.3.15	Synthesis of Mn(NTf ₂) ₂	39
2.3.16	Preparation of Mn(NTf ₂) ₂ doped ionic liquids.....	39
2.4	CONCLUSIONS	40
2.5	REFERENCES.....	41
3	IONIC LIQUID BASED LASER	44
3.1	ABSTRACT.....	44
3.2	INTRODUCTION	45
3.3	RESULTS AND DISCUSSION	48
3.3.1	Photostability performances.....	48
3.3.2	Absorption and luminescence studies	58
3.3.3	EPR investigations	59
3.4	EXPERIMENTAL SECTION	66
3.4.1	Chemicals	66
3.4.2	General procedure for the purification of Ionic Liquids purchased from chemical suppliers	66
3.4.3	EPR measurements	66
3.4.4	Photostability measurements	66
3.4.5	Luminescence and absorbance studies.....	67
3.5	GENERAL PROCEDURE FOR THE PRODUCTION OF THE LASER MATERIAL	67
3.5.1	Doping the LASER material with organic quenchers.....	67
3.5.2	Synthesis of Rhodamine 6 G NTf ₂	67
3.5.3	General procedure for the synthesis of 1- <i>N</i> -alkyl-3-methylimidazolium and trihexyl- tetradecylphosphonium bis(trifluoromethane)sulfonylimides and triflates	68
3.5.4	Synthesis of Ionogels.....	69
3.5.5	Synthesis of Mn(NTf ₂) ₂	69
3.5.6	Synthesis of bistrifluoromethansulfonic acid.....	69
3.6	CONCLUSION.....	70
3.7	REFERENCES.....	72
4	LANTHANIDES IN IONIC LIQUIDS: SPECTROSCOPICAL AND ELECTROCHEMICAL INVESTIGATIONS	75
4.1	ABSTRACT.....	75
4.2	INTRODUCTION	76
4.3	RESULTS AND DISCUSSION	76
4.3.1	EXAFS spectroscopy.....	76

4.3.2	Cyclic voltammetry	79
4.4	EXPERIMENTAL SECTION	82
4.4.1	EXAFS	82
4.4.2	Cyclic voltammetry	82
4.4.3	Chemicals and Synthesis	82
4.4.4	General procedure for the fabrication of the investigated samples.....	83
4.4.5	General procedure for the work up of ILs from chemical suppliers	83
4.4.6	General procedure for the synthesis of Eu(NTf ₂) ₃ and Yb(NTf ₂) ₃	83
4.4.7	Synthesis of 1- <i>N</i> -butyl-1-methylpyrrolidinium and 1- <i>N</i> -butyl-3-methylimidazolium dicyanamide	83
4.4.8	General procedure for the synthesis of 1- <i>n</i> -alkyl-1-methylpyrrolidinium and 1- <i>n</i> -alkyl- 1-methylimidazolium triflates	84
4.4.9	General procedure for the synthesis of 1- <i>n</i> -alkyl-3-methylimidazolium bis(trifluoro- methane)sulfonylimides.....	84
4.5	CONCLUSION.....	85
4.6	REFERENCE	86
5	EXPERIMENTAL SECTION	88
5.1	USED CHEMICALS	88
5.2	USED SOFTWARE	91
5.3	USED EQUIPMENT AND HARDWARE.....	92
6	APPENDIX A.....	94
6.1	DSC	94
6.2	RAMAN	99
6.3	INFRARED	102
6.4	PHOTOLUMINESCENCE	107
6.5	EMISSION DECAY SPECTRA AT -196°C	126
6.6	UV/VIS.....	131
7	APPENDIX B.....	136
8	APPENDIX C.....	137
8.1	UV/Vis.....	137
9	APPENDIX D	144
9.1	EXAFS SPECTROSCOPY.....	144
9.2	CYCLIC VOLTAMMETRY	151

1 Synthesis, structural and physic-optical properties of Manganate(II) based ionic liquids



1.1 Abstract

Several ionic liquids (ILs) based on complex manganate(II) anions with chloro, bromo and bis(trifluoromethanesulfonyl)imide (NTf₂) ligands were synthesized. As counterions n-alkyl-methylimidazolium cations of different chain length (alkyl = ethyl (C₂), propyl (C₃), butyl (C₄), hexyl (C₆)) were chosen. Except for the 1-hexyl-3-methylimidazolium ILs all compounds could be obtained in the crystalline state at room temperature. However, for all compounds an extreme tendency to form supercooled liquids when cooling from the liquid above the melting point. Generally solidification via glass transition took place below -40° C. Consequently, all compounds can be regarded as ionic liquids.

Depending on the local coordination environment of Mn²⁺ green (tetrahedrally coordinated) or red (octahedrally coordinated) luminescence emission from the ⁴T(G) level is observed. The local coordination of the luminescent Mn²⁺ centre was established unequivocally by UV/Vis as well as Raman and IR vibrational spectroscopy. Emission decay times measured at room temperature in the solid (crystalline or powder) were generally a few ms. Depending on the ligand values up to 25 ms were found. For the bromo compounds the luminescence decay times were nearly independent on the state of matter and the temperature. However, for chloro and bis(trifluoromethanesulfonyl)imide IL the emission decay times were even in the solid state dependent on the temperature, indicating that the measured values are strongly influenced by nuclear motion and vibration of the atoms. In the liquid state luminescence of tetrahedrally coordinated Mn²⁺ could only be observed when the tetrachloromanganate ILs were diluted with the respective halide ILs. However, for [C₃mim]₂[Mn(NTf₂)₃] where Mn²⁺ is in an octahedral coordination environment a weak red emission of the pure compound is found even in the liquid state at elevated temperatures.

1.2 Introduction

Mn^{2+} is known to exhibit interesting photophysical properties like fluorescence or phosphorescence.^[1] Well known phosphors are $[Zn(Mn)]_2SiO_4$ ^[1], but also in simple halogenido complexes.^[2] Depending on the coordination environment either green (tetrahedrally coordinated Mn^{2+}) or red to pink (octahedrally coordinated Mn^{2+}) luminescence can be observed.^[3] Aside from photoluminescence, triboluminescence^[4] as well as electroluminescence^[5] have been observed for certain tetra-alkyl ammonium salts. In an astonishing number of the studied optically active Mn^{2+} salts the counterions are organic ammonium ions. Often they obey the general composition $[NR_4][MnX_4]$ (R = H, alkyl; X = Cl, Br, I). This composition is strongly reminiscent of recently studied tetrachloroferrate ionic liquids such as $[C_4mim][FeCl_4]$ ^[6] which also contain with Fe^{3+} a d^5 ion. Because of the high single ion magnetism they can be manipulated by an external magnetic field.^[7]

In general, ionic liquids as salt-like compounds with a low melting point (below 100 °C) offer generally the possibility to engineer the properties of a material to the needs of a special application by the choice of the respective cation-anion combination.^[8] In case of complex manganate salts this was already realized by Seddon and Earle who suggested that complex manganate anions in combination with organic cations might be interesting light emitting materials for use in cathode ray tubes, fluorescent tubes, X-ray imaging screens, radiation detectors but also toys, signs etc.^[9] However, all the compounds described except for one were solid at room temperature and unfortunately lost their luminescent properties at temperatures when solid-solid phase transitions or melting occurred.

Low melting compounds composed of an organic cation and an optically active rare earth ion as for example $[C_4mpyr]_2[Pr(NTf_2)_5]$ ^[10], $[C_3mim][Eu(NTf_2)_4]$, $[C_4mim][Eu(NTf_2)_5]$ and $[C_4mpyr][Eu(NTf_2)_5]$ ^[11] and $[C_4mim]_{3-x}[Dy(SCN)_{8-x}(H_2O)_x]$ ^[12] exhibit excellent luminescent properties. For these systems unexpectedly good luminescent properties can be even maintained in the molten/liquid state due to the favourable coordination environment of the lanthanide ion. Furthermore, replacement of conventional solvents by carefully designed ionic liquids can generally lead to a dramatic increase of emission decays of the excited state and quantum yields of emission – even for NIR luminescence.^[13]

Therefore light transition metal based ILs with their interesting luminescent properties were studied.

1.3 Results and Discussion

1.3.1 Thermal Analysis

Thermal data of the investigated manganate(II) complex compounds are compiled in Table 1. Graphical representation of all DSC thermograms together with detailed information on the transition enthalpies are collected in the Appendix A. For all DSC scans the heating and cooling cycles were twice repeated to check for any change in the thermal properties in the second cycle. The repeated cycles could be reproduced for all compounds if not stated otherwise.

The investigated compounds show all to be true ionic liquids. All short chain (C_2 – C_4) compounds could be obtained as crystalline samples whereas C_6 chain shows an extremely strong tendency to supercool and solidify as glasses. Thus, none of the 1-*n*-hexyl-3-methylimidazolium manganate compounds could be crystallized - neither by homogeneous nor by non-homogeneous crystallization techniques.

Three types of different thermal behaviour can be observed for the studied ILs. For the first type (Fig. 1, left), to which the 1-ethyl and 1-*n*-propyl-3-methyl-imidazolium halide containing ILs belong, distinct melting points upon heating and distinct crystallization temperatures upon cooling are observed.^[14] A typical DSC scan of this kind of IL is given in Fig. 1. Thermal events occurring at lower temperatures than the melting point to solid-solid phase transitions. The samples solidify partially as a glass and recrystallize upon heating before melting. The tendency to solidify as a glass becomes more and more pronounced when the alkyl chain gets longer.

In case of the 1-*n*-butyl-3-methylimidazolium ILs (type two) after melting of the crystalline material (which was obtained by inhomogeneous crystallization, hence, crystallization from solution) to the liquid state only glass transitions can be observed when cooling the samples (type two; Fig. 1, middle). By repeated heating these glasses form supercooled liquids which showed no tendency for homogeneous crystallization. Finally, the 1-hexyl-3-methylimidazolium ionic liquids even could not be crystallized from solution (Fig. 1, right). This third type of ILs has no real melting or freezing points and only glass transitions are observed.

Extension of the alkyl chain from C_2 to C_3 leads in case of the tetrahalogenomanganates to a depression of the melting point. Further extension of the alkyl chain seems to inhibit the crystallization. Here rather the formation of a glass is preferred. Not only an extension of the alkyl chain of the cation but also a change of the anion from the higher symmetric halide to the less symmetric bis(trifluoromethanesulfonyl)imide favours the solidification as a glass. In both cases packing frustrations seem to be the main reason for this behaviour. The less symmetric the cation the more tendencies to form glasses rather than crystalline substances are given.

Table 1. Thermal data acquired by DSC measurements of 1-*n*-alkyl-3-methyl imidazolium manganate(II) ionic liquids. Data are given in [°C].

compound	Cooling			heating			
	glass transition	crystallization	solid-solid phase transition	glass transition	crystallization	melting	solid-solid phase transition
[C ₂ mim] ₂ [MnCl ₄]	-	39.2	14.8	-	-	77.3	-
[C ₃ mim] ₂ [MnCl ₄]	-65.8	-7.8	-27.5	-54.4	-35.5	-	-
[C ₄ mim] ₂ [MnCl ₄]	-54.0	-	-	-49.2	-	62.0	-
[C ₆ mim] ₂ [MnCl ₄]	-51.8	-	-	-50.1	-	-	-
[C ₂ mim] ₂ [MnBr ₄]	-	39.5	-	-	10.2	72.0	-
[C ₃ mim] ₂ [MnBr ₄]	-	18.2	-54.1	-	-10.4	53.8	-24.8
[C ₄ mim] ₂ [MnBr ₄]	-55.4	-	-	-49.9	-	44.2	-
[C ₆ mim] ₂ [MnBr ₄]	-54.2	-	-	-49.5	-	-	-
[C ₂ mim][Mn(NTf ₂) ₃]	-45.2	-	-	-47.2	22.7	-	-
[C ₃ mim][Mn(NTf ₂) ₃]	-44.4	-	-	-44.1	-	36.7	0.7
[C ₄ mim][Mn(NTf ₂) ₃]	-48.5	-	-	-40.3	-	66.0	-
[C ₆ mim][Mn(NTf ₂) ₃]	-56.4	-	-	-50.8	-	-	-

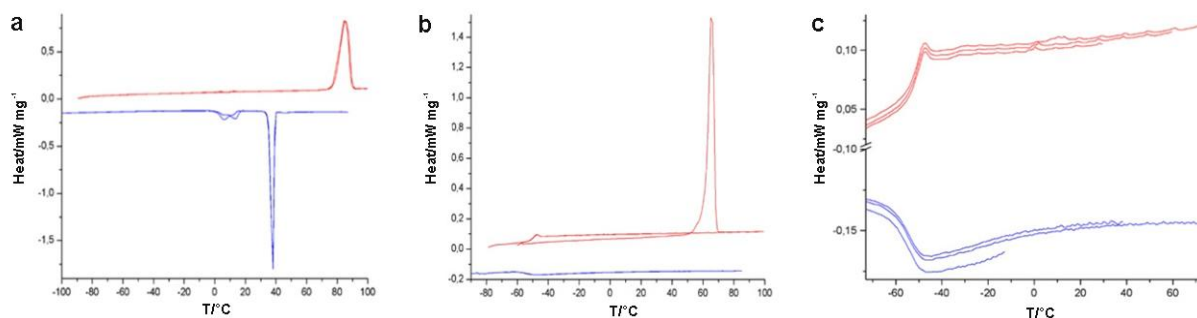


Fig. 1. Representative thermograms of a) $[\text{C}_2\text{mim}]_2[\text{MnCl}_4]$ as a typical manganate (II) ionic liquid of type one; b) of $[\text{C}_4\text{mim}]_2[\text{MnCl}_4]$ as a typical manganate (II) ionic liquid of type two and c) of $[\text{C}_6\text{mim}]_2[\text{MnCl}_4]$ as a typical manganate (II) ionic liquid of type three (right). Heating cycle (top); cooling cycle (bottom), heating rate 5 K/min.

1.3.2 Infrared and Raman Spectroscopy

The expected vibrations of the imidazolium ring are clearly visible in the infrared and Raman spectra of the Mn-based ILs (see Fig. 2 and Appendix A). The C-H deformation modes can be found in the range $1300\text{--}1550\text{ cm}^{-1}$ and the C-H stretching modes in the range $2800\text{--}3200\text{ cm}^{-1}$ as well as the C-H rocking modes at 720 cm^{-1} . All vibrational modes of the respective cations of the manganese containing ILs found in the MIR region correlate well with the respective neat halide IL.

No significant influence of the anion on the counter cation can be found. Metal-ligand vibrations of tetrahedrally coordinated Mn^{2+} are infrared and Raman active whilst for the octahedrally coordinated compounds the F_{1u} and A_{1g} modes are only Raman active. The metal-ligand vibrations are usually observed in the FIR (far infrared) range at 200 cm^{-1} to 400 cm^{-1} . In the FIR region the sharp Mn-Cl stretching mode has typically its maximum absorbance around 290 cm^{-1} , also accompanied by shoulders at lower or higher frequencies, whereas the Mn-Br modes appear as a broad band at 220 cm^{-1} (see Fig. 2 (a)). The bromo compounds exhibit in the FIR spectra a much lower intensity of absorbance than the respective chloro compounds. The symmetric manganese-halide vibrations in Fig. 2(d) are marked with arrows. Typical values of the ν_s (Mn-Cl) are 255 cm^{-1} and of ν_s (Mn-Br) are ca. 160 cm^{-1} which are in good agreement with the literature.^[15] Generally, these Mn-halogenido vibrations have only weak intensities and appear typically in regions below 400 cm^{-1} .^[16]

As all the NTf_2 derivatives of the Mn-based ILs are optically thick the MIR spectra of the NTf_2 derivatives of the Mn-based ILs had to be recorded in solution of their respective room temperature liquid IL to trace any transmission.

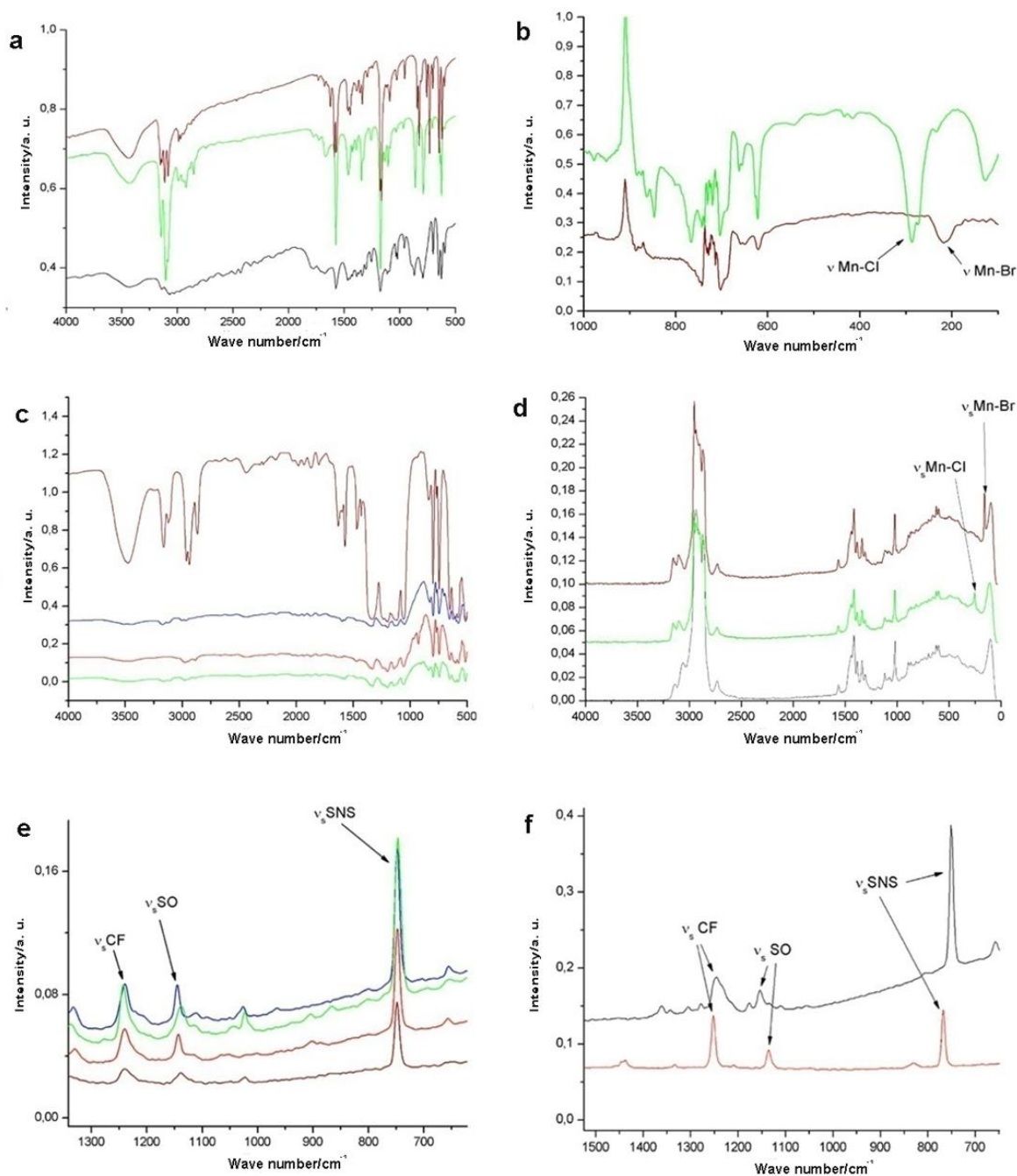


Fig. 2. a) mid-infra-red spectra of $[\text{C}_6\text{mim}]_2[\text{MnBr}_4]$ (top), $[\text{C}_2\text{mim}]_2[\text{MnCl}_4]$ (middle) and $[\text{C}_6\text{mim}]\text{Br}$ (bottom); b) far-infra-red spectra of $[\text{C}_6\text{mim}]_2[\text{MnCl}_4]$ (top) and $[\text{C}_6\text{mim}]_2[\text{MnBr}_4]$ (bottom); c) mid-infra-red spectra of $[\text{C}_2\text{mim}][\text{Mn}(\text{NTf}_2)_3]$ (2nd from top), $[\text{C}_3\text{mim}][\text{Mn}(\text{NTf}_2)_3]$ (bottom), $[\text{C}_4\text{mim}][\text{Mn}(\text{NTf}_2)_3]$ (2nd from bottom) and $[\text{C}_6\text{mim}][\text{Mn}(\text{NTf}_2)_3]$ (top); d) Raman spectra of $[\text{C}_6\text{mim}]_2[\text{MnBr}_4]$ (top), $[\text{C}_6\text{mim}]_2[\text{MnCl}_4]$ (middle) and $[\text{C}_6\text{mim}]\text{Br}$ (bottom); e) section of the Raman spectra of $[\text{C}_2\text{mim}][\text{Mn}(\text{NTf}_2)_3]$ (top), $[\text{C}_3\text{mim}][\text{Mn}(\text{NTf}_2)_3]$ (2nd from top), $[\text{C}_4\text{mim}][\text{Mn}(\text{NTf}_2)_3]$ (2nd from bottom) and $[\text{C}_6\text{mim}][\text{Mn}(\text{NTf}_2)_3]$ (bottom); f) section of the Raman spectra of $\text{Mn}(\text{NTf}_2)_2$ (top) and HNTf_2 (bottom).

As can be seen in Fig. 2 (c) only $[\text{C}_6\text{mim}][\text{Mn}(\text{NTf}_2)_3]$ shows a significant transmission. Compared to the tetrahalogeno ILs the NTf_2 derivatives do not exhibit such a pronounced fine splitting of their bands. The bands exhibit a much lower intensity for the C-H stretching and deformation modes than observed in the spectra of the respective halide ILs. The ν_s (S-N-S) modes at 748 cm^{-1} in the $\text{NTf}_2\text{ Mn}^{2+}$ derivatives are shifted about 20 cm^{-1} to lower wave numbers compared to H NTf_2 (ν_s (S-N-S) modes at 767 cm^{-1}) but provide the same intensities. In the IL $\text{C}_4\text{mpyrNTf}_2$ this stretching mode of the “free” anion lies around 740 cm^{-1} .^[17] As expected, upon coordination to a Lewis acid centre (here Mn^{2+}) the ν_s (S-N-S) frequency increases. Also the symmetric stretching modes ν_s (S-O) (see Fig. 2(e); $[\text{C}_2\text{mim}][\text{Mn}(\text{NTf}_2)_3]$: ν_s (S-O) at 1145 cm^{-1} , $[\text{C}_3\text{mim}][\text{Mn}(\text{NTf}_2)_3]$: ν_s (S-O) at 1139 cm^{-1} , $[\text{C}_4\text{mim}][\text{Mn}(\text{NTf}_2)_3]$: ν_s (S-O) at 1143 cm^{-1} and $[\text{C}_6\text{mim}][\text{Mn}(\text{NTf}_2)_3]$: ν_s (S-O) at 1138 cm^{-1}) are sensitive towards complexation to Lewis acid centres. Apparently the S-O bond is weakened upon coordination of NTf_2 to Mn^{2+} . The S-O stretching modes appear in the same region as the homoleptic alkaline rare earth NTf_2 compounds but remain unsplit indicating only one coordination mode.^[17]

For comparison, Fig. 2(f) shows the Raman spectra of HNTf_2 and $\text{Mn}(\text{NTf}_2)_2$. The symmetric stretching mode of the C-F bonds appears at the same wave number supporting that this mode is not perturbed by the cation nature or its coordination. In the opposite the ν_s S-N-S deviate only slightly for both components whereas the ν_s S-O of the $\text{Mn}(\text{NTf}_2)_2$ (1154 cm^{-1}) is as well shifted about 18 cm^{-1} to lower wave numbers compared to the free acid HNTf_2 (ν_s S-O 1136 cm^{-1}) due to interactions of the oxygens of the SO_2 groups with the manganese Lewis acid centre.

1.3.3 Optical spectroscopy – general aspects

In case of Mn^{2+} its electronic d^5 configuration is its own hole equivalent. Thus the TANABE-SUGANO^[18] energy level diagrams for both the tetrahedral and octahedral coordination are identical. To the first order the electronic states of Mn^{2+} are unperturbed by the nuclear motion for all motions that reduce symmetry. The upper ${}^4\text{E}$, ${}^4\text{A}_1(\text{G})$, ${}^4\text{E}$, ${}^4\text{A}_1(\text{D})$ and states and the ${}^6\text{A}_1$ state have the same slopes on the energy level diagrams.^[2] This accounts for the comparatively sharp lines observed for the ${}^6\text{A}_1 \rightarrow {}^4\text{E}$, ${}^4\text{A}_1(\text{G})$ as well as the ${}^6\text{A}_1 \rightarrow {}^4\text{A}_1(\text{D})$ transitions in the absorption spectra.

Electric dipole transitions within high-spin (*hs*) centrosymmetric, octahedral Mn^{2+} complexes are both spin and parity forbidden indicating a long lifetime of the excited electronic states. Non-centrosymmetric *hs*- Mn^{2+} compounds have LaPORTE-allowed d-d transitions but are still spin forbidden. The emission decay of their excited states is generally lower by a factor of 5 compared to those of the Mn^{2+} systems with an inversion centre.^[14]

1.3.4 UV/Vis

The coordination environment of Mn^{2+} can be easily judged from the colour. Compounds with Mn^{2+} in tetrahedral environment usually are of yellow-greenish colour while octahedrally coordinated Mn^{2+} appear in a pale red to pink colour. Transitions observed in the range of 300-800 nm can be assigned to the expected intraconfigurational transitions for Mn^{2+} ion (Fig. 3).^[4, 20] For tetrahedrally coordinated Mn^{2+} electronic transitions are LapORTE allowed and show thus higher absorbances than in an octahedral environment (factor of 100). UV/Vis spectra of the compounds under investigation are in excellent agreement with the literature.^[4, 20, 21] No significant impact of the counter cation on the colour of the compounds could be detected. Solid and liquid state absorption spectra of the Mn^{2+} ILs do not differ significantly. In agreement with a smaller ligand field splitting for the tetrahedral complex anions compared to the octahedral complex anions electronic transitions of the MnX_4^{2-} compounds were found at longer wavelength.

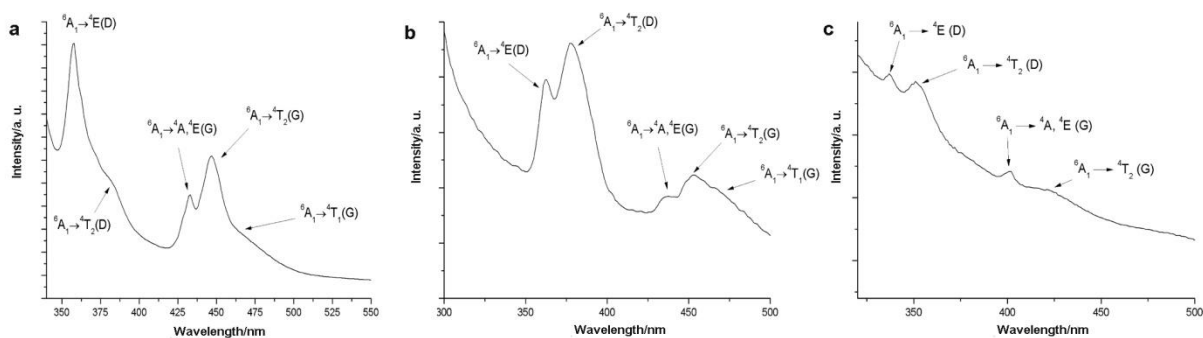


Fig. 3. UV/Vis spectrum of $[C_4mim]_2[MnCl_4]$ (left), $[C_4mim]_2[MnBr_4]$ (middle) and $[C_3mim][Mn(NTf_2)_3]$ (right).

Typical UV/Vis spectra of a representative tetrahedrally coordinated Mn^{2+} IL is shown in Fig. 3 (a) and (b). Two distinct groups of bands are observed in the UV/Vis region for all studied ILs. The first group of absorption bands belong to transitions to D-term states with strong ligand field splitting whereas the second group of bands originate from the small ligand field splitted G-terms. In general the bands of the G-terms appear with much lower intensities than the bands of the D-terms.

For the tetrachloromanganates the most intense band in the UV region of the tetrachloromanganates corresponds to the ${}^6A_1 \rightarrow {}^4E(D)$ transition. Other bands are the very weak ${}^6A_1 \rightarrow {}^4T_2(D)$, the weak ${}^6A_1 \rightarrow {}^4A, {}^4E(G)$ and the intense ${}^6A_1 \rightarrow {}^4T_2(G)$ transition. The broad band at 470-475 nm is most likely due to an energy transfer band ${}^6A_1 \rightarrow {}^4T_1(G)$. In comparison with the tetrachloromanganates the ${}^6A_1 \rightarrow {}^4A, {}^4E(D)$ transition is generally of lower intensity than the ${}^6A_1 \rightarrow {}^4T_2(D)$ band and the absorption bands are blue shifted by 2-6 nm. According to the TANABE-SUGANO diagram of d^5 ions the ${}^6A_1 \rightarrow {}^4E(D)$ transition is depends on the ligand field strength. In

consequence, from the absorption maximum the electron donor ability of the ligand can be estimated. As the absorption maximum of the tetrabromo compounds lies at lower wavelength compared to the tetrachloromanganates as the tetrabromo compounds have a higher degree of covalency.

As the spectra of the solid ionic liquids with complex Mn-NTf₂ cations showed a low signal/noise ration, they were diluted with the respective Mn-free IL for UV/Vis measurements (except for the ethylimidazolium derivatives). Two separated groups of bands are observed – one group consisting of two bands at 337 nm ${}^6A_{1g} \rightarrow {}^4E_g(D)$ and at 351 nm ${}^6A_{1g} \rightarrow {}^4T_{2g}(D)$ and a second group at larger wavelengths with transitions at 401 nm ${}^6A_{1g} \rightarrow {}^4A_g, {}^4E_g(G)$ and at 422 nm ${}^6A_{1g} \rightarrow {}^4T_{2g}(G)$. The observed electronic transitions are similar to the ones found for MnF₂^[22], where Mn²⁺ is octahedrally coordinated by F⁻.

Table 2. Assigned transitions of the collected UV/Vis data of the tetrahalomanganate complexes. Wavelengths are in [nm].

Compound	${}^6A_1 \rightarrow {}^4E(D)$	${}^6A_1 \rightarrow {}^4T_2(D)$	${}^6A_1 \rightarrow {}^4A, {}^4E(G)$	${}^6A_1 \rightarrow {}^4T_2(G)$	${}^6A_1 \rightarrow {}^4T_1(G)$
[C ₂ mim] ₂ [MnCl ₄]	357	381	433	446	472
[C ₃ mim] ₂ [MnCl ₄]	358	381	433	447	470
[C ₄ mim] ₂ [MnCl ₄]	358	383	433	447	470
[C ₆ mim] ₂ [MnCl ₄]	358	381	433	446	472
[C ₂ mim] ₂ [MnBr ₄]	362	380	435	453	470
[C ₃ mim] ₂ [MnBr ₄]	362	379	435	452	471
[C ₄ mim] ₂ [MnBr ₄]	362	377	436	453	470
[C ₆ mim] ₂ [MnBr ₄]	363	380	436	454	472

Table 3. Assigned transitions of the collected UV/Vis data of the NTf₂ derivatives of the manganate complexes. Wavelengths are in [nm].

Compound	${}^6A_{1g} \rightarrow {}^4E_g (D)$	${}^6A_{1g} \rightarrow {}^4T_{2g} (D)$	${}^6A_{1g} \rightarrow {}^4A_g, {}^4E_g (G)$	${}^6A_{1g} \rightarrow {}^4T_{2g} (G)$
[C ₂ mim][Mn(NTf ₂) ₃]	337	351	402	424
[C ₃ mim][Mn(NTf ₂) ₃]	337	351	401	422
[C ₄ mim][Mn(NTf ₂) ₃]	336	351	401	421
[C ₆ mim][Mn(NTf ₂) ₃]	337	351	402	421

1.3.5 Luminescence spectroscopy

Excitation and photoluminescence spectra were recorded at room temperature. The luminescence decay times were measured at room temperature and at the temperature of liquid nitrogen. For the [C₃mim] salts also the temperature dependence of the luminescence decay times was investigated.

To record the excitation spectra, the emission intensity of the most intense transition was monitored while the excitation wavelength was continuously changed between 300 to 500 nm. In the excitation spectra (Fig. 4; Appendix A), the d-d transitions of the Mn²⁺ ion are clearly visible. These transitions can be assigned to the expected intraconfigurational transitions for a tetrahedrally (in case of the halide compounds) or octahedrally (in case of the NTf₂ compounds) coordinated Mn²⁺ ion.^[22] The excitation spectra are in excellent agreement with the previously recorded UV spectra.

All emission spectra were recorded after direct excitation from the 6A_1 to the ${}^4E(D), {}^4T_2(D)$ states of Mn²⁺. These transitions are the most intense absorption bands in the UV region of all compounds. In the emission spectra only one intraconfigurational transition can be observed between 400 and 700 nm (see Appendix A). In case of tetrahedrally coordinated Mn²⁺ the ${}^4T_1(G) \rightarrow {}^6A_1$ radiative transition is observed with the characteristic visible yellow-greenish emission around 520 nm. For octahedrally coordinated Mn²⁺ compounds the ${}^4T_{1g}(G) \rightarrow {}^6A_{1g}$ transition is observed with a reddish colour at about 590 nm (see Table 6).

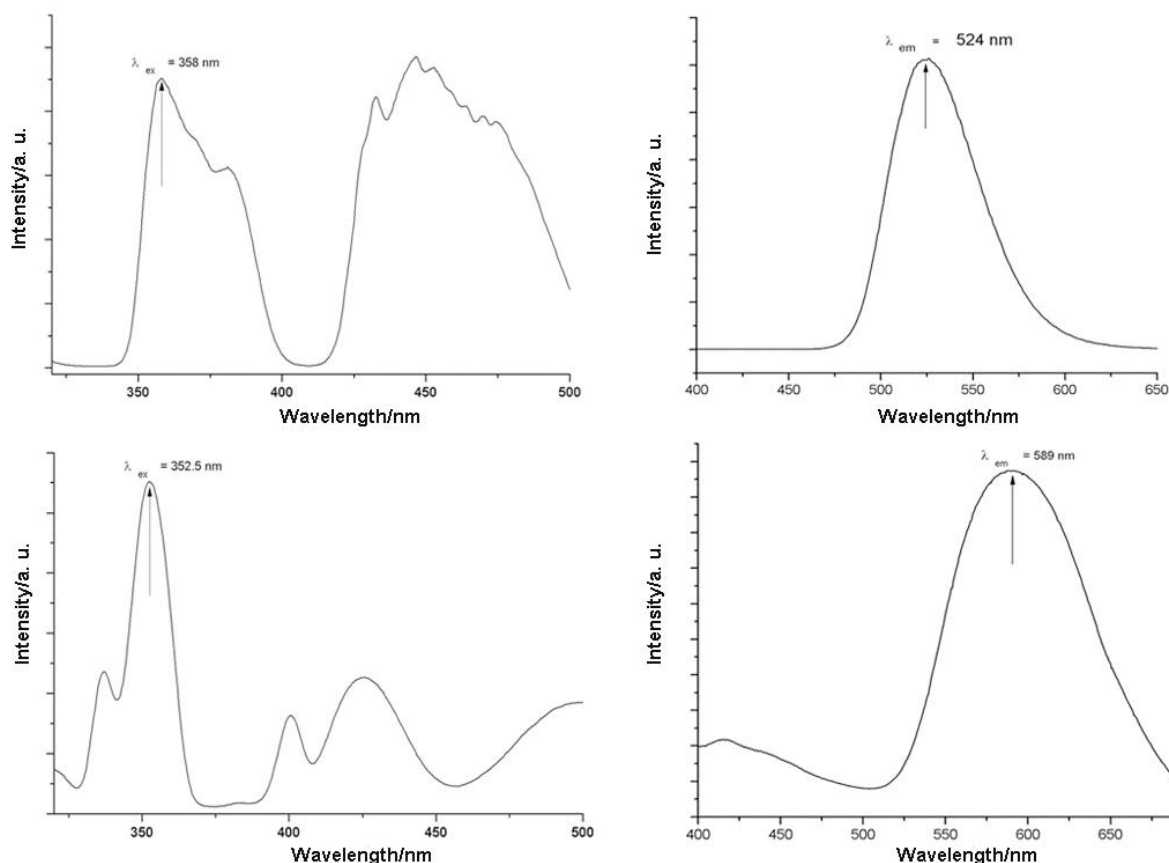


Fig. 4. Excitation (left) and emission (right) spectra of $[\text{C}_2\text{mim}]_2[\text{MnCl}_4]$ (top) and $[\text{C}_2\text{mim}][\text{Mn}(\text{NTf}_2)_3]$ (bottom).

All samples containing shorter alkyl chains than hexyl exhibit appreciably intense photoluminescence (Fig. 4; see also Appendix A Fig. 28-72). Emission band half widths of around 50 nm (200 cm^{-1}) are observed in all emission spectra. Appreciable shifts of the emission maxima are observed especially for the chloro and bromo derivatives (see Table 4) depending on the counter cation. Upon melting all values in the photoluminescence spectra shift about 5-10 nm ($100\text{-}200\text{ cm}^{-1}$) to lower wavelengths indicating weaker intramolecular interactions. The discrepancy in the STOKES-shift between the Mn^{2+} based halido and the NTf_2 -derivatives derive from the symmetry and MO contribution of each ligands. The four halide ligands overlap stronger with the manganese d-orbitals than the six weakly coordinating oxygens of the NTf_2 anions. It suffers due to symmetric aspects of the bond length and lower overlap contribution.

Table 4. List of the observed emission maxima in [nm] of the investigated manganese compounds at RT.

	[MnCl ₄]	[MnBr ₄]	[Mn(NTf ₂) ₃]
[C ₂ mim] ₂	524	514	589
[C ₃ mim] ₂	510	518	592
[C ₄ mim] ₂	516	519	589
[C ₆ mim] ₂)*)*)*

)* to weak/short-lived to detect with the used experimental setup

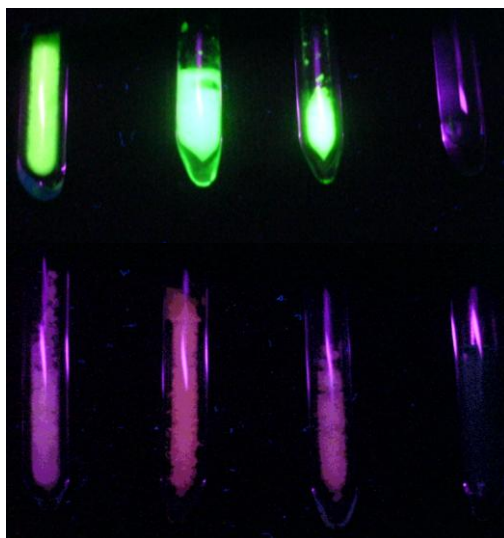


Fig. 5. From left to right in the top row [C₂mim]₂[MnCl₄], [C₃mim]₂[MnCl₄], [C₄mim]₂[MnCl₄] and [C₆mim]₂[MnCl₄], in the bottom row [C₂mim][Mn(NTf₂)₃], [C₃mim][Mn(NTf₂)₃], [C₄mim][Mn(NTf₂)₃], [C₆mim][Mn(NTf₂)₃] excited at room temperature with UV light ($\lambda_{\text{ex}} = 366 \text{ nm}$).

1.3.6 Emission decay studies

The luminescence decay curves of the ${}^4T_1(G) \rightarrow {}^6A_1$ radiative transition were measured and a single exponential function could be fitted to the data confirming that just one optical Mn^{2+} species is present. The experimental luminescence emission decays at room temperature and at -196°C are compiled in Table 5. Upon melting or in the metastable liquid state at room temperature no appreciable emission could be detected for the halogenido ILs due to vibrational quenching.^[22]

Tetrabromomanganates exhibit emission decays of the excited Mn^{2+} states of about 0.4 ms at room temperature which is in good agreement with literature values.^[14] In contrast the respective excited state of the tetrachloromanganate compounds live for about 3 to 5 ms.^[23] The stronger degree of covalency in the complex bromides compared to the chlorides leads to a higher degree of vibronic coupling and hence to a reduction of the lifetime of the excited state. This assumption is backed by comparing the respective Mn-X modes in the vibrational spectra (see above).

The NTf_2 derivatives of the Mn-based ILs exhibit – to our knowledge – the largest reported phosphorescence decay of Mn^{2+} . These compounds reach emission decays of about 30 ms (see Table 5). Generally lifetimes of about 12-15 ms are reported.^[22] Mn^{2+} features in these compounds in the crystalline solid state octahedral site symmetry. Both the LaPORTE forbiddance and the spin forbidden transitions lead to very long excited state decay times up to 25 ms at room temperature and 34 ms at 77 K for $[C_3mim][Mn(NTf_2)_3]$. In case of the tetrachloro and tris(bis(trifluoromethanesulfonyl)imide) manganates where there is less covalent bonding between the metal and the ligand compared to the bromido compounds there is the lifetimes are strongly dependent on the temperature. Non-radiative deactivation processes are more likely to occur at higher temperatures. In consequence, the lifetimes of the excited states at 77 K are higher compared to those at 298 K. For the tetrabromomanganates the lifetimes remain constant between 77 K and 298 K. This observation is in agreement with studies on other tetrabromomanganates with organic counter cations.^[24]

To study the temperature dependence of the lifetime of the excited states in more detail for $[C_3mim]_2[MnCl_4]$, $[C_3mim]_2[MnBr_4]$ and $[C_3mim][Mn(NTf_2)_3]$ the temperature dependence of the emission decay was determined in liquid nitrogen and in a temperature range from 10°C to 70°C in steps of $2-15^\circ$. Fig. 6 shows the temperature dependence on the emission decays of the C_3mim compounds of Mn^{2+} . Increasing temperature of the samples results in decreasing the emission decay lifetimes of the excited ${}^4T_1(G)$ state due to thermal collision deactivation mechanisms. Starting with the solid samples at 10°C and increasing temperature by steps of $2^\circ-15^\circ$ a sudden drop of the measured emission decay occurs at the respective melting points. In case of the halogenido compounds no luminescence could be detected while for $[C_3mim][Mn(NTf_2)_3]$ a weak reddish luminescence was observed. The deactivation via thermal motion collision is attenuated by the NTf_2

anion and favoured by the octahedral site symmetry of Mn^{2+} in the NTf_2 complex. Surprisingly in the liquid state the NTf_2 derivatives a detectable emission decay can be observed which presents the efficiency of the shielding of the anions.

Table 5. Emission decays of the Mn-based ILs at room temperature (RT) and at $-196^\circ C$ (liquid nitrogen). Emission decay values are in [ms].

Compound	RT	$-196^\circ C$
$[C_2mim]_2[MnCl_4]$	1.5 (s)	3.4 (s)
$[C_3mim]_2[MnCl_4]$	4.6 (s)	5.5 (s)
$[C_4mim]_2[MnCl_4]$	3.9 (s)	4.2 (s)
$[C_6mim]_2[MnCl_4]$	(l)*	4.0 (s)
$[C_2mim]_2[MnBr_4]$	0.4 (s)	0.4 (s)
$[C_3mim]_2[MnBr_4]$	0.4 (s)	0.4 (s)
$[C_4mim]_2[MnBr_4]$	0.4 (s)	0.4 (s)
$[C_6mim]_2[MnBr_4]$	(l)*	0.4 (s)
$[C_2mim][Mn(NTf_2)_3]$	22.8 (s)	29.7 (s)
$[C_3mim][Mn(NTf_2)_3]$	24.8 (s)	33.9 (s)
$[C_4mim][Mn(NTf_2)_3]$	18.8 (s)	32.4 (s)
$[C_6mim][Mn(NTf_2)_3]$	(l)*	32.7 (s)
$Mn(NTf_2)_2$	17.3 (s)	38.3 (s)

* to weak/short-lived to detect with the used experimental setup

s solid; l liquid

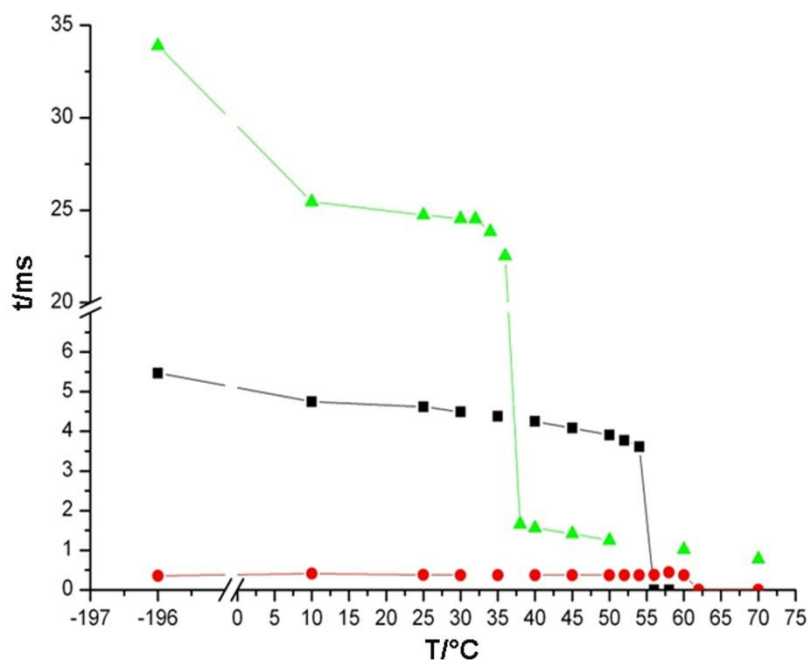


Fig. 6. Temperature dependence of the emission decays of $[\text{C}_3\text{mim}]_2[\text{MnCl}_4]$ (black), $[\text{C}_3\text{mim}]_2[\text{MnBr}_4]$ (red) and $[\text{C}_3\text{mim}][\text{Mn}(\text{NTf}_2)_3]$ (green) upon melting.

1.3.7 Triboluminescence

Tetrahalogenomanganates are well known emitters for triboinduced radiation due to their piezoelectrical properties. Excitation via mechanical exposure when an applied electrical field induces the electric polarisation of suitable strength.^[5, 20] This results in a characteristic greenish emission when rubbing crystals of Mn^{2+} compounds. Triboluminescence of only tetrahalogenomanganate ILs was observed when the crystals of the tetrahalogenido salts were rubbed with a glass stick. The emitted light flashes of the manganate complexes were of greenish colour and observed by eye for only a fractional amount of a second.

1.3.8 Electroluminescence

If a high voltage was applied to samples of solid Mn-IL samples, electroluminescence could be observed. As expected, the bromido and chlorido compounds show a greenish luminescence whereas the NTf_2 compounds emit red light. No visible emission could be observed for all hexylimidazolium containing samples.

1.4 Experimental section

1.4.1 Synthesis of MnCl_2

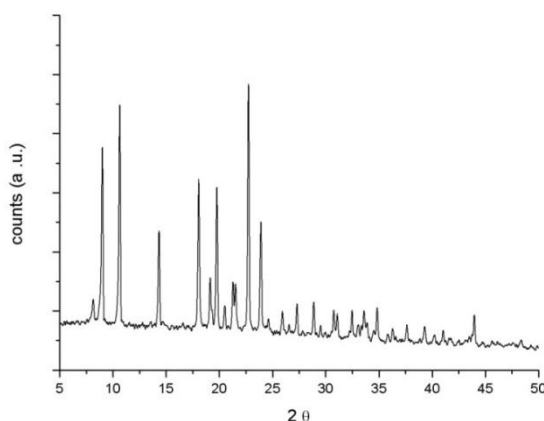
MnCO_3 was suspended in deionized water and an excess of concentrated hydrochlorid acid was added. The mixture was stirred until complete dissolution of the carbonate. Then the water and HCl were boiled off. The residual solid was heated in a SCHLENK tube at 140-160°C under high vacuum for two hours. Afterwards the solid was heated at 300°C under high vacuum.

EA MnCl_2 calc. N 0.00%, C 0.00%, H 0.00%, S 0.00%; found N 0.00%, C 0.00%, H 0.00%, S 0.00%.

1.4.2 Synthesis of $\text{Mn}(\text{NTf}_2)_2$

MnCO_3 was suspended in deionized water and the at least two- or threefold molar amount of HNTf_2 in aqueous solution was added dropwise. After complete dissolution of the samples the water was boiled off until a slurry solid appeared. This solid compound was transferred into a SCHLENK tube and pre-dried at 140-160°C under high vacuum. The residual solid was then sublimed under high vacuum at 270°C over night.

EA $\text{Mn}(\text{NTf}_2)_2$ calc. N 4.55%, C 7.80%, H 0.00%, S 20.81%; found N 7.78%, C 7.78%, H 0.10%, S 21.40%.



1.4.3 Synthesis of bistrifluoromethansulfonic acid

HNTf_2 was synthesized by sublimation from a solution of LiNTf_2 in an excess sulfuric acid. The reaction mixture was stirred for two days at 80-100°C. The colourless product crystallized upon cooling in yields of about 90%.

$^1\text{H-NMR}$ (300 MHz, D_2O): $\delta = 4.77$ (s, 1H)

^{19}F -NMR (300 MHz, D_2O): $\delta = -79.16$ (s, 6F)

$^{13}\text{C}\{^{19}\text{F}\}$ -NMR (300 MHz, D_2O): $\delta = 19.27$ (s, 2C)

1.4.4 General procedure for the synthesis of 1-*n*-alkyl-3-methylimidazolium chlorides and bromides

Generally, the chloride and bromide ILs were synthesized using by alkylation of *N*-Methylimidazole with the respective halogenalkane.^[21, 24] For all ILs ($\text{C}_n\text{mimBr/Cl}$, $n = 2, 3, 4$) except for C_6mimBr and C_6mimCl crystalline white powders were obtained.

C_2mimCl was synthesized by adding a fourfold excess of cold ethyl chloride to dry *N*-methylimidazole in a teflon cartridge (Parr Instruments Comp., Illinois, USA). The filled teflon cartridge was inserted into an autoclave (Parr Instruments Comp., Illinois, USA) and stirred at 90°C for four days. The reaction mixture was then allowed to cool to room temperature and the excess ethyl chloride was boiled off. The obtained very hygroscopic white powder was dried at 95°C under reduced pressure for several days.

C_2mimCl ^1H -NMR (300 MHz, D_2O): $\delta = 1.46$ (t, 3H); 3.87 (s, 3H); 4.21 (q, 2H); 7.45 (d, 2H); 8.72 (s, 1H)

C_3mimCl ^1H -NMR (300 MHz, D_2O): $\delta = 0.5$ (t, 3H); 1.81 (q, 2H); 3.83 (s, 3H); 4.09 (t, 2H); 7.39 (d, 2H); 8.66 (s, 1H)

C_4mimCl ^1H -NMR (300 MHz, D_2O): $\delta = 0.82$ (t, 3H); 1.18 (m, 2H); 1.72 (quin, 2H); 3.76 (s, 3H); 4.01 (t, 2H); 7.30 (d, 2H); 8.57 (s, 1H)

C_6mimCl ^1H -NMR (300 MHz, D_2O): $\delta = 0.78$ (t, 3H); 1.22 (m, 6H); 1.80 (t, 2H); 3.83 (s, 3H); 4.13 (t, 2H); 7.40 (d, 2H); 8.67 (s, 1H)

C_2mimBr ^1H -NMR (300 MHz, CDCl_3): $\delta = 1.23$ (t, 3H); 3.75 (s, 3H); 4.06 (q, 2H); 7.39 (s, 2H); 9.82 (s, 1H)

C_3mimBr ^1H -NMR (300 MHz, CDCl_3): $\delta = 0.44$ (t, 3H); 1.45 (hex, 2H); 3.61 (s, 3H); 3.82 (t, 2H); 7.82 (d, 2H); 9.67 (s, 1H)

C_4mimBr ^1H -NMR (300 MHz, CDCl_3): $\delta = 0.85$ (t, 3H); 1.27 (hex, 2H); 1.81 (pen, 2H); 4.02 (s, 3H); 4.24 (t, 2H); 7.56 (d, 2H); 10.19 (s, 1H)

C_6mimBr ^1H -NMR (300 MHz, CDCl_3): $\delta = 0.75$ (t, 3H); 1.20 (m, 6H); 1.81 (pen, 2H); 2.05 (s, 2H); 4.03 (s, 3H); 4.22 (t, 2H); 7.55 (d, 2H); 10.24 (s, 1H)

1.4.5 General procedure for the synthesis of 1-*n*-alkyl-3-methylimidazolium bis(trifluoromethane)sulfonylimides

The 1-*n*-alkyl-3-methylimidazolium bis(trifluoromethane)sulfonates were synthesized by metathesis reaction of the 1-*n*-alkyl-3-methylimidazolium halides with lithium bis(trifluoromethane-sulfonyl)imides.^[19, 21, 24]

C₂mimNTf₂ ¹H-NMR (300 MHz, CDCl₃): δ = 1.58 (t, 3H); 4.06 (q, 2H); 7.73 (d, 2H); 9.00 (s, 1H)

¹⁹F-NMR (300 MHz, CDCl₃): δ = -79.96 (s, 6H)

IC (halides): 119.6 ppm

C₃mimNTf₂ ¹H-NMR (300 MHz, CDCl₃): δ = 0.87 (t, 3H); 1.82 (hex, 2H); 3.84 (s, 3H); 4.05 (t, 2H); 7.29 (d, 2H); 8.53 (s, 1H)

¹⁹F-NMR (300 MHz, CDCl₃): δ = -79.43 (s, 6H)

IC (halides): 110.6 ppm

C₄mimNTf₂ ¹H-NMR (300 MHz, CDCl₃): δ = 0.89 (t, 3H); 1.31 (hex, 2H); 1.80 (pen, 2H); 3.87 (s, 3H); 4.11 (t, 2H); 7.30 (d, 2H); 8.59 (s, 1H)

¹⁹F-NMR (300 MHz, CDCl₃): δ = -79.32 (s, 6H)

IC (halides) 126.4 ppm

C₆mimNTf₂ ¹H-NMR (300 MHz, CDCl₃): δ = 0.83 (t, 3H); 1.26 (m, 6H); 1.81 (pen, 2H); 3.87 (s, 3H); 4.11 (t, 2H); 7.30 (d, 2H); 8.61 (s, 1H)

¹⁹F-NMR (300 MHz, CDCl₃): δ = -79.27 (s, 6H)

IC (halides): 113.3 ppm

1.4.6 General procedure for the synthesis of the bis(1-alkyl-3-methylimidazolium) tetrahalogenomanganates

According to $2 \text{ RmimX} + \text{MnX}_2 \rightarrow [\text{Rmim}]_2[\text{MnX}_4]$ (R = alkyl, X = Cl, Br) equimolar amounts of the respective dry 1-alkyl-3-methylimidazolium halide and MnX₂ were placed in a SCHLENK tube and heated to 80°C. After completion of the reaction which can be traced visibly by the complete dissolution of MnX₂ the product was kept at 90°C under reduced pressure for 1 day. In all cases the yields of the ionic liquids were quantitative. The liquid products were washed several times with

isopropanol to remove unreacted starting materials. Alternatively, the reaction can be driven in anhydrous methanol or isopropanol followed by crystallization of the products by removal of the solvent. These were recrystallized several times from methanol/isopropanol (1 : 0.5 to 1 : 1).

EA [C₂mim]₂[MnCl₄] calc. N 13.37%, C 34.39%, H 5.29%; found N 13.34%, C 34.26%, H 5.49%.

EA [C₃mim]₂[MnCl₄] calc. N 12.59%, C 37.75%, H 5.89%; found N 12.48%, C 37.67%, H 6.20%.

EA [C₄mim]₂[MnCl₄] calc. N 11.79%, C 40.44%, H 6.36%; found N 11.63%, C 40.36%, H 6.37%.

EA [C₆mim]₂[MnCl₄] calc. N 10.55%, C 45.21%, H 7.21%; found N 10.25%, C 44.71%, H 7.77%.

EA [C₂mim]₂[MnBr₄] calc. N 9.39%, C 24.15%, H 3.72%; found N 9.45%, C 24.51%, H 3.48%.

EA [C₃mim]₂[MnBr₄] calc. N 8.97%, C 26.91%, H 4.19%; found N 8.94%, C 26.90%, H 4.30%.

EA [C₄mim]₂[MnBr₄] calc. N 8.63%, C 29.59%, H 4.66%; found N 8.65%, C 29.71%, H 4.70%.

EA [C₆mim]₂[MnBr₄] calc. N 7.90%, C 33.88%, H 5.40%; found N 7.72%, C 33.27%, H 5.49%.

1.4.7 General procedure for the synthesis of the 1-alkyl-3-methylimidazolium tris(bis(trifluoromethanesulfonyl)imide)manganates(II)

According to $RmimNTf_2 + Mn(NTf_2)_2 \rightarrow [Rmim][Mn(NTf_2)_3]$ (R = alkyl) the respective 1-alkyl-3-methylimidazolium bis(trifluoromethanesulfonyl)imide ionic liquid was placed in a SCHLENK tube and anhydrous $Mn(NTf_2)_2$ was added. The mixture was then dissolved in anhydrous acetonitrile and stirred for 1-2 days at 60°C. After completion of the reaction the solvent was removed and the product dried under reduced pressure for 2 days at 80°C. In all cases the yield was quantitative.

EA [C₂mim][Mn(NTf₂)₃] calc. N 6.96%, C 14.32%, H 1.10%, S 19.10%; found N 7.00%, C 14.67%, H 1.30%, S 18.54%.

EA [C₃mim][Mn(NTf₂)₃] calc. N 6.86%, C 15.30%, H 1.28%, S 18.85%; found N 6.88%, C 15.21%, H 1.16%.

EA [C₄mim][Mn(NTf₂)₃] calc. N 6.77%, C 16.25%, H 1.46%, S 18.56%; found N 5.23%, C 16.85%, H 2.90%, S 18.36%.

EA [C₆mim][Mn(NTf₂)₃] calc. N 6.59%, C 18.08%, H 1.80%, S 18.11%; found N 6.70%, C 17.88%, H 2.82%, S 17.35%.

1.5 Conclusions

In this study the synthesis and optical properties of a series of imidazolium based Mn^{2+} containing ionic liquids are reported. The imidazolium rings were derivatized with *n*-alkyl chains from C_2 to C_6 . All ILs show to be true ionic liquids with melting points below $100^\circ C$. Since all ILs are solid at room temperature except the hexyl derivatives these compounds show luminescent properties in the visible region. However, the luminescence phenomena are completely quenched when the solid samples of the halogeno derivatives were molten because of thermal collision deactivation. In one case we were able to show luminescence phenomena in the liquid state.

The optical properties of the studied ILs were confirmed by comparison with literature values and are in excellent agreement with recent measurements. Hereby no significant perturbation of the optical properties of the luminescent manganese centre could be observed due to exchange of the alkyl chain at the Imidazolium ring. When the local environment of the manganese centre changes from tetrahedral to octahedral coordination site symmetry the optical properties are strongly influenced. Tetrahedrally coordinated solid tetrabromo and tetrachloromanganates exhibit intense greenish fluorescent and phosphorescent emission whilst solid Mn^{2+} based ILs octahedrally coordinated by NTf_2 emit weakly reddish. These emission phenomena could also be observed when solid samples were rubbed with a glass stick or excited by a high voltage amplifier.

Depending on the local environment and the electron donor abilities of the ligands the emission decays of the excited states of Mn^{2+} vary from 0.4 ms up to more than 25 ms at room temperature. Low temperature emission decay studies exhibited that ligands with low donor abilities like the shielding NTf_2 enlarge the emission decay of the excited Mn^{2+} based IL whereas the higher the electron donor ability the lower the emission decay of the excited state will be. Even in case of molten $[C_3mim][Mn(NTf_2)_3]$ we were successful to observe phosphorescence with a emission decay about 0.8 ms at $70^\circ C$ could be observed. In the molten liquid state $[C_3mim][Mn(NTf_2)_3]$ shows a very weak reddish light emission proving that the NTf_2 anion is effectively shielding against thermal collision deactivation.

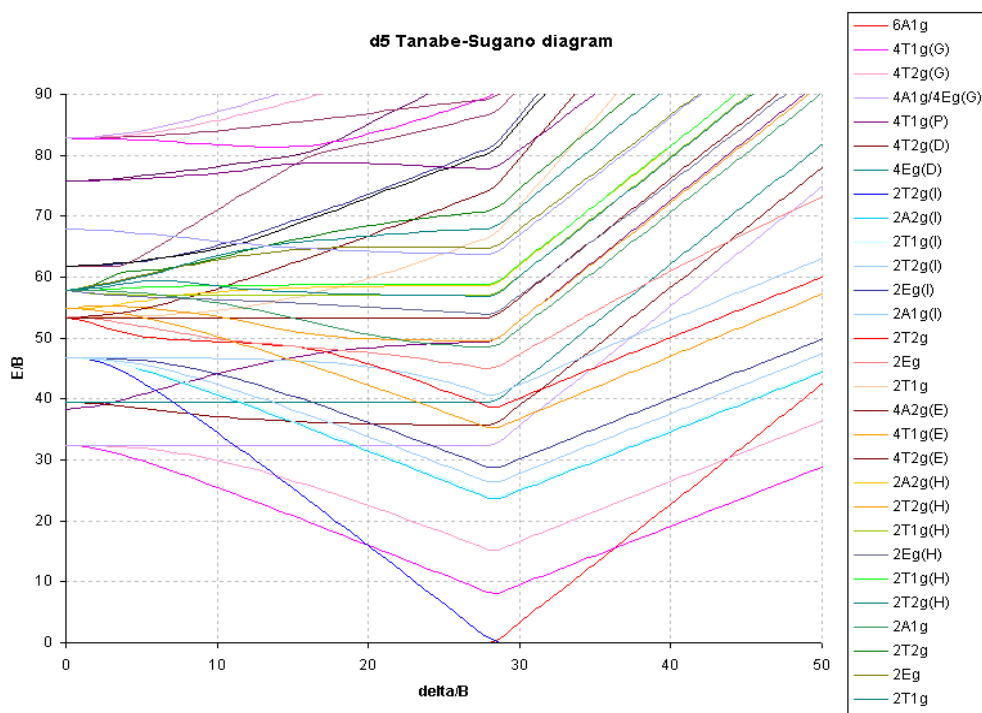
1.6 References

- [1] H. W. Lawrence, *An Introduction to Luminescence of Solids*, Wiley, New York, **1950**.
- [2] L. E. Orgel, *J. Chem. Phys.* **1955**, *23*, 1958.
- [3] K. E. Lawson, *J. Chem. Phys.* **1967**, *47*, 3627.
- [4] F. A. Cotton, D. M. L. Goodgame, M. Goodgame, *J. Am. Chem. Soc.* **1962**, *84*, 167; F. A. Cotton, *Inorg. Chem.* **2001**, *40*, 3576.
- [5] K. Sato, M. Morita, S. Okamoto, S. Morita, T. Kambara, K. I. Gondaira, H. Takenoshita, *Progress in Crystal Growth and Characterization*, **1984**, *10*, 311; G. O. Müller, *Phys. State Solidi A* **1993**, *139*, 263; J. Benoit, *Phys. State Solidi A* **1988**, *105*, 637; E. Chimczak, J. W. Allen, *J. Phys. D: Appl. Phys.* **1985**, *18*, 951; M. F. Bulanyi, A. V. Kovalenko, B. A. Polezhaev, *Inorganic Materials (Translation of Neorganicheskie Materialy)* **2002**, *36*, 222; N. T. Gurin, O. Y. Sabitov, *Technical Physics* **2006**, *51*, 1012.
- [6] B. Mallick, Diploma thesis (Cologne) **2007**; S. Hayashi, H. Hamaguchi, *Chemistry Letters* **2004**, *33*, 1590; Y. Yoshida, A. Otsuka, G. Saito, S. Natsume, E. Nishibori, M. Takata, M. Sakata, T. Yoko, *Bull. Chem. Soc. Jpn* **2005**, *78*, 1921; Y. Yoshida, G. Saito, *J. Mater. Chem.* **2006**, *16*, 1254; C. Zhong, T. Sasaki, E. Fujiwara, A. Kobayashi, Y. Iwasawa, *Bull. Chem. Soc. Jpn* **2007**, *80*, 2365; R. D. Sesto, P. Williams, *Chem. Comm.* **2008**, 447.
- [7] N. Sabbatini, M. Guardigli, J.-M. Lehn, *Coord. Chem. Rev.* **1993**, *123*, 201.
- [8] P. Wasserscheid, T. Welton, *Ionic liquids in synthesis, Vol. 1*, Wiley-VCH, Weinheim, **2002**.
- [9] K. Seddon, M. Earle, *PCT/GB2005/004121*, United Kingdom, **2006**.
- [10] A. Babai, A.-V. Mudring, *Chem. Mat.* **2005**, *17*, 6230.
- [11] S. Tang, A.-V. Mudring, *Angew. Chem. Int. Ed.* **2008**, *47*, 7568.
- [12] B. Mallick, B. Balke, C. Felser, A.-V. Mudring, *Angew. Chem. Int. Ed.* **2008**, *47*, 7635
- [13] A. Babai, S. Arenz, R. Giernoth, K. Driesen, P. Nockemann, A.-V. Mudring, *J. Alloys Compd.* **2005**, *418*, 204; S. Arenz, A. Babai, K. Binnemans, K. Driesen, R. Giernoth, A.-V. Mudring, *Chem. Phys. Lett.* **2005**, *402*, 75.

- [14] K. Vögtle, PhD thesis, University of Karlsruhe (Karsruhe), **1982**; C. P. Fredlake, J. M. Crosthwaite, J. F. Brennecke, *J. Chem. Eng. Data* **2004**, *49*, 954.
- [15] M. J. Gall, M. J. Ware, *Spectrochimica Acta* **1970**, *26A*, 287; H. D. Lutz, H. J. Schneider, *Z. anorg. allg. Chem.* **1991**, 592; F. Guillaume, A. J. Dianoux, *J. Chem. Phys.* **1990**, *94*, 3438; R. Callaghan, O. Siiman, *Inorg. Chem.* **1981**, *20*, 1723; Y. Jeon, D. Kim, *J. Phys. Chem. B* **2008**, *112*, 4735; Y. Jeon, D. Kim, *J. Chem. Phys. B* **2008**, *112*, 928; P. W. W. Hunter, G. A. Webb, *J. Inorg. Nucl. Chem.* **1972**, *34*, 1511; A. Lucken, H. Bill, *J. Phys.: Cond. Matter* **1991**, *3*, 5085; H. G. M. Edwards, L. A. Woodward, *Chem. Comm.* **1968**, 541; J. S. Avery, D. M. L. Goodgame, *Spectrochimica Acta* **1967**, *24A*, 1721; K. Wussow, H. D. Lütz, *J. Solid State Chem.* **1989**, *78*, 117; A. R. Parent, M. M. Trulli, *Inorg. Chim. Acta* **2007**, *360*, 1943.
- [16] J. Weidlein, U. Müller, K. Dehnicke, *Schwingungsfrequenzen II, Vol. 1*, Georg Thieme Verlag, Göppingen, **1986**.
- [17] A. Babai, A.-V. Mudring, *Inorg. Chem.* **2006**, *45*, 3249; M. Castriota, T. Caruso, *J. Phys. Chem. A* **2005**, *109*, 92; I. Rey, L. Servant, *Electrochimica Acta* **1998**, *43*, 1505; K. Fujii, S. Ishiguro, *J. Phys. Chem. B* **2007**, *111*, 12829; S. Riviera-Rubero, S. Baldelli, *J. Chem. Phys. B* **2006**, *110*, 4756; L. J. Hardwick, P. Novak, *J. Raman Spectr.* **2007**, *38*, 551; J. C. Lassegues, P. Johansson, *J. Raman Spectr.* **2007**, *38*, 551; A. Bakker, K. Hermansson, *Polymer* **1995**, *36*, 4371; K. Iwata, H. Hamaguchi, *Acc. Chem. Res.* **2007**, *40*, 1174; P. A. Madden, F. Hutchinson, *J. Chem. Phys.* **2003**, *120*, 6609; R. Ozawa, H. Hamaguchi, *Chem. Lett.* **2003**, *32*, 948; S. A. Katsyuba, A. Vidiis, *Helvetica Chimica Acta* **2004**, *87*, 2556; R. W. Berg, J. M. Thompson, *J. Chem. Phys. B* **2005**, *109*, 19018; H.-C. Chang, S. H. Liu, *J. Chem. Phys. A* **2007**, *111*, 9201; A. Blaschette, H. Bürger, *Z. anorg. allg. Chem.* **1970**, *378*, 104; E. R. Talaty, W. R. Carper, *J. Chem. Phys. B* **2004**, *108*, 13177.
- [18] Y. Tanabe, S. Sugano, *J. Phys. Soc. Japan* **1954**, *9*, 753; Y. Tanabe, S. Sugano, *J. Phys. Soc. Japan* **1954**, *9*, 766.
- [19] P. A. Thiessen, K. Meyer, *Naturwissenschaften* **1970**, *9*, 423.
- [20] G. E. Hardy, J. I. Zink, *Inorg. Chem.* **1976**, *15*, 3061; N. Islam, *Applied Spectroscopy* **1975**, *29*, 266; M. T. Vala, S. L. Holt, *Molecular Physics* **1972**, *23*, 217; A. J. MacFarlane, R. J. P. Williams, *J. Chem. Soc. A* **1969**, 1519; J. J. Foster, N. S. Gill, *J. Chem. Soc. A* **1968**, 2625; C. Furlani, A. Furlani, *J. Inorg. Nucl. Chem.* **1961**, *19*, 51; S. J. Chan, H. Lütje, *J. Chem. Phys.* **1967**, *47*, 2121; A. Mehra, P. Venkateswarlu, *J. Chem. Phys.* **1966**, *45*, 3381; S. Buffagni, T. M. Dunn, *Nature* **1960**, *188*, 937; R. Lissilour, M. A. Makhyoun, *J. de chimie physique* **1981**, *78*, 335; D. Oelkrug,

- A. Wölpl, *Ber. d. Bunsen-Ges.* **1972**, 76, 680; R. Parrot, K. Nikolic, *J. of Luminescence* **1979**, 18/19, 154; W. D. Perry, L. M. Vallerino, *Inorg. Chim. Acta*, 7 **1973**, 2, 175; R. Pappalardo, *J. Chem. Phys.* **1959**, 31, 1050; C. Naud, R. Parrot, *Phys. Rev. B* **1979**, 20, 3333.
- [21] V. Gutmann, K. Fenkart, *Monatshefte f. Chemie* **1966**, 45, 286.
- [22] G. Blasse, C. Grabmaier, *Luminescent materials*, Springer Verlag, Berlin, **1994**.
- [22] P. Manning, *Can. Mineralogist* **1969**, 9, 237; L. Burlamacchi, E. Tiezzi, *J. Phys. Chem.* **1970**, 74, 3980.
- [23] M. D. C. M. de Lucas, M. Lorenzo, *Ferroelectrics* **1990**, 109, 21; N. Presser, B. R. Sundheim, *Chem. Phys.* **1978**, 31, 281; B. R. Sundheim, B. Howard, *J. Chem. Phys.* **1972**, 57, 4492; B. R. Sundheim, J. L. Painter, *J. Coord. Chem.* **1984**, 13, 185; K. Nikolic, F. Lignou, *J. of Luminescence* **1973**, 8, 137; M. Whrigton, D. Ginley, *Chem. Phys.* **1974**, 4, 295.
- [24] N. Presser, M. Ratner, B.R. Sundheim, *Chem. Phys.* **1978**, 31, 281.

2 Optical basicity of ionic liquids



2.1 Abstract

The concept of optical basicities initially developed by DUFFY for solid oxides was successfully transferred to low melting salts such as ionic liquids. Several ILs were doped with $\text{Mn}(\text{NTf}_2)_2$ ($\text{NTf}_2 =$ bistrifluoromethanesulfonyl)imide) as a probe to investigate the IL anion basicity by means of UV/Vis spectroscopy. The ${}^6\text{A}_1 \rightarrow {}^4\text{A}$, ${}^4\text{E}(\text{G})$ transition band of Mn^{2+} is influenced by the electron donor properties, hence, Lewis basicity, of the coordinating ligands but remains – to the first order – independent from the ligand field. It turned out that the change in the optical spectra for various $\text{Mn}(\text{NTf}_2)_2$ doped ILs is predominantly dependent on the anion. No significant influence of the IL cation could be detected for the ILs under investigations. This allows to rank the ILs with respect to their (optical) anion basicity. For the most prominent IL anions an order of

$\text{BF}_4 < \text{ClO}_4 < \text{NTf}_2 \sim \text{MeSO}_3 < \text{NO}_3 < \text{DCA} < \text{TFA} < \text{EtSO}_4 \sim \text{OTos} < \text{Cl} < \text{Br}$

with respect to rising optical basicity could be determined.

2.2 Introduction

Ionic liquids (ILs) are becoming increasingly popular as solvents and reactants for a wide range of applications.^[1] One of the many advantages that ionic liquids are able to offer over conventional organic solvents (and water) is the tuneability of the solvent properties through the choice of the respective cation/anion combination. Different combinations of cations and anions lead to a nearly infinite number of ionic liquids with certain properties. It is estimated that roughly 10^{18} ionic liquids are accessible.^[2] Because of this ionic liquids are also called “designer solvents”.^[3] For the design of such solvents it is important to know and also to be able to predict their properties. Important physicochemical solvent properties are its polarity and acidity. Solvent polarity can determine the solubility of substances and is able to decisively influence the outcome of chemical reactions, the position of chemical equilibria, reaction rates and much more.^[4] The rate of a reaction that goes through a charge separated transition state (as in case of S_N2 nucleophilic substitutions) is generally increased in more polar solvents. This observation has been rationalized in the HUGHES-INGOLD rules.^[5] Often continuum properties such as the dielectric constant, refractive index (optical polarizability) and dipole moment are seen as a measure for the solvation power. However, this can be misleading. For example, perchloric acid does not dissociate in anhydrous sulphuric acid with a dielectric constant ϵ of 85 but is dissociated in acetic anhydride with $\epsilon = 7$; anhydrous HCN ($\epsilon = 125$) turns out to be a bad solvent for most salts but pyridine ($\epsilon = 12$) a good one.^[6] It was initially thought that a highly polar medium like ionic liquids would easily dissolve other salts. It has been realized that ordinary metal salts have sometimes an astonishing low solubility in many ionic liquids – although one often assumes that similar dissolves similar. But solvent-solute interactions take place at a molecular level and a variety of different solvent-solute interactions have to be taken into account. Solvent-solute interactions can be either specific or non-specific interactions.^[7] Non-specific interactions are instantaneous/induced dipole forces (dispersion or London forces), dipole/induced dipole forces (induction or Debye forces), dipole/dipole forces (orientation or Keesom forces) and ion/dipole forces (Coulomb forces). Specific interactions include hydrogen bond donor and/or hydrogen bond acceptor interactions, electron pair donor/electron pair acceptor or charge-transfer interactions, solvophobic interactions (which can become important in highly structured solvents like ILs).

Several methods have been used to determine the solvent power of ionic liquids determined addressing their polarity and nucleophilicity (donor power). A common approach for determining the solvent polarity is to evaluate the UV/Vis spectra of optical probes such as solvatochromic dyes or transition metal complexes in the solvents under investigation.^[7] The absorption or emission bands of the probe show a strong shift in their optical spectra (solvatochromic shift) according to the polarity of the solvent in which they are dissolved.^[8] As probes for solvent polarities, different dyes

and transition metal have been used, e.g., Nile Red^[9], REICHARTD's Dye^[10], $[\text{Fe}(\text{tmphen})_2(\text{CN})_2]$ ^[11] (tmphen = 3, 4, 7, 8-tetramethyl-1, 10-phenanthroline) or $\text{Cu}(\text{tmen})(\text{acac})^+$ (tmen = tetramethylenediamine = 1,2-bis(dimethylamino)ethane, acac = acetyl-acetonate).^[12] KAMLET-TAFT parameters^[13] have been derived for many ionic liquids using solvatochromic, organic dyes.^[14] Here ϵ^* reports the effect of the dipolarity and polarizability of the solvent, ϵ is largely controlled by the cation of the ionic liquid and ENT seems to be specially sensitive to the hydrogen bond donor ability of the cation of the ionic liquid. ϵ is dependent on the hydrogen bond basicity of the solvent and is dominated by the nature of the anion. In addition, a hydrogen bond accepting ability scale has been set up by ¹H-NMR spectroscopy and using the solvatochromic dye 3-(4-amino-3-methylphenyl)-7-phenyl-benzo-[1,2-b:4,5-b0]-difuran-2,6-di-one.^[15] Solvatochromic shifts of $[\text{Fe}(\text{phen})_2(\text{CN})_2]\text{ClO}_4$ have also been used for that purpose.^[16] Efforts to spectroscopically determine acidity/basicity scales for ionic liquids have recently be reviewed^[17] and it has been noted that results from these measurements are, as a whole, strongly dominated by the cation. However, an important property of ionic liquids as already noted for molten salts is their Lewis basicity or electron or coordinaton power of the anion. Lux and Flood have developed an acid-base theory for oxide materials relying basically on the Lewis acidity of the oxide anion.^[18] It has been widely realized that the determination of acidity of non-aqueous solutions is not an easy task especially for molten salts.^[19]

In a new approach which mainly addressed the donor strength, coordination power or LEWIS basicity of the anion, a spectroscopic probe-ion method is developed which allows for the determination of ionic liquid acidity. The method is based on DUFFY's concept of the optical basicity.^[20] DUFFY originally developed the concept of optical basicity to determine the electron donation power of different oxide host lattices. d-d spectra of transition metal ions provide valuable information on the environment of a metal ion when it undergoes complexation or changes in the ligand sphere. Ligands mainly exert two important effects on the metal central ion which are on the one hand the crystal field splitting of the energy levels of the central ion and on the other hand the nephelauxetic effect (expansion of its atomic orbitals).^[21] Especially the second effect indicates the extent of electron density provided by the ligands for the metal ion (degree of covalency). Mn^{2+} and Fe^{3+} with a d^5 electron configuration are particularly suitable transition metal cations. By evaluating the absorption spectrum of the d^5 ion in the respective coordination environment the so-called orbital expansion effect h can be determined. The energy difference between the ${}^6\text{A}_{1g}$ (${}^6\text{S}$ term) ground state and the ${}^4\text{A}_{1g}$ and ${}^4\text{E}_g$ (${}^4\text{G}$ term) is independent of the crystal field and relies primarily on the reduction of inter-electronic repulsion by expansion of the 3d orbitals:

$$hk \cdot \nu_{S \rightarrow G}^f = \nu_{S \rightarrow G}^f - \nu_{S \rightarrow G}$$

$\nu_{S \rightarrow G}^f$: frequency of the free ion

$\nu_{S \rightarrow G}$: frequency of the complexed ion

The parameters h and k are specific to the ligand set and the metal ion. k is nearly independent from the coordination number and is 0.069 for Mn^{2+} .^[22] $hs-d^5-Mn^{2+}$ features in a tetrahedral coordination site LaPORTE-allowed but spin-forbidden transitions whereas the electronic transitions of octahedrally coordinated Mn^{2+} are LaPORTE-forbidden and spin forbidden which results in low absorbances. In case of both site symmetries the TANABE-SUGANO diagrams are identical as the d^5 ion is its own hole equivalent which facilitates the interpretation of the absorption spectra.^[23]

To adapt DUFFY's approach to low temperature molten salts, hence, ionic liquids, $Mn(NTf_2)_2$ as a $Mn-d^5$ source was doped into several ILs and the shift of the ${}^6A_1({}^6S) \rightarrow {}^4A, {}^4E(G)$ transition band maxima in the UV/Vis spectra was evaluated.

2.3 Results and Discussion

An ideal $Mn-d^5$ probe would be the free ion. For our systems under investigation $Mn(NTf_2)_2$ ($NTf_2 =$ bis(trifluoromethanesulfonyl)imide) was chosen as the best approximation of a free Mn^{2+} source. The NTf_2 anion belongs to the class of weakly coordinating anions^[24], its transition metal compounds show only a weak ligand field splitting and $Mn(NTf_2)_2$ can be easily synthesized. As we have shown previously for other metal bis(trifluoromethanesulfonyl)imides replacement of NTf_2 by anions of the ionic liquid (IL) occur readily upon dissolution of the salt in an ionic liquid with stronger coordinating, more LEWIS basic, anions.^[25] Thus by dissolving $Mn(NTf_2)_2$ in various ionic liquids the respective IL can be probed for its optical basicity.

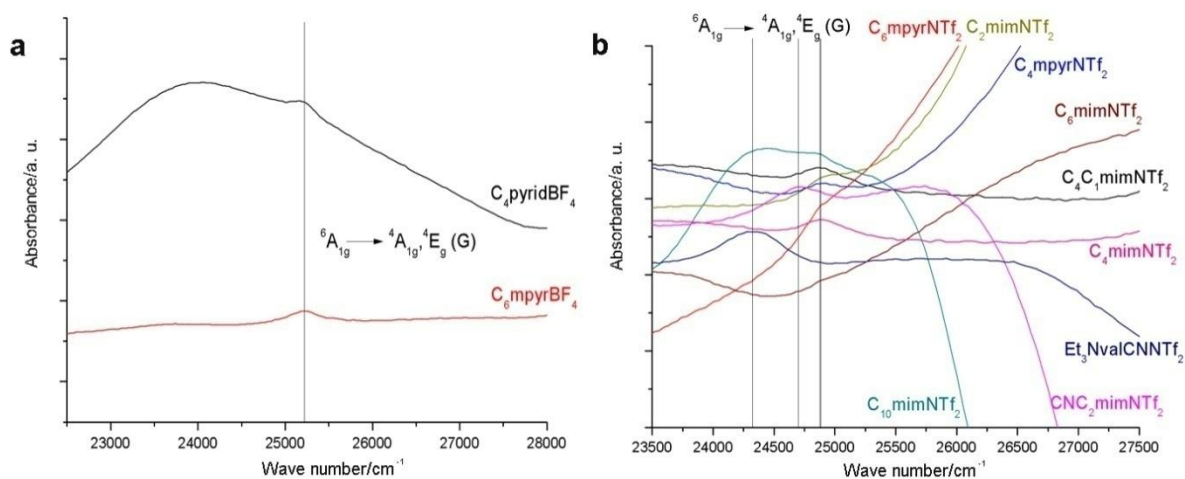


Fig. 1 UV/Vis spectra of a) different C_4 mim-ILs and b) different NTf_2^- -ILs doped with $Mn(NTf_2)_2$. The ${}^6A_1({}^6S) \rightarrow {}^4A, {}^4E(G)$ transition bands are depicted by straight lines.

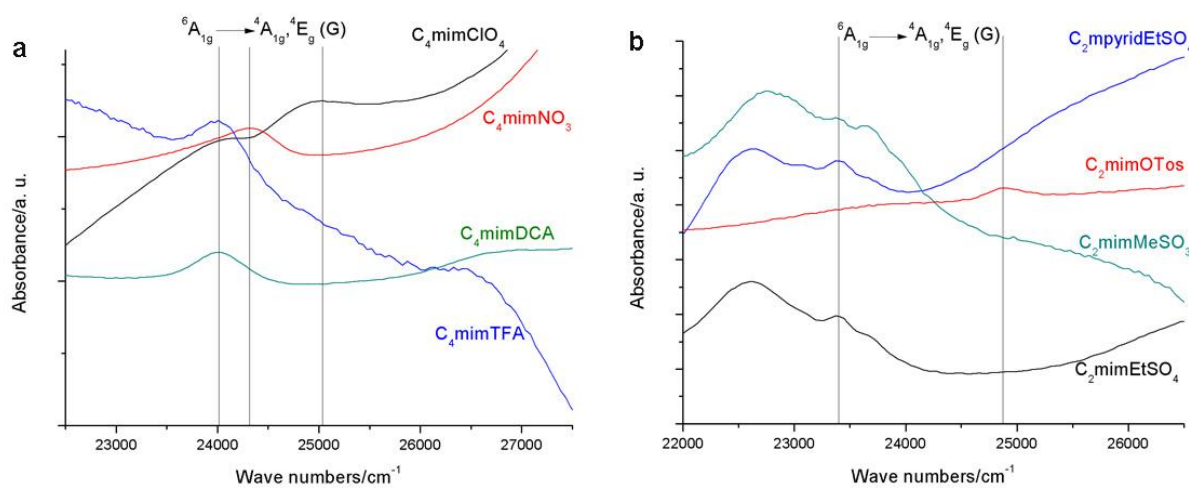


Fig. 2 UV/Vis spectra of a) different C_4 mim-ILs and b) different NTf_2^- -ILs doped with $Mn(NTf_2)_2$. The ${}^6A_1({}^6S) \rightarrow {}^4A, {}^4E(G)$ transition bands are depicted by straight lines.

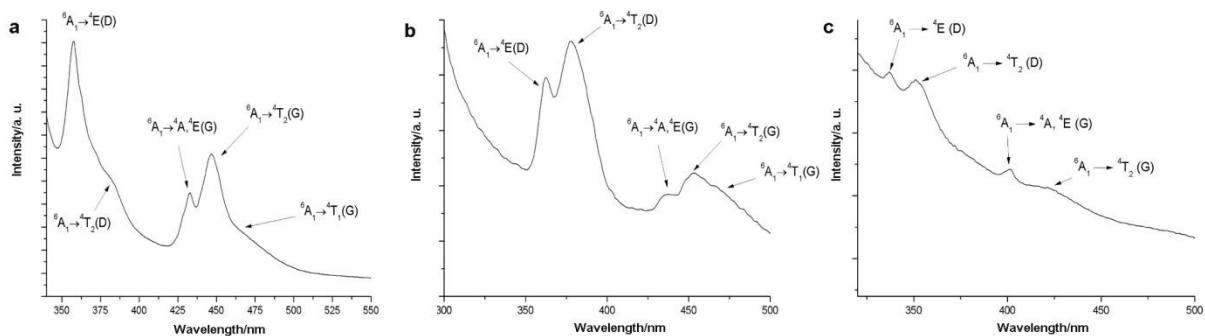


Fig. 3 UV/Vis spectra of $[C_4mim]_2[MnCl_4]$ (left), $[C_4mim]_2[MnBr_4]$ (middle) and $[C_3mim][Mn(NTf_2)_3]$ (right).

Table 1. ${}^6A_1 \rightarrow {}^4A, {}^4E(G)$ transition maxima of $Mn(NTf_2)_2$ doped ILs and their nephelauxetic parameter h at RT. The site symmetry of Mn^{2+} is assigned to be either tet (tetrahedral) or oct (octahedral).

sample	${}^6A_1 \rightarrow {}^4A, {}^4E(G)$ transition band/ cm^{-1}	approx. Mn^{2+} site symmetry	nephelauxetic parameter h
[C ₂ mim][NTf ₂]	24902	oct	-0.01
[C ₄ mim][NTf ₂]	24887	oct	-0.01
[C ₆ mim][NTf ₂]	24879	oct	0.00
[C ₄ C ₁ mim][NTf ₂]	24881	oct	0.00
[C ₁₀ mim][NTf ₂]	24868	oct	-0.01
[CNC ₂ mim][NTf ₂]	24713	oct	0.09
[C ₄ mpyr][NTf ₂]	24893	oct	-0.01
[C ₆ mpyr][NTf ₂]	24898	oct	-0.01
[Et ₃ NvalCN][NTf ₂]	24350	oct	0.30
[C ₂ mim][MeSO ₃]	24868	oct	0.00
[C ₂ mim][EtSO ₄]	23388	tet	0.85
[C ₂ mpyrid][EtSO ₄]	23400	tet	0.85
[C ₂ mim][OTos]	23395	tet	0.85
[C ₄ mim][ClO ₄]	25022	oct	-0.08
[C ₄ mim][NO ₃]	24327	oct	0.32
[C ₄ mim][TFA]	24006	oct	0.50
[C ₄ mim][DCA]	24339	oct	0.33
[C ₄ pyrid][BF ₄]	25204	oct	-0.19
[C ₆ mpyrid][BF ₄]	25239	oct	-0.21
acetonitrile	24200/24378 ¹	oct	0.39/0.29
water	24904	oct	0.02

¹ This transition band is splitted into two broad and overlying bands

Table 2. ${}^6A_1 \rightarrow {}^4A, {}^4E(G)$ transition maxima of Mn^{2+} -based ILs and their nephelauxetic parameter h at RT. The site symmetry of Mn^{2+} is assigned to be either tet (tetrahedral) or oct (octahedral).

sample	${}^6A_1 \rightarrow {}^4A, {}^4E(G)$ transition band/ cm^{-1}	approx. Mn^{2+} site symmetry	nephelauxetic parameter h
$[C_2mim]_2[MnCl_4]$	23095	tet	1.02
$[C_3mim]_2[MnCl_4]$	23095	tet	1.02
$[C_4mim]_2[MnCl_4]$	23095	tet	1.02
$[C_6mim]_2[MnCl_4]$	23095	tet	1.02
$[C_2mim]_2[MnBr_4]$	22989	tet	1.08
$[C_3mim]_2[MnBr_4]$	22989	tet	1.08
$[C_6mim]_2[MnBr_4]$	22936	tet	1.11
$[C_6mim]_2[MnBr_4]$	22936	tet	1.11
$[C_2mim]_2[Mn(NTf_2)_4]$	24876	oct	0.00
$[C_3mim]_2[Mn(NTf_2)_4]$	24938	oct	-0.04
$[C_4mim]_2[Mn(NTf_2)_4]$	24938	oct	-0.04
$[C_6mim]_2[Mn(NTf_2)_4]$	24876	oct	0.00

At first glance at the recorded UV/Vis spectra of ionic liquid doped with $Mn(NTf_2)_2$ show low absorbances and broad transition bands due to thermal vibrations (see Fig. 1-3). The frequencies of the ${}^6A_1({}^6S) \rightarrow {}^4A, {}^4E(G)$ transition span a range from about 23000-25000 cm^{-1} depending on the ionic liquid (see table 1). From table 1 it becomes obvious that mostly the anion of the ionic liquid influences the position of the ${}^6A_1({}^6S) \rightarrow {}^4A, {}^4E(G)$ transition of Mn^{2+} . For the most common ionic liquid cations such as alkylimidazolium, alkylpyridinium or alkylpyrrolidinium no significant cation influence could be detected. However, when the cation is functionalized with a potential electron donor functionality such as a nitrile group the cation influence becomes important and the anion basicity cannot be determined as a mixed effect of both the cation and the anion on the shift of the

absorption maximum is observed. Thus for the determination of the optical basicity only innocent cations without donor functions will be considered.

The nephelauxetic parameter h calculated from the absorption maximum of the ranges ${}^6A_1({}^6S) \rightarrow {}^4A, {}^4E(G)$ transition from -0.2 for tetrafluoroborate ILs to 1.1 for bromide ILs. Less coordinating IL anion evoke in general to an octahedral site symmetry for Mn^{2+} whilst stronger coordination anion like chloride and bromide or diethylsulfate and tosylate lead to a tetrahedral site symmetry. The nephelauxetic parameter grows in the direction of OR ($R = EtSO_4$) $< Cl < Br$ from $0.85 < 1.02 < 1.1$ indicating rising covalent bonding between Mn^{2+} and the ionic liquid anion which results in an increased electron density at Mn^{2+} .

The nephelauxetic parameters h for octahedrally coordinated Mn^{2+} range from -0.19 ($[C_4pyrid][BF_4]$) to 0.50 ($[C_4mim][TFA]$). Thus BF_4 has the lowest tendency to donate electron density amongst the ILs under investigation. In general it appears that highly symmetric anions like ClO_4 and BF_4 (point group T_d) have lower h parameters compared to less symmetric anions (NTf_2, TFA). Judging from the nephelauxetic parameter h the electron donor tendency and thus, the optical basicity of the ionic liquid anions under investigation rises according to $BF_4 < ClO_4 < NTf_2 \sim MeSO_3 < NO_3 < DCA < TFA$.

The nephelauxetic parameters h for tetrahedrally coordinated Mn^{2+} range from 0.85 (ethylsulfate, tosylate) to about 1 (chloride and bromide).

In summary according to rising optical basicity the investigated anion can be arranged as follows:



2.3 Experimental

2.3.1 Materials

Acetonitrile (98%, Biesterfeld, Hamburg, D), activated charcoal (KMF, St. Augustin, D), aluminum oxide (Brockmann I, neutral, Acros, Geel, B), dichloromethane (99%), lithium triflate (98%, Acros, Geel, B), lithium bistrifluoromethanesulfonamide (99%, IoLiTec, Denzlingen, D), manganese carbonate (44-46% Mn, KMF, St. Augustin, D) and concentrated sulfuric acid (99%+) were used as received. Acetonitrile (99.8%, <10 ppm water) was purchased from Acros, Geel, B and used as received.

Chloroacetonitrile (98%), methyltrifluoroacetate (99%), *N*-methylimidazole (98%), pyrrolidine (98%) and diethylsulfate (98%) were purchased from Sigma-Aldrich, Schnelldorf, D and distilled prior to use. 1,2-dimethylimidazole (98%) was purchased from Sigma-Aldrich, Schnelldorf, D and recrystallized from toluene prior to use. Triethylamine (98%) was purchased from Acros, Geel, B and distilled prior to use. Silver nitrate (99%) was purchased from KMF, St. Augustin, D and dried at high vacuum at 220°C over night prior to use.

The ionic liquids 1-ethyl-3-methylimidazolium methylsulfite (99%), 1-ethyl-3-methylimidazolium tosylate (99%), 1-ethyl-4-methylpyridinium ethylsulfate (99%), *N*-hexyl-*N*-methylpyrrolidinium tetrafluoroborate (98%) and *N*-butyl-*N*-methylpyrrolidinium hexafluorophosphate (99%) were purchased from IoLiTec, Denzlingen, D. *N*-butyl-*N*-methylpyrrolidinium (trifluoro)(tris(perfluoroethyl)phosphate (pure) was received from Merck, Darmstadt, D. To purify the commercial ILs they were diluted with CH₂Cl₂ or CHCl₃ and washed several times with deionized water to remove any excess of halides or alkaline salts (AgNO₃ test) as well as other contaminations. After filtration over a column filled with neutral Al₂O₃ and active charcoal the solvent of the organic phase was removed under dynamic vacuum and the product dried under reduced pressure at 80-90°C for 1-2 days.

2.3.2 Syntheses

Synthesis and sample handling were carried out under standard SCHLENK and Argon-glove box techniques. All solvents were dried using standard procedures.^[26]

2.3.3 UV/Vis measurements

The UV/Vis spectra of these samples were recorded on a Bruker Cary 5000 using sealed one-way cuvettes. Difference spectra of the $\text{Mn}(\text{NTf}_2)_2$ containing and pure ionic liquid were measured in the range from 250-700 nm with a scan rate of 400 nm/s.

2.3.4 General synthesis procedure for nitrile-ILs

An excess of the respective chloronitrile in acetonitrile was added dropwise to a solution of triethylamine or methylimidazole in acetonitrile, respectively.

To obtain CNC_2mimCl the reaction mixture was stirred at 0°C while adding the starting materials. Afterwards the temperature was raised to 70°C and the reaction mixture was stirred for 1 day.

For Et_3NvalCN the reaction mixture was placed in a teflon lined Parr autoclave and heated to 90°C for 4 days.

After completion of the reaction acetonitrile was removed under vacuum and the obtained raw products were recrystallized from CH_2Cl_2 . The dried products were then dissolved in acetone/acetonitrile (50 : 50) and an equimolar amount of LiNTf_2 dissolved in acetonitrile added. After stirring at 60°C for 1 day the organic phase removed at the rotatory evaporator and the raw product washed halide free with deionized water (AgNO_3 test). After filtration over a column filled with neutral or acidic Al_2O_3 the residual organic phase removed and dried under high vacuum for 1 day at 80-90°C.

$[\text{Et}_3\text{NvalCN}][\text{NTf}_2]$: $^1\text{H-NMR}$ (300 MHz, CDCl_3): δ = 0.86 (t, 3H); 1.22 (m, 6H); 1.80 (t, 2H); 3.83 (s, 3H); 4.13 (t, 2H); 7.40 (d, 2H); 8.67 (s, 1H)

$[\text{CNC}_2\text{mim}][\text{NTf}_2]$: $^{13}\text{C-NMR}$ (300 MHz, acetone- d_6): δ = 35.89 (s); 36.23 (s); 36.90 (s); 113.22 (s); 113.49 (s); 117.75 (s); 121.99 (s); 122.66 (s); 127.87 (s); 126.24 (s); 137.48 (s)

$^1\text{H-NMR}$ (300 MHz, Aceton- d_6): δ = 4.02 (s, 3H); 5.51 (s, 2H); 7.71 (d, 2H); 9.00 (s, 2H)

2.3.5 General synthesis procedure for 1-*n*-alkyl-3-methylimidazolium chlorides and bromides

Generally, the chloride and bromide ILs were synthesized using by direct alkylation of N-methylimidazole with the respective halogenalkane using standard literature procedures.^[27] For

C_nmimBr/Cl, C = 2, 3, 4 a crystalline white powder was obtained. C₆mimBr and C₆mimCl were obtained as liquid products of high viscosity.

C₂mimCl was synthesized by adding a fourfold excess of cold ethyl chloride to dry N-methylimidazole in a teflon cartridge (Parr Instruments Comp., Illinois, USA). The filled teflon cartridge was inserted into an autoclave (Parr Instruments Comp., Illinois, USA) and stirred at 90°C for four days. The reaction mixture was then allowed to cool to room temperature and the excess ethyl chloride was boiled off. The very hygroscopic white powder obtained was dried at 95°C under reduced pressure for several days.

[C₂mim]Cl: ¹H-NMR (300 MHz, D₂O): δ = 1.46 (t, 3H); 3.87 (s, 3H); 4.21 (q, 2H); 7.45 (d, 2H); 8.72 (s, 1H)

[C₃mim]Cl: ¹H-NMR (300 MHz, D₂O): δ = 0.85 (t, 3H); 1.81 (q, 2H); 3.83 (s, 3H); 4.09 (t, 2H); 7.39 (d, 2H); 8.66 (s, 1H)

[C₄mim]Cl: ¹H-NMR (300 MHz, D₂O): δ = 0.82 (t, 3H); 1.18 (m, 2H); 1.72 (quin, 2H); 3.76 (s, 3H); 4.01 (t, 2H); 7.30 (d, 2H); 8.57 (s, 1H)

[C₆mim]Cl: ¹H-NMR (300 MHz, D₂O): δ = 0,78 (t, 3H); 1.22 (m, 6H); 1.80 (t, 2H); 3.83 (s, 3H); 4.13 (t, 2H); 7.40 (d, 2H); 8.67 (s, 1H)

[C₂mim]Br: ¹H-NMR (300 MHz, CDCl₃): δ = 1.23 (t, 3H); 3.75 (s, 3H); 4.06 (q, 2H); 7.39 (s, 2H); 9.82 (s, 1H)

[C₃mim]Br: ¹H-NMR (300 MHz, CDCl₃): δ = 0.44 (t, 3H); 1.45 (hex, 2H); 3.61 (s, 3H); 3.82 (t, 2H); 7.82 (d, 2H); 9.67 (s, 1H)

[C₄mim]Br: ¹H-NMR (300 MHz, CDCl₃): δ = 0.85 (t, 3H); 1.27 (hex, 2H); 1.81 (pen, 2H); 4.02 (s, 3H); 4.24 (t, 2H); 7.56 (d, 2H); 10.19 (s, 1H)

[C₆mim]Br: ¹H-NMR (300 MHz, CDCl₃): δ = 0.75 (t, 3H); 1.20 (m, 6H); 1.81 (pen, 2H); 2.05 (s, 2H); 4.03 (s, 3H); 4.22 (t, 2H); 7.55 (d, 2H); 10.24 (s, 1H)

2.3.6 General synthesis procedure bis(trifluoromethane)sulfonylamide ionic liquids

The 1-*n*-alkyl-3-methylimidazolium and trihexyltetradecylphosphonium bis(trifluoromethane)-sulfonates were synthesized by metathesis reaction of 1-*n*-alkyl-3-methylimidazolium halides with lithium bis(trifluoromethane-sulfonyl)amide. The respective halide IL was dissolved in

acetone/acetonitrile (50 : 50) in case of P_{666 14} ILs or in deionized water in case of C_xmimNTf₂ and an equimolar amount of LiNTf₂ dissolved in the respective solvent was added. After stirring at 60°C for one day the organic phase was separated and washed halide free with deionized water (AgNO₃ test). The solution was then filtered over a column filled with neutral Al₂O₃ and active charcoal. The residual organic phase was freed from solvent and dried under high vacuum for 1-2 days at 80-90°C.

[C₂mim][NTf₂]: ¹H-NMR (300 MHz, CDCl₃): δ = 1.58 (t, 3H); 4.06 (q, 2H); 7.73 (d, 2H); 9.00 (s, 1H)

¹⁹F-NMR (300 MHz, CDCl₃): δ = -79.96 (s, 6H)

[C₃mim][NTf₂]: ¹H-NMR (300 MHz, CDCl₃): δ = 0.87 (t, 3H); 1.82 (hex, 2H); 3.84 (s, 3H); 4.05 (t, 2H); 7.29 (d, 2H); 8.53 (s, 1H)

¹⁹F-NMR (300 MHz, CDCl₃): δ = -79.43 (s, 6H)

[C₄mim][NTf₂]: ¹H-NMR (300 MHz, CDCl₃): δ = 0.89 (t, 3H); 1.31 (hex, 2H); 1.80 (pen, 2H); 3.87 (s, 3H); 4.11 (t, 2H); 7.30 (d, 2H); 8.59 (s, 1H)

¹⁹F-NMR (300 MHz, CDCl₃): δ = -79.32 (s, 6H)

[C₆mim][NTf₂]: ¹H-NMR (300 MHz, CDCl₃): δ = 0.83 (t, 3H); 1.26 (m, 6H); 1.81 (pen, 2H); 3.87 (s, 3H); 4.11 (t, 2H); 7.30 (d, 2H); 8.61 (s, 1H)

¹⁹F-NMR (300 MHz, CDCl₃): δ = -79.27 (s, 6H)

[C₁₀mim][NTf₂]: ¹H-NMR (300 MHz, DMSO-d₆): δ = 0.81 (t, 3H); 1.20 (s, 14H); 1.73 (pen, 2H); 3.80 (s, 3H); 4.11 (t, 2H); 7.68 (d, 2H); 9.06 (s, 1H)

¹⁹F-NMR (300 MHz, DMSO-d₆): δ = -78.84 (s, 6H)

[C₄C₁mim][NTf₂]: ¹H-NMR (300 MHz, CDCl₃): δ = 0.95 (t, 3H); 1.39 (hex, 2H); 1.84 (pen, 2H); 2.76 (s, 3H); 2.94 (s, 2H); 3.92 (s, 3H); 4.26 (t, 2H); 7.57 (d, 2H)

¹⁹F-NMR (300 MHz, CDCl₃): δ = -79.89 (s, 6H)

2.3.7 General synthesis procedure for trifluoroacetate ionic liquids

Freshly distilled butylimidazole was cooled to -10°C and treated dropwise in a round flask with an equimolar amount of freshly distilled methyltrifluoroacetate. The resulting mixture was allowed to warm to room temperature and stirred for 1 day. To this mixture CH₂Cl₂ and fine powdered active charcoal were added and the suspension was stirred for 1 day at room temperature. After filtration

of the mixture over a column filled with neutral or acidic Al_2O_3 the residual organic phase was freed from solvent under vacuum and then dried under high vacuum for 1 day at 80-90°C.

$[\text{C}_4\text{mim}][\text{TFA}]$: $^1\text{H-NMR}$ (300 MHz, CDCl_3): $\delta = 0.85$ (t, 3H); 1.27 (hex, 2H); 1.81 (pen, 2H); 4.02 (s, 3H); 4.24 (t, 2H); 7.56 (d, 2H); 10.19 (s, 1H)

2.3.8 General synthesis procedure for dicyanamide ionic liquids

The respective halide IL was dissolved in deionized water and an equimolar amount of AgDCA was added. The reaction mixture was stirred for 2 hours at 60°C. The unreacted material and the alkali metal halide were then filtered off and the solvent of the remaining solution was removed under vacuum. The residual was then dissolved in CH_2Cl_2 and washed several times with deionized water. After filtration of the mixture over a column filled with neutral or acidic Al_2O_3 the solvent was removed from the residual organic phase and the product was dried under high vacuum for 1 day at 80-90°C.

$[\text{C}_4\text{mim}][\text{DCA}]$: $^1\text{H-NMR}$ (300 MHz, CDCl_3): $\delta = 0.85$ (t, 3H); 1.27 (hex, 2H); 1.81 (pen, 2H); 4.02 (s, 3H); 4.24 (t, 2H); 7.56 (d, 2H); 10.19 (s, 1H)

$[\text{C}_4\text{mpyr}][\text{DCA}]$: $^1\text{H-NMR}$ (300 MHz, CDCl_3): $\delta = 0.44$ (t, 3H); 1.45 (hex, 2H); 3.61 (s, 3H); 3.82 (t, 2H); 7.82 (d, 2H); 9.67 (s, 1H)

2.3.9 General synthesis procedure for diethylsulfate ionic liquids

Et_2SO_4 was added dropwise to an equimolar amount of dry methylimidazole. After complete addition of the starting materials the resulting mixture was stirred for 1 day at 60°C. After cooling to room temperature the mixture was diluted with CH_2Cl_2 and filtered over a column filled with neutral or acidic Al_2O_3 and active charcoal. The solvent was removed under vacuum and the residual dried under high vacuum for 1-2 days at 80-90°C.

$[\text{C}_2\text{mim}][\text{EtSO}_4]$: $^1\text{H-NMR}$ (300 MHz, CDCl_3): $\delta = 0.85$ (t, 3H); 1.27 (hex, 2H); 1.81 (pen, 2H); 4.02 (s, 3H); 4.24 (t, 2H); 7.56 (d, 2H); 10.19 (s, 1H)

2.3.10 General synthesis procedure for nitrate ionic liquids

The respective halide IL was dissolved in deionized water in a flask and an equimolar amount of AgNO_3 also dissolved in deionized water was added dropwise. The resulting mixture was stirred for 1

day at 60°C. The precipitated silverhalide was filtered off and the solvent was removed. After cooling to room temperature the mixture was diluted with CH₂Cl₂. The solution was then washed halide free (AgNO₃ test). After filtration of the mixture over a column filled with neutral or acidic Al₂O₃ and active charcoal the residual organic phase was freed from solvent and dried under high vacuum for 1-2 days at 80-90°C.

[C₄mim][NO₃]: ¹H-NMR (300 MHz, CDCl₃): δ = 0.89 (t, 3H); 1.32 (hex, 2H); 1.88 (pen, 2H); 4.03 (s, 3H); 4.35 (t, 2H); 7.88 (d, 2H); 9.65 (s, 1H)

2.3.11 General synthesis procedure for perchlorate ionic liquids

The respective halide IL was dissolved in CH₂Cl₂ in a flask and an equimolar amount of NaClO₄·H₂O suspended in CH₂Cl₂ was added. Additionally Na₂SO₄ were added to remove the crystal water of the sodium salt. The resulting mixture was stirred for 3 days at RT. The precipitated alkaline halide was filtered off and then washed halide free (AgNO₃ test). After filtration of the solution over a column filled with neutral or acidic Al₂O₃ and active charcoal the residual organic phase was freed from solvent and dried under high vacuum for 1-2 days at 80-90°C.

[C₄mim][ClO₄]: ¹H-NMR (300 MHz, DMSO-d₆): δ = 0.86 (t, 3H); 1.24 (hex, 2H); 1.76 (pen, 2H); 3.84 (s, 3H); 4.14 (t, 2H); 7.61 (d, 2H); 8.99 (s, 1H)

¹³C-NMR (300 MHz, DMSO-d₆): δ = 12.5 (s); 18.1 (s); 30.6 (s); 35.0 (s); 47.9 (s); 121.5 (s); 122.8 (s); 135.7 (s)

2.3.12 General synthesis procedure for tetrahalogenomanganate ionic liquids

According to $2 \text{ RmimX} + \text{MnX}_2 \rightarrow [\text{Rmim}]_2[\text{MnX}_4]$ (R = alkyl, X = Cl, Br) equimolar amounts of the respective dry 1-alkyl-3-methylimidazolium halide and MnX₂ were placed in a SCHLENK tube and heated to 80°C. After completion of the reaction which can be traced visibly by the complete dissolution of MnX₂ the product was kept at 90°C under reduced pressure for 1d. In all cases the yields of the yellow-green to brownish ionic liquids were quantitative. The liquid products were washed several times with isopropanol to remove unreacted starting materials. Alternatively, the reaction can be driven in anhydrous methanol or isopropanol followed by crystallization of the products by after removal of the solvent. For purification the halide compounds were washed several times with isopropanol and recrystallized several times from a methanol/isopropanol (1:0.5-1) mixture.

[C₂mim]₂[MnCl₄] calc. N 13.37%, C 34.39%, H 5.29%; found N 13.34%, C 34.26%, H 5.49%.

[C₃mim]₂[MnCl₄] calc. N 12.59%, C 37.75%, H 5.89%; found N 12.48%, C 37.67%, H 6.20%.

[C₄mim]₂[MnCl₄] calc. N 11.79%, C 40.44%, H 6.36%; found N 11.63%, C 40.36%, H 6.37%.

[C₆mim]₂[MnCl₄] calc. N 10.55%, C 45.21%, H 7.21%; found N 10.25%, C 44.71%, H 7.77%.

[C₂mim]₂[MnBr₄] calc. N 9.39%, C 24.15%, H 3.72%; found N 9.45%, C 24.51%, H 3.48%.

[C₃mim]₂[MnBr₄] calc. N 8.97%, C 26.91%, H 4.19%; found N 8.94%, C 26.90%, H 4.30%.

[C₄mim]₂[MnBr₄] calc. N 8.63%, C 29.59%, H 4.66%; found N 8.65%, C 29.71%, H 4.70%.

2.3.13 General synthesis procedure for tris(bis(trifluoromethanesulfonyl)amide)manganate(II) ionic liquids

According to $RmimNTf_2 + Mn(NTf_2)_2 \rightarrow [Rmim][Mn(NTf_2)_3]$ (R = alkyl) the respective 1-alkyl-3-methylimidazolium bis(trifluoromethanesulfonyl)amide ionic liquid was placed in a SCHLENK tube and anhydrous Mn(NTf₂)₂ was added. The mixture was then dissolved in anhydrous acetonitrile and stirred for 1-2 days at 60°C. After completion of the reaction the solvent was removed and the product dried under reduced pressure for 2 days at 80°C. In all cases the yield of the product was quantitative.

[C₂mim][Mn(NTf₂)₃] calc. N 6.96%, C 14.32%, H 1.10%, S 19.10%; found N 7.00%, C 14.67%, H 1.30%, S 18.54%.

IC (halides): 119.6 ppm

[C₃mim][Mn(NTf₂)₃] calc. N 6.86%, C 15.30%, H 1.28%, S 18.85%; found N 6.88%, C 15.21%, H 1.16%.

IC (halides): 110.6 ppm

[C₄mim][Mn(NTf₂)₃] calc. N 6.77%, C 16.25%, H 1.46%, S 18.56%; found N 5.23%, C 16.85%, H 2.90%, S 18.36%.

IC (halides): 126.4 ppm

[C₆mim][Mn(NTf₂)₃] calc. N 6.59%, C 18.08%, H 1.80%, S 18.11%; found N 6.70%, C 17.88%, H 2.82%, S 17.35%.

IC (halides): 113.3 ppm

2.3.14 Synthesis of bistrifluoromethanesulfonic acid

HNTf₂ was synthesized by sublimation from a solution of LiNTf₂ in an excess sulfuric acid. The reaction mixture was stirred for two days at 80-100°C. This procedure was once repeated to obtain a colourless product which crystallized upon cooling in yields of about 90%.

¹H-NMR (300 MHz, D₂O): δ = 4.77 (s, 1H)

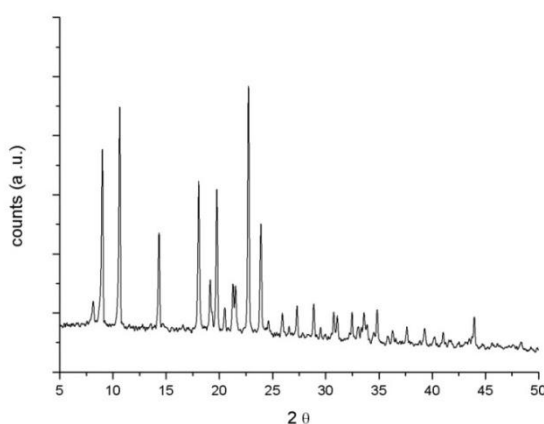
¹⁹F-NMR (300 MHz, D₂O): δ = -79.16 (s, 6F)

¹³C{¹⁹F}-NMR (300 MHz, D₂O): δ = 19.27 (s, 2C)

2.3.15 Synthesis of Mn(NTf₂)₂

MnCO₃ was suspended in deionized water and the at least two- or threefold molar amount of HNTf₂ in aqueous solution was added dropwise. After stirring for 2 hours at 60°C the unreacted material was filtered off and water was boiled off until a solid appeared. This solid compound was transferred into a SCHLENK tube and dried at 140-160°C under high vacuum, then sublimed under high vacuum at 270°C over night.

Elemental analysis calc. N 4.55%, C 7.80%, H 0.00%, S 20.81%; found N 7.78%, C 7.78%, H 0.10%, S 21.40%.



2.3.16 Preparation of Mn(NTf₂)₂ doped ionic liquids

Mn(NTf₂)₂ was dissolved in an IL as 0.05 M solution by heating or irradiating with ultrasound until complete dissolution was achieved.

2.4 Conclusions

Although the estimation of the acid-base properties of ionic, liquid, non-aqueous systems still is a difficult task the concept of optical basicity was successfully transferred to determine acid-base properties of the non-aqueous ILs. $\text{Mn}(\text{NTf}_2)_2$ turned out to be suitable probe for ionic liquids. Several ILs were doped with $\text{Mn}(\text{NTf}_2)_2$ salts and the shift of the ${}^6\text{A}_1 \rightarrow {}^4\text{A}, {}^4\text{E}(\text{G})$ transition band of Mn^{2+} investigated by UV/Vis spectroscopy. In case of ionic liquid cations with no electron donor functions the solvatochromic shift turned out to be only dependent on the ionic liquid anion. The nephelauxetic parameters h calculated from the ${}^6\text{A}_1 \rightarrow {}^4\text{A}, {}^4\text{E}(\text{G})$ absorption maximum allowed to rank the most common ionic liquid anions with respect to their optical basicity. The anion donor power and the optical basicity develops according to the following row:

$\text{BF}_4 < \text{ClO}_4 < \text{NTf}_2 \sim \text{MeSO}_3 < \text{NO}_3 < \text{DCA} < \text{TFA} < \text{EtSO}_4 \sim \text{OTos} < \text{Cl} < \text{Br}$.

In summary, the described method presents a simple and quick method to estimate the electron donor power and coordinating properties of RTIL anions independent on the cation. We hope that this will lead to improve the rational design of ionic liquids for specific applications.

2.5 References

- [1] T. Welton, *Chem. Rev.* **1999**, *99*, 2071; P. Wasserscheid, W. Keim, *Angew. Chem. Int. Ed. Engl.* **2000**, *39*, 3772; T. Welton, Peter Wasserscheid, *Ionic liquids in synthesis*, VCH-Wiley, Weinheim, **2002**; K. R. Seddon, *Kinet. Katal.* **1996**, *37*, 743'; C. L. Hussey, *Adv. Molten Salt Chem.* **1983**, *5*, 185; M. J. Earle, P. B. McCormac, K. R. Seddon, *Green Chem.* **1999**, *1*, 23.
- [2] K.R. Seddon, in *The International George Papatheodorou Symposium:Proceedings*, S. Boghosian, V. Dracopoulos, C.G. Kontoyannis, G.A. Voyiatzis (Eds.), Patras, **1999**, 131.
- [3] K. R. Seddon, *J. Chem. Tech. Biotechnol.* **1997**, *68*, 351; N. V. Plechkova, K. R.Seddon, *Chem. Soc. Rev.* **2008**, *37*, 123.
- [4] Ch. Reichardt, *Pure Appl. Chem.* **2004**, *76*, 1903; Ch. Reichardt, *Solvents and Solvent Effects in Organic Chemistry* (2nd Ed.), Wiley-VCH, Weinheim, **1988**.
- [5] C.K. Ingold, *Structure and Mechanism in Organic Chemistry*, Bell, London, **1969**; E.D. Hughes, C.J. Ingold, *J. Chem. Soc.* **1953**, 244; E.D. Hughes, *Trans. Faraday Soc.* **1941**, *37*, 603; E.D. Hughes, C.K. Ingold, *Trans. Faraday Soc.* **1941**, *37*, 657; K.A. Cooper, M.L. Dhar, E.D. Hughes, C.K. Ingold, B.J. MacNulty, L.I. Woolf, *J. Chem. Soc.* **1948**, 2043.
- [6] V. Gutmann: *Coordination Chemistry in Non-Aqueous Solution*. Springer-Verlag, Wien, New York, **1968**.
- [7] Ch. Reichardt, *Solvents and Solvent Effects in Organic Chemistry* (2nd Ed.), Wiley-VCH, Weinheim, **1988**.
- [8] Ch. Reichardt, *Chem. Soc. Rev.* **1992**, *21*, 147; Ch. Reichardt, *Chem. Rev.* **1994**, *94*, 2319; E. Buncel, S. Rajagopal, *Acc. Chem. Res.* **1990**, *23*, 226; Y. Marcus, *Chem. Soc. Rev.* **1993**, *22*, 409. S. Spange, A. Reuter, W. Linert, *Langmuir.* **1998**, *14*, 3479; H. Jin, B. O'Hare, J. Dong., S. Arzhantsev, G. A. Baker, J. F. Wishart, A. J. Benesi, M. Maroncelli, *J. Phys. Chem. B* **2008**, *112*, 81.
- [9] J. F. Deye, T. A. Berger, A. G. Anderson, *Anal. Chem.* **1990**, *62*, 615; A. K. Dutta, K. Kamada, K. Ohta, *J. Photochem. Photobiol. A: Chem* **1996**, *93*, 57; M. S. Uusi-Penttilä, R. J. Richards, B. K. Torgerson, K. A. Berglund, *Ind. Eng. Chem. Res.* **1997**, *36*, 510; P. K. Kipkemboi, A. J. Easreal, *Aust. J. Chem.* **1994**, *47*, 1771.
- [10] Ch. Reichardt, *Green Chem.* **2005**, *7*, 339; L. Crowhurst, P. R. Mawdsley, J. M. Perez-Arlandis, P. A. Salter, T. Welton, *Phys. Chem. Chem. Phys.* **2003**, *5*, 2790.

- [11] R. W. Soukup, *Chemie in unserer Zeit*, **1983**, 129; J. Burgess, *Spectrochim. Acta* **1969**, 26a, 1396; A. A. Schilt, *J. Am. Chem. Soc.* **1957**, 79, 5421; S. Spange, D. Keutel, *Liebigs Ann. Chem.* **1992**, 423.
- [12] W. Linert, R. F. Jameson, A. Taha, *J. Chem. Soc. Dalton Trans.* **1993**, 1381; D. Bourdin, D. Lavabre, J. P. Béteille, G. Levy, J. C. Micheau, *Bull. Chem. Soc. Jpn.* **1990**, 63, 2985.
- [13] R.W. Taft, M.J. Kamlet, *J. Am. Chem. Soc.* **1976**, 98, 2886.
- [14] T. Welton, Peter Wasserscheid, *Ionic liquids in synthesis*, VCH-Wiley, Weinheim, **2002**.; I.-M. Herfort, H. Schneider, *Liebigs Ann. Chem.* **1991**, 27; P. Shetty, P.J. Youngberg, B.R. Kersten, C.F. Poole, *J. Chromatogr.* **1987**, 411, 61; S. K. Poole, P.H. Shetty, C.F. Poole, *Anal. Chim. Acta* **1989**, 218, 241; W.B. Harrod, N.J. Penta, *J. Phys. Org. Chem.* **1990**, 3, 534; J.L. Kaar, A.M. Jesionowski, J.A. Berberich, R. Moulton, A.J. Russel, *J. Am. Chem. Soc.* **2003**, 125, 4125; S.N.V.K. Aki, J.F. Brennecke, A. Samanta, *J. Chem. Soc. Chem. Commun.* **2001**, 413; J. G. Huddleston, G. Broker, H. Willauer, R. D. Rogers, in *Ionic Liquids – Industrial Applications for Green Chemistry*, ed. R.D. Rogers, K. Seddon, *Am. Chem. Soc. Washington DC*, **2002**; S.V. Dzyuba, R.A. Bartsch, *Tetrahedron Lett.* **2002**, 43, 4657; C. Chiappe in Ch. Reichardt, *Green Chem.* **2005**, 7, 339; K.A. Fletcher, S. Pandey, *J. Phys. Chem. B* **2003**, 107, 7340; M. Koel, *Proc. Estonian Acad. Sci. Chem.* **2005**, 54, 3; R. A. Bartsch, S.V. Dzyuba in: *Ionic Liquids as Green Solvents – Progress and Prospects*, *A. Chem. Soc., Washington*, **2003**; J.-M. Lee, S Ruckes, J. M. Prausnitz, *J. Phys. Chem. B* **2008**, 112, 1473; S. Park, R.J. Kazlauskas, *J. Org. Chem.* **2001**, 66, 8395; R. Karmakar, A. Samata, *J. Phys. Chem. A* **2002**, 106, 66, 4447; P. Wasserscheid, C.M. Gordon, C. Hilgers, M. J. Muldoon, I.R. Dunkin, *J. Chem. Soc. Chem. Commun.* **2001**, 1186; K.A. Fletcher, S. Pandey, *Appl. Spectrosc.* **2002**, 56, 1498; W. Schroth, H.-D. Schädler, J. Andersch, *Z. Chem.* **1989**, 29, 56; Y. Wu, T. Sasaki, K. Kazushi, T. Seo, K. Sakurai, *J. Phys. Chem. B* **2008**, 112, 7530.
- [15] A. Oehlke, K. Hofmann and S. Spange, *New J. Chem.* **2006**, 30, 533.
- [16] R. Lungwitz, M. Friedrich, W. Linert, S. Spange, *New J. Chem.* **2008**, 32, 1493.
- [17] A.-V. Mudring in B. Kirchner, *Topics in Current Chemistry* **2009**, 209.
- [18] H. Flood, T. Forland, *Acta Chem. Scand.* **1947**, 1, 592.
- [19] J.E. Huheey, E.A. Keiter, R.L. Keiter, *Inorganic Chemistry: Principles, of Structure and Reactivity*, 4th ed. Prentice Hall, **1997**.

- [20] J. A. Duffy, *Bonding, Energy levels & Bands in Inorganic Solids*, New York, **1990**; J. A. Duffy, *Eur. J. of Glass Sci. Tech. Part B* **2008**, *49*, 317; J. A. Duffy, *J. Phys. Chem.* **2006**, *110*, 13245; J. A. Duffy, *Compt. Ren. Chimie* **2002**, *5*, 797; J. A. Duffy, *Sol. State Ionics* **1998**, *105*, 87; J. A. Duffy, *J. Am. Cer. Soc.* **1997**, *80*, 1416; J. A. Duffy, *J. Chem. Edu.* **1996**, *73*, 1138; J. A. Duffy, *Phys. Chem. of Glasses* **1996**, *37*, 45; J. A. Duffy, *Phys. Chem. of Glasses* **1995**, *36*, 53; J. A. Duffy, *Geochim. et Cosmochim. Acta* **1993**, *57*, 3961; J. A. Duffy, *Opt. Prop. Glass* **1991**, 159; J. A. Duffy, *Phys. Chem. of Glasses* **1991**, *32*, 211; J. A. Duffy, *Phys. Chem. of Glasses* **1989**, *30*, 1; J. A. Duffy, *J. of non-cryst. solids* **1976**, *21*, 373; J. A. Duffy, *J. Phys. Chem.* **1975**, *79*, 2780; J. A. Duffy, *J. Inorg. Nucl. Chem.* **1975**, *37*, 1203.
- [21] C.K. Jørgensen, *Oxidation Numbers and Oxidation States*, Springer Verlag, Berlin, **1969**, chapter 5.
- [22] A.P.Lever, *Inorganic Electronic Spectroscopy*, Elsevier, The Netherlands, **1968**, chapter 7 &9m
- [23] Y. Tanabe, S. Sugano, *J. Phys. Soc. J.* **1954**, *9*, 766; Y. Tanabe, S. Sugano, *J. Phys. Soc. J.* **1954**, *9*, 753; Y. Tanabe, S. Sugano, *J. Phys. Soc. J.* **1954**, *9*, 753.
- [24] Steven H. Strauss. *Chem. Rev.* **1993**, *93*, 3, 927.
- [25] A. Babai, PhD Thesis, University of Cologne (Cologne), **2006**; A. Babai, A.-V. Mudring, *Eur. J. Inorg. Chem.* **2009**, submitted.
- [26] W. L. F. Armarego, C. L. L. Chai, *Purification of laboratory chemicals*, Elsevier Science, The Netherlands, **2003**.
- [27] A. Babai, A.-V. Mudring, *Chem. Mat.* **2005**, *17*, 6230.

3 Ionic liquid based LASER



3.1 Abstract

The long term photostability performances of commonly available organic dyes doped in several ILs under different atmospheric conditions were studied. The focus was laid primarily onto the well-known Rhodamine 6 G dye family. All samples exhibited extended lifetimes compared to standard alcoholic dye solutions. However, by doping dye-IL solutions additionally with unusual but potent quenchers the photostability of Rhodamine dyes was increased by orders of magnitudes. Even under ambient conditions the photostability of the dye solution was enhanced when using the secondary metabolites β -carotene. It was also found that Mn^{2+} and ascorbic acid showed excellent results and exceeded the photostabilities of common used quenchers like 2,2-bipyridin or alkyl iodides discussed throughout the literature. From photoemission and absorbance spectra no direct influence of the Mn^{2+} species can be observed leaving the emission properties of the investigated dye unchanged. Hydrophobic and thermally stable phosphonium ILs can be used to minimize contact and side reactions with water *in situ*. Photostability tests, EPR and luminescence spectroscopy gave information about the dye photodegradation and a qualitative view to the quenching mechanisms. Mn^{2+} quenches the radical species formed through photoexcitation of the dye. In quencher-free dye-IL solution generated dye radicals could be trapped over several days after exposure to light.

3.2 Introduction

Organic closed-shell chromophors, i. e. organic dyes^[1] consist of an extended π -backbone and are well-known since ancient times for colouring or marking purposes^[2] and are used today also for light emitting compounds.^[3] Their application ranges from the UV (300-400 nm) over the visible (400-800 nm) up to the NIR region (800-900 nm). For the past 40 years different dyes were derived mainly from already high absorbing chromophoric organic compounds which are also found in nature. The emission range of the chromophoric π -system can be tuned by using groups with different electronic structure. Dyes are usually dissolved in alcohols or dispersed in other solvents for further applications. However, these alcoholic dye solutions lose their optical properties after some minutes of photoexcitation with an external light source.^[4] Due to the irreversible photodegradation and the following persistent loss of the emissive properties^[5] special design with steric alkyl- or phenyl groups of the dyes was forced to enhance their photostabilities. The addition of quenching species to dye solutions was studied by several groups but with only slight advantages to the common used dye solutions.^[6]

The usage of dyes for LASER applications was independently discovered by SOROKIN and SCHÄFER in 1966 when samples of dye solution were hit accidentally by a light beam of a rubin LASER.^[1] Since then many effort were done to keep the dye solutions longer emissive. Up to date, commercially available dye LASER devices are built of a pumping system which injects the dye solution through a jet into the resonator chamber (Fig. 1).^[7]

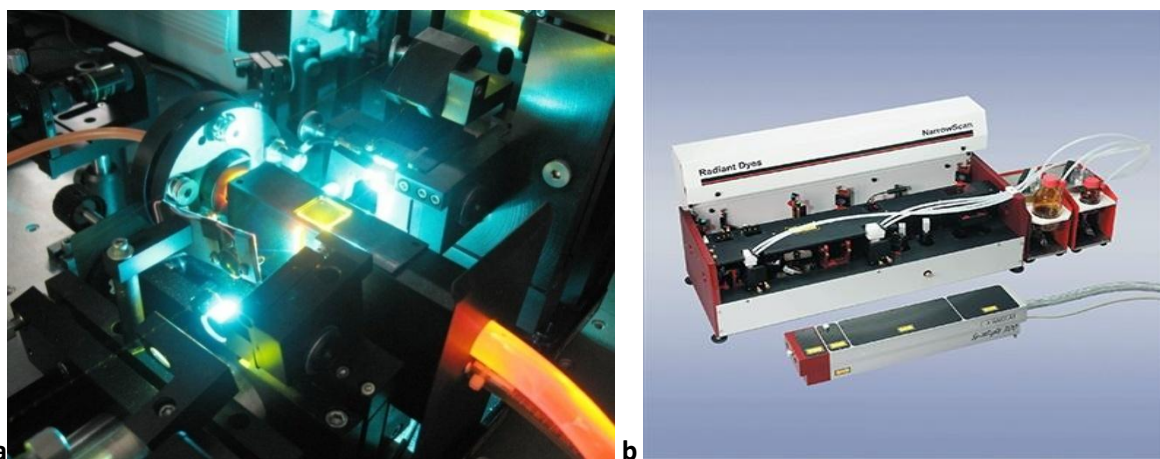
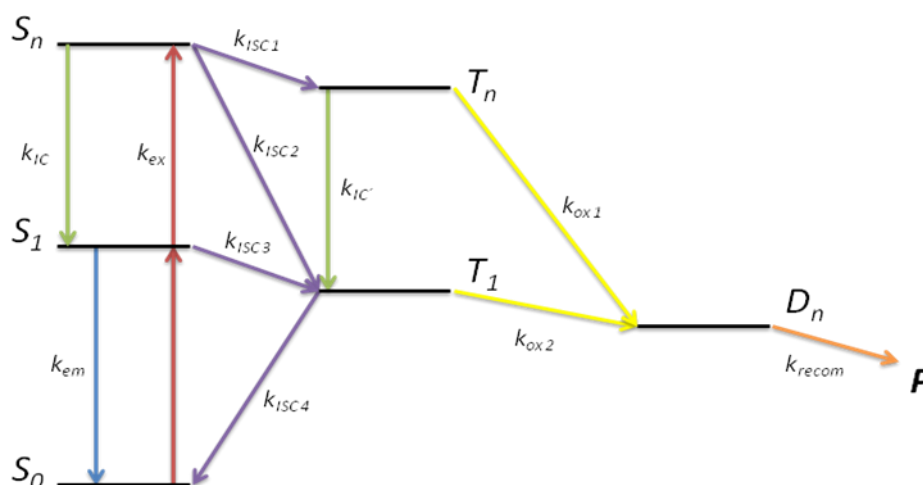


Fig. 1 a) Dye LASER resonator chamber including jet; b) common dye LASER device. On the very right the dye solution bins are seen.

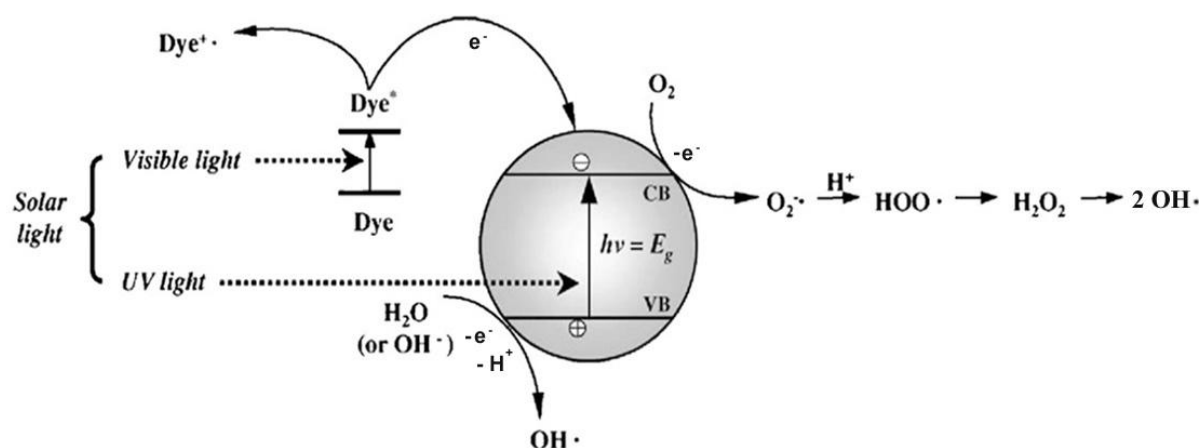
This open system has the disadvantages requiring a spacious and expensive pump system. Furthermore, the dye solution is exposed to air. Since oxygen promotes the degradation drastically the used dye solution has to be exchanged frequently.

Electrons in the *HOMO* of the organic dye are excited by light absorbance from the S_0 ground state to higher singlet states S_n ($n \in \mathbb{N}$). Relaxation via *ISC* lead to the occupation of lower triplet states T_n next to the relaxation to S_1 via *IC*. According to KASHA's rule^[8] the emission of electromagnetic waves of an excited closed shell molecule is assumed to occur only from the S_1 state. The considered initial photodegradation steps are the generation of radicals D_n - so called "dark states" - out of the electroactive triplet states (see Scheme 1).^{[9] [10]}



Scheme 1 Energy diagram of initial photoexcitation steps for a closed shell organic chromophor. After excitation from S_0 with k_{ex} to higher singlets S_n , emission from S_1 or eventually *ISC* to lower triplets T_n is achieved. The electroactive triplets T_n can undergo electron transfer k_{ox} to form D_n radical species or again undergo *ISC* to singlet states. From D_n further degradation with k_{recom} is considered ensuing in non-emissive products P .^[7, 8]

In presence of 3O_2 the dye triplet states are quenched and the spin energy is transferred resulting in excited and reactive 1O_2 species. Several mechanisms of photodegradation of dyes are discussed,^[11] e. g. for heterogenous doped systems the LANGMUIR-HINSHELWOOD or the ELEY-RIDEAL processes.^[12] In all cases initial degradation are believed to start by occasional radical generation in presence of a catalyst (Scheme 2). Electron transfer from an excited donor dye molecule occurs towards an acceptor molecule – namely water or protic solvent molecules – or other dye molecules. The reduced species start the arbitrary radical chain reaction. The end products are assumed to be non-emissive dimers or oxidized products.^[13] Thereby the long-living triplet states are the key intermediates.^[14]



Scheme 2 Initial degradation of dyes in solution in presence of water on a TiO_2 surface (CB = conductive band; VB = valence band)(picture from ^[10]).

Additives such as transition metal salts, semiconductors or other quenchers, e. g. organic compounds enhance the photostability.^[15] The introduction of dyes into solid matrices, i. e. xerogels reduces air contact and results in easy handling of devices.^[16]

The emissivity of a fresh dye solution decreases first rapidly (blinking) to reach a steady state at which it remains constant (see Fig. 2). By successive excitation bleaching, the irreversible photodegradation starts ensuing in the total loss of any emission properties. Single-molecule spectroscopy and studies of dye molecule ensembles show that blinking arises from the population of long-living (ca. ms) “dark states” – by photoexcitation-generated radicals. The reduction of these dark states can be achieved using ROXS (reducing and oxidizing systems).^[8]

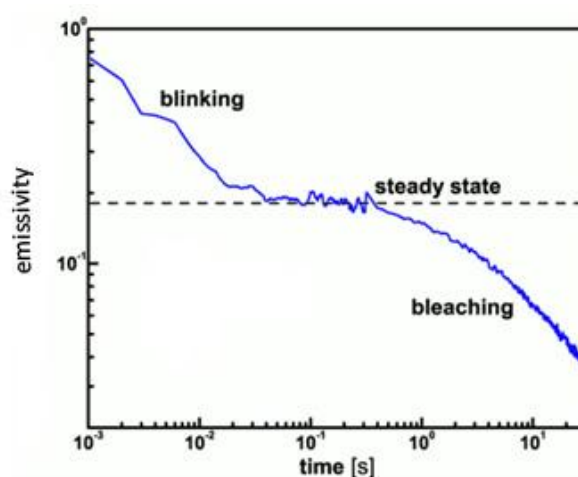


Fig. 2 Emissivity of a solid dye sample against time (doubly logarithmic scales) at RT to display photodegradation over time under LASER irradiation (picture from ^[8]).

Decrease in temperature leads directly to a decrease in bleaching processes. However, even in solid matrices tunneling processes deliver the charge to the dye at low temperatures (10 K). Diffusion in solution plays no role because oxidative photodegradation occurs only when oxygen and dye interact directly.^[5]

Concerning IL-dye solutions KAWAI et al. proved first the stabilization of Rhodamine 6 G Cl in $C_4mimNTf_2$ finding small improvement compared to alcoholic dye solutions.^[17] After two hours the emissivity of the dye solution decreased around 20%. The emission and absorption spectra of alcoholic and ionic solutions were shown to be nearly identical.

So far, photostability studies dealt only on short time scales. Most work groups concentrated on the blinking processes which are observable only for minutes or hours so that there is still much uncertainty about long term behaviour of dyes.^[18] The present work shows on a qualitative scale the improvement of dye photostability by dissolution in ILs which is focusing on Rhodamine 6 G dyes. Additionally several tailor-made and natural quenchers were tested on their impact on the dye photostability.

3.3 Results and discussion

3.3.1 Photostability performances

A variety of dyes were doped into several ILs eventually with or without a quencher. Table 1-2 compile the recorded emissivities of these samples including the reference system ethanol/Rhodamine 6 G Cl. Samples doped with quenchers exhibit extended photostabilities compared to undoped dye solutions. In order to reduce contact to water, to have an optically pure compound and to have a large thermal stability hydrophobic tetraalkylphosphonium ILs were chosen for further investigations.

The photostability is changing dramatically depending on the atmospheric conditions like air, N_2 , Ar or vacuum (see Fig. 3). Ar-flushed and evaporated samples exhibit similar photostabilities while nitrogen containing samples show bleaching after 50 h of constant photoexcitation. Even dry methanolic dye solutions under vacuum appear to emit much longer than common commercially available alcoholic dye solutions. Air containing IL-dye solutions decrease their emissivities shortly after starting of the photoexcitation.

In all photostability tests the emissivity decrease in the first hours of excitation period. Successive excitation results then in increasing emissivities. According to the previous discussed phenomena of the *dark states*, the initial decrease in emissivity points to the generation of non-

emissive excited products. The relaxation of these species over time enhances the emissivity due to reformation of emissive species (see Fig. 3 enlarged sections of the diagrams). The stabilization of dyes in ILs compared to alcoholic dye solutions under the same ambient conditions may be attributed to their high electrochemical stabilities and high viscosities.^[19] Diffusion of excited dye molecules is suppressed in ILs due to the high viscosity compared to common organic solvents.

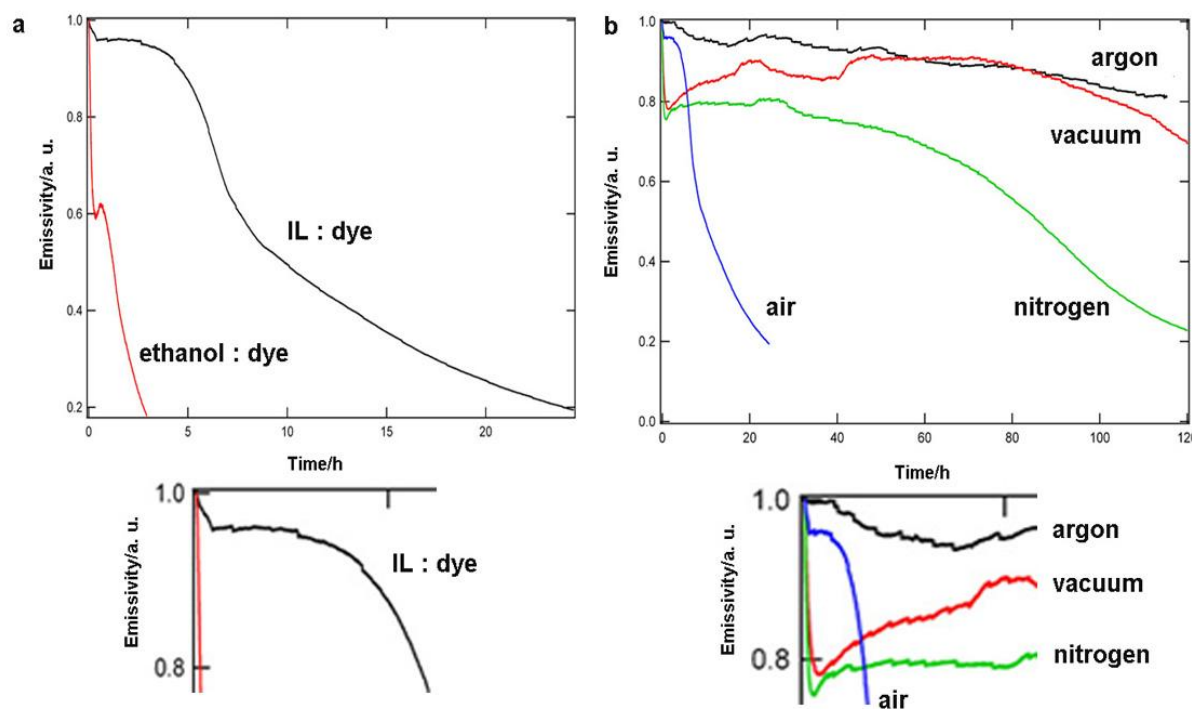


Fig. 3 Photostability of a) $P_{66614}NTf_2/Rhodamine\ 6\ G\ ClO_4$ (black) and ethanol/Rhodamine 6 G ClO_4 (red) in air b) $P_{66614}NTf_2/Rhodamine\ 6\ G\ ClO_4$ in air (blue); N_2 (green); vacuum (red) and Ar (black) (data compiled and provided by Dipl.-Ing. (FH) J. KRAUSE).

The photostability of the dyes in ILs can be further improved by orders of magnitudes by simple doping the dye-solutions with suitable quenchers. Especially Mn^{2+} , ascorbic acid and secondary metabolites like β -carotene under vacuum or inert gas atmosphere turn out to be promising quenchers.^[20] Surprisingly also under air conditions the emissivity can be enhanced up by factors using ILs doped with β -carotene.

The initial decrease of the emissivity like in the undoped samples is also observed in the Mn^{2+} -doped samples (see Fig. 4). Different Mn^{2+} -doped ILs show different photostabilities. In Fig. 4 the highest photostability is obtained with the $P_{66614}NTf_2$ -IL. The cation and the anion nature seem to have a certain impact on the dye stabilization. Due to the long term photostability of $P_{66614}NTf_2/Rhodamine\ 6\ G\ ClO_4/Mn(NTf_2)_2$ the 50% emissivity threshold has to be estimated to be ca. 65 years. This is an improvement to alcoholic dye solutions of a factor of 1,500. In concentration

studies it is carried out that the dye to Mn^{2+} ratio fits best to 1 : 4 of dye to Mn^{2+} . Other Mn^{2+} to dye ratios resulted in lower photostabilities (see table 1).

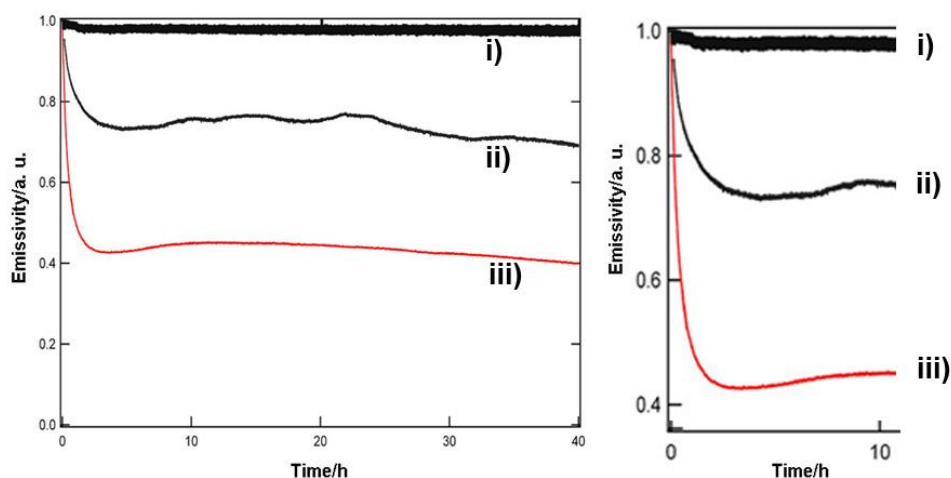


Fig. 4 Photostability of i) $\text{P}_{66614}\text{NTf}_2/\text{Rhodamine 6 G ClO}_4/\text{Mn}(\text{NTf}_2)_2$, ii) $\text{C}_4\text{C}_1\text{mimNTf}_2/\text{Rhodamine 6 G ClO}_4/\text{Mn}(\text{NTf}_2)_2$ and iii) $\text{C}_4\text{mpyrFAP}/\text{Rhodamine 6 G ClO}_4/\text{Mn}(\text{NTf}_2)_2$ (data compiled and provided by Dipl.-Ing. (FH) J. KRAUSE).

The role of the additive Mn^{2+} can be ascribed to the removing of traces of oxygen left in the IL. Hereby residual oxygen oxidizes Mn^{2+} to Mn^{4+} in presence of halides and oxygen which can be traced visibly by the precipitation of a green-brownish solid in $\text{P}_{66614}\text{NTf}_2/\text{Rhodamine 6 G Cl}/\text{Mn}(\text{NTf}_2)_2$ samples. In electrochemistry this reaction is referred as the key step of the WINKLER method for the determination of oxygen in solution.^[21] By exchanging the anion of the Rhodamine dye with ClO_4 the precipitation of the solid is suppressed. High order atoms are known for the heavy atom effect.^[22] This effect may be also involved to quench the triplet states of the excited dye molecules.^{[15] [23]}

β -carotene was chosen as *green* quencher for further investigations. From Fig. 5 different β -carotene concentration samples exhibit dramatic changes in their photostabilities. At low β -carotene concentrations the emissivity falls first and rises afterwards. Lower dye to β -carotene ratios are favoured over high β -carotene concentrations (see Fig. 5). Even in air this system shows a high photostability compared to the air open alcoholic dye solution (see table 2). In air-open systems the loss of the dye luminescence performance results from the constant dissolution of oxygen into the IL degrading the dye faster than β -carotene relax the triplet energy. The 1 : 1 dye to β -carotene sample and the N_2 -flushed sample (dye to β -carotene is 10 : 1) increase their emissivities directly after exposure to exciting light beam but decreases after three hours and constantly loses their emissivities.

To monitor the influence of radicals to the photostability of β -carotene doped IL-dye samples a common organic radical starter was introduced. Co-doping the 10 : 1 (dye to β -carotene) $P_{666\ 14}NTf_2/Rhodamine\ 6\ G\ ClO_4$ sample with the radical starter NCS results in initial emissivity decrease followed by high emissivity like in the case of equimolar and the N_2 -flushed sample (dye to β -carotene is 10 : 1). Afterwards the emissivity decreases and reaches a steady-state (see Fig. 5).

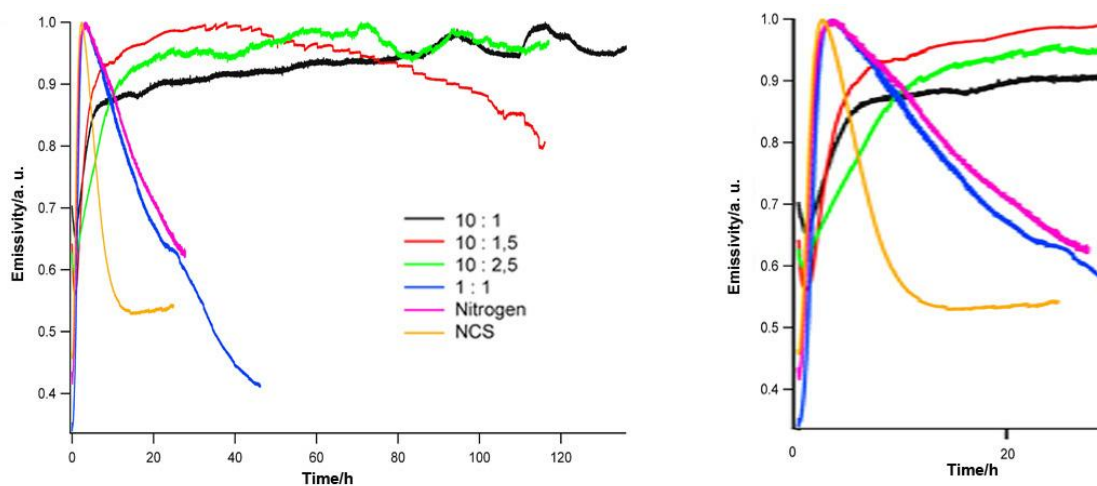


Fig. 5 Photostability of $P_{666\ 14}NTf_2/Rhodamine\ 6\ G\ ClO_4$ doped with β -carotene; dye to β -carotene ratio 10 : 1 (black), 10 : 1.5 (red), 10 : 2.5 (green), 1 : 1 (blue) under vacuum conditions; 10 : 1 (magenta) in N_2 ; 10 : 1 co-doped with NCS under vacuum (data compiled and provided by Dipl.-Ing. (FH) J. KRAUSE).

The secondary metabolite β -carotene converts nearly 100% of any triplet species of the cytochroms found in plant cells and protects the chromophoric chlorophyll group from reactive singlet oxygen.^[24] Triplet energy is thereby dissipated by β -carotene via vibronic relaxation of the floppy π -backbone. Thus the excited dye molecules are assumed to transfer energy of their triplet states via FRET (FÖRSTER resonance energy transfer) or a DEXTER-like dipole-dipole energy transfer to the β -carotene.^[25] The behaviour in case of the NCS co-doped sample remains unclear. NCS forms by heating radicals which react arbitrary in solution. In the present case the emissivity of the sample reaches a steady state. The initialized radicals could react with the *dark states* to form nonreactive products.

Ascorbic acid is already known to be an antioxidizing agent in nature^[26] – it readily reduces oxygen to water *in vivo*. The ascorbic acid saturated $P_{666\ 14}NTf_2/Rhodamine\ 6\ G\ ClO_4$ dye solution under vacuum exhibits the best photostability performance of all samples without any loss of luminescence performance of the dye tending that traces of oxygen are still left in the IL and cannot be removed by evaporation alone (see Fig. 6).^[27]

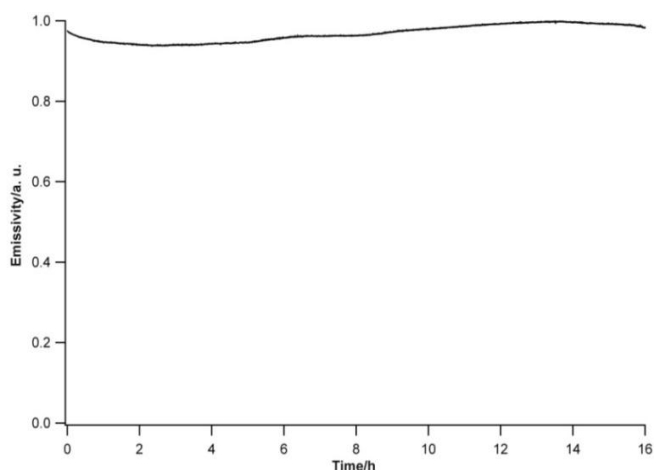


Fig. 6 Photostability of $P_{66614}NTf_2/Rhodamine\ 6\ G\ ClO_4$ saturated with ascorbic acid (data compiled and provided by Dipl.-Ing. (FH) J. KRAUSE).

Ionogels containing $P_{66614}NTf_2/Rhodamine\ 6\ G\ ClO_4$ were produced to incorporate dyes into solid ionic liquid matrices according to BINNEMANS.^[28] Next to the difficulty to establish dense and homogenous samples the dye-doped, ionogels offer only four hours to reach 50% initial emissivity (see table 2, Fig. 7). The dye-doped ionogels were prepared under air conditions and treatment with an ultra sonic bath to establish gelation. Because of the constant diffusion of oxygen into the mixture while gelation the degradation takes place in the solid state.

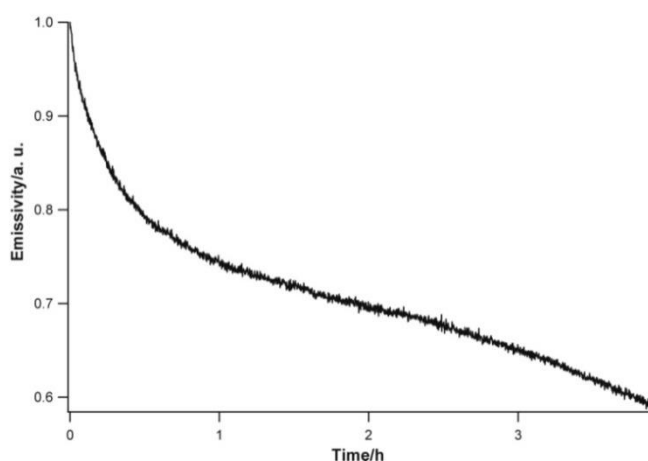


Fig. 7 Photostability of Ionogel with $P_{66614}NTf_2/Rhodamine\ 6\ G\ ClO_4$ (data compiled and provided by Dipl.-Ing. (FH) J. KRAUSE).

Coumarine 6 in P_{66614} IL exceeds the photostability of the respective alcoholic solution but do not reach the Rhodamine 6 G performance in ILs (see Fig. 8). After 20 hours of excitation the 50% initial emissivity threshold is reached. Because Coumarine 6 is hardly soluble in $P_{66614}NTf_2$, it was dissolved in the more hydrophilic and more viscous $P_{66614}OTf$. Indeed the photostability is slightly improved in $P_{66614}OTf$. Thus considerations about the dye-solvent interaction take the solubility and the viscosity

of the matrix into account. In general, Coumarine dyes are well-known to undergo faster and more readily photodegradation than Rhodamine dyes.

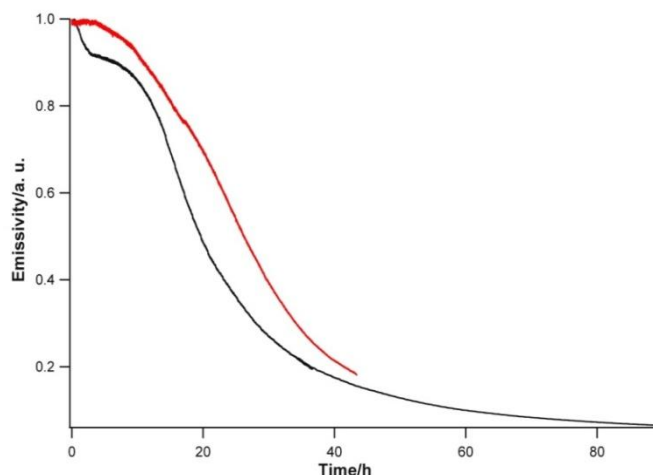


Fig. 8 Photostability of P₆₆₆₁₄NTf₂/Coumarine 6 (black) and P₆₆₆₁₄OTf/Coumarine 6 (red) under vacuum conditions (data compiled and provided by Dipl.-Ing. (FH) J. KRAUSE).

Since halides can still interact with the dye, their exchange to electrochemically stable WCAs should increase dye photochemical stability. By simple anion metathesis the chloride of Rhodamine 6 G Cl was exchanged by the NTF₂ anion. P₆₆₆₁₄NTf₂/Rhodamine 6 G NTF₂ exhibits under vacuum a highly stable dye system (table 2). The melting point of the dye is also decreased about 100°C (Fig. 9) with the tendency of strong undercooling.² The photostability data show that the anion has a certain influence on the thermal and photostability properties which takes consideration of anion effects to the degradation steps because of redox stability into account.

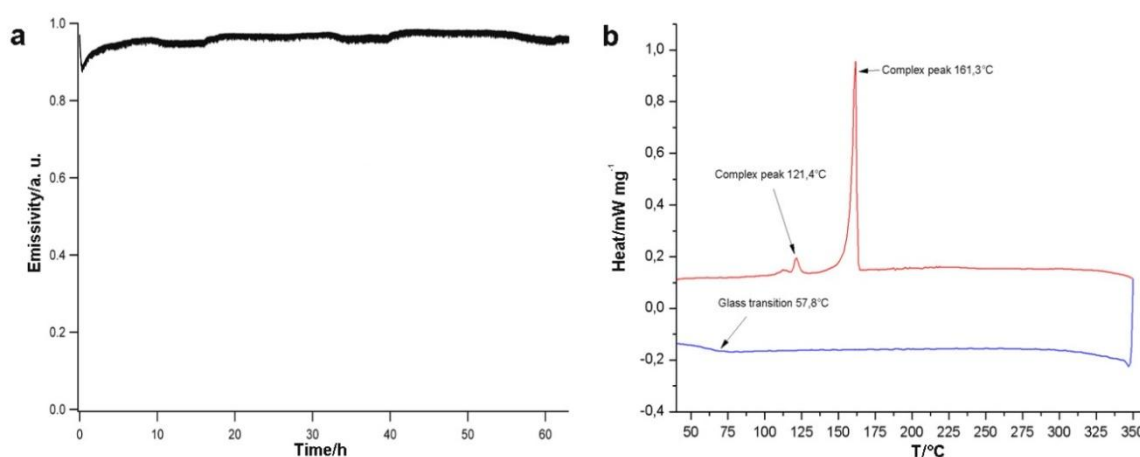


Fig. 9 a) Photostability data of P₆₆₆₁₄NTf₂/Rhodamine 6 G NTF₂ (data compiled and provided by Dipl.-Ing. (FH) J. KRAUSE) and b) DSC thermogram of synthesized Rhodamine 6 G NTF₂.

² Rhodamine 6 G ClO₄, m. p. 263-265°C

Table 1 Compiled data of the photostability performances of the different ILs doped with several quenchers at different conditions (DPSS pumped Ar-LASER, 500-1000 mW; al = all line; optical pumping using all wavelengths; data compiled and provided by Dipl.-Ing. (FH) J. KRAUSE). The irradiation was proceeded until 50% of initial emissivity was reached (otherwise stated).

	LASER pump wavelength/ nm	exciting intensity/ mW	recorded emission wavelength/ nm	vacuum	total irradiation time/h	down to 50% emissivity time/h	sample volume/ ml
MeOH							
2·10⁻⁶ M Rhodamine 6 G	al	500	570	n	2.916	1.21	0.2
	al	500	570	n	1.063	to 71%	0.1
	al	1000	550	n	3.722	2.20	0.2
	480	480	550	n	1.861	1.07	0.2
	476	500	550	n	1.861	0.71	0.1
8·10⁻⁶ M Mn(NTf₂)₂ 2·10⁻⁶ M Rhodamine 6 G	al	500	570	n	14.174	to 37%	0.2
	al	1000	570	n	1.593	to 68%	0.2
	al	2500	550	n	1.487	increasing	0.2
	514	470	550	n	1.861	to 90%	0.2
	514	550	550	n	1.591	to 67%	0.2
8·10⁻⁶ M Mn(NTf₂)₂ 2·10⁻⁶ M Rhodamine 6 G	al	500	570	n	1.861	1.35	0.2
	EtOH						
2·10⁻⁶ M Rhodamine 6 G ClO₄	488	500	570	n	2.900		0.2
C₂mimNTf₂							
2·10⁻⁶ M Rhodamine 6 G	476	500	566	n	1.861	to 79%	0.2
	514	470	550	n	1.861	0.79	0.2
8·10⁻⁶ M Mn(NTf₂)₂ 2·10⁻⁶ M Rhodamine 6 G	al	500	550	y	18.611	7.67	0.2
	al	500	570	n	0.869	0.37	0.2
8·10⁻⁶ M Mn(NTf₂)₂ 1·10⁻⁶ M Rhodamine 6 G	al	500	570	n	2.732	0.01	0.2
6·10⁻⁵ M Mn(NTf₂)₂ 2·10⁻⁶ M Rhodamine 6 G	al	500	570	n	0.808	0.51	0.2

Table 1(continue) Compiled data of the photostability performances of the different ILs doped with several quenchers at different conditions (DPSS pumped Ar-LASER, 500-1000 mW; al = all line; optical pumping using all wavelengths; data compiled and provided by Dipl.-Ing. (FH) J. KRAUSE). The irradiation was proceed until 50% of initial emissivity was reached (otherwise stated).

	LASER pump wavelength/ nm	exciting intensity/ mW	recorded emission wavelength/ nm	vacuum	total irradiation time/h	down to 50% emissivity time/h	sample volume/ ml
C₄C₁mimPF₆							
2·10⁻⁶ M Rhodamine 6 G	532	500	550	y	1.861	to 89%	0.2
	532	500	550	y	28.343	15.03	0.2
8·10⁻⁶ M Mn(NTf₂)₂ 2·10⁻⁶ M Rhodamine 6 G	al	500	550	n	1.861	to 81%	0.2
	al	500	570	n	1.076	to 63%	0.2
	al	500	550	n	2.561	to 51%	0.2
	al	500	550	y	46.565	to 43%	0.2
	al	500	550	y	41.367	16.31	0.2
P_{666 14}NTf₂							
8·10⁻⁶ M Mn(NTf₂)₂ 2·10⁻⁶ M Rhodamine 6 G ClO₄	532	500	550	y	69.723	to 82%	0.2
	532	500	620	y	93.843	73.58	0.2
2·10⁻⁷ M β-carotene 2·10⁻⁶ M Rhodamine 6 G ClO₄	al	350	550	y	91.650	to 61%	0.1
	532	500	550	n	140.769	to 60%	0.2
8·10⁻⁶ M Mn(NTf₂)₂ 2·10⁻⁶ M Rhodamine 6 G ClO₄	al	500	570	n	1.861	0.77	0.2
	al	500	550	y	18.611		0.2
	al	500	550	y	70.713	to 74%	0.2
	al	500	550	y	1.470		0.2
	al	500	550	y	19.754	to 88%	0.2
	532	500	550	y	65.405	stable	0.2
8·10⁻⁶ M Mn(NTf₂)₂ 8·10⁻⁶ M Tb(OTf)₃ 2·10⁻⁶ M Rhodamine 6 G	532	500	550	y	153.285	to 78%	0.2
	488	500	550	y	161.000	stable	0.1

Table 1(continue) Compiled data of the photostability performances of the different ILs doped with several quenchers at different conditions (DPSS pumped Ar-LASER, 500-1000 mW; al = all line; optical pumping using all wavelengths; data compiled and provided by Dipl.-Ing. (FH) J. KRAUSE). The irradiation was proceed until 50% of initial emissivity was reached (otherwise stated).

	LASER pump wavelength/ nm	exciting intensity/ mW	recorded emission wavelength/ nm	vacuum	total irradiation time/h	down to 50% emissivity time/h	sample volume/ ml
C₂mimEtSO₄							
8·10 ⁻⁶ M Mn(NTf ₂) ₂ 2·10 ⁻⁶ M Rhodamine 6 G	al	500	550	y	1.861	increasing	0.2
	al	500	550	y	22.093	to 66%	0.2
N₁₄₄₄NTf₂							
8·10 ⁻⁶ M Mn(NTf ₂) ₂ 2·10 ⁻⁶ M Rhodamine 6 G	al	500	550	n	1.861	0.65	0.2

Table 2 Compiled data of the photostability performances of the different ILs doped with several quenchers at different conditions (DPSS pumped Ar-LASER, 500-1000 mW; al = all line; optical pumping using all wavelengths; data compiled and provided by Dipl.-Ing. (FH) J. KRAUSE).

	LASER pump wavelength/ nm	exciting intensity/ mW	recorded emission wave-length/ nm	total irradiation time/h	sample volume/ ml	vacuum
P₆₆₆₁₄NTf₂						
8·10 ⁻⁶ M Mn(NTf ₂) ₂ 2·10 ⁻⁶ M Rhodamine 6 G ClO ₄	488	500	550	93.1	0.1	y
2·10 ⁻⁶ M Rhodamine 6 G ClO ₄ 6·10 ⁻⁵ M ascorbic acid	488	500	550	16.2	0.1	y
2·10 ⁻⁶ M Rhodamine 6 G NTf ₂	488	500	550	63.4	0.1	y
P₆₆₆₁₄OTf						
2·10 ⁻⁶ M Coumarine 6	488	500	550	43.4	0.1	y

Table 2 (continue) Compiled data of the photostability performances of the different ILs doped with several quenchers at different conditions (DPSS pumped Ar-LASER, 500-1000 mW; al = all line; optical pumping using all wavelengths; data compiled and provided by Dipl.-Ing. (FH) J. KRAUSE).

	LASER pump wavelength/ nm	exciting intensity/ mW	recorded emission wave-length/ nm	total irradiation time/h	sample volume/ ml	vacuum
C₄C₁minNTf₂/						
Mn(NTf ₂) ₂ 2·10 ⁻⁶ M Rhodamine 6 G ClO ₄	488	500	550	40.2	0.1	y
C₄mpyrFAP						
8·10 ⁻⁶ M Mn(NTf ₂) ₂ 2·10 ⁻⁶ M Rhodamine 6 G ClO ₄	488	500	550	40.2	0.1	y
Ionogel						
2·10 ⁻⁶ M Rhodamine 6 G ClO ₄	488	500	550	3.9	0.1	n
P₆₆₆₁₄NTf₂						
2·10 ⁻⁶ M Rhodamine 6 G ClO ₄ (vacuum)	488	500	550	161.0	0.1	y
2·10 ⁻⁶ M Rhodamine 6 G ClO ₄ (Ar)	488	500	550	115.3	0.1	n
2·10 ⁻⁶ M Rhodamine 6 G ClO ₄ (N ₂)	488	500	550	139.0	0.1	n
2·10 ⁻⁶ M Rhodamine 6 G ClO ₄ / 2·10 ⁻⁷ M β-carotene (10 : 1)	488	500	550	136.0	0.1	y
2·10 ⁻⁶ M Rhodamine 6 G ClO ₄ / 3·10 ⁻⁷ M β-carotene (10 : 1.5)	488	500	550	116.1	0.1	y
2·10 ⁻⁶ M Rhodamine 6 G ClO ₄ / 4.5·10 ⁻⁷ M β-carotene (10 : 2.5)	488	500	550	117.0	0.1	y
2·10 ⁻⁶ M Rhodamine 6 G ClO ₄ / 2·10 ⁻⁶ M β-carotene (1 : 1)	488	500	550	46.2	0.1	y
2·10 ⁻⁶ M Rhodamine 6 G ClO ₄ / 4.5·10 ⁻⁷ M β-carotene (N ₂)	488	500	550	25.0	0.1	n
2·10 ⁻⁶ M Coumarine 6	488	500	550	90.0	0.1	y

3.3.2 Absorption and luminescence studies

The emission maximum of Rhodamine 6 G depends on the matrix, i. e. in methanol/Rhodamine 6 G ClO_4 and $\text{P}_{666.14}\text{NTf}_2$ /Rhodamine 6 G NTf_2 emission maxima are at 575 nm compared to $\text{P}_{666.14}\text{NTf}_2$ /Rhodamine 6 G Cl ($\lambda_{\text{em}} = 557 \text{ nm}$) and $\text{P}_{666.14}\text{NTf}_2$ /Rhodamine 6 G ClO_4 / β -carotene ($\lambda_{\text{em}} = 568 \text{ nm}$) respectively. However, the emission properties are influenced by the anion nature of the Rhodamine counterion which is in coincidence with recent results.^[29] In the β -carotene co-doped sample the dye emission maximum shifts bathochromic (see Fig. 10).

In Fig. 11 absorption and fluorescence emission spectra of Mn^{2+} doped IL-dye samples are displayed. The overlaid spectra appear in high coincidence presenting identical emission properties for all Mn^{2+} concentrations ($\lambda_{\text{em}} = 577 \text{ nm}$) and are in very good agreement with the emission maximum of $\text{P}_{666.14}\text{NTf}_2$ /Rhodamine 6 G ClO_4 solution ($\lambda_{\text{em}} = 577 \text{ nm}$). From recent studies Mn^{2+} is known to be octahedrally coordinated in NTf_2 -ILs. Its ${}^6\text{A}_{1g} \rightarrow {}^4\text{A}_g, {}^4\text{E}_g(\text{G})$ transition band is located at 352 nm and superposes an absorption band of the dye. The dye absorption maximum reveals unperturbed at 528 nm as well as the emission maximum at 577 nm.

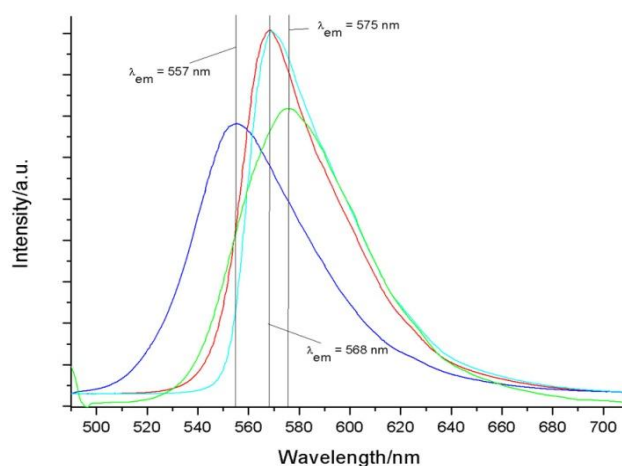


Fig. 10 Comparison of emission maxima of $\text{P}_{666.14}\text{NTf}_2$ doped with Rhodamine 6 G Cl (blue), β -carotene (green), Rhodamine 6 G NTf_2 (red) and $\text{MeOH}/\text{Rhodamine 6 G ClO}_4$ (cyan)(data compiled and provided by Dipl.-Ing. (FH) J. KRAUSE).

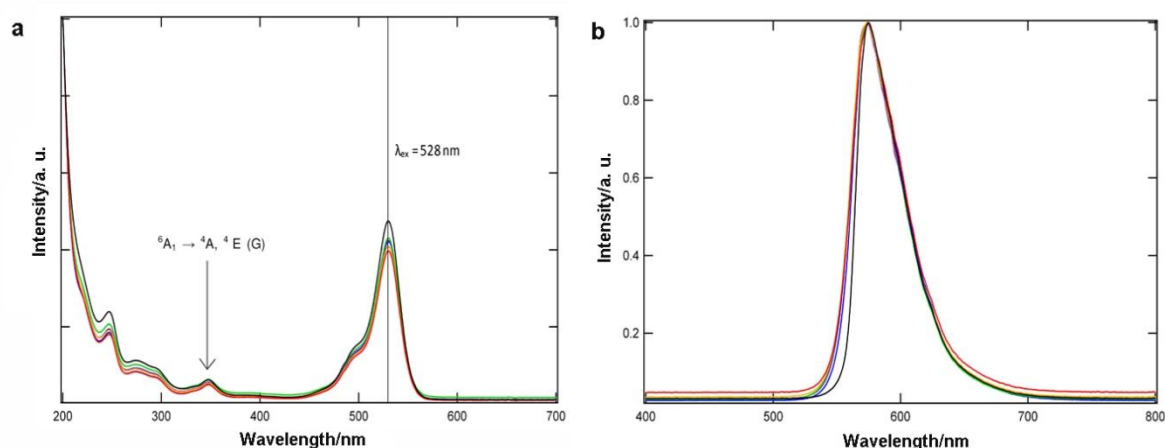


Fig. 11 Comparison of a) absorption spectra (depicted are the ${}^6A_{1g} \rightarrow {}^4A_g, {}^4E_g(G)$ transition band of Mn^{2+} and the absorption maximum at 528 nm) and b) emission spectra of $P_{66614}NTf_2/Rhodamine\ 6\ G\ ClO_4$ doped with different concentrations of $Mn(NTf_2)_2$; undoped (black), 1 : 1.5 (green), 1 : 3 (purple), 1 : 3.2 (blue), 1 : 4 (orange) and 1 : 6 (red)(data compiled and provided by Dipl.-Ing. (FH) J. KRAUSE).

3.3.3 EPR investigations

The present EPR investigations are focused on the Rhodamine 6 G dyes and also their interaction with Mn^{2+} . In the magnetic field the Mn^{2+} ($I = 5/2$)^[30]-EPR signal splits into a single hexet with the common hyperfine splitting of 92-96 G.^[31] It holds also for common organic solvents like CH_2Cl_2 which can be seen in Fig. 12. A further splitting can also be observed with $J = 24-29$ G (Fig. 11c-e) at RT, 110 K and down to 5 K. Apparently further splitting could thus originate from the proximity to another EPR active nucleus. In highly concentrated samples HEISENBERG exchange^[32] leads to the collapse of the hyperfine splitting to a singlet (Fig. 12a). Table 3 deals with the collected data from the EPR spectra. All g -values are in excellent agreement with literature data. The single resonance signal – singlet or hexet – points to a spherical Mn^{2+} environment due to magnetic isotropy.^[27]

Table 3 Collected data from the EPR investigations of several Mn²⁺ doped dye solutions at different conditions. The splitting patterns are assigned to (s) singlet or (hex) hextet.

sample	<i>g</i>	J/G
Mn(NTf₂)₂	2.01086 (s)	-
P_{666 14}NTf₂/Mn(NTf₂)₂	2.01398 (hex)	93
C₁C₄mimPF₆/Rhodamine 6 G Cl/Mn(NTf₂)₂	2.02039 (hex)	92
C₁C₄mimPF₆/Rhodamine 6 G Cl/Mn(NTf₂)₂ @ 5 K	2.02846 (hex)	96
P_{666 14}NTf₂/Rhodamine 6 G Cl/Mn(NTf₂)₂	2.01625 (hex)	96
P_{666 14}NTf₂/Rhodamine 6 G Cl/Mn(NTf₂)₂ photoexcited	i) 2.01952 (hex) ii) 2.00275 (s)	93 -
N_{1 444}NTf₂/Rhodamine 6 G Cl/Mn(NTf₂)₂	2.01656 (hex)	93
P_{666 14}NTf₂/Rhodamine 6 G Cl/Mn(NTf₂)₂ @ 110 K	2.02540 (hex)	96

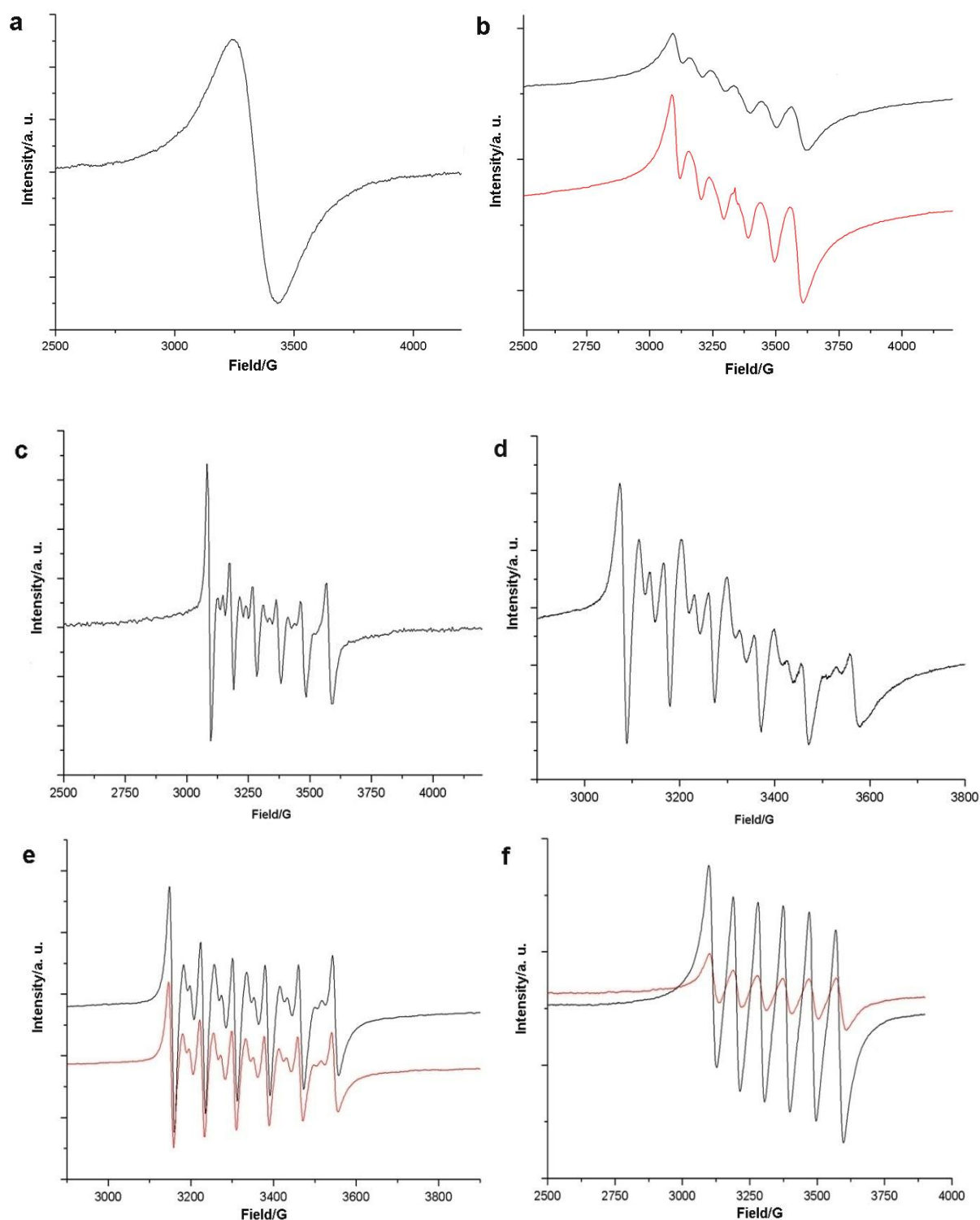


Fig. 12 EPR spectra of a) solid $\text{Mn}(\text{NTf}_2)_2$, b) $\text{P}_{66614}\text{NTf}_2/\text{Rhodamine 6 G Cl}/\text{Mn}(\text{NTf}_2)_2$ (red) and $\text{N}_{1444}\text{NTf}_2/\text{Rhodamine 6 G Cl}/\text{Mn}(\text{NTf}_2)_2$ (black), c) $\text{C}_{14}\text{mimPF}_6/\text{Rhodamine 6 G Cl}/\text{Mn}(\text{NTf}_2)_2$ (1 : 4), d) $\text{C}_{14}\text{mimPF}_6/\text{Rhodamine 6 G Cl}/\text{Mn}(\text{NTf}_2)_2$ (1 : 4) @ 5K, e) $\text{P}_{66614}\text{NTf}_2/\text{Rhodamine 6 G ClO}_4/\text{Mn}(\text{NTf}_2)_2$ @ 110 K (black) and $\text{P}_{66614}\text{NTf}_2/\text{Mn}(\text{NTf}_2)_2$ (red), f) $\text{Mn}(\text{NTf}_2)_2$ in CH_2Cl_2 @ RT (red) and @ 200 K (black).

A photodegraded $C_1C_4mimPF_6/Rhodamine\ 6\ G\ Cl/Mn(NTf_2)_2$ sample exhibits dramatical changes compared to a fresh sample (see Fig. 13). Herein a second signal overlays the Mn^{2+} hextet.^[33] Since degradation of the dye occurred prior to the EPR measurement a reaction of the dye and the Mn^{2+} could be considered. Taking into account that excited dye molecules are electroactive and can undergo redox reactions,³ Mn^{2+} could have reacted via electron transfer with the excited dye molecules.⁴ The cubic symmetry of the Mn^{2+} environment is still present in the photodegraded sample. It appears that a second species was generated and overlays the Mn^{2+} hextet (Fig. 12b).

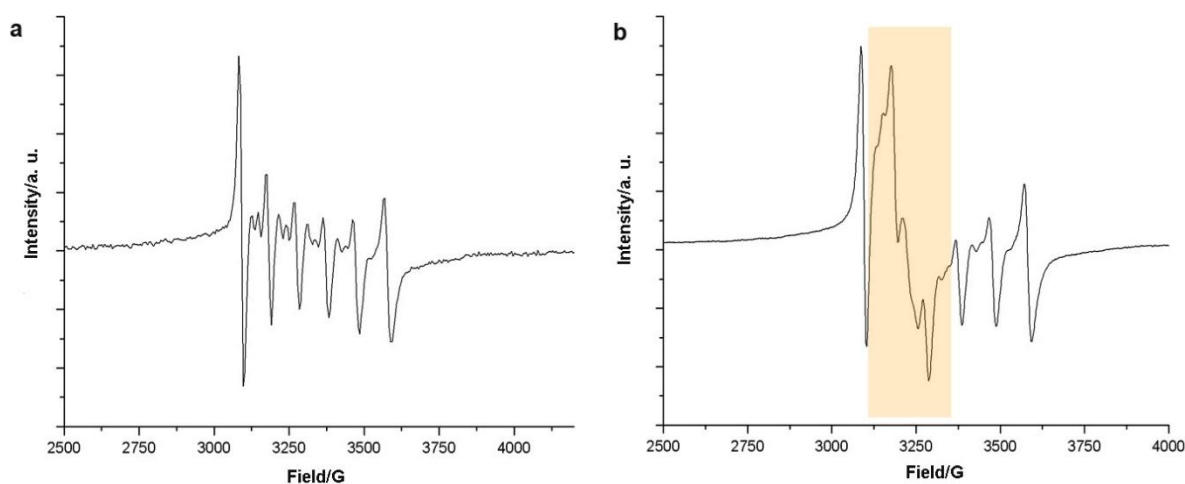


Fig. 13 EPR section of a) fresh and b) photodegraded $C_1C_4mimPF_6/Rhodamine\ 6\ G\ Cl/Mn(NTf_2)_2$ (1 : 4) at RT.

In situ EPR experiments on photoexcited (diode LASER 200 mW; $\lambda_{ex} = 532\ nm$) quencher-free dye solution samples show a singlet (see Fig. 14a). In the $P_{666\ 14}NTf_2/Rhodamine\ 6\ G\ ClO_4/Mn(NTf_2)_2$ sample a singlet is obtained by LASER irradiation with a g -value of $g = 2.0028$ (dpph $g = 2.0036$; see Fig. 14b). Before the irradiation in both samples – the Mn^{2+} -doped and the undoped $P_{666\ 14}NTf_2/Rhodamine\ 6\ G\ ClO_4$ solution – no EPR signal of any radical species with $g = 2.0028$ could be detected. The radical resonances are first obtained when the samples are irradiated by the LASER light beam.^[34] In case of the Mn^{2+} doped sample the singlet of the organic radical overlays the Mn^{2+} -hextet. By studying the relaxation of the radical with EPR technique it appears that the signal vanishes directly when the LASER light beam is shut down. In the $P_{666\ 14}NTf_2/Rhodamine\ 6\ G\ ClO_4$ solution the singlet is still traceable after exposure to exciting light beam. However, this tends to the stabilization of radical species in ILs due to their electrochemical stability.^[19] Mn^{2+} eases the spin-forbidden transitions and generates spin allowed electronic relaxation transitions in the π -backbone.^[22] The relaxation mechanism can be ascribed as a spin-lattice relaxation mechanism.^[25]

³ A greenish-brownish solid precipitated by photoexcitation in presence of halides

⁴ The same system is chemical stable for weeks if not photoexcited

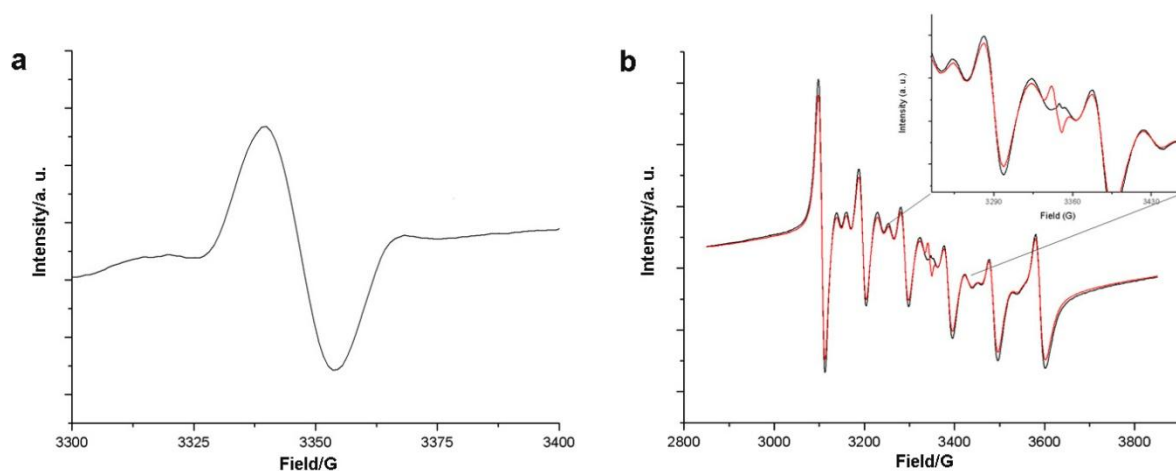


Fig. 14 EPR spectrum of a sample of Rhodamine 6 G ClO_4 doped in a) $\text{P}_{66614}\text{NTf}_2$ (smoothed results)⁵ and b) $\text{P}_{66614}\text{NTf}_2/\text{Mn}(\text{NTf}_2)_2$ excited by a LASER light beam ($\lambda = 532 \text{ nm}$).

Kinetic EPR studies of $\text{P}_{66614}\text{NTf}_2/\text{Rhodamine 6 G ClO}_4$ show that two signals are observed when irradiated by a LASER light beam (Fig. 15). Two distinct singlets are observed with similar but distinct g -values. One singlet is sharp ($g = 2.00174$) and relaxes after exposure to the LASER beam very slowly for a couple of days. In contrast the other floppy signal with not determinable g -value ($g \sim 2.0001$) disappears within several minutes after ending of the excitation.

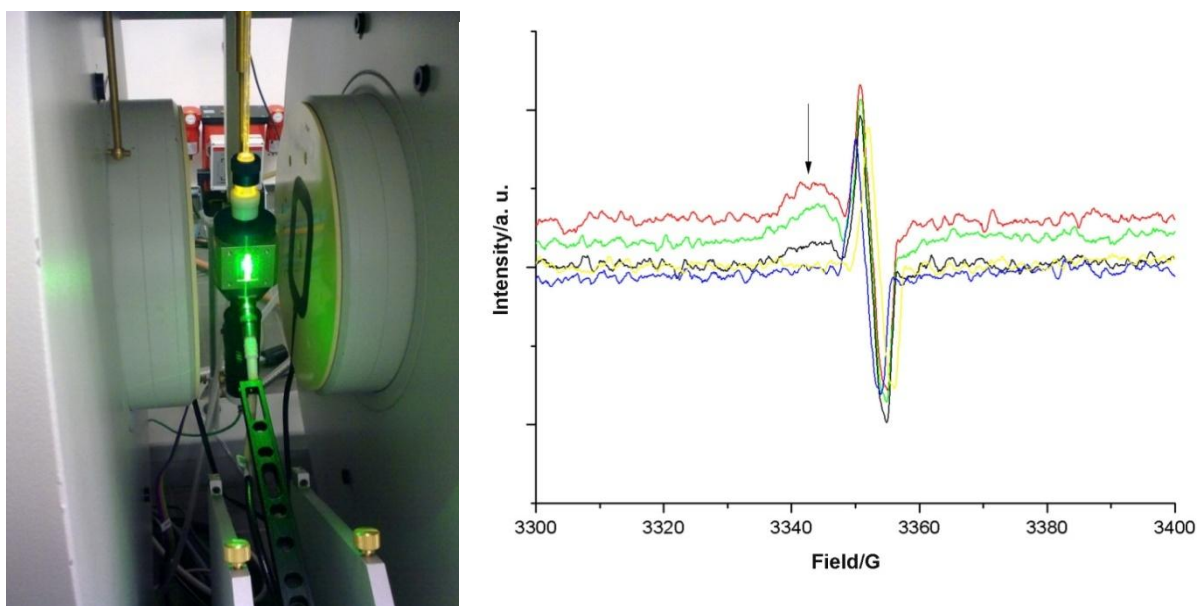


Fig. 15 Experimental setup for the *in situ* photoexcitation of IL-dye solution samples. The LASER ($\lambda = 532 \text{ nm}$) has a power output of 200 mW and the beam is widened through a lens to fully cover the sample capillary surface (left). Smoothed EPR spectra^[7] of $\text{P}_{66614}\text{NTf}_2/\text{Rhodamine 6 G ClO}_4$ recorded in time intervals after ending irradiation: 10 min. (red); 15 min. (green); 25 min. (black), 3 h 20 min. (blue) and 3 h 30 min. (yellow). The fast relaxing signal is depicted by the arrow (right).

⁵ Savitzky-Golay algorithm in polynomial third order with 20 points

The g -values of the sharp singlet signal of the excited sample are not shifting significantly in the first hours (see table 4). After two days the g -values are decreasing slightly about ca. $\Delta g = 0.0005$.

Table 4 Compiled g -values of the *in situ* experiments on photoexcited $P_{666\ 14}NTf_2$ /Rhodamine 6 G ClO_4 .

time/min after exposure to LASER light beam	g -value
0	2.00059
10	2.00152
15	2.00143
20	2.00146
25	2.00148
200	2.00137
210	2.00160
1740 (29 h)	2.00154
2700 (45 h)	2.00097
6000 (100 h)	2.00110

Using simple considerations an estimation of radical dye molecule species can be applied; the detection limit of EPR technique is required to be 10^{-11} mol. The concentrations of Mn^{2+} and dye of each are 10^{-16} mol. Because the signal-to-noise ratio is high, the lower detection limits are reached. The upper boundary is assumed by comparison of the FOURIER-transformed EPR signal areas of the Mn^{2+} salt and the EPR signal area of the organic dye radical. From Fig. 16 and table 5 the area of the EPR signal of the Mn^{2+} species **A** is roughly 200-times the resonance intensity area **C** of the dye.⁶ Since the unfavoured population of the triplet states for molecules bearing low order atoms, most excited dye molecules will relax via IC to lower singlets. The amount of existing radical dyes will thus be roughly 10^{-11} to 10^{-13} mol which means a former singlet to triplet ratio of $10^5 : 1$ to $10^3 : 1$.

⁶ Integration of the fast FOURIER transformation of the cw-EPR signals

Additionally the photodegradation has to be assumed as exponential growing (see Fig. 2) because of low concentrations of degraded byproducts.

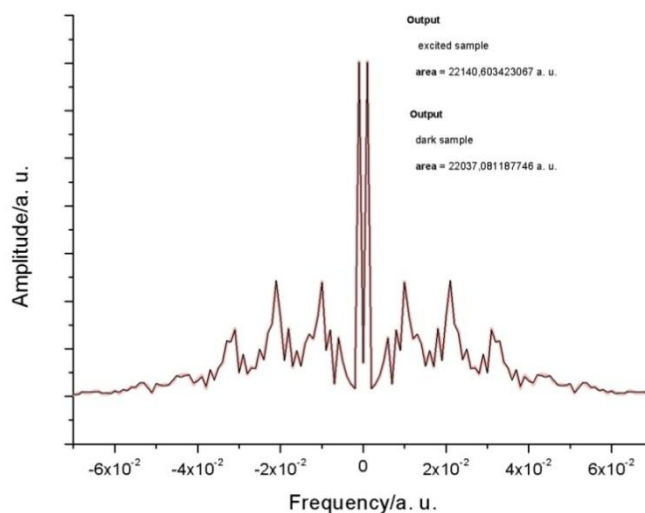


Fig. 16 Compared fast FOURIER transformed of EPR signals of $P_{666.14}NTf_2/Rhodamine\ 6\ G\ ClO_4/Mn(NTf_2)_2$ samples: excited sample (purple) and dark sample (black).

Table 5 Results of the integration of the cw-EPR signals of $P_{666.14}NTf_2/Rhodamine\ 6\ G\ ClO_4/Mn(NTf_2)_2$.

	dark sample A	excited sample B	substracted sample C
Integrated EPR area/a. u.	22037.1	22140.6	103.5
EPR area ratio	213	214	1

The photochemical radical generation as well as the low initial radical concentration and the exponential decay of the emissivity of the dye tend to a photoinduced radical chain degradation mechanism of first order due to concentration influence of only one species – the dye. The solvent has a certain influence on the stabilization of the radicals. ILs proved here to stabilize radicals over days while being electrochemical inert to redox processes induced by photoexcited dyes.

3.4 Experimental section

3.4.1 Chemicals

$P_{666-14}Cl$ was purchased from Cytec Corp., USA and washed with deionized water prior to use. $LiNTf_2$ (99%) was purchased from IoLiTec, Freiburg i. Br., D and used as received. $LiOTf$ (99%) was purchased from Acros, Geel, B and used as received. $C_4C_1mimPF_6$ (99%) was purchased from IoLiTec, Freiburg i. Br., D and worked up prior to use. $C_4mpyrFAP$ (99%) was purchased from Merck, Darmstadt, D and worked up prior to use. Dry Methanol (99.8%, <50 ppm water) was purchased from Acros and used as received. Tetramethylsiloxane (TMOS, 98%) and Methyltrimethoxysiloxane (MTMS, 99%) were purchased from Acros, Geel, B and distilled prior to use. DODC (99%), Rhodamine 6 G (for fluorescence), Rhodamine 6 G ClO_4 (for fluorescence), β -carotene (97%), NCS (99%) and formic acid (99%) were purchased from Sigma-Aldrich, Steinheim, D and used as received. $Tb(OTf)_3$ was gently provided by Dr. B. MALLICK, AG MUDRING, RUB, D. $MnCO_3$ (44-46% Mn, KMF, St. Augustin, D) was used as received.

3.4.2 General procedure for the purification of Ionic Liquids purchased from chemical suppliers

The purchased IL was diluted with CH_2Cl_2 or $CHCl_3$ and washed several times with deionized water to remove excess of halides ($AgNO_3$ test) or alkaline salts as well as unreacted starting material. After filtration of the solution over a column filled with neutral Al_2O_3 and active charcoal the residual organic phase was freed from solvent and dried under high vacuum for 1-2 days at 80-90°C.

3.4.3 EPR measurements

EPR spectra were recorded in the X-band on a Bruker ELEXSYS 500E equipped with a variable temperature unit. The g -values were determined with a dpph sample as reference.

3.4.4 Photostability measurements

The photostability performances were tested by Dipl.-Ing. (FH) J. KRAUSE from the I. Physikalisches Institut, University of Cologne. The dye solutions were excited with an argon ion LASER at wavelengths 488 nm and 514 nm or with a diode-pumped solid-state LASER (DPSS) at 532 nm (500-1000 mW, cw or pulsed, 20 kHz, 12 ns pulse width, 25 μJ per pulse). The beam was focussed with a lens to a diameter of 1 cm, yielding an average intensity of 0.637 W/cm^2 . The luminescence radiation was focused on the entrance slit of a monochromator and detected with a CCD camera. The laser line was blocked with an edge filter for 488 nm.

3.4.5 Luminescence and absorbance studies

The luminescence (CCD camera) and absorbance (Shimadzu UV-3600, Shimadzu, Duisburg, D) measurements of the materials were performed by Dipl.-Ing. (FH) J. KRAUSE from the I. Physikalisches Institut, University of Cologne.

3.5 General procedure for the production of the LASER material

To yield a typical LASER sample, to 2 ml of $P_{666\ 14}NTf_2$ or $P_{666\ 14}OTf$ 1.1 mg Rhodamine 6 G ClO_4 (Sigma-Aldrich, for fluorescence) or corresponding molar amount of any other dye (Coumarine 6) and 5.0 mg $Mn(NTf_2)_2$ were added. The mixture was heated at 80-90 °C and treated in an ultrasonic bath until complete dissolution of the educts. About 0.1 or 0.2 ml of the solutions were transferred into fused Duran capillaries which were sealed under vacuum using Quickfit technique. For EPR studies Quartz capillaries with 4 mm diameter and for photophysical studies Duran capillaries with 5 mm diameter were used.

3.5.1 Doping the LASER material with organic quenchers

The prepared Mn^{2+} -free $P_{666\ 14}NTf_2$ /Rhodamine 6 G ClO_4 solutions were doped with different concentrations of β -Carotene by simple mixing with a β -Carotene-IL solution ($2 \cdot 10^{-6}$ M β -carotene/IL). To yield the ascorbic acid doped IL-dye solution a $6 \cdot 10^{-5}$ M solution of ascorbic acid in IL was prepared by dissolution of solid ascorbic acid into a 2 ml dye-IL solution.

3.5.2 Synthesis of Rhodamine 6 G NTf_2

Rhodamine 6 G was dissolved in dry Methanol under dry N_2 and an equimolar amount of $LiNTf_2$ in Methanol was added to stir at 50°C for 1 day. The Methanol phase was washed with dry CH_2Cl_2 . Then the CH_2Cl_2 phase was washed with deionized water under dry N_2 to remove excess halides and Lithium salts. The raw product was then freed from solvent and dried at 80°C for 1 day under high vacuum.

EA Rhodamine 6 G NTf_2 calc. N 5.81%, C 49.79%, H 4.32%, S 8.86%; found N 6.23%, C 50.26%, H 4.33%, S 8.77%.

^{19}F -NMR (300 MHz, $CDCl_3$): $\delta = -78.79$ (s, 6F)

3.5.3 General procedure for the synthesis of 1-*N*-alkyl-3-methylimidazolium and trihexyl-tetradecylphosphonium bis(trifluoromethane)sulfonylimides and triflates

The 1-*N*-alkyl-3-methylimidazolium and trihexyltetradecylphosphonium bis(trifluoromethane)-sulfonates were synthesized by metathesis reaction of the 1-*N*-alkyl-3-methylimidazolium halides with lithium bis(trifluoromethanesulfonyl)imides or lithium triflate. The respective halide IL was dissolved in acetone/acetonitrile (50 : 50) (in case of P_{666 14} ILs) or in deionized water (in case of C_xmimNTf₂) and the equimolar amount of the dissolved LiNTf₂ or LiOTf salt in was added. After stirring at 60°C for 1 day the organic phase was separated and washed halide free with deionized water (AgNO₃ test). The solution was then filtered over a column filled with neutral Al₂O₃ and active charcoal. The residual organic phase was freed from solvent and dried under high vacuum for 1-2 days at 80-90°C.

C₂mimNTf₂: ¹H-NMR (300 MHz, CDCl₃): δ = 1.58 (t, 3H); 4.06 (q, 2H); 7.73 (d, 2H); 9.00 (s, 1H)

¹⁹F-NMR (300 MHz, CDCl₃): δ = -79.96 (s, 6F)

IC (halides): 119.6 ppm

C₄mimNTf₂: ¹H-NMR (300 MHz, CDCl₃): δ = 0.89 (t, 3H); 1.31 (hex, 2H); 1.80 (pen, 2H); 3.87 (s, 3H); 4.11 (t, 2H); 7.30 (d, 2H); 8.59 (s, 1H)

¹⁹F-NMR (300 MHz, CDCl₃): δ = -79.32 (s, 6F)

IC (halides): 126.4 ppm

P_{666 14}NTf₂: ¹H-NMR (300 MHz, CDCl₃): δ = 0.91 (m, 3H); 1.28 (m, 18H); 1.81 (pen, 2H); 3.87 (s, 3H); 4.11 (t, 2H); 7.30 (d, 2H); 8.61 (s, 1H)

¹⁹F-NMR (300 MHz, CDCl₃): δ = -78.93 (s, 6F)

³¹P-NMR (300 MHz, CDCl₃): δ = 32.89 (s, 1P)

P_{666 14}OTf: ¹H-NMR (300 MHz, CDCl₃): δ = 0.85(m, 12H); 1.22 (s, 18H); 1.28 (m, 13H); 1.33 (m, 16H); 2.12 (m, 8H)

¹⁹F-NMR (300 MHz, CDCl₃): δ = -78.27 (s, 3F)

³¹P-NMR (300 MHz, CDCl₃): δ = 32.05 (s, 1P)

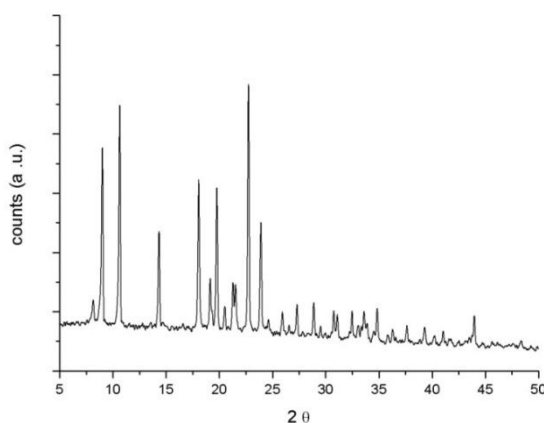
3.5.4 Synthesis of Ionogels

Ionogels were prepared according to a procedure of BINNEMANS.^[25] 1.00 ml P_{666 14}NTf₂ and 0.5 mg Rhodamine 6 G ClO₄ were dissolved in 3.76 ml of a solution of TMOS and MTMS (50 : 50) (both redistilled). To this mixture 0.12 ml formic acid was added and irradiated with ultra sonic sound bath. The mixture was allowed to gelate at air conditions.

3.5.5 Synthesis of Mn(NTf₂)₂

MnCO₃ was suspended in deionized water and a two- to threefold molar amount of HNTf₂ in aqueous solution was added dropwise. After stirring for 2 hours at 60°C the unreacted material was filtered off, the water was boiled off until a slurry solid appeared. This solid compound was transferred into a SCHLENK tube and pre-dried at 140-160°C under high vacuum. The residual solid was then sublimed under high vacuum at 270°C over night.

EA Mn(NTf₂)₂ calc. N 4.55%, C 7.80%, H 0.00%, S 20.81%; found N 4.35%, C 7.78%, H 0.10%, S 21.40%.



3.5.6 Synthesis of bistrifluoromethansulfonic acid

HNTf₂ was synthesized by sublimation from a solution of LiNTf₂ in an excess sulfuric acid.^[52] The reaction mixture was stirred for two days at 80-100°C. The colourless product crystallized upon cooling in yields of about 90%.

¹H-NMR (300 MHz, D₂O): δ = 4.77 (s, 1H)

¹⁹F-NMR (300 MHz, D₂O): δ = -79.16 (s, 6F)

¹³C{¹⁹F}-NMR (300 MHz, D₂O): δ = 19.27 (s, 2C)

3.6 Conclusion

Organic dye photostability performances can be improved by orders of magnitudes. The emissivity of these IL-dye solutions exhibits in the beginning of excitation an equilibrium-like behaviour until a steady state is reached. Further excitation leads to no significant reduction of the emissivity. Since ILs can be electrochemically stable, non-flammable, show only very low vapor pressure and are assumed to be “green solvents” the application of these IL-dye solutions may become of industrial reference. Additionally doping these solutions with suitable quenchers like Mn^{2+} or secondary metabolites also increases the photostability performances compared to common commercially available dye solutions. Very high dye photostability is achieved in $P_{666,14}NTf_2/Rhodamine\ 6\ G\ ClO_4/Mn(NTf_2)_2$. The Mn^{2+} -doping results in no impact on the luminescence properties of the dyes. In β -carotene doped $P_{666,14}NTf_2/Rhodamine\ 6\ G\ ClO_4$ samples bathochromic shifts in the emission maxima are observed concerning an interaction of the secondary metabolite with the dye. The exchange of the counterion of the Rhodamine dye moves the emission maximum in ILs hypsochromic and also improves the photostability.

From EPR and optical spectroscopy no significant impact of Mn^{2+} to the luminescent properties of the dye is observed. The role of Mn^{2+} is ambiguous and can be summarized considering several facts; first Mn^{2+} removes oxygen like in the WINKLER key step reaction, second it eases the ISC of triplet dyes towards their singlet ground states. However, the Mn^{2+} doped dye solution has to be halide-free.

Secondary metabolites, i. e. β -carotene and ascorbic acid also enhance the emissivity lifetime of organic dyes in ILs. Investigations show prolonged photostabilities in all atmospheres – even under air. From photoluminescence spectra the emission maximum in these samples is bathochromic shifted indicating interactions to the dye. Best photostability performances are found in ascorbic acid saturated dye-IL solutions. Because ILs readily dissolve gases in high concentrations ascorbic acid removes the residual left oxygen. In general, photodegradation of dye solutions starts via arbitrary radical reaction. The dye doped medium must therefore be freed from oxygen.

In kinetic EPR studies non-emissive radicals – so called “dark states” – are detected when dye solutions is irradiated using LASER light beam in excellent agreement with literature data. These two distinct EPR signals show different g -values and have different relaxation times. Initially generated radicals in ionic liquid media relax over several days in contrast to alcoholic dye solutions. This stabilization is attributed to the electrochemical stability of the IL.

An estimation of the *in situ* by photoexcitation generated radical dye species found that in an evacuated quencher-free IL/dye-sample ca. 1 of 10^4 excited dye molecules are turned to radicals.

In conclusion, organic dye photodegradation is promoted especially by oxygen. Since an evaporated methanolic dye solution exhibited also extended photostability, no clear evidence for the participation of other factors to the photodegradation of dyes could be determined.

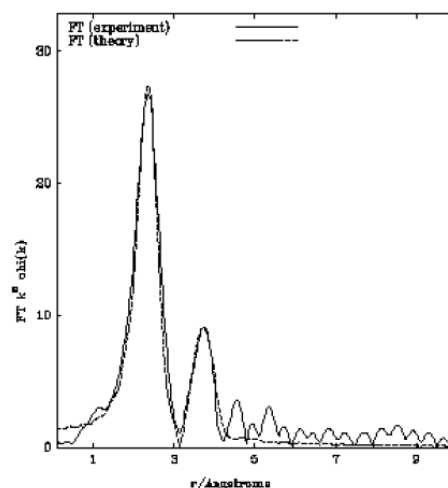
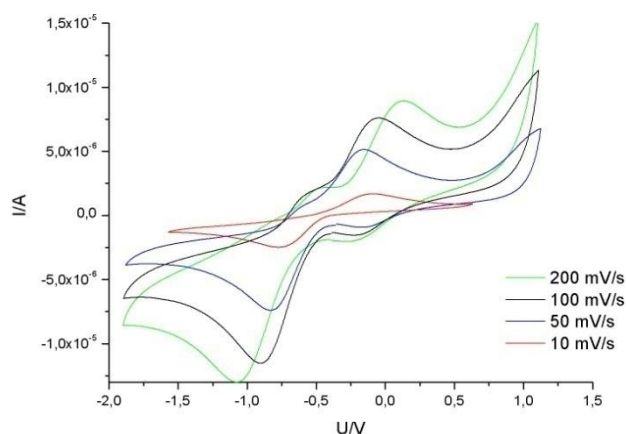
3.7 References

- [1] *Beilstein*, 18, V, 12, 283; U. Brackmann, *LASER dyes*, Lambda Physik AG, **2000**, Göttingen, D; H. Zollinger, A. Iqbal: *Color Chemistry: Syntheses, Properties and Applications of Organic Dyes and Pigments*. 3. Ed. Wiley-VCH, Weinheim **2003**
- [2] A. Baeyer, *Chem. News J. of Ind. Sci.*, **1902**, 85, 243.
- [3] O. Svelto et al., *Handbook of Lasers and Optics*, Springer, **2007**, New York, 777; F. P. Schäfer, *Dye Lasers*, **1990**, Springer-Verlag, Berlin; F. J. Duarte and L. W. Hillman (Eds.), *Dye Laser Principles*, **1990**, Academic, New York; S. P. McGlynn, A.T. Kinoshita, *Molecular Spectroscopy of the Triplet State*, **1969**, Englewood Cliffs, NJ: Prentice-Hall; T. Hamann, *Energy Environ. Sci.*, **2008**, 1, 66.
- [4] T. Cordes, J. Vogelsang, P. Tinnefeld, *J. Am. Chem. Soc.* **2009**, 131, 5018.
- [5] R. Zondervan, F. Kulzer, M. Orrit, *J. Phys. Chem. A*, **2004**, 108, 1657; R. Zondervan, F. Kulzer, M. Orrit, *J. Phys. Chem. A*, **2003**, 107, 6770.
- [6] R.E. Benesch, *Science*, **1953**, 118, 447; Gingell R, Walker R. *Xenobiotics* **1971**, 1, 3, 231; V. E. Korobov, A. K. Chibisov, *J. of Photochem.*, **1978**, 9, 411; F. P. Schäfer, *Laser Chem.* **1983**, 3, 265; G. E. Krichevsky, G. T. Khachaturova, O. M. Anissimova/Intern, *J. Polymeric Mater.*, **1990**, 13, 6.
- [7] <http://www.fine-adjustment.com/de/products/list/path/1/laser>.
- [8] M. Kasha, *Discussions Faraday Soc.* **1950**, 9, 14.
- [9] J. Vogelsang, R. Kasper, P. Tinnefeld, *Angew. Chem. Int. Ed.* **2008**, 47, 5465.
- [10] Ch. Bräuchle, H. Fuchs, K. Müllen, *J. Phys. Chem. A* **1998**, 102, 9109; F. Cannone, G. Chirico, A. Diaspro, *J. of Biomed. Optics*, **2003**, 8, 3, 391.
- [11] S.-H. Chun, M.-F Chien, K-C Lau, and W.-K. Li, *J. Phys. Chem. A*, **2005**, 109, 33, 7509; I. Corral, L. Gonzalez, *J Comput Chem*, **2008**, 29, 1982; N. Kakeya, M. Nojima, N. Tokura, J.C.S. Perkin I, **1976**, 87; N. Sugiyama, M. Iwata, H. Aoyama, *Chem. Comm.*, **1968**, 1563; S. P. Zingg, R. M. Pagni, J. H. Burns, *Tetrahedron Letters*, **1991**, 32, 41, 5737; H. Kotani, K. Ohkubo, S. Fukuzumi, *J. Am. Chem. Soc.*, **2004**, 126, 49, 15999; Y. Takahashi, S.-I. Morishima, K. Wakamatsu, J.

- Chem. Soc. Chem. Comm.* **1994**, 13; A. Ravikumar R. Bendikov, M. Bendikov, *Chem. Commun.*, **2006**, 1179; R. Dabestani, K. J. Ellis, M. E. Sigman, *J. of Photochem. Photobio.* **1995**, 86, 231.
- [12] M.A. Rauf , S. S. Ashraf, *Chem. Eng. J.*, **2009**, 151, 10.
- [13] R. N. Goyal, S. K. Srivastava, R. Agarwal, *Bulletin de la Societe Chimique de France*, **1985**, 4, 656; M. Ahmad, M. D. Rahn, T. A. King, *Appl. Optics*, **1999**, 38, 30, 6337; N. Oshima, T. O. Sugano, H. Hirai, *Can. J. Chem.* **1984**, 62, 2047; T. Stanoeva, D. Neshchadin, G. Gescheidt, S. N. Batchelor, *J. Phys. Chem. A*, **2005**, 109, 49, 11103; J. R. Lenhard, R. L. Parton, *J. Am. Soc.*, **1987**, 109, 19, 5808.
- [14] R. W. Chambers, D. R. Kearns, *J. Phys. Chem.*, **1968**, 72, 13, 4718.
- [15] B. Marciniak, G. E. Buono-Core, *J. of Photochem. Photobio A*, **1990**, 52, 1, 1; B. Marciniak, G. L. Hug, *J. of Photochem. Photobio A*, **1994**, 78, 1, 7.
- [16] R. E. Majors, L. B. Rogers, *Analytical Chemistry* **1969**, 41, 8, 1052.
- [17] Kawai et al. WO **2007/088703**, PCT/JP2007/00003.
- [18] Bornemann et al. *Optical Letters*, **2006**, 1669; Yi Fu, Jian Zhang, and Joseph R. Lakowicz, *Langmuir*, **2008**, 24, 3429; Ch. Bräuchle, H. Fuchs, K. Müllen, *J. Phys. Chem. A* **1998**, 102, 9109; *J. of Biomed. Optics*, **2003**, 8, 3, 391; I. Rasnik, S. A McKinney, T. Ha, *Nature Methods*, **2006**, 3, 11, 891; T. Gensch, M. Böhmer, Pedro F. Aramendia, *J. Phys. Chem. A*, **2005**, 109, 6652.
- [19] T. Welton, Peter Wasserscheid, *Ionic liquids in synthesis*, VCH-Wiley, Weinheim, **2002**.
- [20] S. Pitula, A.-V. Mudring, D. Schaniel, J. Krause, DE 102009000784; B. Marciniak, G. E. Buono-Core, *Spec. Lett.* **1990**, 23, 2, 149.
- [21] J. A. Whitehead, J. Zhang, G. A. Lawrence, *Hydrometallurgy*, **2007**, 88, 109; G. H. Jeffrey, J. Bassett, R. C. Denney, *Vogel's textbook of quantitative chemical analysis*, **1989**, 5th ed. John Wiley & sons, New York; L. Winkler, *Berichte der Deutschen Chemischen Gesellschaft*, **1888**, 21, 2843.
- [22] T. V. Dinh, E. L. Yen, J. D. Winefordner, *Anal. Chem.*, **1976**, 48, 8, 1186; K. N. Solovyov, E. A. Borisevich, *Physics Uspekhi* **2005**, 48, 3, 231; M. A. El-Sayed, *Acc. Chem. Res.*, **1968**, 1, 1, 8.

- [23] M. N. Berberan-Santos, *Phys. Chem. Comm.* **2000**, 5.
- [24] R. Schödel, PhD Thesis, Freie Universität Berlin (Berlin) **1999**.
- [25] D. Kumar Das, D. Kumar Sasmal, K. Bhattacharyya, *J. Phys. Chem. A*, **2009**, *113*, 16, 3737; T. Förster, *Ann. Physik*, **1948**, *6*, 2, 55.
- [26] J. L. Svirbely, A. Szent-Gyorgyi, *The Biochemical Journal*, **1933**, *27*, 279; G. Becher, K. Winsel, *Zeitschrift für Erkrankungen der Atmungsorgane* **1989**, *173*, 100.
- [27] K. Seddon, personal communication.
- [28] K. Binnemans, S. Bellayer, J. Le Bideau, *Chem. Mater.*, **2006**, *18*, 24, 5711; K. Binnemans, S. Bellayer, L. Viau, *Dalton Trans.*, **2009**, 298.
- [29] S. Pitula, A.-V. Mudring, *Inorg. Chem.* **2010**, in press; Ch. Reichardt, *Pure Appl. Chem.* **2004**, *76*, 1903; Ch. Reichardt, *Solvents and Solvent Effects in Organic Chemistry* (2nd Ed.), Wiley-VCH, Weinheim, **1988**.
- [30] G. Jeschke, "Einführung in die ESR-Spektroskopie", **1998**, manuscript, MPI Mainz.
- [31] M. Francesca Ottaviani, F. Montalti, M. Romanelli, *J. Phys. Chem.* **1996**, *100*, 26; A. Murali, *Physica B* **2005**, *538*, 19; R. S. Bansal, V. P. Seth, *Physica Scripta*. **1991**, *44*, 493; R. P. Sreekanth Chakradhar, *J. of Non-Crystalline Solids* **2007**, *353*, 2355; E. M. Glebov, V. P. Grivin, V. F. Plyus, *J.I of Structural Chemistry*. **2006**, *47*, 3, 476.
- [32] A. Schüren, A. Uthe, personal communication.
- [33] Gmelin, *Handbook, Mn*, Vol. C 10, 6, **1982**.
- [34] L. Toupet, C. Andraud, O. Maury, *Org. Lett.* **2008**, *10*, 19, 4159; L. Storaro, M. Lenarda, M. Brustolon, *Phys. Chem. Chem. Phys.* **2006**, *8*, 5069; B. A. Coles, G. M. Stearn, A. M. Waller, *J. Chem. Soc., Faraday Trans. I* **1988**, *84*, 7, 2357; I. G. Kytina, V. G. Kytin, K. Lips, *Appl. Phys. Lett.* **2004**, *84*, 24, 4902; V. Vattanen, J. A. Pedersen, *J. Chem. Soc., Perkin Trans.* **1996**, *2*, 2207; Y. Nie, C. Hu, J. Qu, *J. of Hazardous Materials* **2008**, *154*, 146.

4 Lanthanides in ionic liquids: Spectroscopical and electrochemical investigations



4.1 Abstract

Lanthanide salts were dissolved in several ILs and studied by EXAFS spectroscopy to receive information about the coordination numbers and interatomic distances. Cyclic voltammetry gave information about their redox behaviour. From EXAFS spectroscopy the coordination of the lanthanide ions in solution exhibited similar bond distances and coordination numbers like in comparable solid compounds. Between eight to nine ligands are coordinating in the first coordination shell to the metal ion center. The redox potentials of the dissolved lanthanide species show diffusion dependent behaviour. Applying different scan rates between 10 to 200 mV/s the cathodic and the anodic peaks are shifting dramatically.

4.2 Introduction

Physical properties of a LEWIS acid centre are influenced by the structure and the arrangement of the ligands around it. Next to single crystal and powder diffractometry information about the environment of the species of interest are obtained from EXAFS X-ray absorption spectroscopy.^[1] The coordination of lanthanides in solution are of special interest but still little is known about the. A viable spectroscopic method is EXAFS which gives information about bond distances and coordination numbers in ordered and disordered structures, i. e. in solutions.^[2] The scattering range of a center is limited up to 3-4 Å. Above this level the electron scattering is damped by other atoms in higher coordination shells. If the scattering atom is of high order number the detection range can be extended to 6-8 Å. HARDACRE et al. described the conformation and dynamic properties of liquid and liquid crystalline IL phases with X-ray and neutron absorption spectroscopy.^[3]

The impact of the structure in solution to physical properties can be studied by examination of the redox behaviour.^[4] Separation of lanthanides and actinides and their mixtures is performed in aqueous solution by liquid-liquid extraction in nuclear chemistry,^[5] for instance in the PUREX process.^[6] The “green solvent” IL is considered to replace the volatile and hazardous organic phase in which the species of interest is dissolved in. BHATT, HOPKINS, SMITH, QUINN and others showed the applicable electrodeposition of actinides in ILs at ambient conditions.^[7] Task-specific ILs indeed showed better extraction performances and moisture-stabilities including high electrochemical windows.^[8] Perturbation of the redox properties by exchange of the solvent offers the chance for selective deposition of a selected species out of a mixture. In fact, recent studies on the electrodeposition of metals and alloys in RTILs show the high interest to this topic.^[9]

4.3 Results and discussion

4.3.1 EXAFS spectroscopy

In table 1 the coordination numbers, distances, DEBYE-WALLER and fit factors of dissolved Eu^{3+} and Yb^{3+} salts in ILs are compiled. The obtained FOURIER-transformed and simulated results are given in the Appendix D. Both, Eu^{3+} and Yb^{3+} exhibit nine coordinating oxygens in their first environment shell when dissolved in NTf_2 -ILs or in the pure salts. Eu-O distances in solid $\text{Eu}(\text{NTf}_2)_3$ range at 242 pm which is excellent agreement with the nine coordinated $[\text{C}_4\text{mpyr}]_2[\text{Eu}(\text{NTf}_2)_5]$ and $[\text{C}_3\text{mim}][\text{Eu}(\text{NTf}_2)_4]$ ^[4] with 239-245 pm from previous work. Also $\text{Yb}(\text{NTf}_2)_3$ shows the same coordination number and Yb-O bond distances (234 pm, see Fig. 1) as in the recent literature ($[\text{C}_4\text{mpyr}][\text{Yb}(\text{NTf}_2)_4]$: Yb-O 227-233 pm).^[4] This also holds for both salts dissolved in NTf_2 -ILs though the distances are slightly (2 pm) longer than in the crystalline compounds.

Oxygens of the OTf anions arrange not regularly. The larger Eu^{3+} is surrounded by only eight oxygens while the smaller Yb^{3+} is nine fold coordinated but with regular Ln-O distances. In the second shell the next scattering atom appears to be the sulfur of the sulfonyl group. In the second coordination shell of Eu^{3+} the OTf-ILs exhibit surprisingly different sulfur arrangements depending on the cation. BF_4 and NTf_2 anions have similar basicities (see Section 2). In $[\text{C}_4\text{mim}][\text{BF}_4] : \text{Yb}[\text{NTf}_2]_3$ and $[\text{C}_4\text{mim}][\text{BF}_4] : \text{Eu}[\text{NTf}_2]_3$ fluorines and oxygens are observed in the coordination shells of the lanthanides. BF_4 anions are found to have distinct coordination numbers for Eu and Yb. Eu is surrounded by three BF_4 , six are found at the Yb centre at also different bond distances. This points to lanthanide coordination shells with mixed ligands. The Yb-F distance is 234 pm, the Eu-F distance with three ligands is 272 pm. It is noteworthy that in the first two shells of Yb 13 atoms were found, the Eu environment exhibits only nine. However, in both cases the DEBYE-WALLER factors for the oxygens are very low compared to other scattering atoms.

Dy^{3+} - Lu^{3+} are discussed to have an eight-fold coordination of oxygens in the first coordination shell while the other bound to nine oxygens.^[4] This fact cannot be transferred to the present data. Herein an average coordination number of nine is obtained for all samples. The close and similar nuclei distances for literature and the collected data state that no water is present around the lanthanide ions.

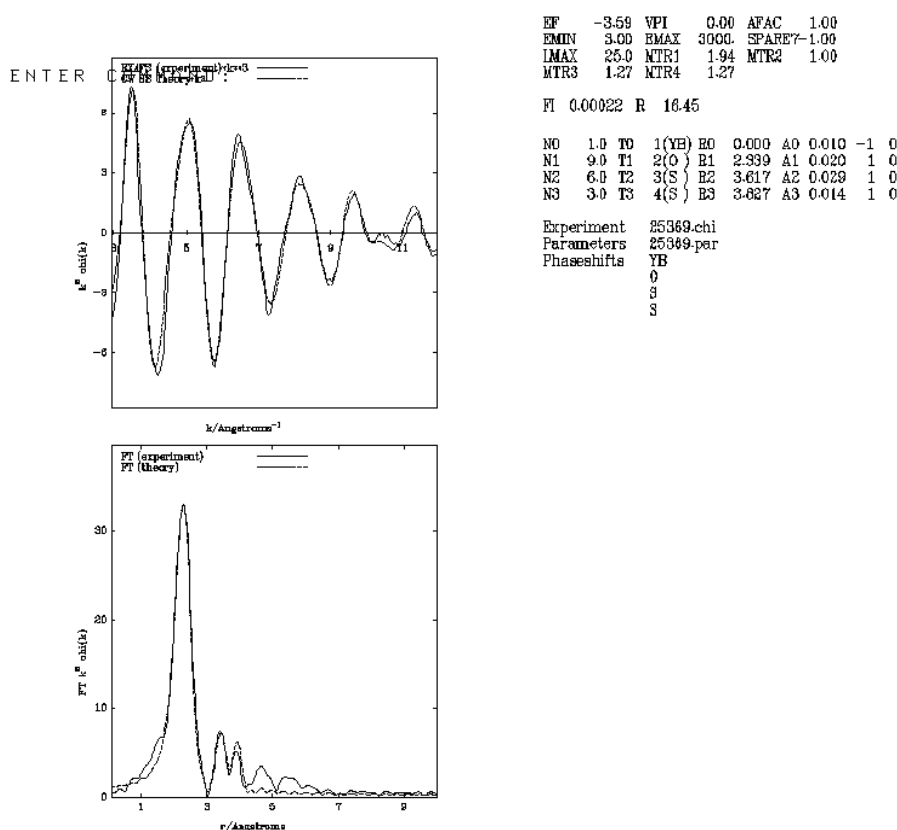


Fig. 1 EXAFS results (top) and FOURIER transformation (bottom) of solid $\text{Yb}(\text{NTf}_2)_3$ (results and data compiled and provided by HARDACRE et al.).

In case of DCA-ILs the nitrogen atom could not be detected whereas oxygen and chlorine were found in the first coordination shell at expected distances and amounts assuming stronger coordinating abilities than DCA anions or due to more probable statistical arrangement of NTf₂ anions bulk solvent.

Table 1. Coordination numbers, distances, DEBYE-WALLER and fit factors for Eu(NTf₂)₃ and Yb(NTf₂)₃ in different ILs derived from EXAFS spectroscopy (data compiled and provided by HARDACRE et al.).

sample	number of shells	scattering atom	distance/Å	co-ordination number	DEBYE-WALLER factor/Å ²	fit factor/%	water content/%
Eu[NTf₂]₃							
solid	2	O	2.422	9	0.023	26.67	
		S	3.724	9	0.040		
[C ₂ mim][OTf]	2	O	2.405	7.9	0.031	35.33	0.11
		S	3.826	4.8	0.037		
[C ₄ mim][DCA]	3	Cl	2.621	7	0.034	21.16	0.13
		O	2.426	2	0.016		
[C ₄ mim][OTf]	3	S	3.377	2	0.029	27.3	0.08
		O	2.385	8.3	0.027		
		S	3.841	7.8	0.044		
[C ₄ mim][NTf ₂]	2	S	4.203	1.9	0.006	39.61	0.07
		O	2.457	8.8	0.044		
		S	3.815	7.8	0.051		
[C ₄ mim][BF ₄]	4	O	2.439	6.4	0.008	18.44	0.14
		F	2.272	3.3	0.046		
		S	3.908	7.7	0.005		
		S	4.110	3.3	0.012		
Yb[NTf₂]₃							
solid	3	O	2.339	9	0.020	16.45	
		S	3.617	6	0.029		
		S	3.827	3	0.014		
[C ₂ mim][OTf]	2	O	2.237	9	0.024	27.84	0.14
		S	3.741	9	0.033		
[C ₄ mim][DCA]	3	O	2.363	8.8	0.025	20.64	0.14
		S	3.105	3.9	0.046		
		S	3.369	4.4	0.023		
[C ₄ mim][OTf]	3	O	2.237	9.1	0.031	33.19	0.09
		S	3.646	7.1	0.043		
		S	3.812	2.6	0.014		
[C ₄ mim][NTf ₂]	2	O	2.329	9.1	0.020	21.97	0.09
		S	3.687	9.2	0.035		
[C ₄ mim][BF ₄]	4	O	2.221	6.8	0.012	13.96	0.12
		F	2.340	6	0.054		
		S	3.525	3	0.003		
		S	3.808	3	0.014		

4.3.2 Cyclic voltammetry

To completely dissolve the lanthanide salts the NTf₂ and OTf salts of Eu³⁺ and Yb³⁺ were synthesized.^[9] These were dissolved in all investigated ILs to get 0.025 M solutions. In case of the DCA and OTf ILs one can suppose that these stronger basic anions will replace the weaker one (NTf₂) in the coordination shell of the lanthanide. The recorded cyclic voltammograms were afterwards referenced against an internal standard – the ferrocen/ferrocenium redox couple. Herein, the formerly used BF₄ and PF₆ ILs could not be investigated due to side reaction of the lanthanide to form the respective lanthanide fluorides.

The redox behaviour of Eu³⁺ in ILs exhibits well separated irreversible one-electron transfers between Eu³⁺ and Eu²⁺ in a range of up to 1.5 V depending on the scan rate. In general, the reduction as well as the oxidation potential of the lanthanide depend on their diffusion in the IL (see Fig. 2). The more viscous the IL is, the more separated the anodic and the cathodic peaks are.

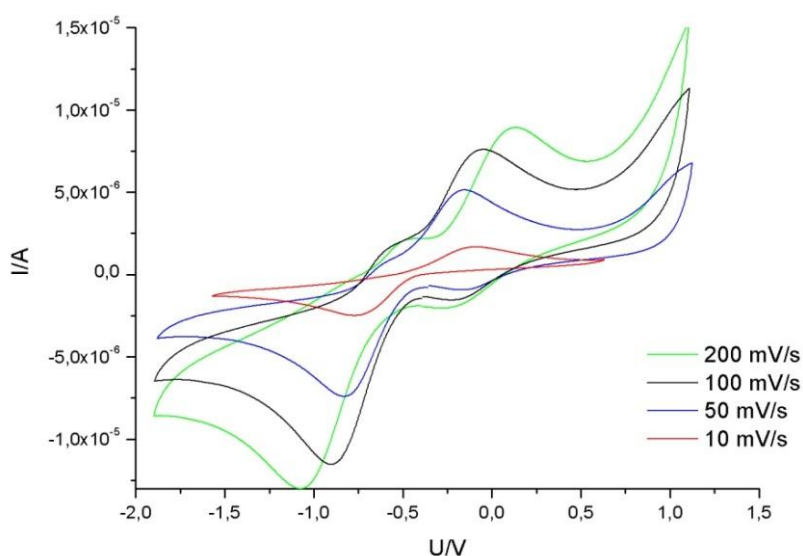


Fig. 2 Overlaid cyclic voltammograms of Eu(NTf₂)₃ in C₄mimNTf₂ vs. Fc^{0/I} measured with four different scan.

Experimentally reducing the trivalent species to the divalent was first done before back-oxidation on the cathodic cycle was applied. The reduction from +3 to +2 state in all studied samples appear to shift stronger than the oxidation potential when changing the scan rate. Decreasing the scan rate regards directly to a decrease in the difference between the cathodic and anodic potentials and to a decrease in the current applied to the electroactive species. Depending on the mass transport due to the viscosity of the IL the half step potentials are also shifting (see Table 2 and 3). The Fig. 3 shows a

typical cyclic voltammogram of $\text{Eu}(\text{NTf}_2)_3$ dissolved in C_4mimOTf . The current applied to the electroactive species is systematically increasing when the scan rate is increased.

The viscosity of an IL is affected by both ions. The difference in the half step potentials of Eu samples of ca. 0.1 V can be assumed due to differences in the viscosities of one order of magnitude ($\eta = 37 \text{ mPa}\cdot\text{s}$ for C_4mimOTf ; $\eta = 158 \text{ mPa}\cdot\text{s}$ for $\text{C}_4\text{mpyrOTf}$).^[10] The diverse cation nature of C_4mimOTf and $\text{C}_4\text{mpyrOTf}$ shows to have no impact because the more striking effect should be the viscosity effect. Herein, the alkyl chain length refers to the change in mass transport. C_2mimOTf ($\eta = 45 \text{ mPa}\cdot\text{s}$) is only slightly more viscous than C_4mimOTf .^[11] Eu^{3+} is surrounded by roughly eight OTf anions in the first coordination shell. Compared to former studies the present results exhibit similar behaviour of the half step potentials.^[4] All OTf ILs show similar half step potentials for the Eu redox couple resulting in nearly viscosity independent half step potentials. Hence, the half step potentials are only influenced by the anion shielding.

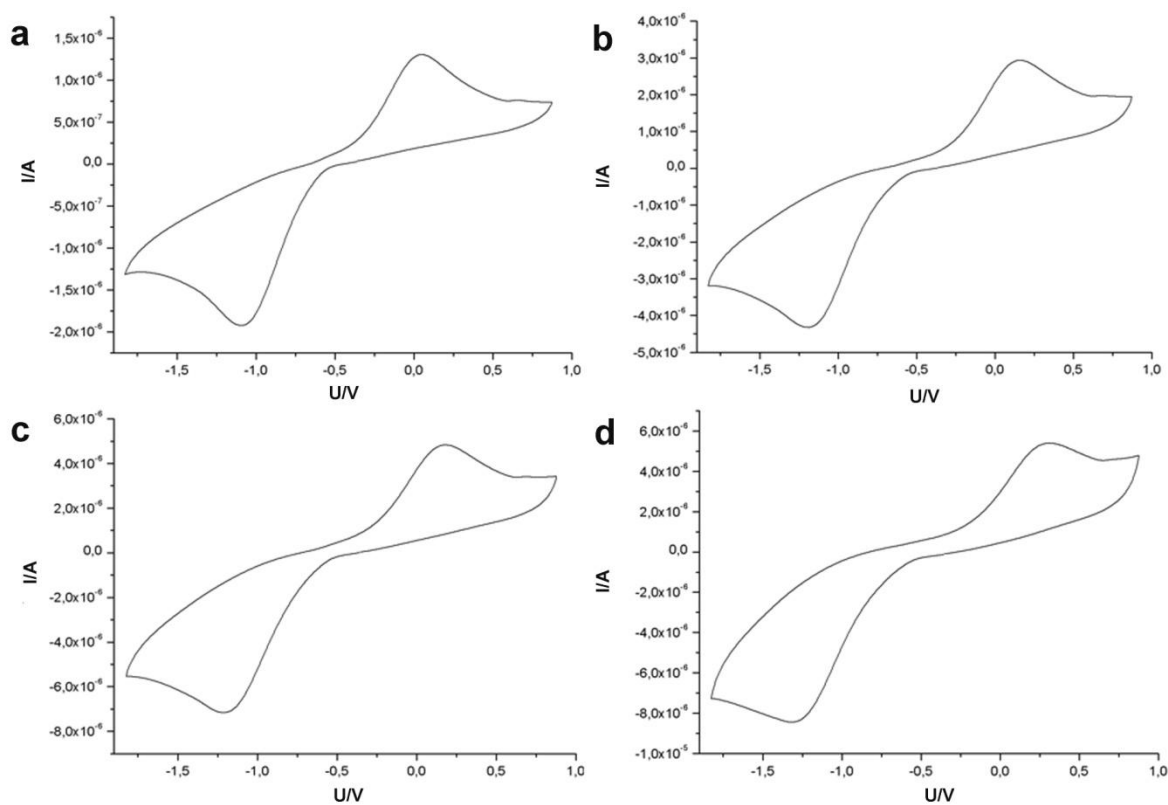


Fig. 3 Cyclic voltammograms of $\text{Eu}(\text{NTf}_2)_3$ in C_4mimOTf vs. Fc/Fc^+ measured with different scan rates a) 10 mV/s, b) 50 mV/s, c) 100 mV/s and d) 200 mV/s.

Table 2 Compiled cyclic voltammetry data of $\text{Eu}^{3+/2+}$ and $\text{Yb}^{3+/2+}$ couples referenced against internal standard redox couple Fc/Fc^+ in different ILs at four scan rates.

sample scan rate/ mV s^{-1}	$E_{1/2}/\text{V}$ ($\text{Eu}^{3+/2+}$)	reduction potential/ V vs. Fc/Fc^+	oxidation potential/ V vs. Fc/Fc^+
$\text{C}_4\text{mimNTf}_2 : \text{Eu}(\text{NTf}_2)_3$			
200	-0.871	-1.474	-0.267
100	-0.875	-1.301	-0.449
50	-0.874	-1.209	-0.539
10	-0.807	-1.142	-0.466
$\text{C}_4\text{mimOTf} : \text{Eu}(\text{NTf}_2)_3$			
200	-0.504	-1.318	0.310
100	-0.512	-1.207	0.183
50	-0.514	-1.188	0.160
10	-0.520	-1.089	0.049
$\text{C}_2\text{mimOTf} : \text{Eu}(\text{NTf}_2)_3$			
200	-0.621	-1.106	-0.136
100	-0.620	-0.954	-0.285
50	-0.669	-0.969	-0.368
10	-0.709	-0.894	-0.524
$\text{C}_4\text{mimDCA} : \text{Eu}(\text{NTf}_2)_3$			
200	-1.077	-1.582	-0.572
100	-1.086	-1.540	-0.632
50	-1.070	-1.442	-0.695
10	-1.081	-1.369	-0.793
$\text{P}_{66614}\text{NTf}_2 : \text{Eu}(\text{NTf}_2)_3$			
200	-0.612	-1.188	-0.036
100	-0.522	-0.974	-0.069
50	-0.433	-0.785	-0.080
10	-0.385	-0.645	-0.125
$\text{C}_4\text{pyridNTf}_2 : \text{Eu}(\text{NTf}_2)_3$			
200	-0.430	-0.910	0.050
100	-0.457	-0.838	-0.076
50	-0.448	-0.797	-0.099
10	-0.442	-0.719	-0.165
$\text{C}_4\text{mpyrOTf} : \text{Eu}(\text{OTf})_3$			
200	-0.626	-1.419	0.168
100	-0.696	-1.352	-0.039
50	-0.721	-1.287	-0.154
10	-0.730	-1.137	-0.322

4.4 Experimental section

4.4.1 EXAFS

EXAFS x-ray absorption spectra were recorded by C. HARDACRE at the SRS (Synchrotron radiation source) in Daresbury, U.K. The simulation and analysis of the spectra was also done by C. HARDACRE.

4.4.2 Cyclic voltammetry

The measurements were done under N_2 protection in a custom-made electrochemical cell (see below) with three electrode alignment. An Ag rod reference electrode (Metrohm AG, Filderstadt, D), a Pt wire counter electrode (Metrohm AG, Filderstadt, D) and a 2 mm diameter Pt wire working electrode were used. Four different scan rates were applied to every sample.



All recorded cyclovoltammograms were referenced against the ferrocene redox couple as internal standard. It was equilibrated 5 s prior to measurement and the 3rd cycle scan was used for data analysis. Between two measurements the built HELMHOLTZ electrical double layer was destroyed by stirring and heating the sample and checked for steady state potential as thermodynamic equilibrium. The steady state potential was then acquired and used for further processing.

4.4.3 Chemicals and Synthesis

HOTf (98%), $Eu(OTf)_3$ (99%) and Eu_2O_3 (99.9%) were purchased from Sigma-Aldrich and used as received. Yb_2O_3 (99.9%) was purchased from Chempur and used as received. For EXAFS studies ILs ($C_2mimOTf$, $C_4mimOTf$, $C_4mimDCA$, $C_4mimNTf_2$) were purchased from Solvent-Innovation, Cologne, D and worked up prior to use. Electrochemical studies were done with ILs synthesized via standard routes.

4.4.4 General procedure for the fabrication of the investigated samples

The resublimed Ln(NTf₂)₃ (Ln = Eu, Yb) salt were dissolved in the IL as 0.025 M solutions in a glovebox. The obtained solutions were treated with ultra sonic bath and gently heated until complete dissolution was obtained.

4.4.5 General procedure for the work up of ILs from chemical suppliers

The respective IL was diluted with CH₂Cl₂ or CHCl₃ and washed several times with deionized water to remove excess of halides or alkaline salts (AgNO₃ test) as well as unreacted raw material. After filtration of the solution over a column filled with neutral Al₂O₃ and active charcoal the residual organic phase was freed from solvent and dried under high vacuum for 1-2 days at 80-90°C.

4.4.6 General procedure for the synthesis of Eu(NTf₂)₃ and Yb(NTf₂)₃

Eu₂O₃ and Yb₂O₃ were suspended in deionized water and the at least sixfold molar amount of HNTf₂ in aqueous solution was added dropwise. After complete dissolution of the oxide the water was boiled off until a slurry solid appeared. This solid compound was transferred into a SCHLENK tube and pre-dried at 140-160°C under high vacuum. The residual solid was then sublimed under high vacuum at 270°C over night.

EA Eu(NTf₂)₃ calc. N 4.23%. C 7.26%, H 0.00%, S 19.39 %; found N 3.95 %. C 6.76%, H 0.00%, S 18.75%.

EA Yb(NTf₂)₃ calc. N 4.23%. C 7.26%, H 0.00%, S 19.39 %; found N 3.95 %. C 6.76%, H 0.00%, S 18.75%.

4.4.7 Synthesis of 1-*N*-butyl-1-methylpyrrolidinium and 1-*N*-butyl-3-methylimidazolium dicyanamide

1-*N*-butyl-1-methylpyrrolidinium bromide was dissolved in deionized water and a slight molar excess of silverdicyanamide suspended in deionized water was added. The mixture was stirred for 2 hours at 60°C and then filtered. The water was removed and the raw product dissolved in CH₂Cl₂ and cooled down. The rest of the halide was then again filtered off. The solution was then filtered over a column filled with neutral Al₂O₃ and activated charcoal. The residual organic phase was freed from solvent and dried under high vacuum for 1-2 days at 80-90°C.

C₄mpyrDCA ¹H-NMR (300 MHz, Acetone-d₆): δ = 0.99 (t, 3H); 1.42 (hex, 2H); 1.88 (m, 2H); 2.29 (s, 4H); 3.22 (t, 3H); 3.53 (m, 2H); 3.69 (m, 4H)

¹³C-NMR (300 MHz, Acetone-d₆): δ = 13.06 (s); 19.61 (s); 21.56 (s); 25.41 (s); 29.01 (hep); 47.99 (t); 63.94 (t); 64.16 (t); 205.80 (m)

C₄mimDCA ¹H-NMR (300 MHz. CDCl₃): δ = 0.85 (t, 3H); 1.27 (hex, 2H); 1.81 (pen, 2H); 4.02 (s, 3H); 4.24 (t, 2H); 7.56 (d, 2H); 10.19 (s, 1H)

¹³C-NMR (300 MHz. Acetone-d₆): δ = 13.12 (s); 19.52 (s); 21.60 (s); 25.47 (s); 28.94 (hep); 48.00 (t); 63.99 (t); 64.14 (t); 205.33 (m)

4.4.8 General procedure for the synthesis of 1-*n*-alkyl-1-methylpyrrolidinium and 1-*n*-alkyl-1-methylimidazolium triflates

The respective halide IL was dissolved in acetone/acetonitrile (50 : 50) and the equimolar amount of LiOTf in acetone was added. The mixture was stirred for 1 day at 60°C and then filtered. The solvent was removed and the raw product dissolved in CH₂Cl₂ and cooled down. The rest of the halide was then again filtered off. The solution was washed halide-free with deionized water (AgNO₃ test). The solution was then filtered over a column filled with neutral Al₂O₃ and activated charcoal. The residual organic phase was freed from solvent and dried under high vacuum for 1-2 days at 80-90°C.

C₄mimOTf ¹H-NMR (300 MHz. Acetone-d₆): δ = 0.96 (t, 3H); 1.40 (hex, 2H); 1.84 (m, 2H); 2.25 (s, 4H); 3.20 (t, 3H); 3.55 (m, 2H); 3.70 (m, 4H)

¹⁹F-NMR (300 MHz. Acetone-d₆): δ = -78.88 (s, 3F)

C₄mpyrOTf ¹H-NMR (300 MHz. Acetone-d₆): δ = 0.96 (t, 3H); 1.40 (hex, 2H); 1.84 (m, 2H); 2.25 (s, 4H); 3.20 (t, 3H); 3.55 (m, 2H); 3.70 (m, 4H)

¹⁹F-NMR (300 MHz. Acetone-d₆): δ = -78.88 (s. 3F)

4.4.9 General procedure for the synthesis of 1-*n*-alkyl-3-methylimidazolium bis(trifluoromethane)sulfonylimides

The 1-*n*-alkyl-3-methylimidazolium bis(trifluoromethane)sulfonates were synthesized by metathesis reaction of the 1-*n*-alkyl-3-methylimidazolium with lithium bis(trifluoromethanesulfonyl)imides.^[19, 21, 24]

C₄mimNTf₂ ¹H-NMR (300 MHz. CDCl₃): δ = 0.89 (t, 3H); 1.31 (hex, 2H); 1.80 (pen, 2H); 3.87 (s, 3H); 4.11 (t, 2H); 7.30 (d, 2H); 8.59 (s, 1H)

¹⁹F-NMR (300 MHz. CDCl₃): δ = -79.32 (s, 6H)

4.5 Conclusion

WCA salts of Eu and Yb were doped into several ILs to receive information about their coordination environment and redox behaviour via EXAFS spectroscopy and cyclic voltammetry. The obtained DEBYE-WALLER factors are in good agreement with results obtained of other high order atoms.^[1] In the first coordination shell of the lanthanide ions the respective anions of the ILs are found to join at bond distances in good agreement with solid samples. Despite Yb³⁺ is discussed to have an eight-fold coordination shell it was found that up to nine ligands are in its first coordination shell.

Irreversible one electron transfer reactions were found for all samples. This can be assigned to the Ln^{3+/2+} redox couples. The redox properties of Eu³⁺ in IL depend strongly on the anion of the used IL. The cation influence seems to be small since the obtained data show only slight differences up to 0.2 V. It was found that DCA shields stronger and shift the half step potential to more negative E_½ values. On the other side OTf is more basic than NTf₂ but appears at more positive E_½ values. In fact, no simple explanation can be given to this behaviour. Moreover, an influence of the cation nature could not be found. It is thus assumed that the change in half step potentials of Eu^{3+/2+} in ILs with identical anion refers to the viscosity induced by the alkyl chain length.

4.6 Reference

- [1] H. Bertagnolli, T. S. Ertel, *Angew. Chem.* **1994**, *106*, 15; C. Hardacre, *Annu. Rev. Mater. Res.* **2005**, *35*, 29.
- [2] P. Nockemann, K. van Hecke, L. van Meervel, *Polyhedron* **2009**, *28*, 1281; J- A. Dzielawa, P. Rickert, M.-L. Dietz, *J. Am. Chem. Soc.* **2002**, *124*, 10664; C. Gaillard, A. El Azzi, I. Billard, *Inorg. Chem.* **2005**, *44*, 852; S. K. Spear, D. C. Stepinski, R. D. Rogers, *Dalton Trans.* **2005**, 1966.
- [3] A. E. Bradley, C. Hardacre, M. Nieuwhuyzen, *Chem. Mater.* **2002**, *14*, 629; A. Triolo, M. A. Ramos, C. Hardacre, *J. Phys. Chem. B* **2006**, *110*, 21357; C. Hardacre, A. K. Soper, D. T. Bowron, *J. Phys.: Condens. Matter* **2003**, 159.
- [4] A. Babai, PhD thesis, University of Cologne (Cologne) **2006**; J. Heinze, *Angew. Chem.* **1984**, *96*, 11, 823; S.-F. Tang, A. Babai, A.-V. Mudring, *Angew. Chem. Int. Ed.* **2008**, *120*, 7631.
- [5] P. Taxil, *J. of Fluorine Chem.* **2009**, *130*, 94.
- [6] V. Kosyakov, V. Marchenko, *Radiochemistry* **2008**, *50*, 4, 333.
- [7] S. I. Nikitenko, C. Cannes, D. Trubert, *Inorg. Chem.* **2005**, *44*, 25, 9497; A. I. Bhatt, I. May, R. G. Lewin, *Inorg. Chem.* **2005**, *44*, 4934; A. Ispas, S. Pitula, A.-V. Mudring, F. Endres, *ECS Transactions*, **2008**, *13*, 113; K. Haerens, E. Matthijs, K. Binnemans, *Green Chem.* **2009**, *11*, 1357; O. Mann, Ge-Bo Pan, W. Freyland, *Electrochimica Acta*, **2009**, *54*, 2487; J. Estager, N. Papaiconomou, M. Draye, *Electrochemistry Comm.* **2008**, *10*, 1661; *Phys. Chem. Chem. Phys.* **2006**, *8*, 4265; M. Galiński, A. Lewandowski, I. Stępnia, *Electrochimica Acta* **2006**, *15*, 5567; S. Lambert, *Circuit World* **2006**, *32*, 4, 36; C. Gaillard, I. Billard, A. Chaumont, *Inorg. Chem.* **2005**, *44*, 23, 8355; C. Hardacre, *Annu. Rev. Mater. Res.* **2005**, *35*, 29; I. Billard, C. Gaillard, K. Binnemans, *Eur. J. Inorg. Chem.* **2007**, 5120; C. Zhong, T. Kume, Y. Iwasawa, *J. of Molecular Catalysis A: Chemical* **2008**, *279*, 200; P. Nockemann, B. Thijs, K. Lunstroot, *Chem. Eur. J.* **2009**, *15*, 1449
- [8] J. Zhang, J. M. Pringle, A. G. Wedd, *Inorg. Chem.* **2005**, *44*, 5123; T. Welton, Peter Wasserscheid, *Ionic liquids in synthesis*, VCH-Wiley, Weinheim, **2002**.
- [9] A. G. M. Barrett, D. C. Braddock, J. P. Henschke, *J. Chem. Soc., Perkin Trans. 1* **1999**, 873; N. Yanagihara, S. Nakamura, M. Nakayama, *Polyhedron* **1998**, *6*, 19, 2514; K. Egashira, Y.

Yoshimura, H. Kanno, *J. of Thermal Analysis and Calorimetry* **2003**, 71, 501

- [10] F. Onink, G. W. Meindersma, A. B. de Haan, *J. of Chem. Eng. Data* **2009**, 54, 10, 2809; P. Husson, A. A. H. Padua, V. Majer, *Green Chem.* **2006**, 8, 172; M. Montanino, S. Passerini, F. Soavi, *Electrochimica Acta* **2008**, 53, 7967
- [11] C.-L. Wong, A. N. Soriano, M.-H. Li, *Fluid Phase Equilibria* **2008**, 271, 43; P. K. Kilaru, P. Scovazzo, *Ind. Eng. Chem. Res.* **2008**, 47, 910

5 Experimental section

5.1 Used chemicals

Al ₂ O ₃ (neutral, activated, Brockmann I)	Acros (Geel, B),
C (purum)	VWR (Darmstadt, D)
Acetone (Selectipur)	BASF (Ludwigshafen, D)
Acetonitrile (>99.5%)	VWR (Darmstadt, D)
	Applichem (Darmstadt, D)
CHCl ₃ (99.8%)	Sigma-Aldrich (Steinheim, D)
	Biesterfeld (Hamburg, D)
CH ₂ Cl ₂ (99.4%)	Sigma-Aldrich (Steinheim, D)
	Biesterfeld (Hamburg, D)
Diethylether (99%)	Applichem (Darmstadt, D)
Ethylacetate (99.8%)	KMF (St. Augustin, D)
Isopropanol (99.8%, < 50 ppm water)	Acros (Geel, B)
Methanol (99.8%, < 50 ppm water)	Acros (Geel, B)
THF (99%)	Biesterfeld (Hamburg, D)
Toluene (99.5%)	Biesterfeld (Hamburg, D)
Bromoethane (98%)	Acros (Geel, B)
Chloroethane (for synthesis)	Merck (Hohenbrunn, D)
1-Bromopropane (98%)	Acros (Geel, B)
1-Chloropropane (99%)	Acros (Geel, B)
1-Bromobutane (>99%)	Acros (Geel, B)

Experimental section

1-Chlorobutane (>99%)	Sigma-Aldrich (Steinheim, D)
1-Bromohexane (>98%)	Sigma-Aldrich (Steinheim, D)
1-Chlorohexane (99%)	Acros (Geel, B)
Diethylsulfate (98%)	Sigma-Aldrich (Steinheim, D)
<i>N</i> -Methylimidazole (>99%)	Acros (Geel, B)
	Sigma-Aldrich (Steinheim, D)
Acetone-d ₆ (99.6%)	Deutero (Kastellaun, D)
CDCl ₃ (99.8%)	Deutero (Kastellaun, D)
D ₂ O (99.9%)	Deutero (Kastellaun, D)
DMSO-d ₆ (99.8%)	Deutero (Kastellaun, D)
Eu(OTf) ₃ (98%)	Acros (Geel, B)
HOTf (98%)	Acros (Geel, B)
LiNTf ₂ (99%)	IoLiTec (Freiburg i. Br. D)
LiOTf (98%)	Acros (Geel, B)
Mn(OTf) ₂	Dr. A. Babai (Cologne, D)
Tb(OTf) ₃	Dr. B. Mallick (Cologne, D)
FeCp ₂ (98%)	Sigma-Aldrich (Steinheim, D)
C ₄ C ₁ mimPF ₆ (98%)	Solvent Innovation (Cologne, D)
C ₂ mimMeSO ₃ (99%)	IoLiTec (Freiburg i. Br. D)
C ₂ mimOTos (99%)	IoLiTec (Freiburg i. Br. D)
C ₂ mpyridEtSO ₄ (99%)	IoLiTec (Freiburg i. Br. D)
C ₈ mimPF ₆ (99%)	IoLiTec (Freiburg i. Br. D)
C ₆ mpyridBF ₄ (99%)	IoLiTec (Freiburg i. Br. D)
C ₄ mpyridPF ₆ (99%)	IoLiTec (Freiburg i. Br. D)

Experimental section

C ₄ mpyrFAP (99%)	Merck (Hohenbrunn, D)
C ₂ mimB(CN) ₄ (99%)	Merck (Hohenbrunn, D)
C ₂ mimFAP (99%)	Merck (Hohenbrunn, D)
C ₄ mimOTf (99%)	Solvent Innovation (Cologne, D)
C ₄ mimN(CN) ₂ (99%)	Solvent Innovation (Cologne, D)
C ₄ C ₁ mimPF ₆ (99%)	IoLiTec (Freiburg i. Br. D)
C ₁₀ mimNTf ₂	AG MUDRING (Bochum, D)
N ₁₈₈₈ NTf ₂	AG MUDRING (Bochum, D)
P _{666 14} Cl (93-95%)	Cyttec (Woodland Park, New Jersey, USA)
P _{666 14} BF ₄ (99%)	Merck (Hohenbrunn, D)
P _{666 14} PF ₆ (99%)	Merck (Hohenbrunn, D)
Eu ₂ O ₃ (99.9%)	Chempur (Karlsruhe, D)
Yb ₂ O ₃ (99.9%)	Chempur (Karlsruhe, D)
MnCO ₃ (44-46% Mn)	Sigma-Aldrich (Steinheim, D)
Coumarine 6 (for fluorescence)	Sigma-Aldrich (Steinheim, D)
DODC (99%)	Sigma-Aldrich (Steinheim, D)
Rhodamine 6 G (for fluorescence)	Sigma-Aldrich (Steinheim, D)
Rhodamine 6 G ClO ₄ (for fluorescence)	Sigma-Aldrich (Steinheim, D)
Ascorbic acid (98%)	Sigma-Aldrich (Steinheim, D)
β-Carotene (97%)	Sigma-Aldrich (Steinheim, D)

5.2 Used software

Adobe Photoshop CS 2 Vers. 9.0	Adobe Systems Incorp. USA
Fluorescence	Luminescence controlling program by Horiba Jobin Yvon, München, D
GPES 4.9.006	Electrochemical analysis program by EcoChem B. V., NL
Proteus 4.7.0	DSC graphical surface program by Netzsch GmbH, Selb, D
CaryScan	UV/VIS analysis program by Varian, Palo Alto, USA
MTW 6.28	Molecular weight calculator program by M. Monroe
Origin 8.0	Table and calculation program by Microcal, Origin Lab Co., Northhampton, USA
SciFinder 2006/2007/web version	Scientific data base by CAS, Columbus, OH, USA
Spinworks 2.5.4 and 3.1	NMR program package, University of Manitoba, Manitoba, CAN
WinSCP 4.1.9	SSH based UNIX/Windows interface by S. Tatham
WinXPow 1.3 and 2.0	XRD program package by STOE&Cie GmbH, Darmstadt, D
XEPR and XEPRView	EPR controlling program package; EPR graphical surface program by Bruker Biospin GmbH, D

5.3 Used equipment and hardware

AC300 Bruker and AC400 Bruker	NMR spectrometer by Bruker Biospin GmbH, D
Netzsch DSC 201 F1	DSC thermograph by Netzsch GmbH, Selb, D
Bruker XEPR X-Band	EPR spectrometer by Bruker Biospin GmbH, D
Cary 05E and Cary 5000	UV/VIS spectrometer by Varian, Palo Alto, USA
Edwards RV12 (max. vacuum ca. $5 \cdot 10^{-3}$ mbar)	Vacuum oil pump from Edwards Inc., UK
Huber G570	XRD powder diffractometer by Huber, Garching, D
Metrohm Autolab and microAutolabIII	CV equipment by Metrohm AG, Filderstadt, D
Metrohm 883 Basic plus	Karl-Fischer Titration device by Metrohm AG, Filderstadt, D
Methrom 881 Compact IC	Ion chromatography device by Metrohm AG, Filderstadt, D
Labmaster 130 and Labstar	Gloveboxes by MBraun, Garching, D
Fluorlog 3	Luminescence spectrophotometer by Horiba Jobin Yvon, München, D
Euro Vektor CHNS-O Euro EA3000	Elemental analyzer by HEKAtech GmbH, Wegberg, D
IFS-66V-S FOURIER Transform	IR spectrometer by Bruker Optik GmbH, Ettlingen, D

Experimental section

FRA 106-S FOURIER Transform

IR spectrometer by Bruker Optik GmbH, Ettlingen, D

Typ VP 20 a (unidentifiable brand)

High frequency generator 20 W; 0.91 A; 220 V

Class 3 b LASER, diode LASER, 532 nm, 200 mW

AG Schaniel, I. Physikalisches Institut (University of Cologne, D)

6 Appendix A

6.1 DSC

All DSC thermograms were recorded at a scan rate of 5 K/min.

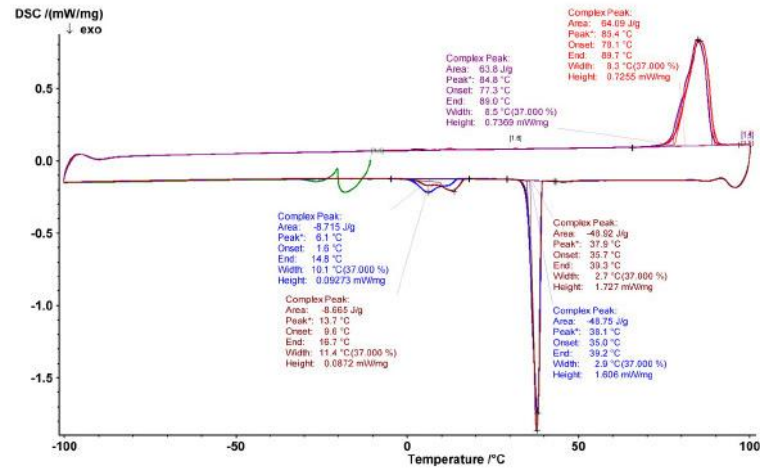


Fig. 1 DSC thermogram of $[\text{C}_2\text{mim}]_2[\text{MnCl}_4]$.

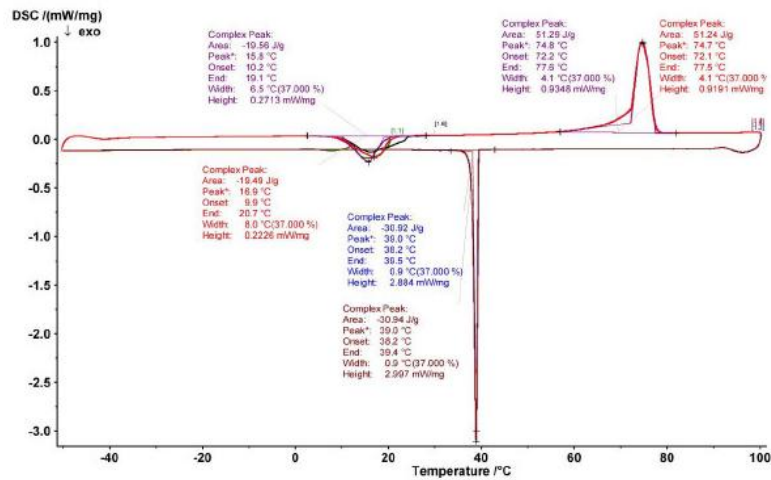


Fig. 2 DSC thermogram of $[\text{C}_2\text{mim}]_2[\text{MnCl}_4]$.

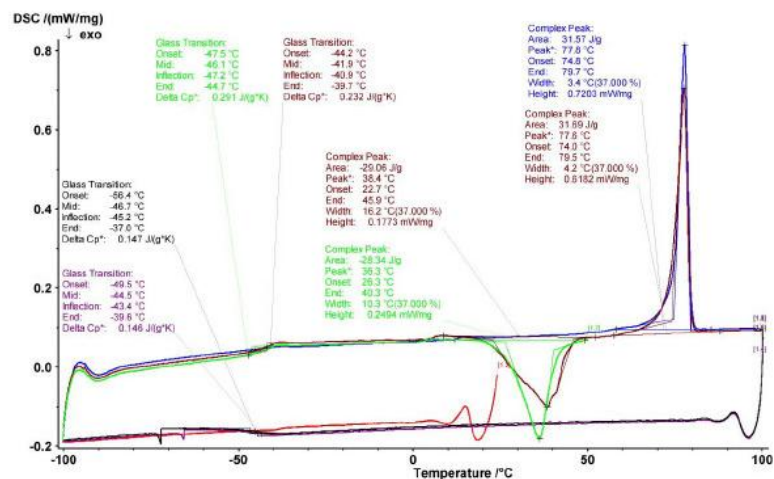


Fig. 3 DSC thermogram of $[C_2mim][Mn(NTf_2)_3]$.

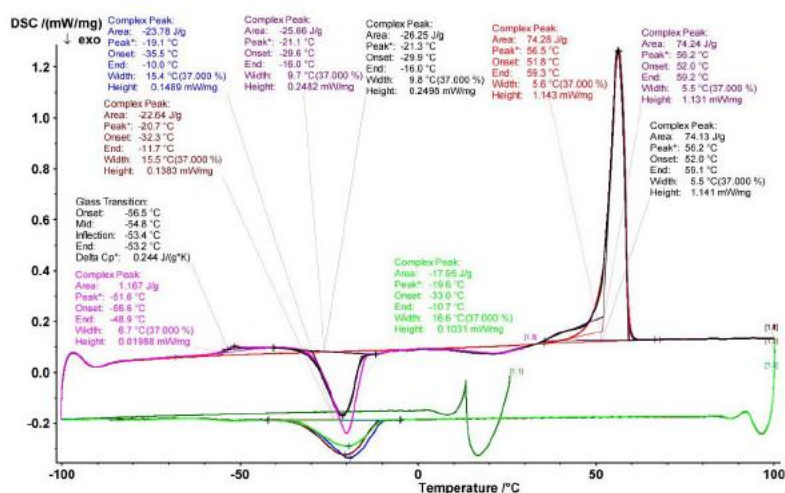


Fig. 4 DSC thermogram of $[C_3mim]_2[MnCl_4]$.

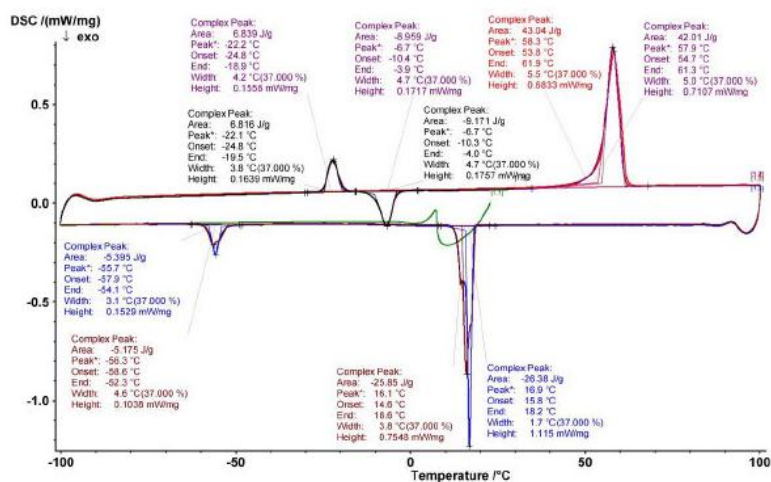


Fig. 5 DSC thermogram of $[C_3mim]_2[MnBr_4]$.

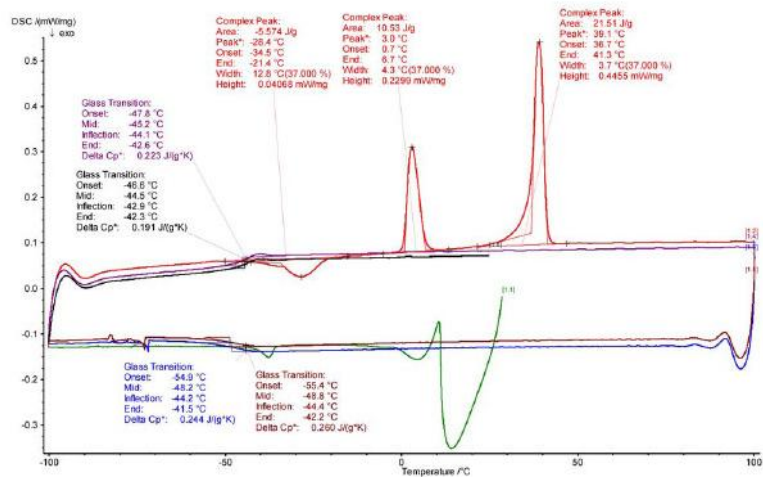


Fig. 6 DSC thermogram of $[C_3mim][Mn(NTf_2)_3]$.

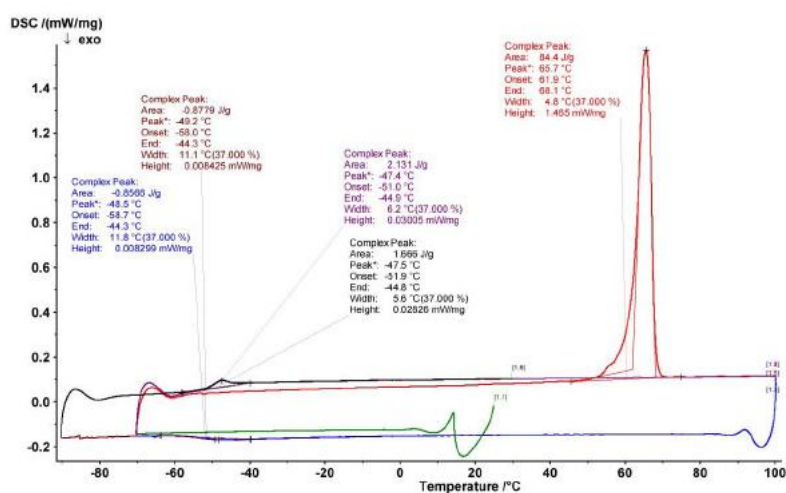


Fig. 7 DSC thermogram of $[C_4mim]_2[MnCl_4]$.

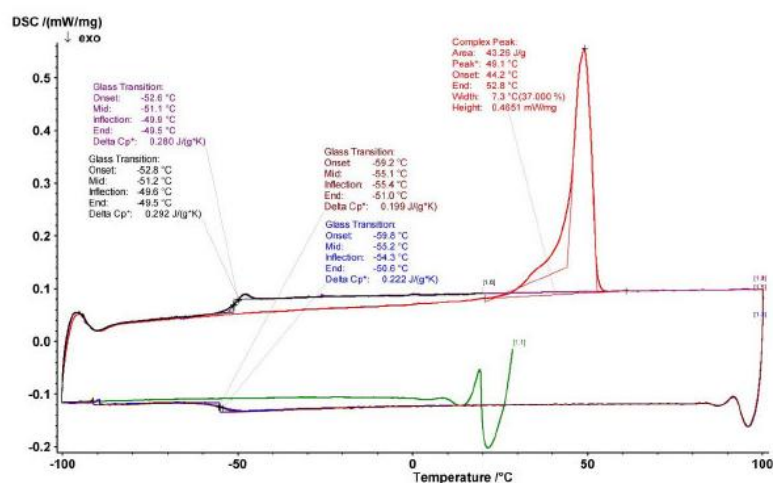


Fig. 8 DSC thermogram of $[C_4mim]_2[MnBr_4]$.

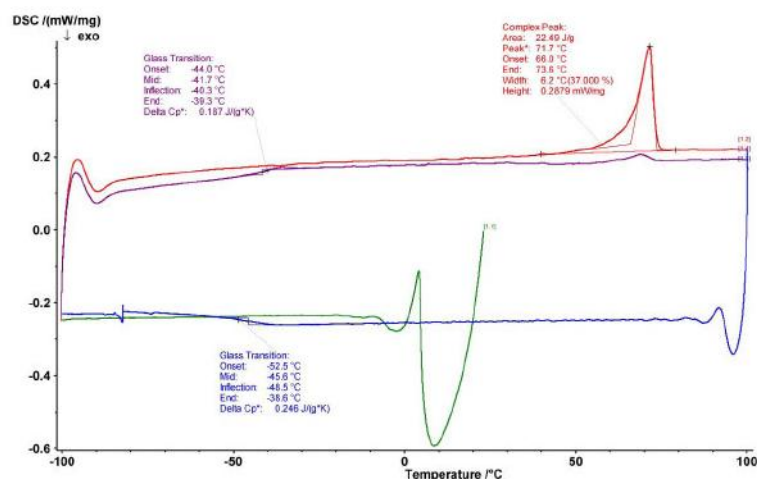


Fig. 9 DSC thermogram of $[C_4mim][Mn(NTf_2)_3]$.

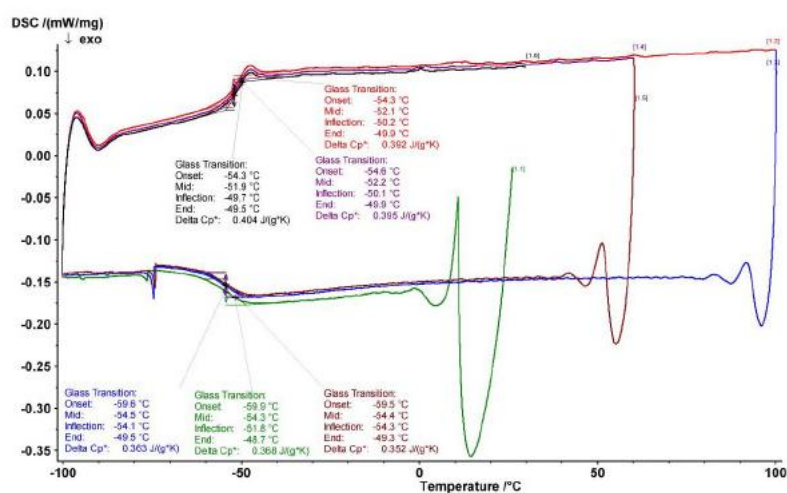


Fig. 10 DSC thermogram of $[C_6mim]_2[MnCl_4]$.

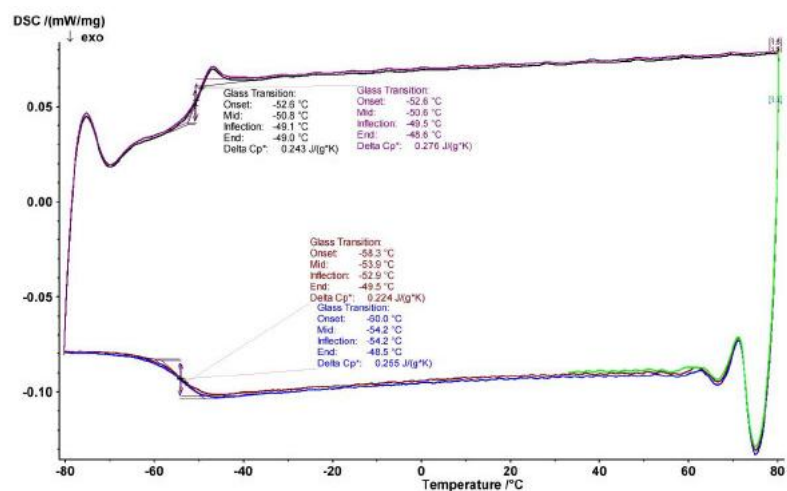


Fig. 11 DSC thermogram of $[C_6mim]_2[MnBr_4]$.

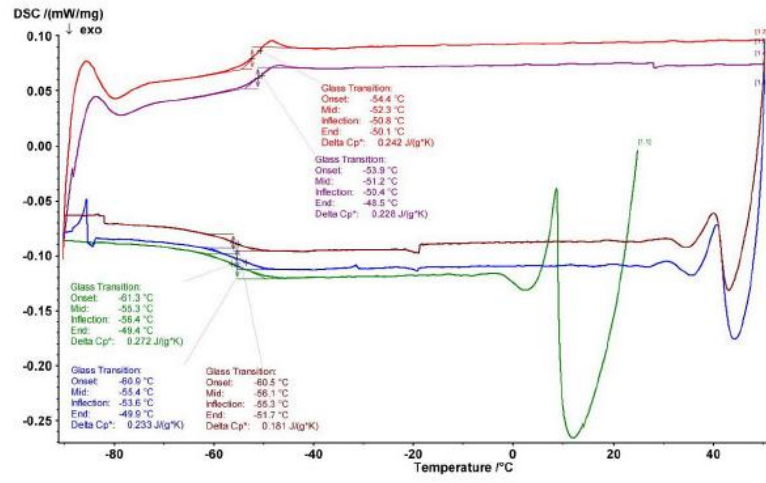


Fig. 12 DSC thermogram of $[C_6mim][Mn(NTf_2)_3]$.

6.2 Raman

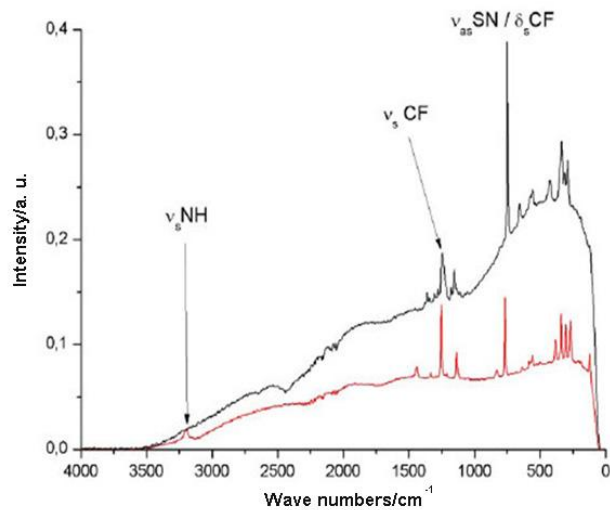


Fig. 13 Raman spectra of Mn(NTf₂)₂ (black) and HNTf₂ (red).

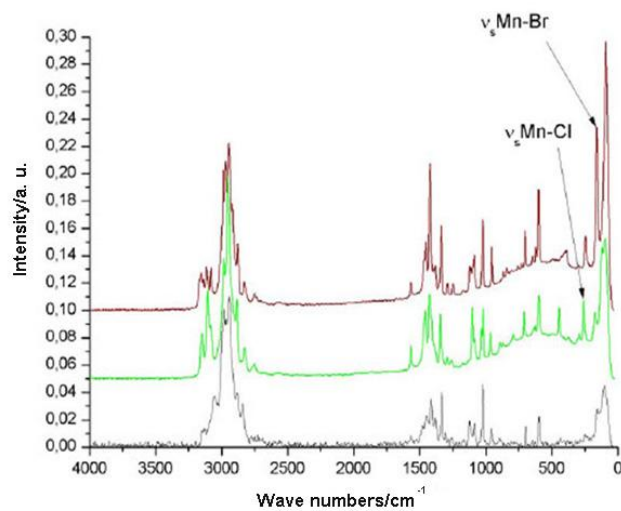


Fig. 14 Raman spectra of C₂mimCl (black), [C₂mim]₂[MnCl₄] (green) and [C₂mim]₂[MnBr₄] (brown).

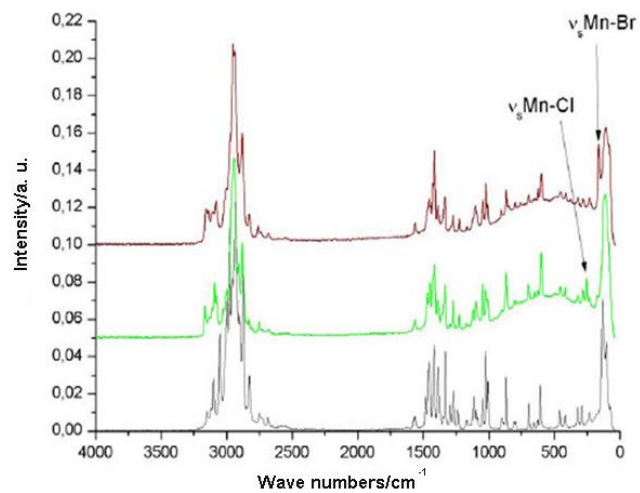


Fig. 15 Raman spectra of C₃mimCl (black), [C₃mim]₂[MnCl₄] (green) and [C₃mim]₂[MnBr₄] (brown).

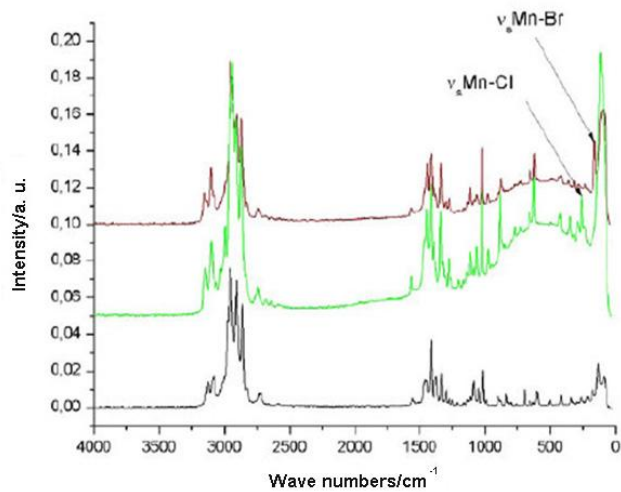


Fig. 16 Raman spectra of C₄mimCl (black), [C₄mim]₂[MnCl₄] (green) and [C₄mim]₂[MnBr₄] (brown).

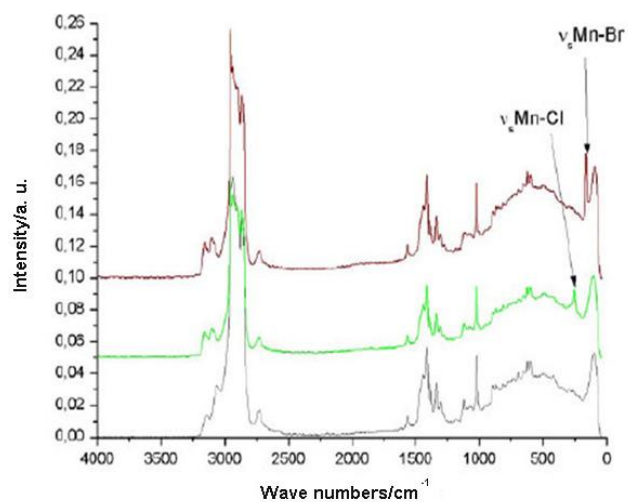


Fig. 17 Raman spectra of C₆mimCl (black), [C₆mim]₂[MnCl₄] (green) and [C₆mim]₂[MnBr₄] (brown).

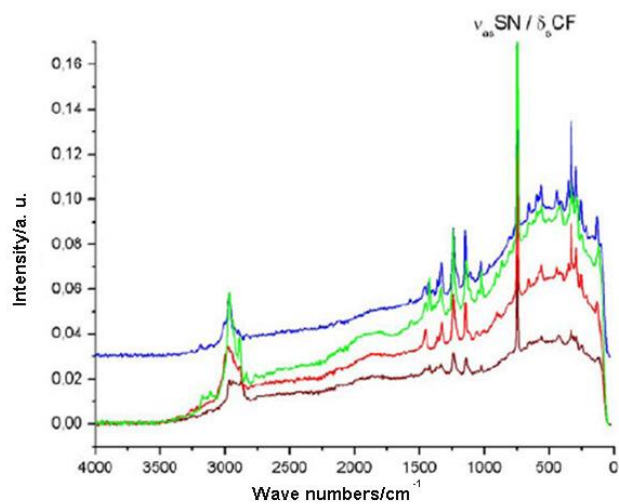


Fig. 18 Raman spectra of [C₂mim][Mn(NTf₂)₃] (blue), [C₃mim][Mn(NTf₂)₃] (green), [C₄mim][Mn(NTf₂)₃] (red) and [C₆mim][Mn(NTf₂)₃] (brown).

6.3 Infrared

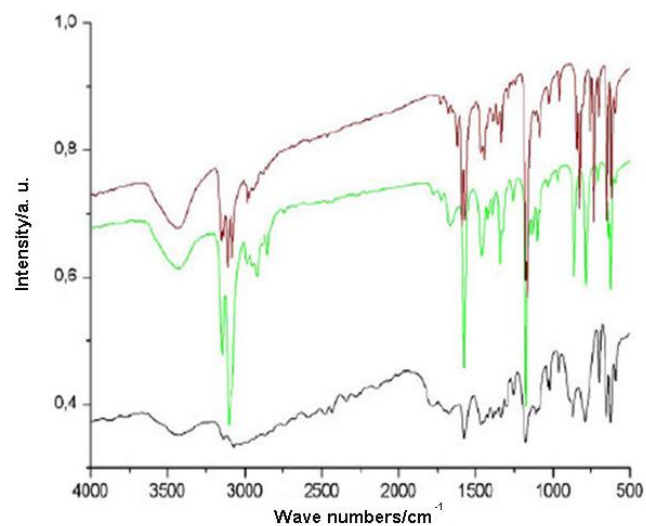


Fig. 19 NIR spectra of C₂mimCl (black), [C₂mim]₂[MnCl₄] (green) and [C₂mim]₂[MnBr₄] (brown).

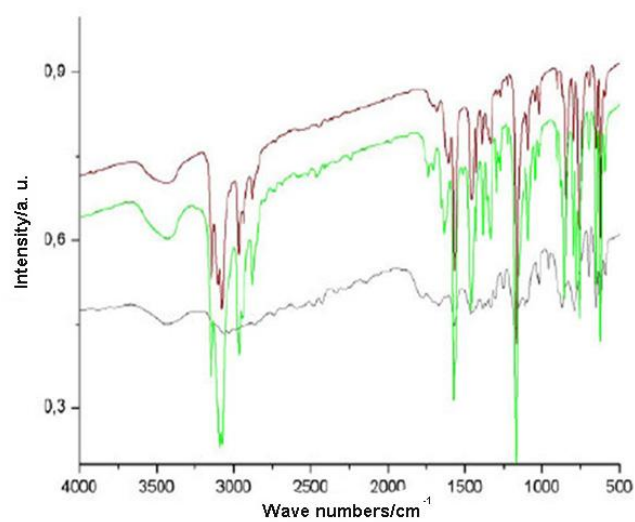


Fig. 20 NIR spectra of C₃mimCl (black), [C₃mim]₂[MnCl₄] (green) and [C₃mim]₂[MnBr₄] (brown).

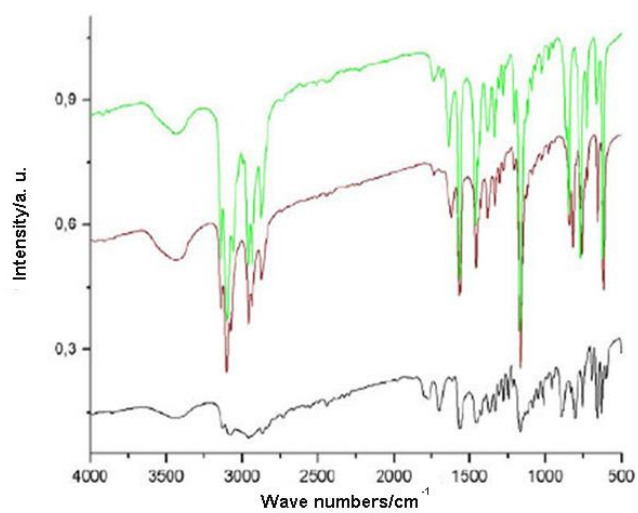


Fig. 21 NIR spectra of C₄mimCl (black), [C₄mim]₂[MnCl₄] (green) and [C₄mim]₂[MnBr₄] (brown).

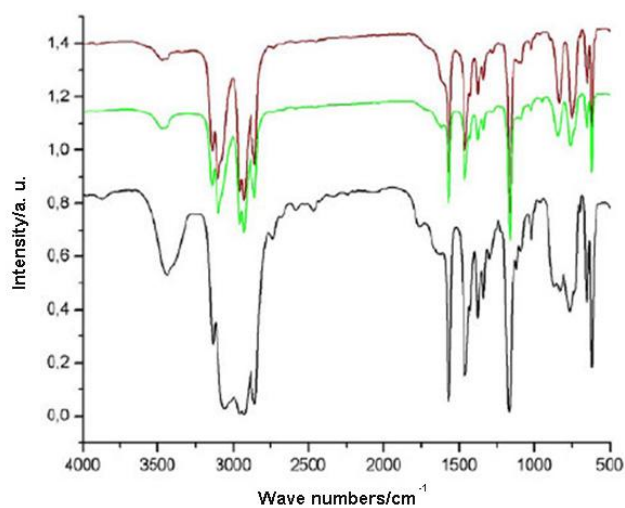


Fig. 22 NIR spectra of C₆mimCl (black), [C₆mim]₂[MnCl₄] (green) and [C₆mim]₂[MnBr₄] (brown).

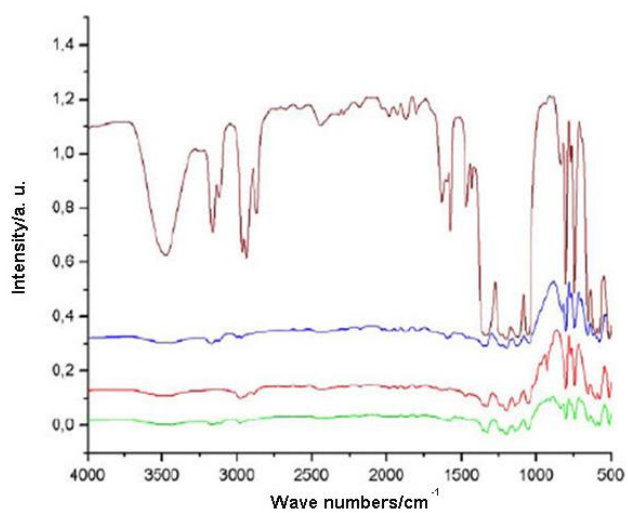


Fig. 23 NIR spectra of $[\text{C}_2\text{mim}][\text{Mn}(\text{NTf}_2)_3]$ (blue), $[\text{C}_3\text{mim}][\text{Mn}(\text{NTf}_2)_3]$ (green), $[\text{C}_4\text{mim}][\text{Mn}(\text{NTf}_2)_3]$ (red) and $[\text{C}_6\text{mim}][\text{Mn}(\text{NTf}_2)_3]$ (brown).

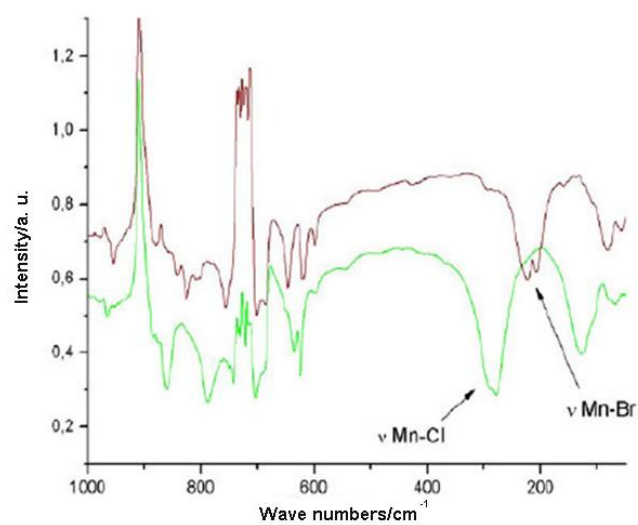


Fig. 24 Far-IR spectra of C_2mimCl (black), $[\text{C}_2\text{mim}]_2[\text{MnCl}_4]$ (green) and $[\text{C}_2\text{mim}]_2[\text{MnBr}_4]$ (brown).

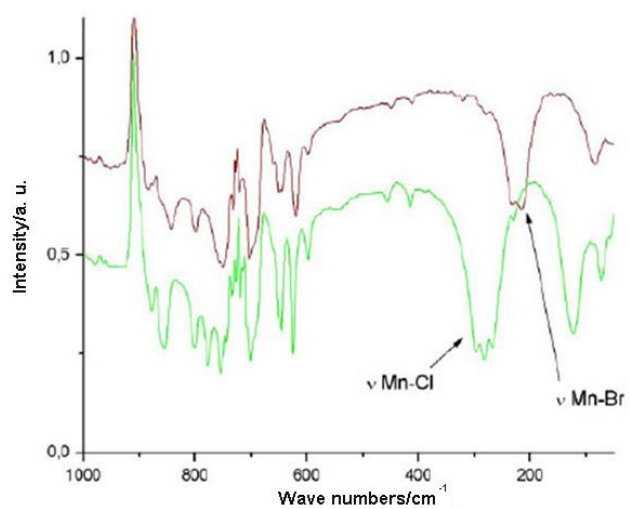


Fig. 25 Far-IR spectra of C₃mimCl (black), [C₃mim]₂[MnCl₄] (green) and [C₃mim]₂[MnBr₄] (brown).

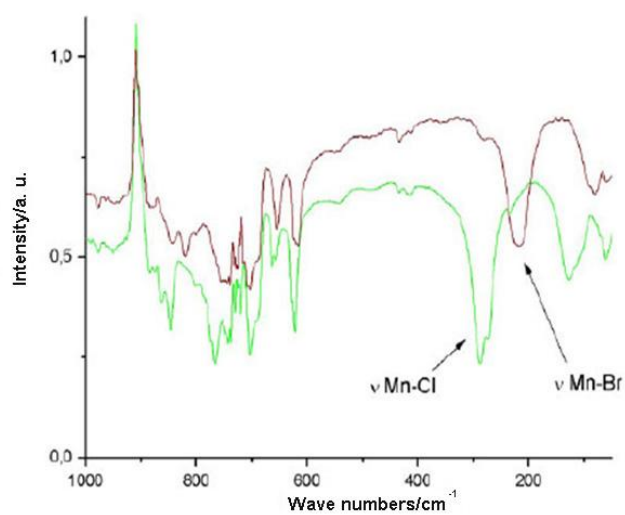


Fig. 26 Far-IR spectra of C₄mimCl (black), [C₄mim]₂[MnCl₄] (green) and [C₄mim]₂[MnBr₄] (brown).

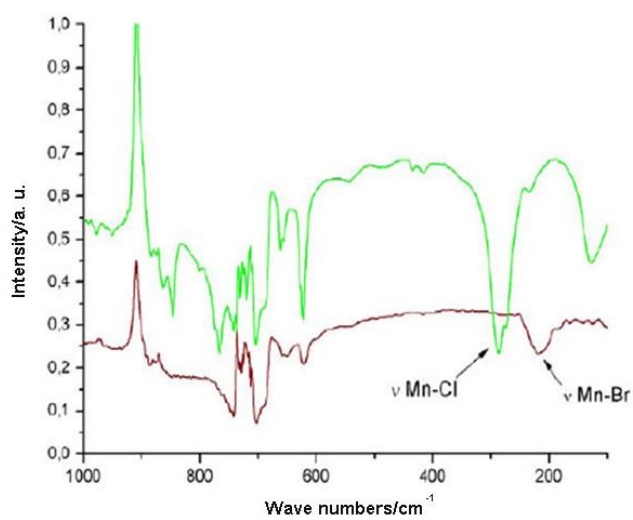


Fig. 27 Far-IR spectra of C_6mimCl (black), $[C_6mim]_2[MnCl_4]$ (green) and $[C_6mim]_2[MnBr_4]$ (brown).

6.4 Photoluminescence

Key

slit	excitation and emission slit width in nm of the detector and beam source of the photospectrometre
sw	sample window; recorded time interval in ms
ex	used excitation wavelength to excite sample
em	emission wavelength; wavelength at which the emission of the excited sample is recorded
fc	flash count; recorded sample emission flashes per time interval in a. u.
id	initial delay; delay in ms between exciting flash and detector opening

slit	1
sw	-
ex	362
em	-
fc	-
id	-

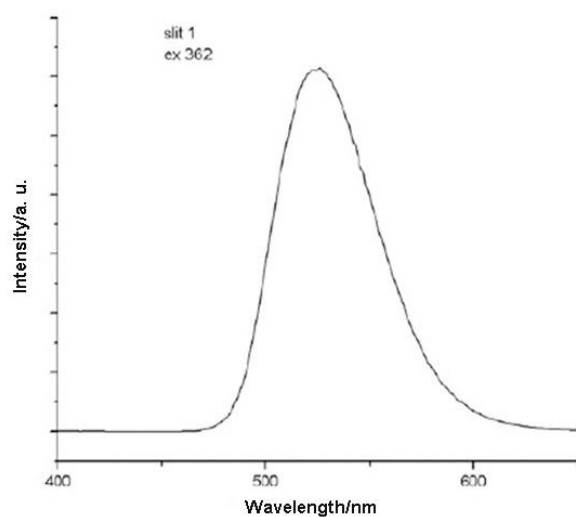


Fig. 28 Fluorescence emission spectrum of $[C_2mim]_2[MnCl_4]$.

slit	2
sw	-
ex	-
em	522.5
fc	-
id	-

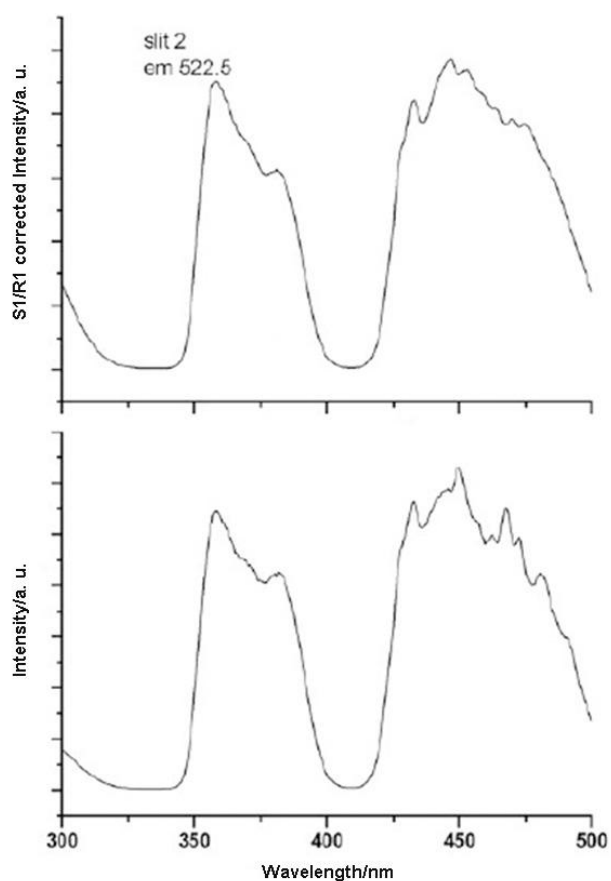


Fig. 29 Fluorescence excitation spectrum of $[C_2mim]_2[MnCl_4]$.

slit	5
sw	2
ex	356
em	-
fc	100
id	0.05

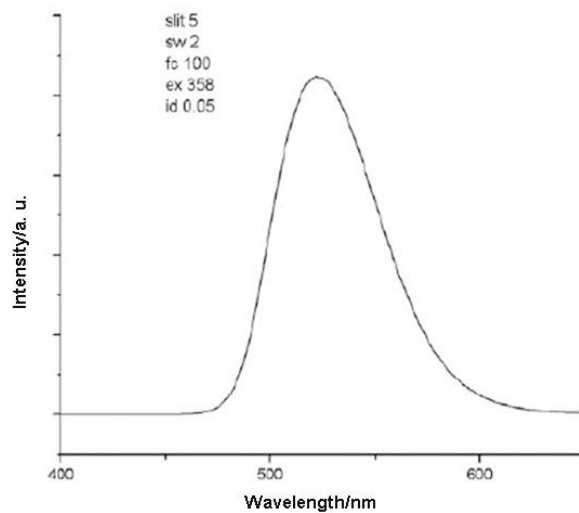


Fig. 30 Phosphorescence emission spectrum of $[\text{C}_2\text{mim}]_2[\text{MnCl}_4]$.

slit	5
sw	2
ex	356
em	-
fc	100
id	0.05

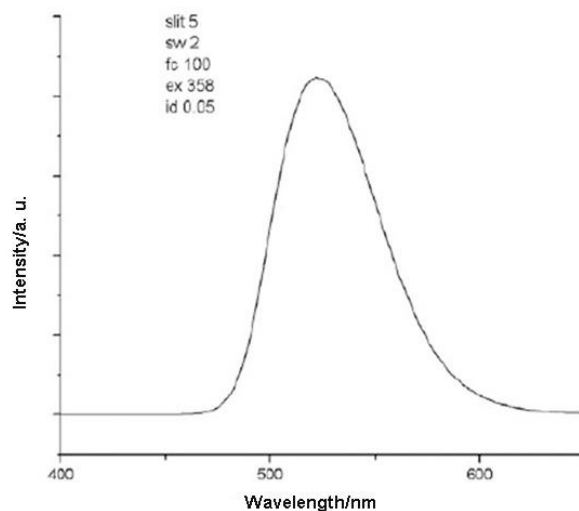


Fig. 31 Phosphorescence excitation spectrum of $[\text{C}_2\text{mim}]_2[\text{MnCl}_4]$.

slit	5
sw	15
ex	361.5
em	522.5
fc	150
id	0.5

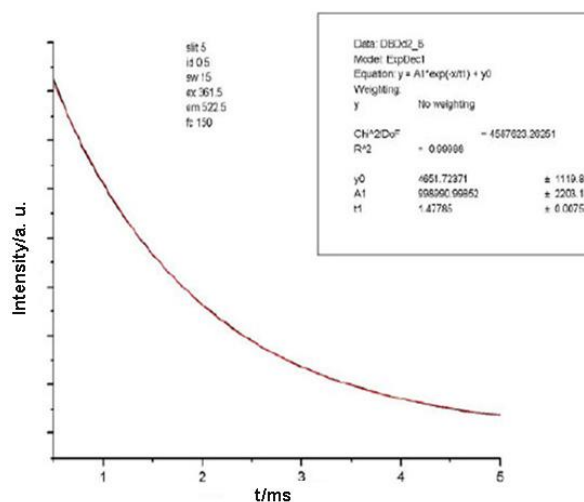


Fig. 32 Emission decay spectrum of $[\text{C}_2\text{mim}]_2[\text{MnCl}_4]$.

slit	2
sw	-
ex	361.5
em	-
fc	-
id	-

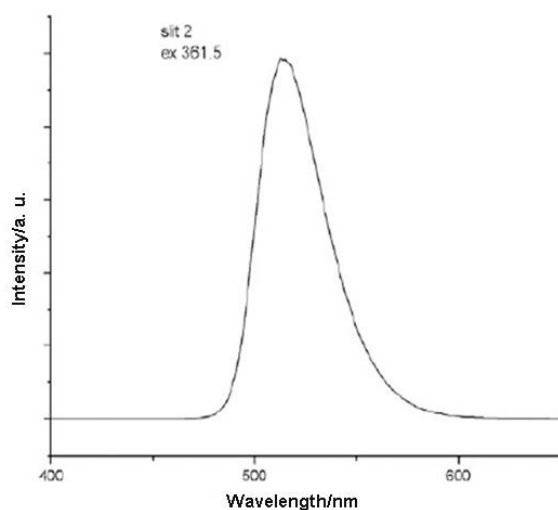


Fig. 33 Fluorescence emission spectrum of $[\text{C}_2\text{mim}]_2[\text{MnBr}_4]$.

slit	1
sw	-
ex	-
em	514
fc	-
id	-

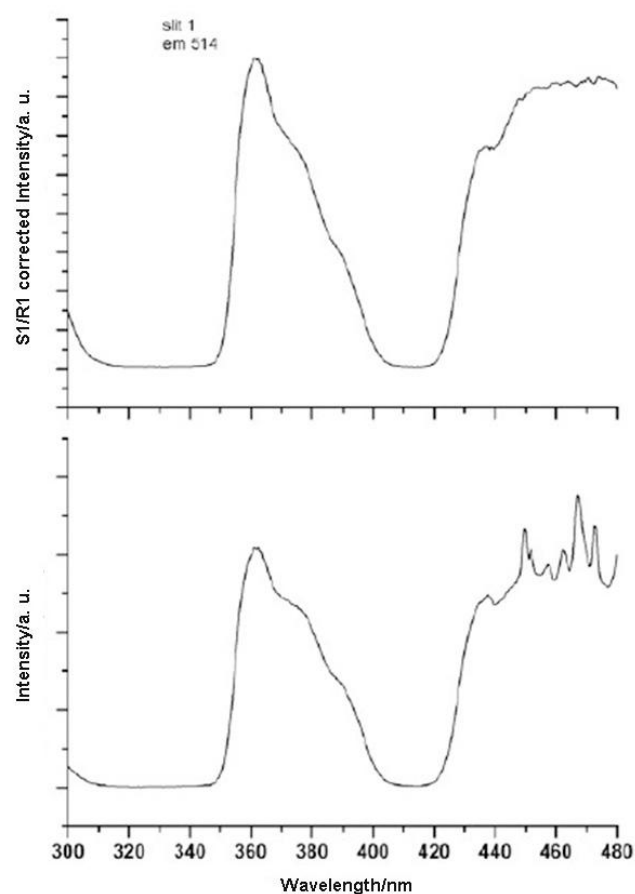


Fig. 34 Fluorescence excitation spectrum of $[\text{C}_2\text{mim}]_2[\text{MnBr}_4]$.

slit	1
sw	10
ex	361.5
em	-
fc	150
id	0.05

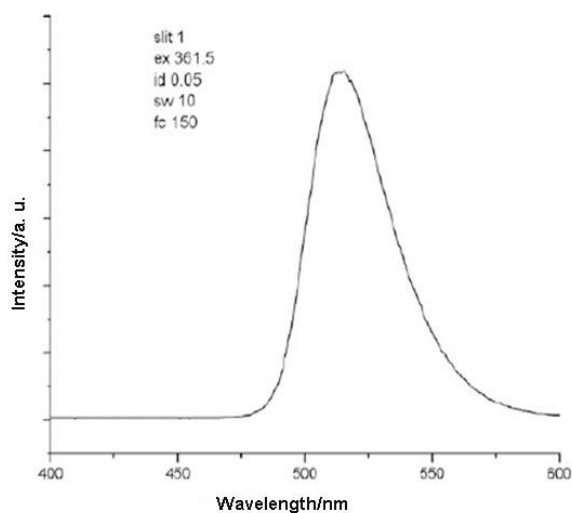


Fig. 35 Phosphorescence emission spectrum of $[C_2mim]_2[MnBr_4]$.

slit	1
sw	10
ex	-
em	514
fc	150
id	0.05

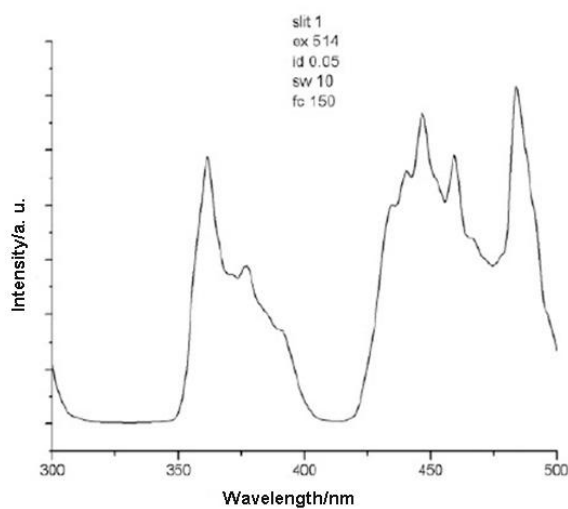


Fig. 36 Phosphorescence excitation spectrum of $[C_2mim]_2[MnBr_4]$.

slit	5
sw	10
ex	361.5
em	514
fc	200
id	0.1

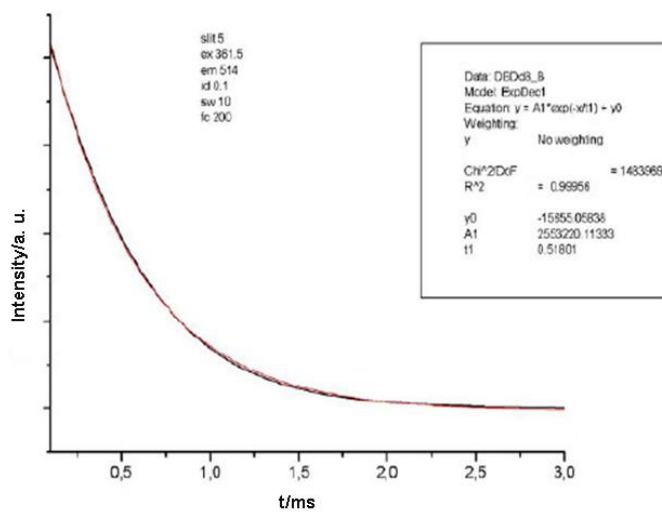


Fig. 37 Emission decay spectrum of $[C_2mim]_2[MnBr_4]$.

slit	3
sw	-
ex	352.5
em	-
fc	-
id	-

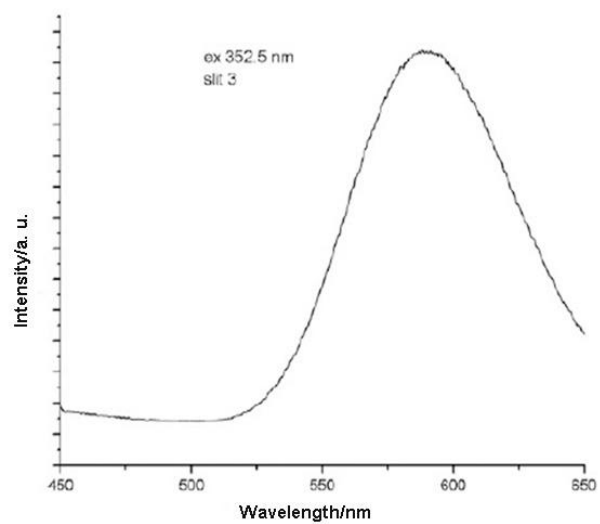


Fig. 38 Fluorescence emission spectrum of $[\text{C}_2\text{mim}][\text{Mn}(\text{NTf}_2)_3]$.

slit	3
sw	-
ex	352.5
em	-
fc	-
id	-

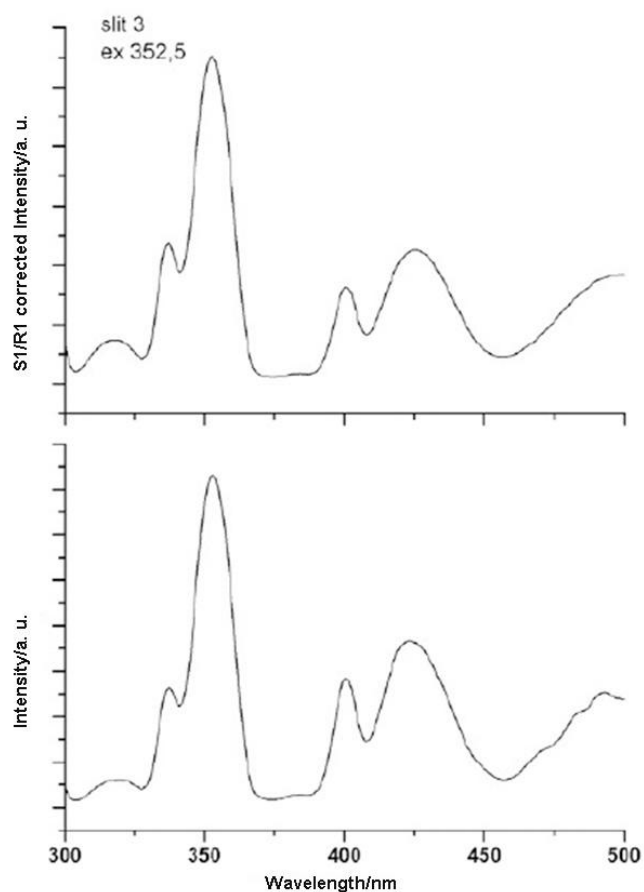


Fig. 39 Fluorescence excitation spectrum of $[\text{C}_2\text{mim}][\text{Mn}(\text{NTf}_2)_3]$.

slit	3
sw	-
ex	352.5
em	-
fc	-
id	-

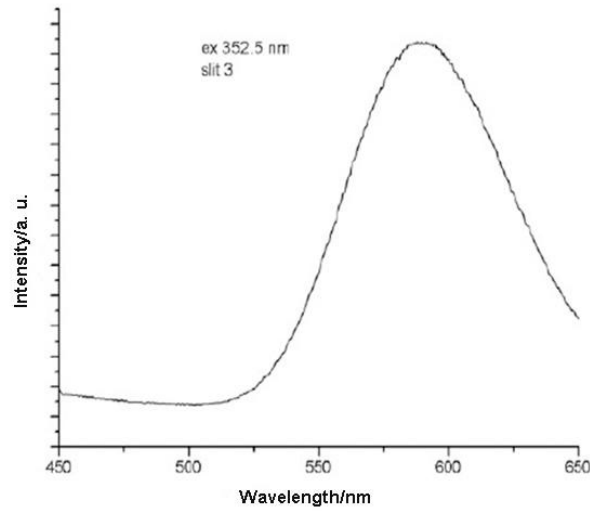


Fig. 40 Phosphorescence emission spectrum of $[C_2mim][Mn(NTf_2)_3]$.

slit	7
sw	5
ex	-
em	589
fc	500
id	0.05

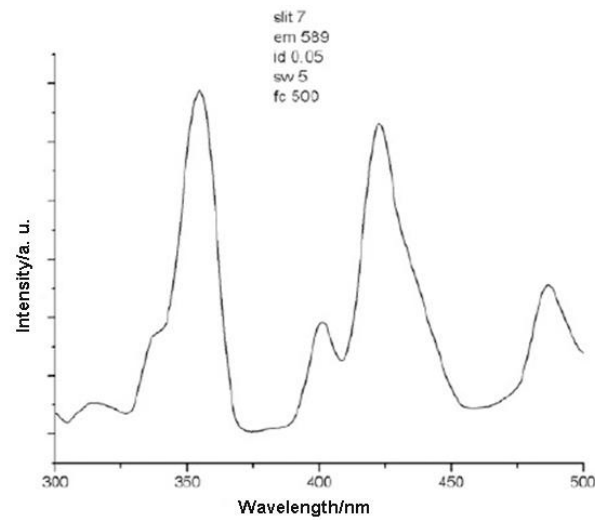


Fig. 41 Phosphorescence excitation spectrum of $[C_2mim][Mn(NTf_2)_3]$.

slit	7
sw	150
ex	352.5
em	589
fc	200
id	10

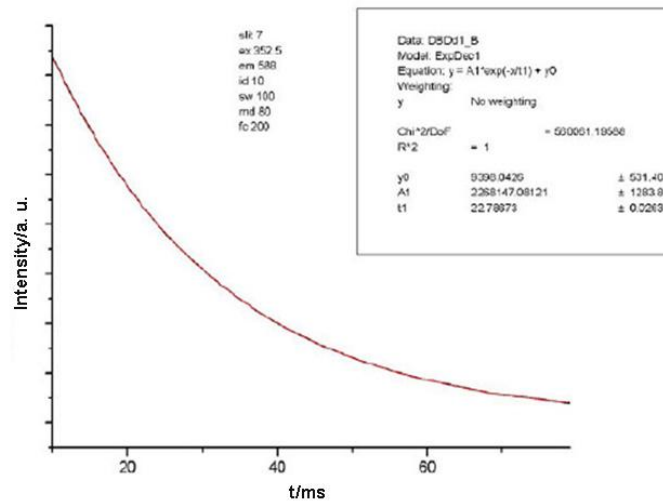


Fig. 42 Emission decay spectrum of $[C_2mim][Mn(NTf_2)_3]$.

slit	1
sw	-
ex	357
em	-
fc	-
id	-

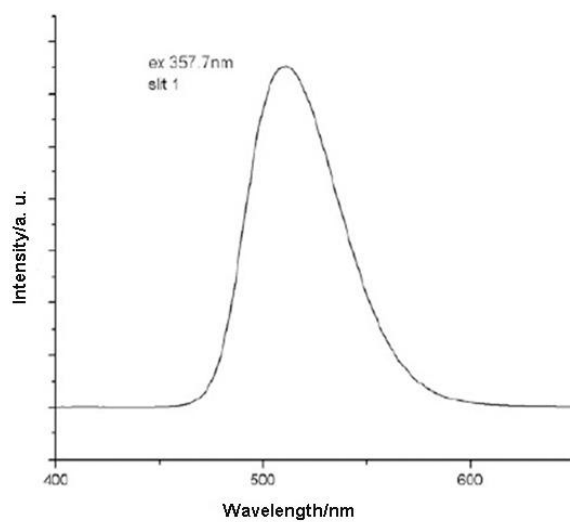


Fig. 43 Fluorescence emission spectrum of $[C_3mim]_2[MnCl_4]$.

slit	1
sw	-
ex	-
em	511
fc	-
id	-

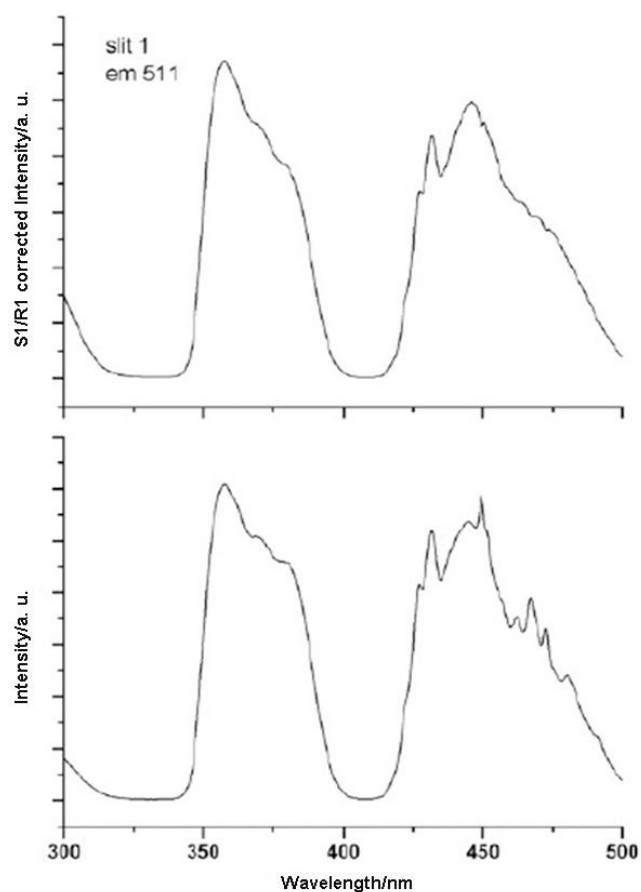


Fig. 44 Fluorescence excitation spectrum of $[C_3mim]_2[MnCl_4]$.

slit	1
sw	5
ex	357.5
em	-
fc	150
id	0.05

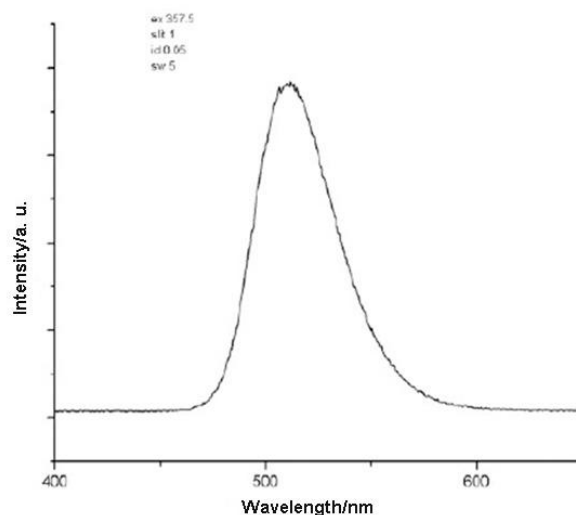


Fig. 45 Phosphorescence emission spectrum of $[C_3mim]_2[MnCl_4]$.

slit	1
sw	10
ex	-
em	511
fc	150
id	0.05

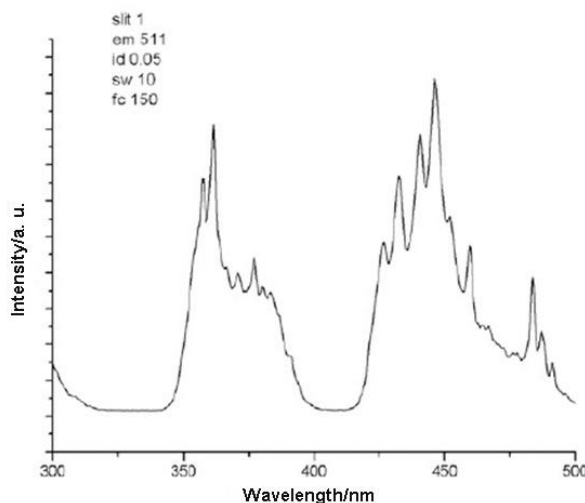


Fig. 46 Phosphorescence excitation spectrum of $[C_3mim]_2[MnCl_4]$.

slit	4
sw	40
ex	357
em	513
fc	200
id	0.5

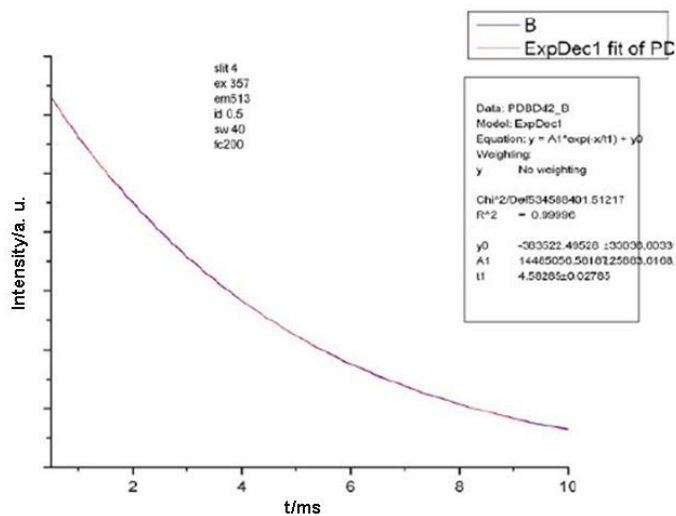


Fig. 47 Emission decay spectrum of $[C_3mim]_2[MnCl_4]$.

slit	1
sw	-
ex	361.5
em	-
fc	-
id	-

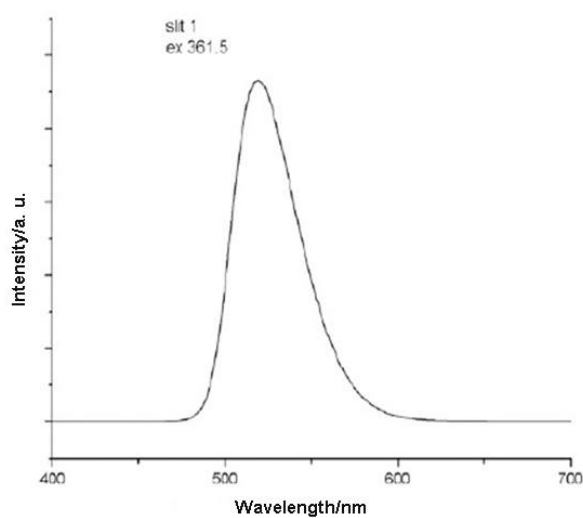


Fig. 48 Fluorescence emission spectrum of $[\text{C}_3\text{mim}]_2[\text{MnBr}_4]$.

slit	1
sw	-
ex	-
em	519
fc	-
id	-

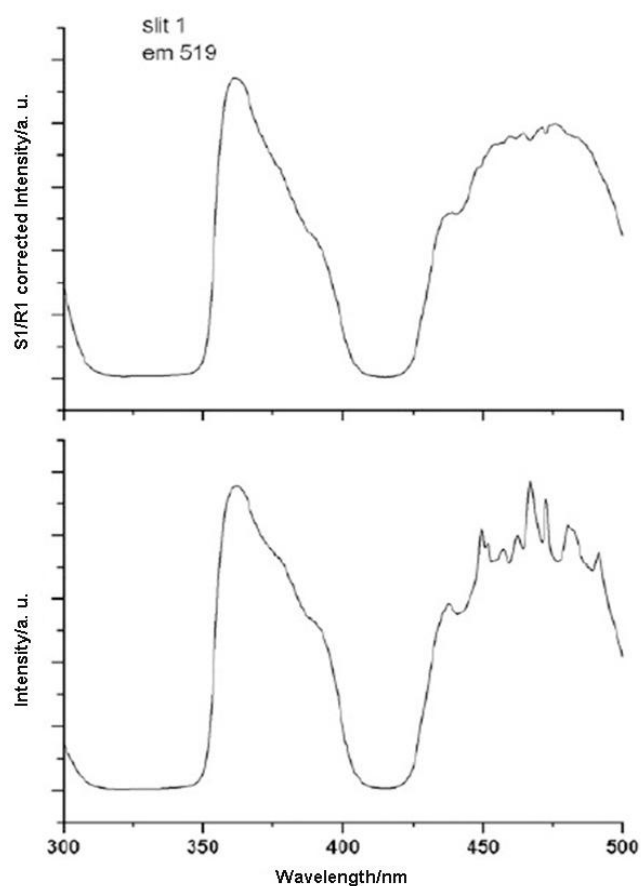


Fig. 49 Fluorescence excitation spectrum of $[\text{C}_3\text{mim}]_2[\text{MnBr}_4]$.

slit	2
sw	10
ex	361.5
em	-
fc	150
id	0.05

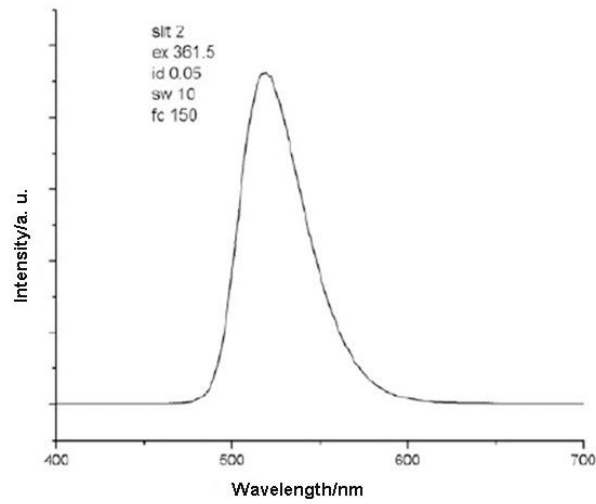


Fig. 50 Phosphorescence emission spectrum of $[C_3mim]_2[MnBr_4]$.

slit	2
sw	10
ex	-
em	519
fc	150
id	0.05

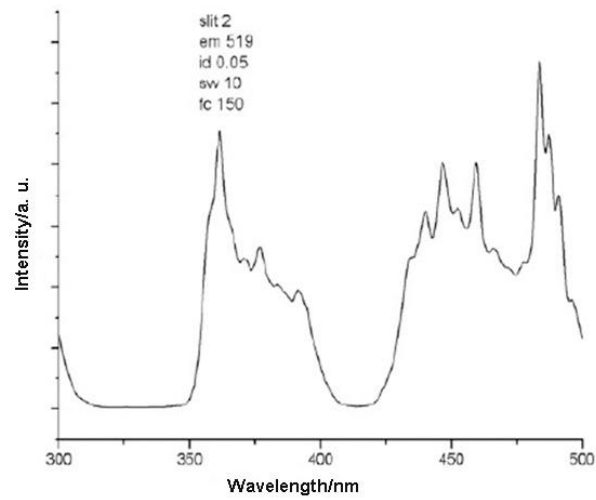


Fig. 51 Phosphorescence excitation spectrum of $[C_3mim]_2[MnBr_4]$.

slit	1
sw	5
ex	362
em	519
fc	150
id	0.01

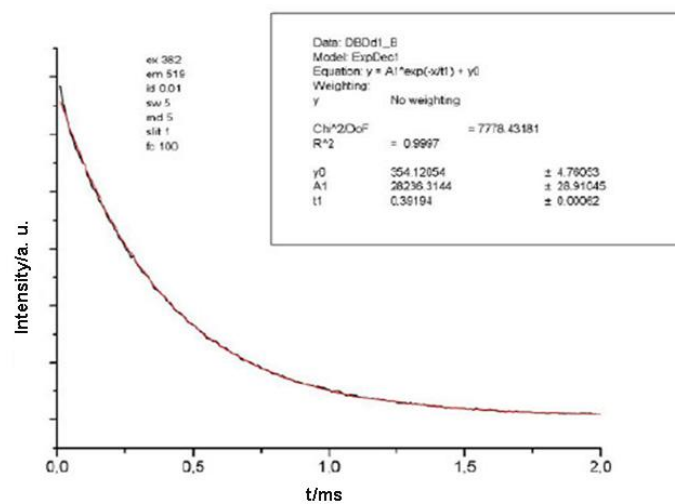


Fig. 52 Emission decay spectrum of $[C_3mim]_2[MnBr_4]$.

slit	2
sw	-
ex	352.5
em	-
fc	-
id	-

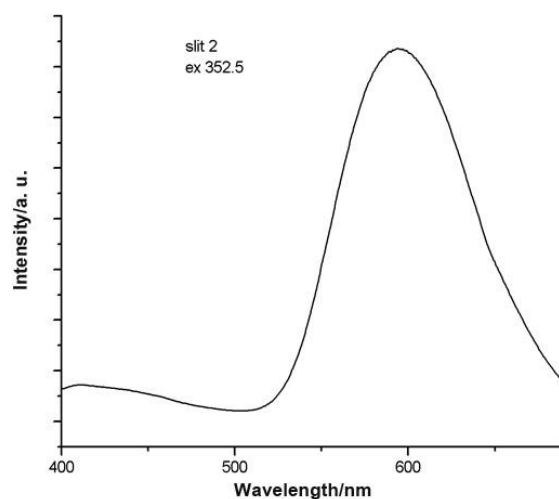


Fig. 53 Fluorescence emission spectrum of $[\text{C}_3\text{mim}][\text{Mn}(\text{NTf}_2)_3]$.

slit	2
sw	-
ex	594
em	-
fc	-
id	-

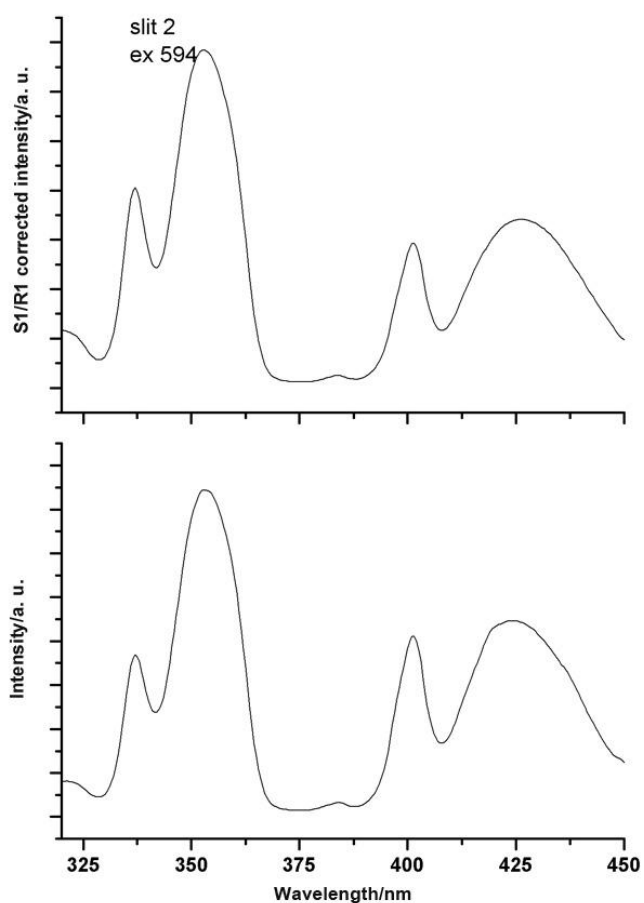


Fig. 54 Fluorescence excitation spectrum of $[\text{C}_3\text{mim}][\text{Mn}(\text{NTf}_2)_3]$.

slit	7
sw	10
ex	353
em	-
fc	500
id	0.05

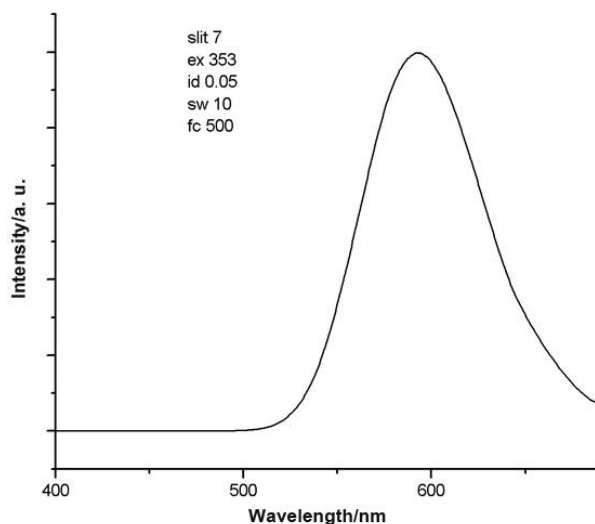


Fig. 55 Phosphorescence emission spectrum of $[C_3mim][Mn(NTf_2)_3]$.

slit	7
sw	10
ex	-
em	592
fc	500
id	0.05

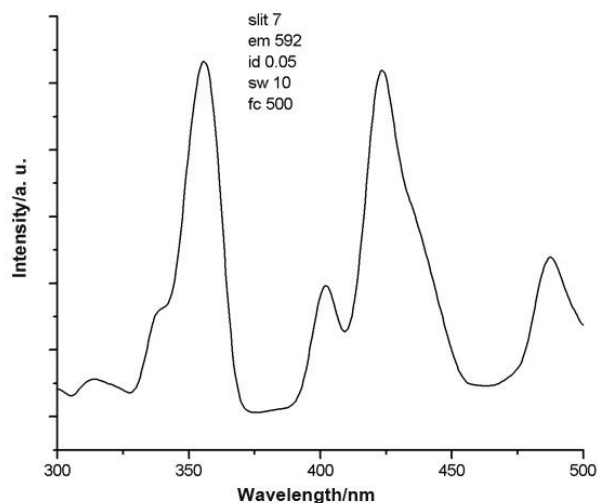


Fig. 56 Phosphorescence excitation spectrum of $[C_3mim][Mn(NTf_2)_3]$.

slit	7
sw	120
ex	355
em	594
fc	400
id	1

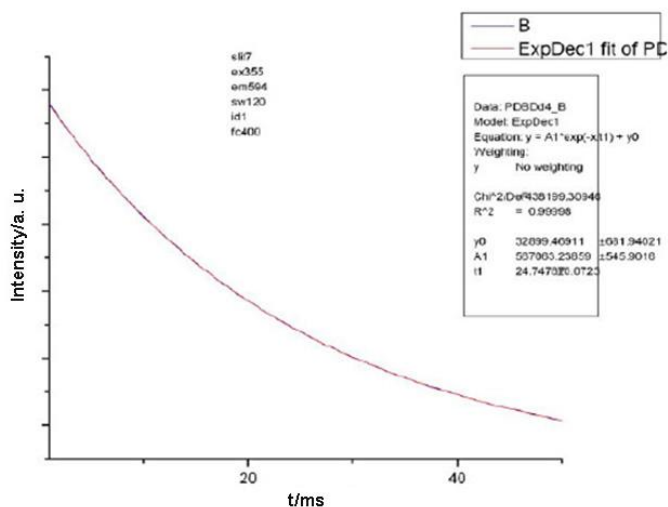


Fig. 57 Emission decay spectrum of $[C_3mim][Mn(NTf_2)_3]$.

slit	1
sw	-
ex	361.5
em	-
fc	-
id	-

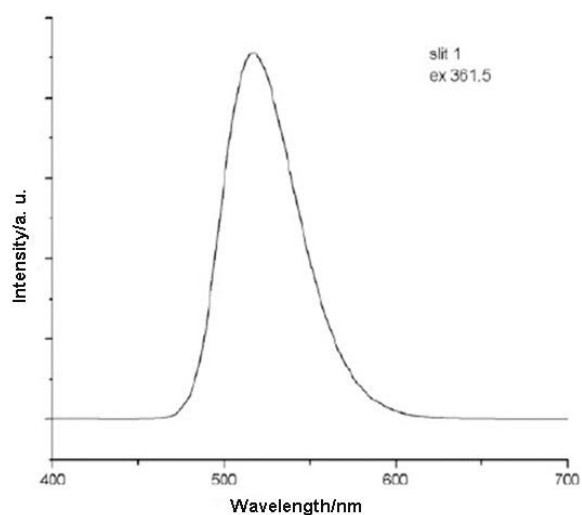


Fig. 58 Fluorescence emission spectrum of $[C_4mim]_2[MnCl_4]$.

slit	1
sw	-
ex	-
em	517
fc	-
id	-

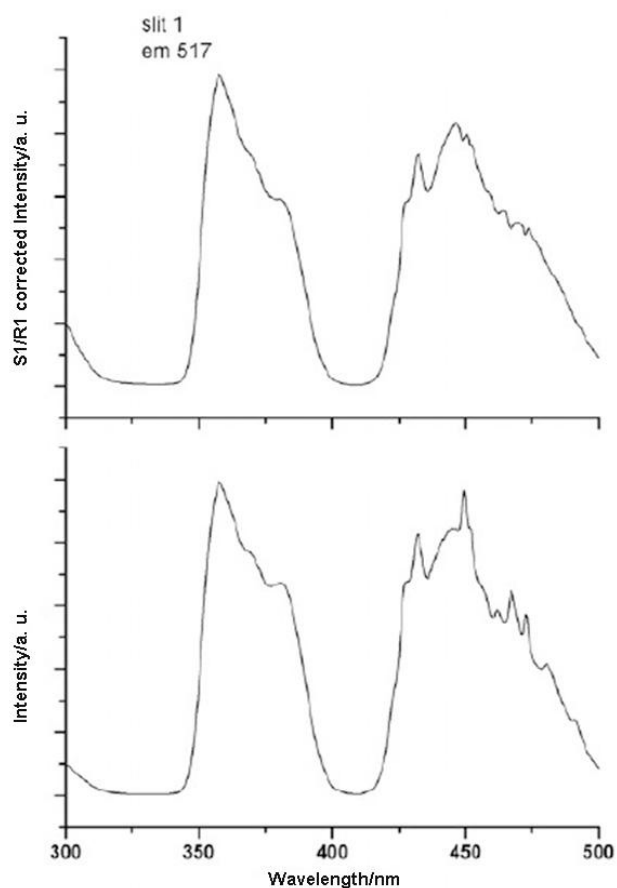


Fig. 59 Fluorescence excitation spectrum of $[C_4mim]_2[MnCl_4]$.

slit	2
sw	4
ex	361.5
em	-
fc	150
id	0.05

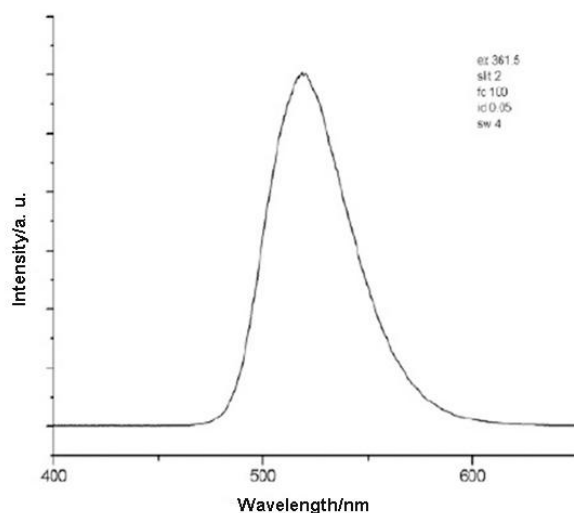


Fig. 60 Phosphorescence emission spectrum of $[C_4mim]_2[MnCl_4]$.

slit	2
sw	20
ex	-
em	517
fc	150
id	0.05

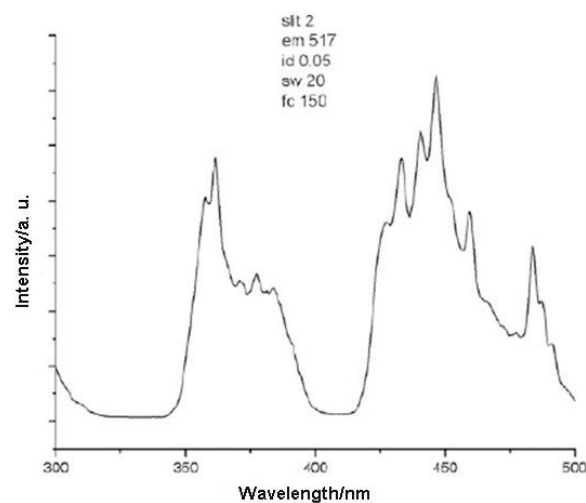


Fig. 61 Phosphorescence excitation spectrum of $[C_4mim]_2[MnCl_4]$.

slit	5
sw	40
ex	361
em	516
fc	300
id	0.5

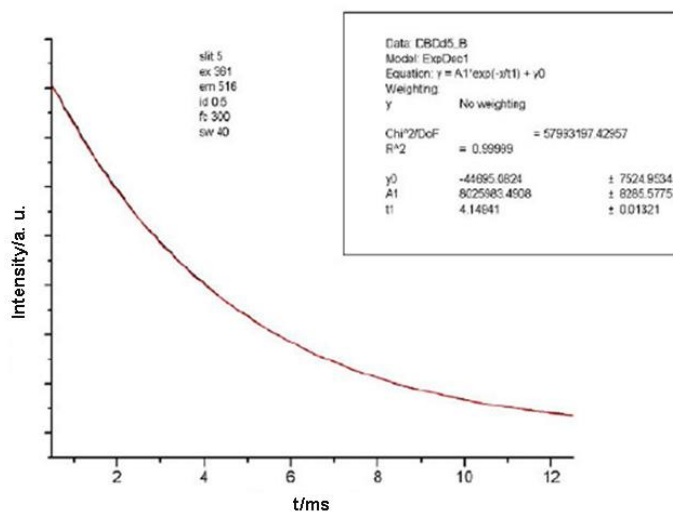


Fig. 62 Emission decay spectrum of $[C_4mim]_2[MnCl_4]$.

slit	2
sw	-
ex	361
em	-
fc	-
id	-

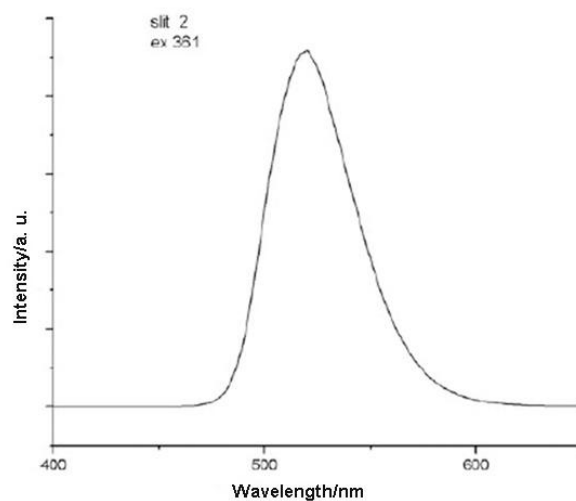


Fig. 63 Fluorescence emission spectrum of $[\text{C}_4\text{mim}]_2[\text{MnBr}_4]$.

slit	1
sw	-
ex	-
em	519.5
fc	-
id	-

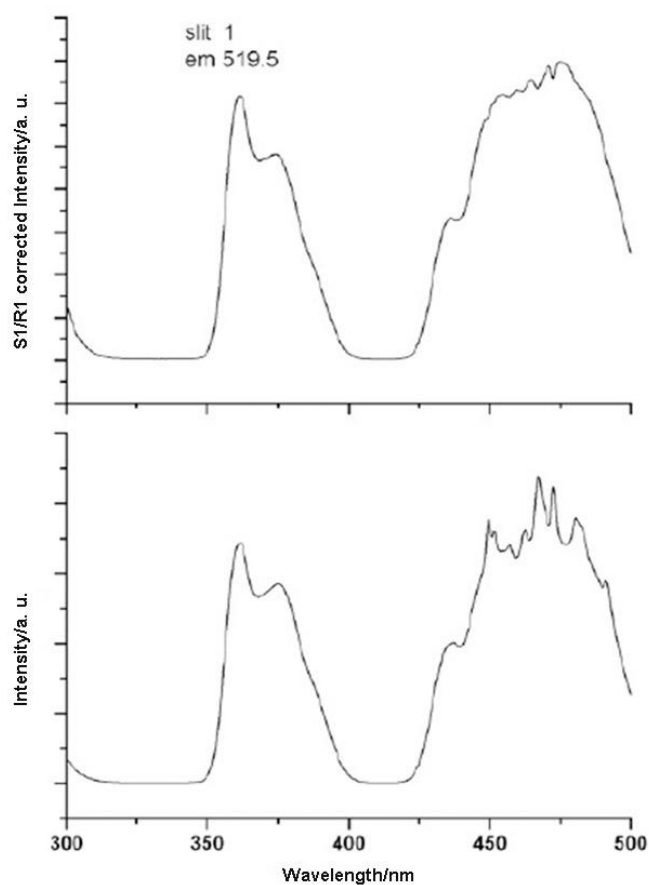


Fig. 64 Fluorescence excitation spectrum of $[\text{C}_4\text{mim}]_2[\text{MnBr}_4]$.

slit	2
sw	4
ex	361.5
em	-
fc	150
id	0.05

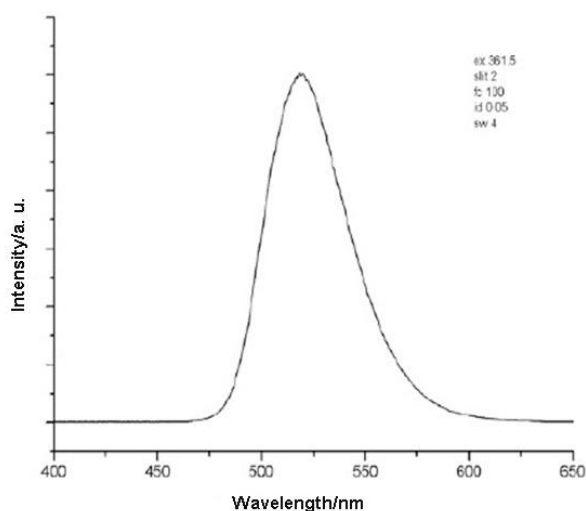


Fig. 65 Phosphorescence emission spectrum of $[C_4mim]_2[MnBr_4]$

slit	3
sw	10
ex	-
em	519.5
fc	150
id	0.05

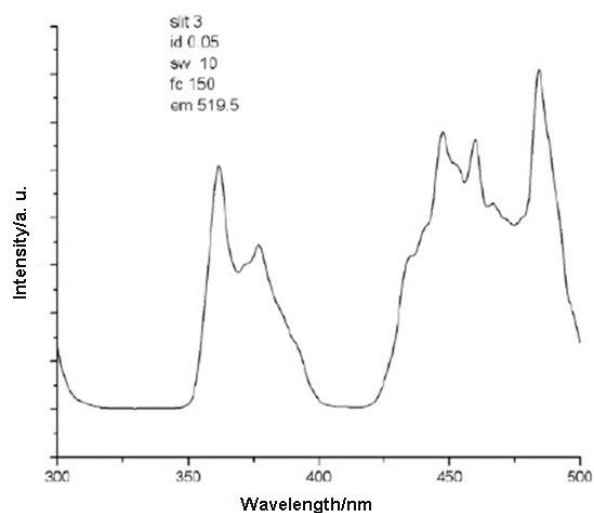


Fig. 66 Phosphorescence excitation spectrum of $[C_4mim]_2[MnBr_4]$.

slit	2
sw	4
ex	361.5
em	519.5
fc	100
id	0.05

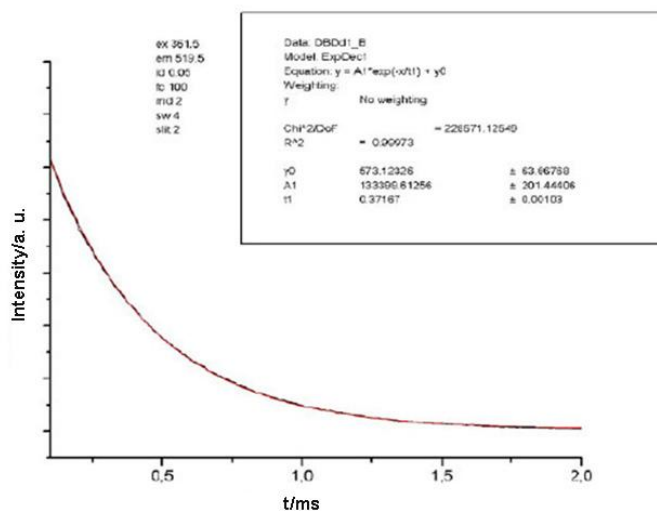


Fig. 67 Emission decay spectrum of $[C_4mim]_2[MnBr_4]$.

slit	2
sw	-
ex	352
em	-
fc	-
id	-

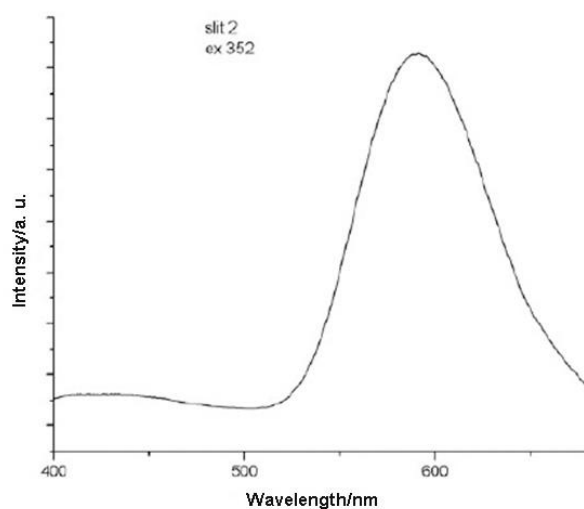


Fig. 68 Fluorescence emission spectrum of $[C_4mim][Mn(NTf_2)_3]$.

slit	2
sw	-
ex	-
em	590.5
fc	-
id	-

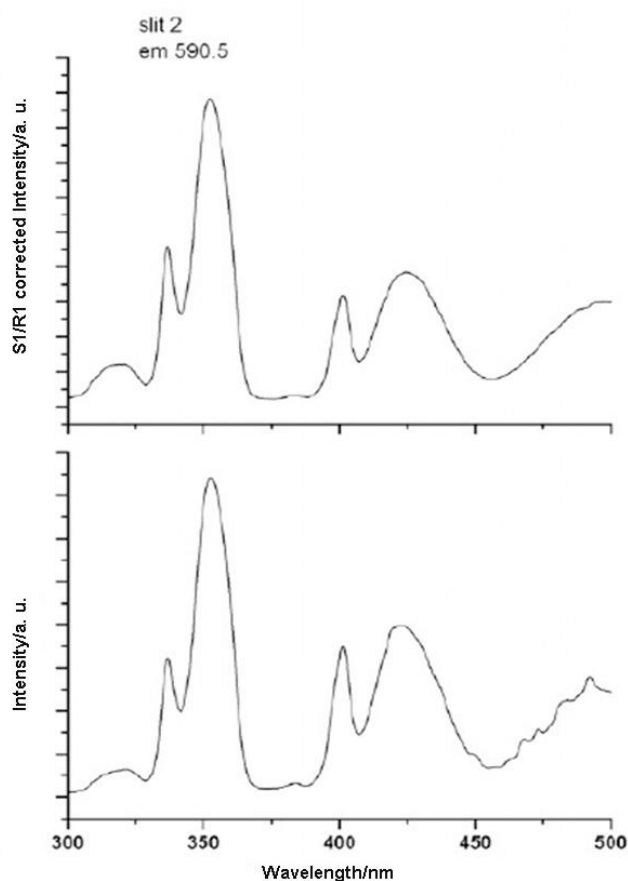


Fig. 69 Fluorescence excitation spectrum of $[C_4mim][Mn(NTf_2)_3]$.

slit	7
sw	20
ex	352.5
em	-
fc	500
id	0.05

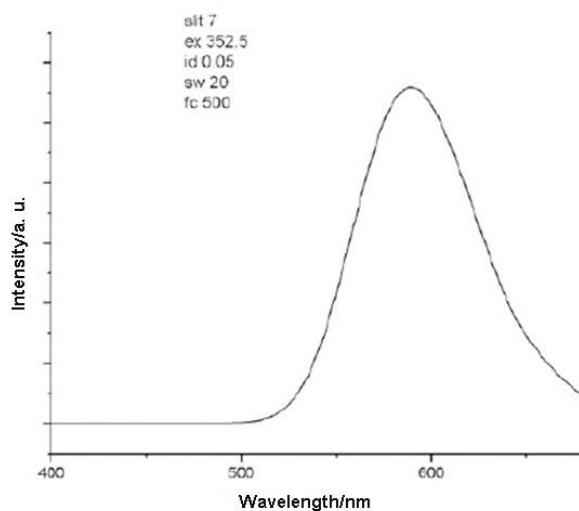


Fig. 70 Phosphorescence emission spectrum of $[C_4mim][Mn(NTf_2)_3]$.

slit	7
sw	20
ex	-
em	589
fc	500
id	0.05

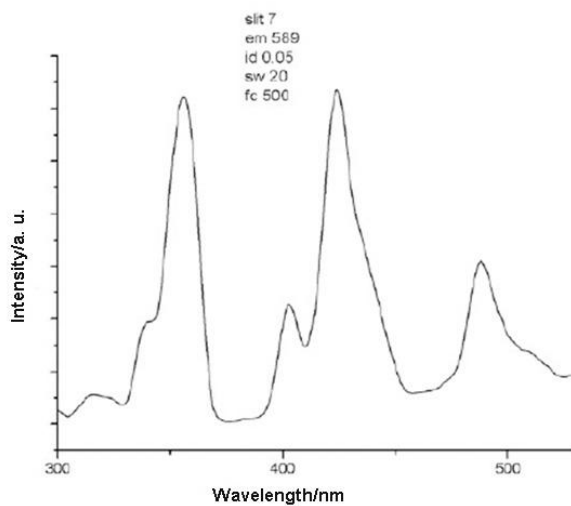


Fig. 71 Phosphorescence excitation spectrum of $[C_4mim][Mn(NTf_2)_3]$.

slit	7
sw	80
ex	356
em	590
fc	300
id	2

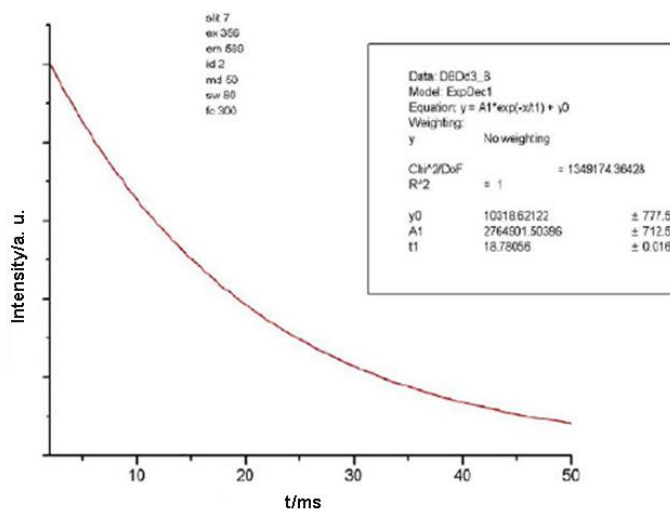


Fig. 72 Emission decay spectrum of $[C_4mim][Mn(NTf_2)_3]$.

6.5 Emission decay spectra at -196°C

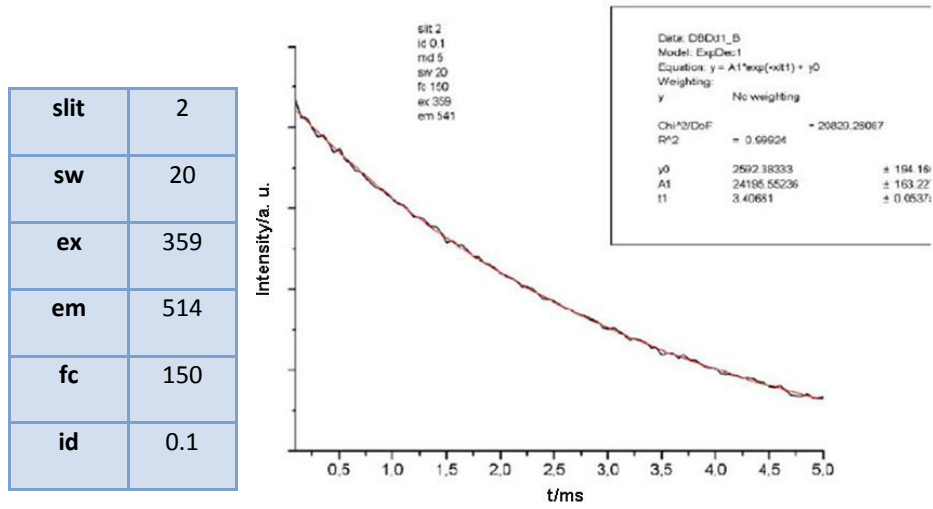


Fig. 73 Emission decay spectrum of $[C_2mim]_2[MnCl_4]$.

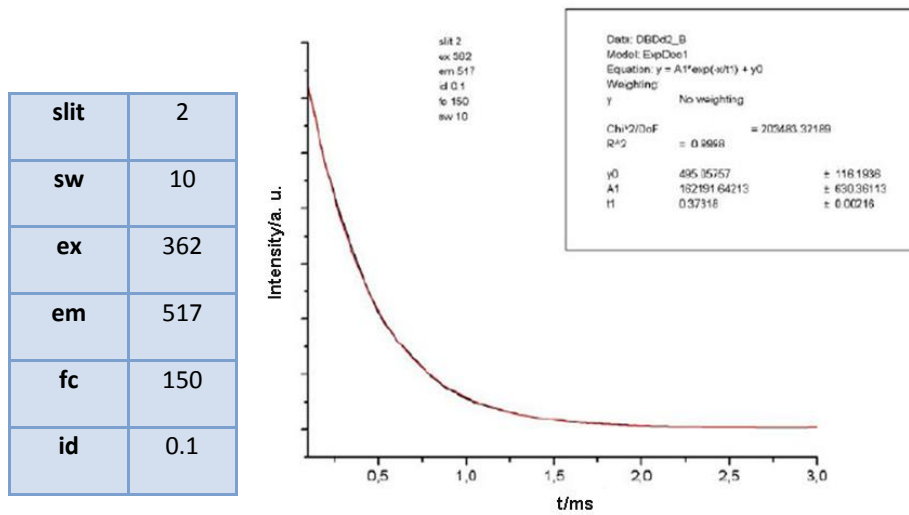


Fig. 74 Emission decay spectrum of $[C_2mim]_2[MnBr_4]$.

slit	7
sw	200
ex	354
em	608
fc	150
id	10

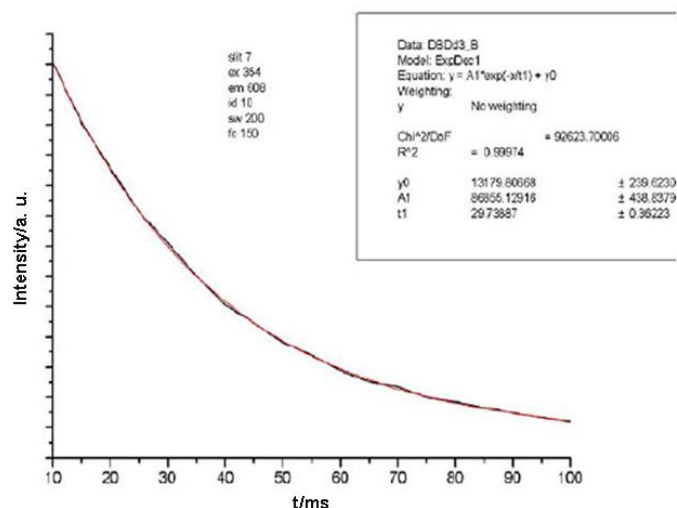


Fig. 74 Emission decay spectrum of $[C_2mim][Mn(NTf_2)_3]$.

slit	5
sw	40
ex	357
em	513
fc	200
id	0.5

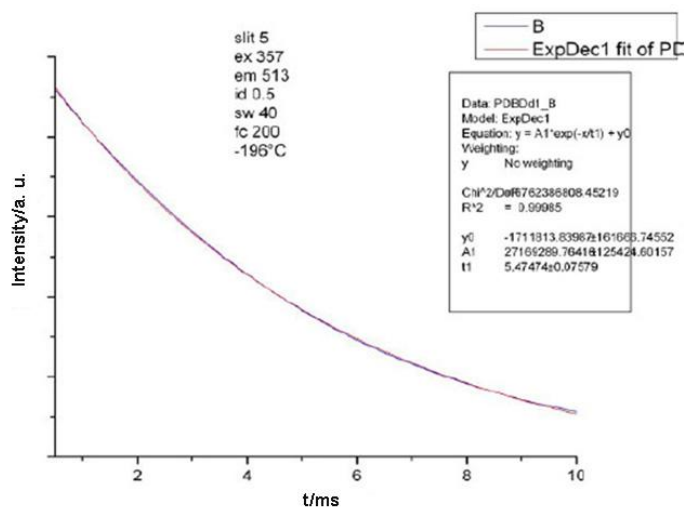


Fig. 75 Emission decay spectrum of $[C_3mim]_2[MnCl_4]$.

slit	2
sw	8
ex	364
em	526
fc	150
id	0.1

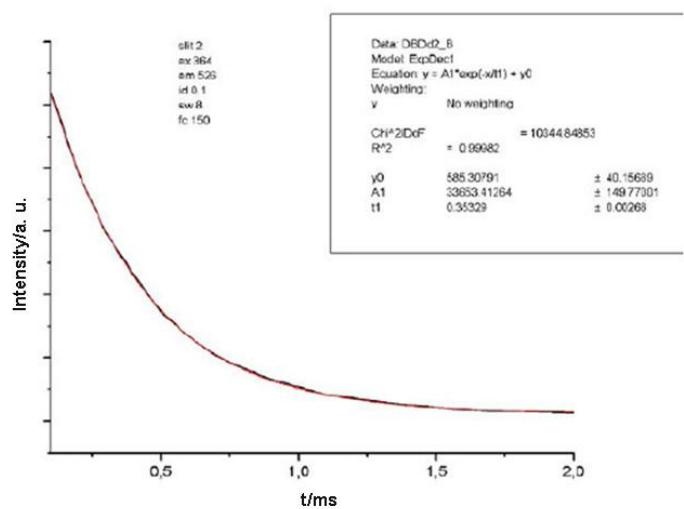


Fig. 76 Emission decay spectrum of $[C_3mim]_2[MnBr_4]$.

slit	7
sw	200
ex	354
em	612
fc	150
id	10

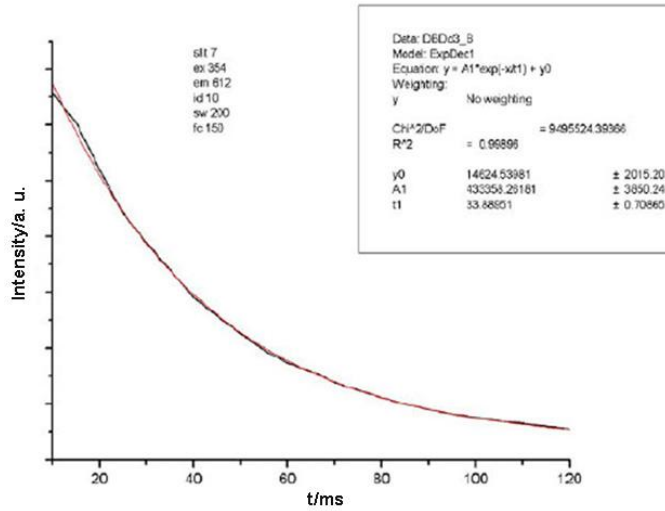


Fig. 77 Emission decay spectrum of $[C_3mim][Mn(NTf_2)_3]$.

slit	3
sw	70
ex	359
em	526
fc	150
id	0.5

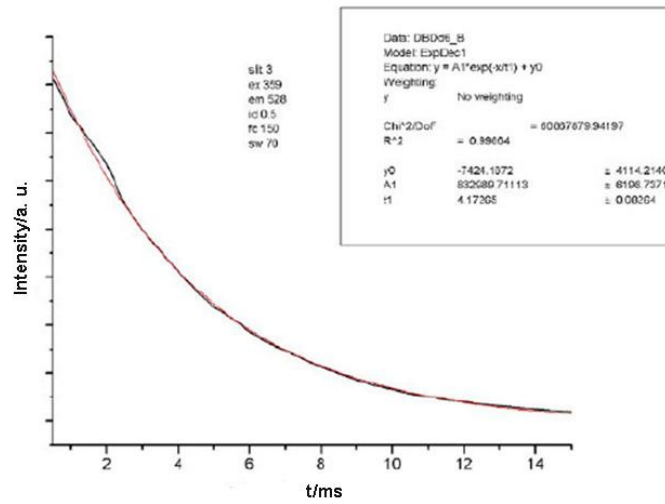


Fig. 78 Emission decay spectrum of $[C_4mim]_2[MnCl_4]$.

slit	3
sw	8
ex	363
em	526
fc	150
id	0.1

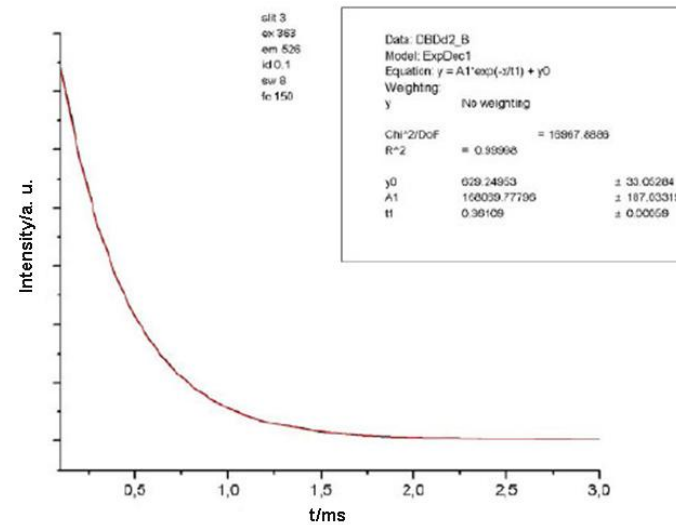


Fig. 79 Emission decay spectrum of $[C_4mim]_2[MnBr_4]$.

slit	3
sw	200
ex	353.5
em	610
fc	150
id	10

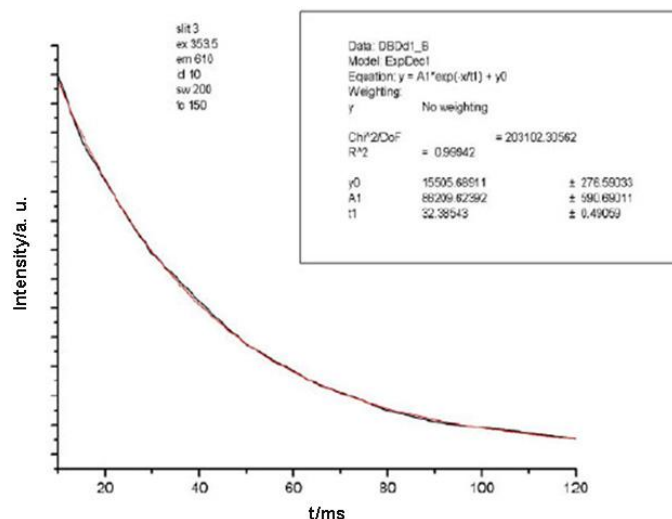


Fig. 80 Emission decay spectrum of $[C_4mim][Mn(NTf_2)_3]$.

slit	3
sw	40
ex	360
em	527
fc	150
id	0.1

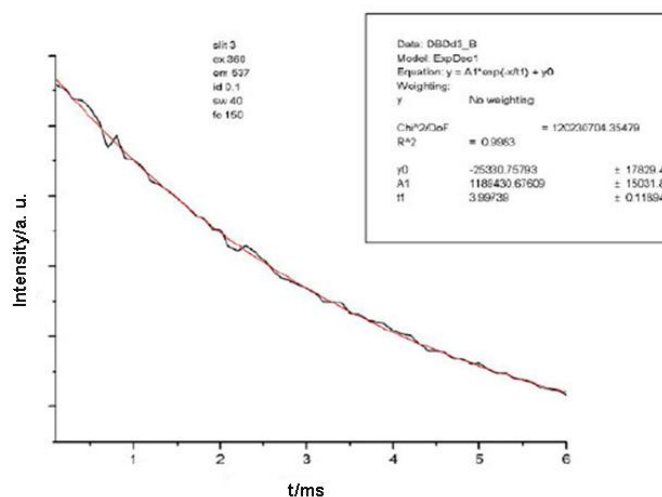


Fig. 81 Emission decay spectrum of $[C_6mim]_2[MnCl_4]$.

slit	2
sw	5
ex	364
em	540
fc	150
id	0.1

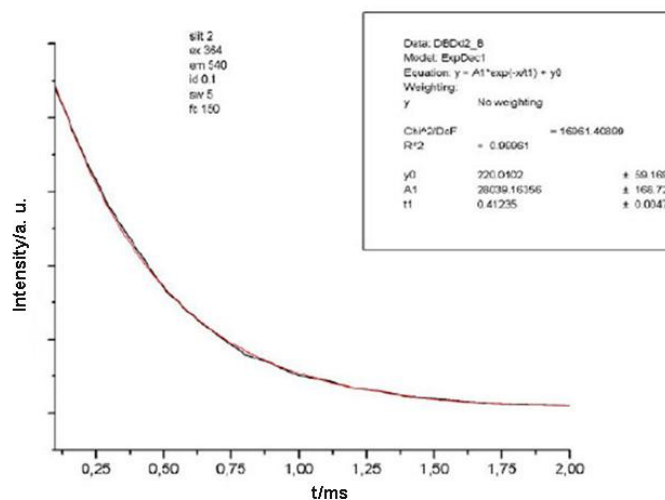


Fig. 82 Emission decay spectrum of $[C_6mim]_2[MnBr_4]$.

slit	5
sw	200
ex	354
em	613.5
fc	150
id	10

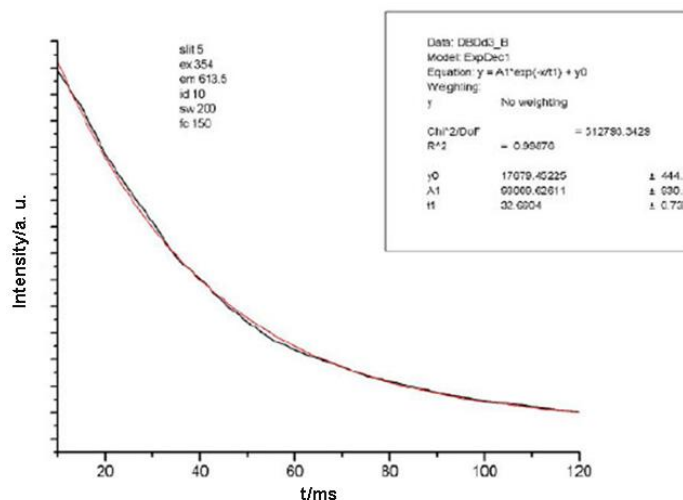


Fig. 83 Emission decay spectrum of $[C_6mim][Mn(NTf_2)_3]$.

slit	7
sw	200
ex	352
em	589
fc	150
id	1

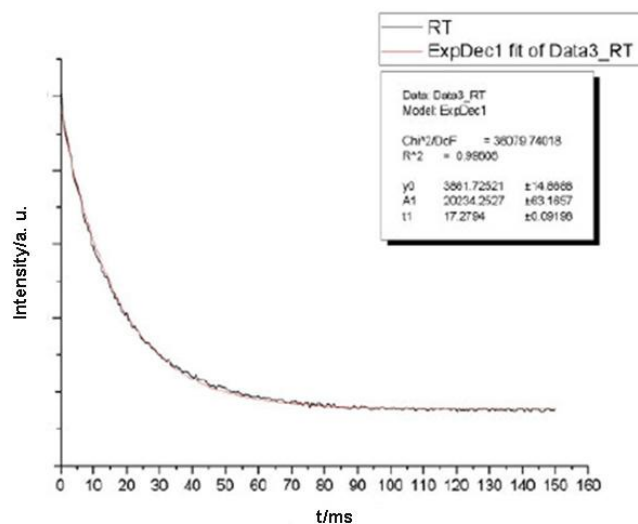


Fig. 84 Emission decay spectrum of $Mn(NTf_2)_2$ at RT.

slit	7
sw	250
ex	353
em	610
fc	150
id	10

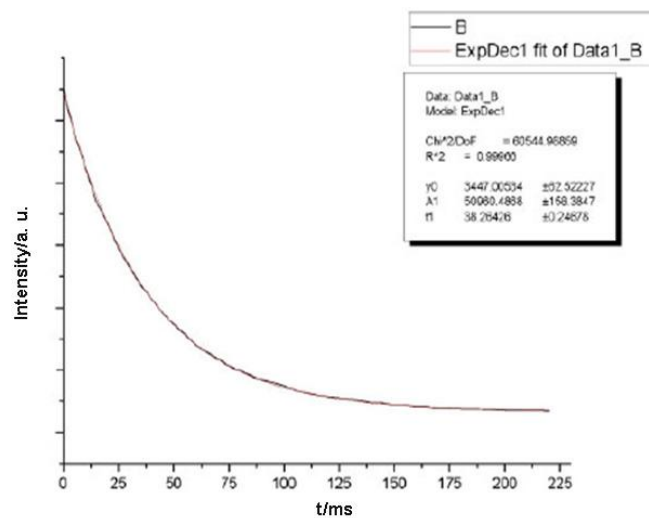


Fig. 85 Emission decay spectrum of $Mn(NTf_2)_2$ at $-196^\circ C$.

6.6 UV/Vis

The UV/Vis spectra were recorded at a scan rate of 600 nm/s.

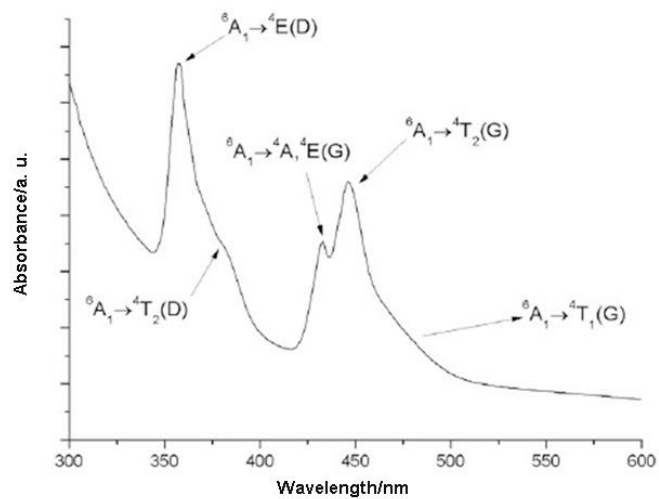


Fig. 86 UV/Vis spectrum of $[\text{C}_2\text{mim}]_2[\text{MnCl}_4]$.

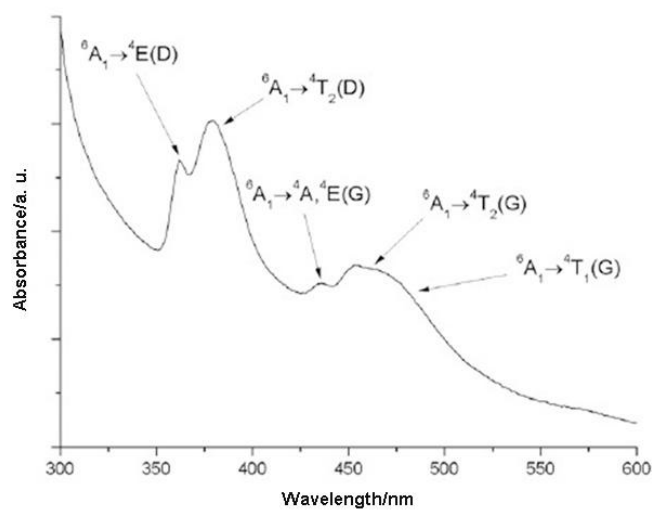


Fig. 87 UV/Vis spectrum of $[\text{C}_2\text{mim}]_2[\text{MnBr}_4]$.

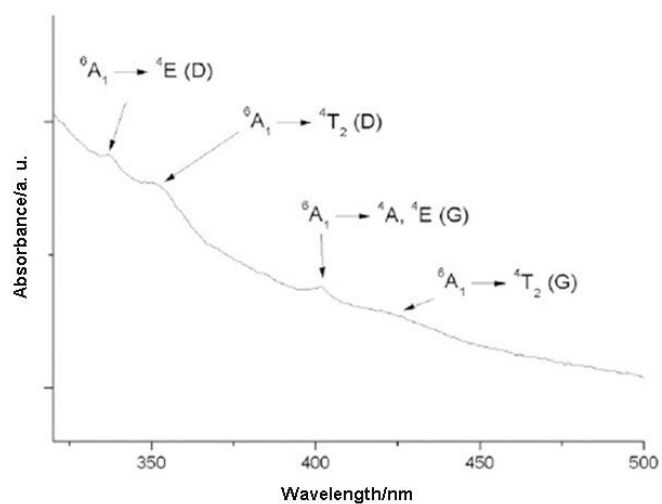


Fig. 88 UV/Vis spectrum of $[\text{C}_2\text{mim}][\text{Mn}(\text{NTf}_2)_3]$.

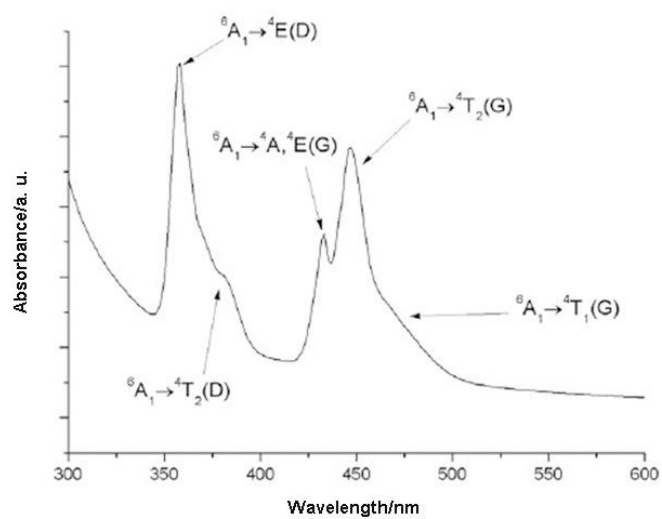


Fig. 89 UV/Vis spectrum of $[\text{C}_3\text{mim}]_2[\text{MnCl}_4]$.

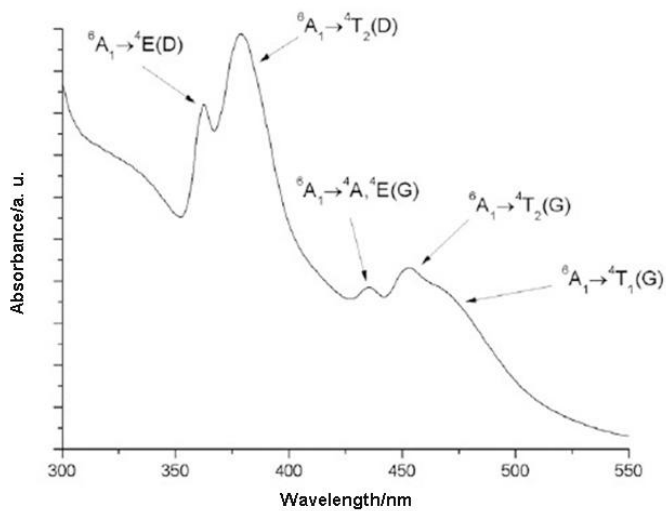


Fig. 90 UV/Vis spectrum of $[\text{C}_3\text{mim}]_2[\text{MnBr}_4]$.

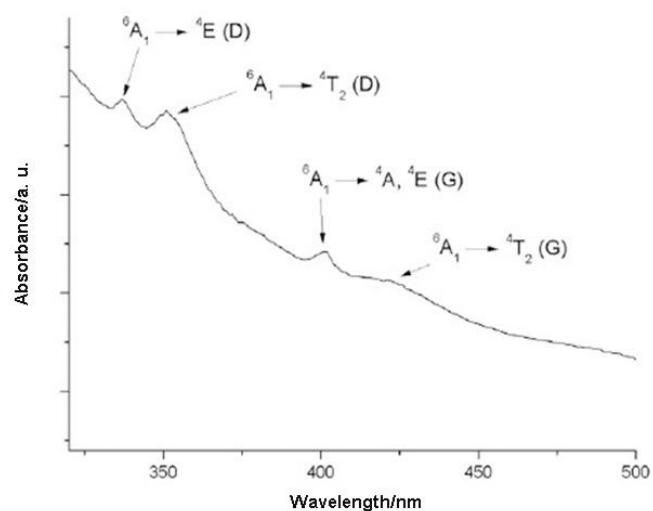


Fig. 91 UV/Vis spectrum of $[\text{C}_3\text{mim}][\text{Mn}(\text{NTf}_2)_3]$.

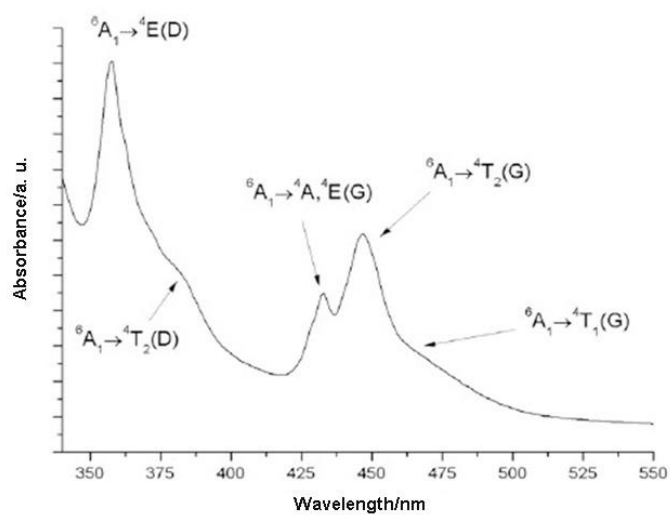


Fig. 92 UV/Vis spectrum of $[\text{C}_4\text{mim}]_2[\text{MnCl}_4]$.

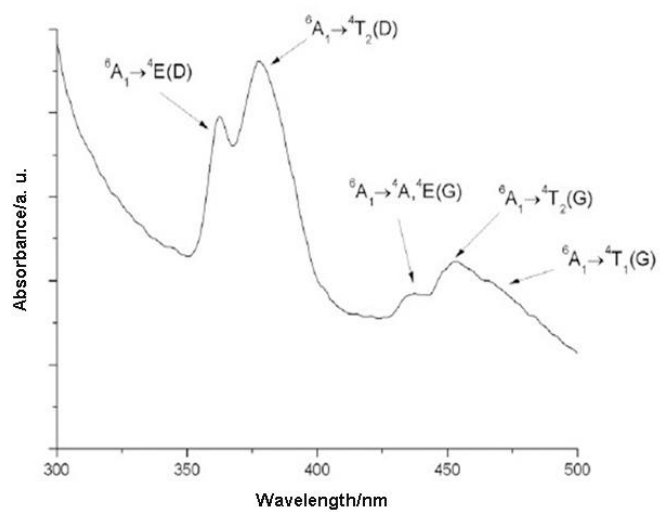


Fig. 93 UV/Vis spectrum of $[\text{C}_4\text{mim}]_2[\text{MnBr}_4]$.

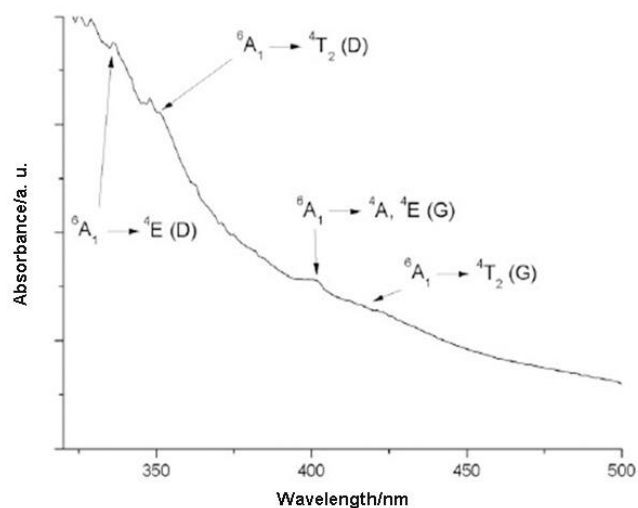


Fig. 94 UV/Vis spectrum of [C₄mim][Mn(NTf₂)₃].

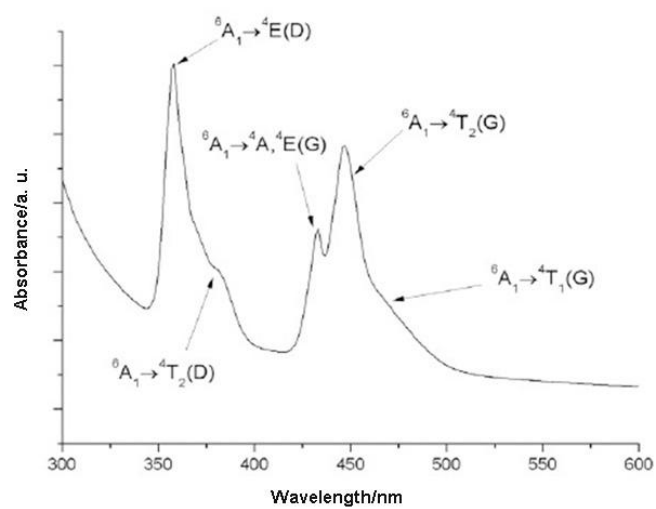


Fig. 95 UV/Vis spectrum of [C₆mim]₂[MnCl₄].

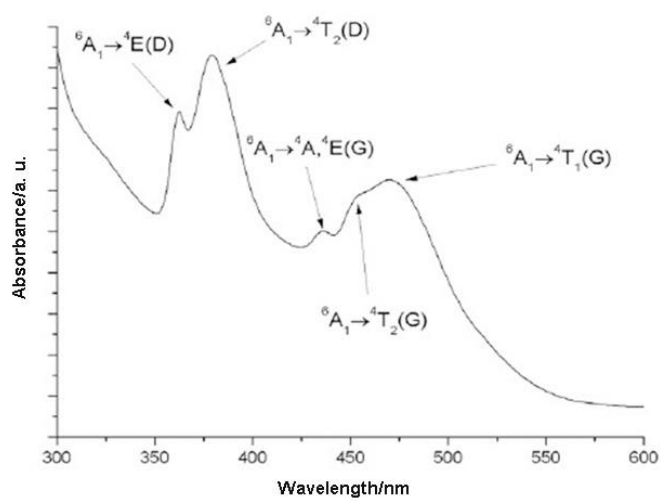


Fig. 96 UV/Vis spectrum of [C₆mim]₂[MnBr₄].

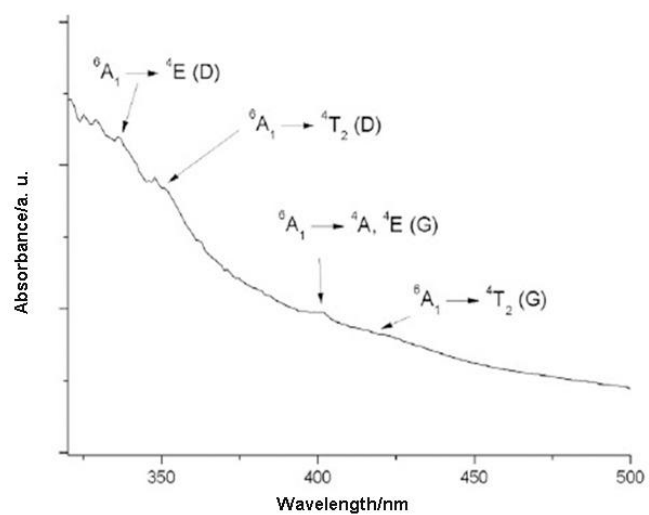


Fig. 97 UV/Vis spectrum of [C₆mim][Mn(NTf₂)₃].

7 Appendix B

The DSC thermogram was recorded at a scan rate of 5 K/min.

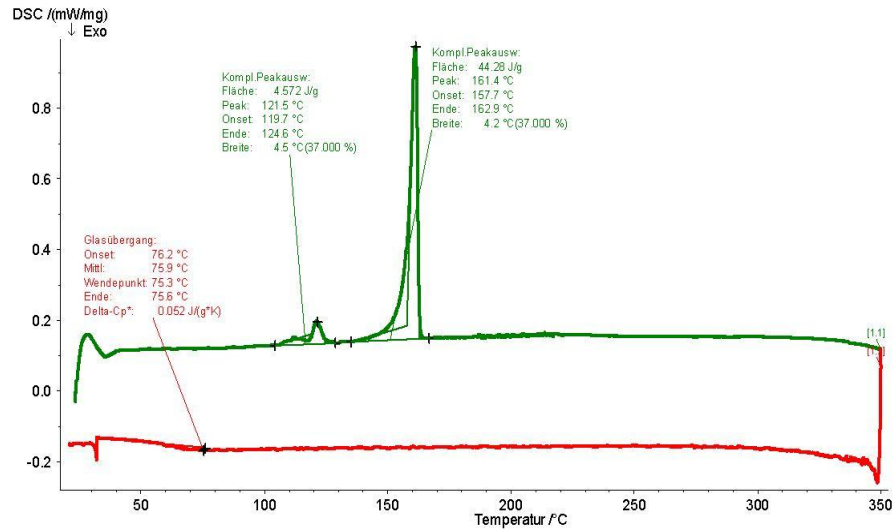


Fig. 1 DSC thermogram of Rhodamine 6 G NTF₂.

8 Appendix C

8.1 UV/Vis

The UV/Vis spectra were recorded at a scan rate of 400 nm/s.

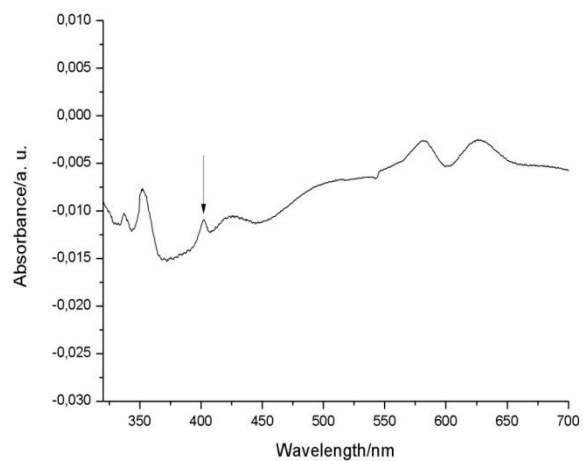


Fig. 1 UV/Vis spectrum of $C_4C_1mimNTf_2$ doped with $Mn(NTf_2)_2$.

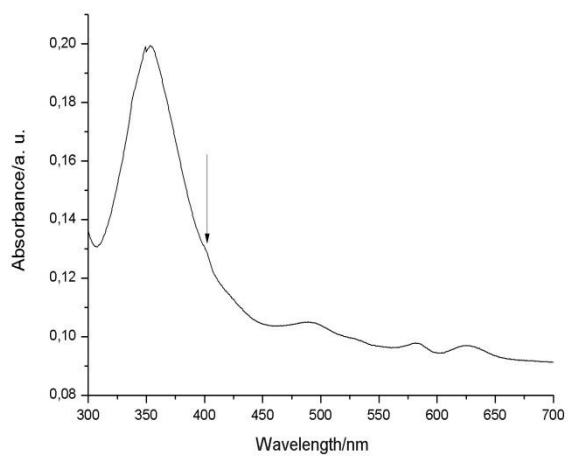


Fig. 2 UV/Vis spectrum of $C_4mimNTf_2$ doped with $Mn(NTf_2)_2$.

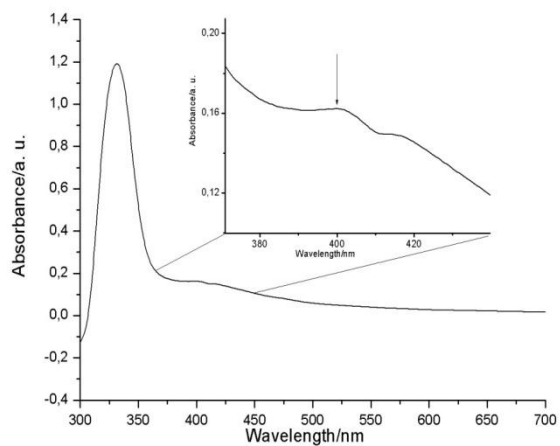


Fig. 3 UV/Vis spectrum of $C_4mimClO_4$ doped with $Mn(NTf_2)_2$.

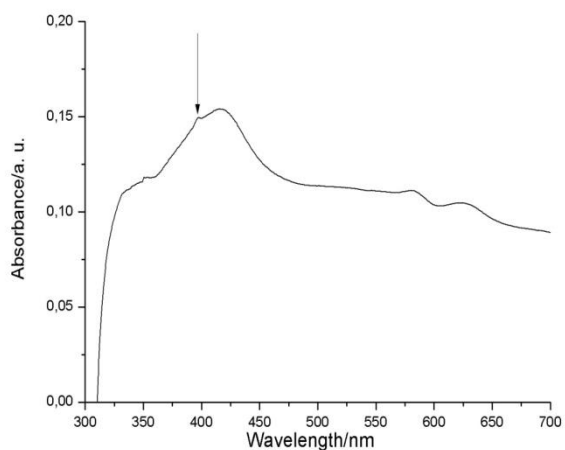


Fig. 4 UV/Vis spectrum of $C_6mpyridBF_4$ doped with $Mn(NTf_2)_2$.

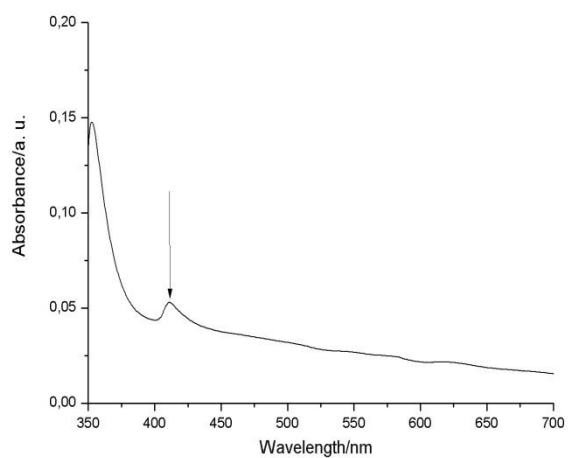


Fig. 5 UV/Vis spectrum of C_4mimNO_3 doped with $Mn(NTf_2)_2$.

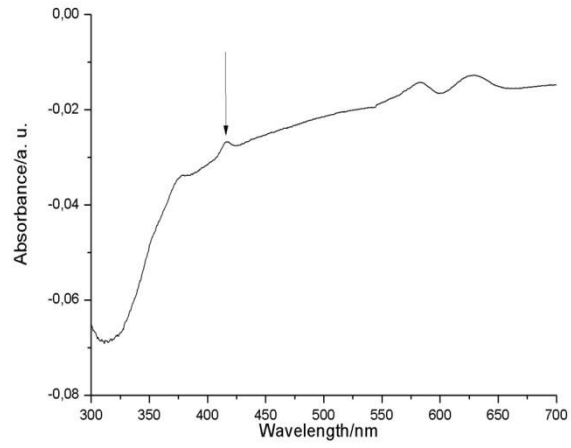


Fig. 6 UV/Vis spectrum of C₄mimTFA doped with Mn(NTf₂)₂.

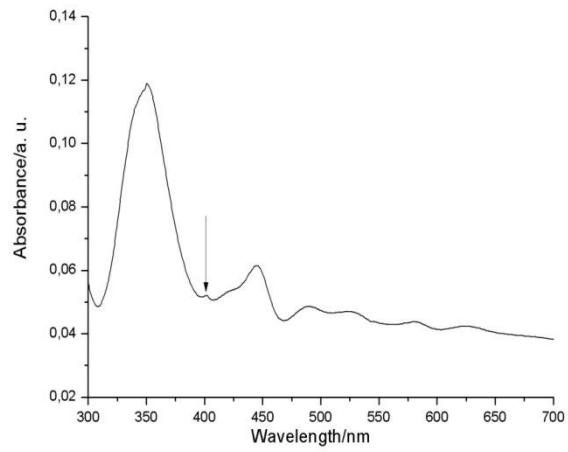


Fig. 7 UV/Vis spectrum of C₄mpyrNTf₂ doped with Mn(NTf₂)₂.

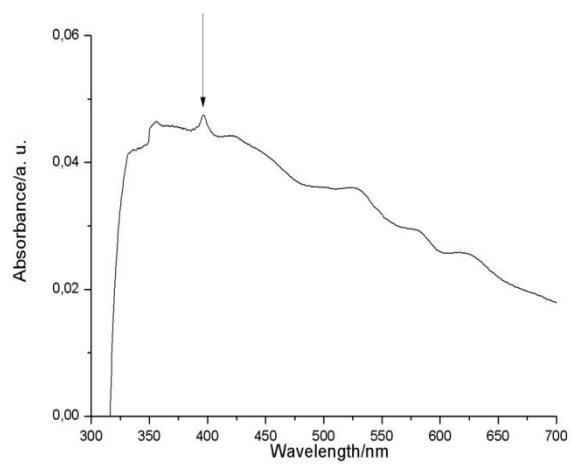


Fig. 8 UV/Vis spectrum of C₄pyridBF₄ doped with Mn(NTf₂)₂.

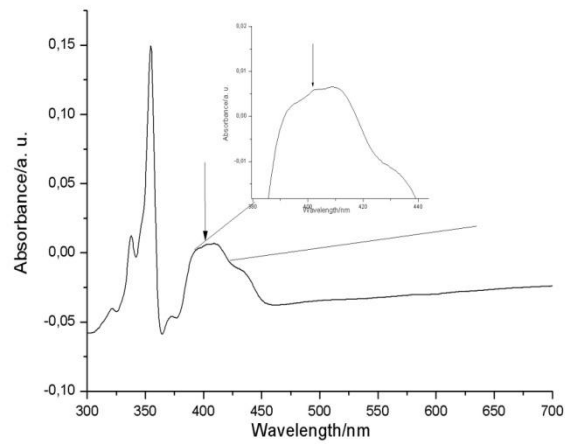


Fig. 9 UV/Vis spectrum of $C_{10}mimNTf_2$ doped with $Mn(NTf_2)_2$.

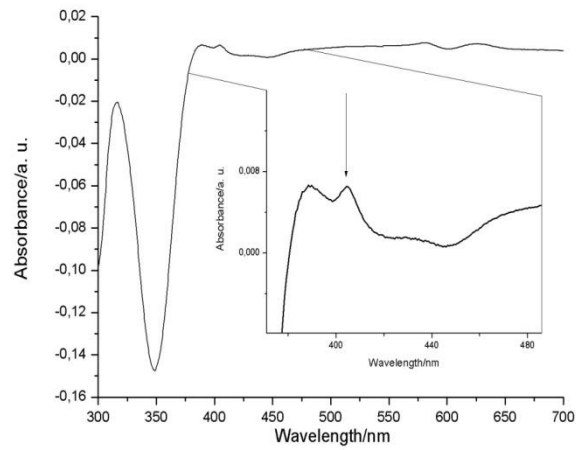


Fig. 10 UV/Vis spectrum of $CNC_2emimNTf_2$ doped with $Mn(NTf_2)_2$.

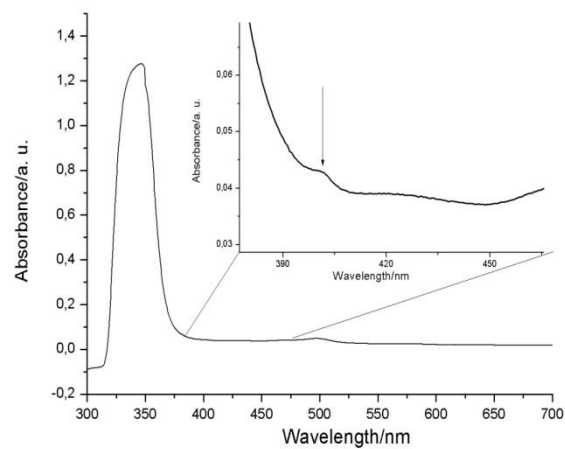


Fig. 11 UV/Vis spectrum of $C_2mimNTf_2$ doped with $Mn(NTf_2)_2$.

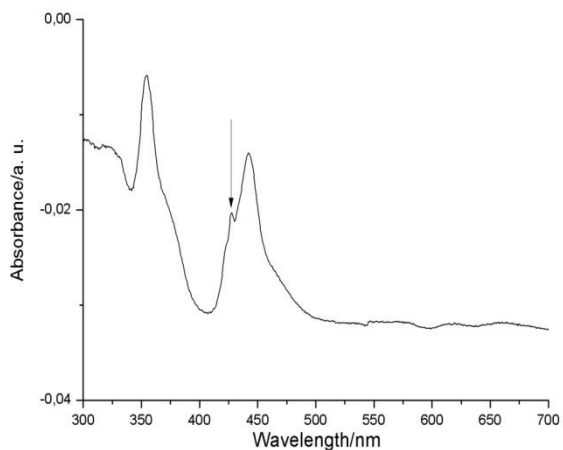


Fig. 12 UV/Vis spectrum of $C_2mimEtSO_4$ doped with $Mn(NTf_2)_2$.

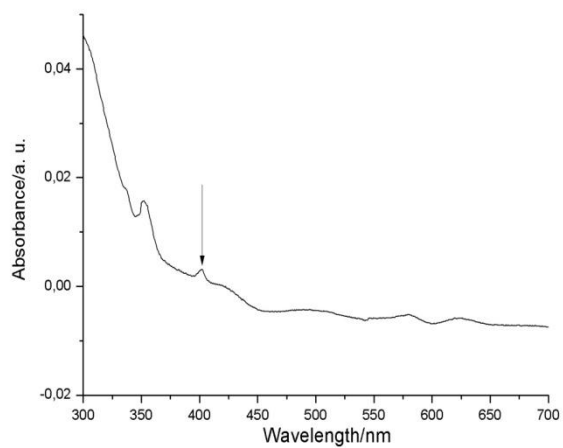


Fig. 13 UV/Vis spectrum of $C_2mimMeSO_3$ doped with $Mn(NTf_2)_2$.

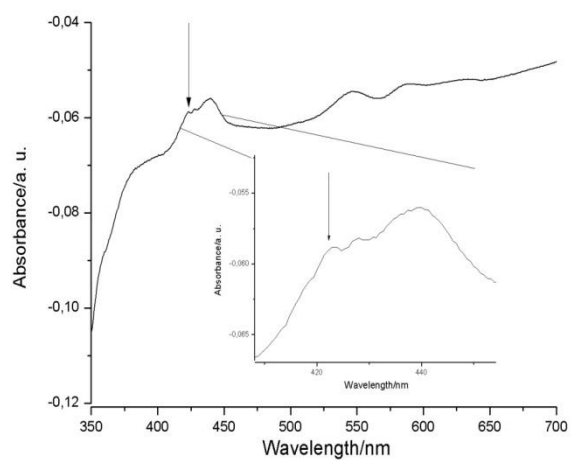


Fig. 14 UV/Vis spectrum of $C_2mimOTos$ doped with $Mn(NTf_2)_2$.

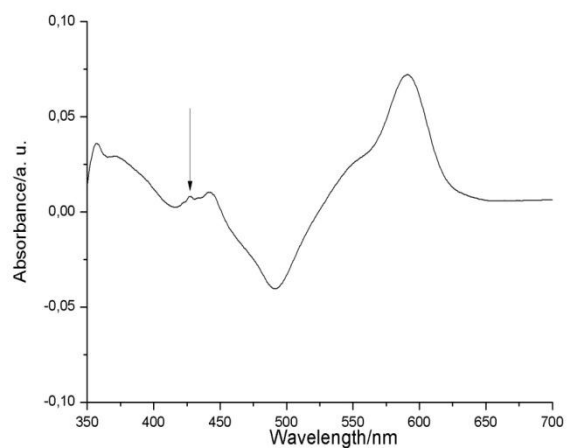


Fig. 15 UV/Vis spectrum of $C_4\text{mpyridEtSO}_4$ doped with $\text{Mn}(\text{NTf}_2)_2$.

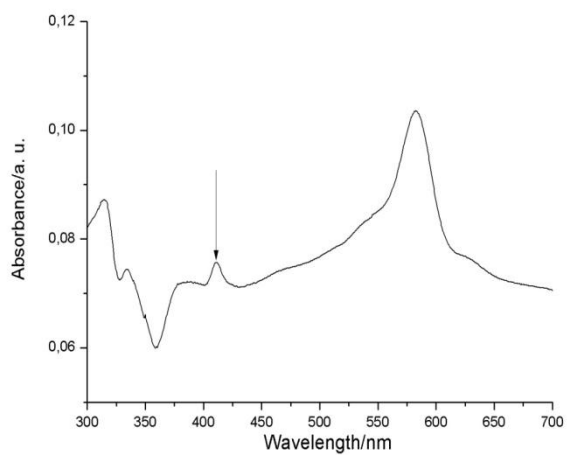


Fig. 16 UV/Vis spectrum of $\text{Et}_3\text{NvalCN NTf}_2$ doped with $\text{Mn}(\text{NTf}_2)_2$.

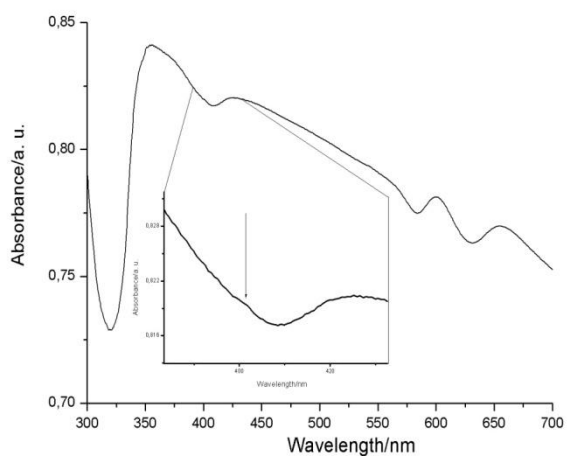


Fig. 17 UV/Vis spectrum of $C_6\text{mimNTf}_2$ doped with $\text{Mn}(\text{NTf}_2)_2$.

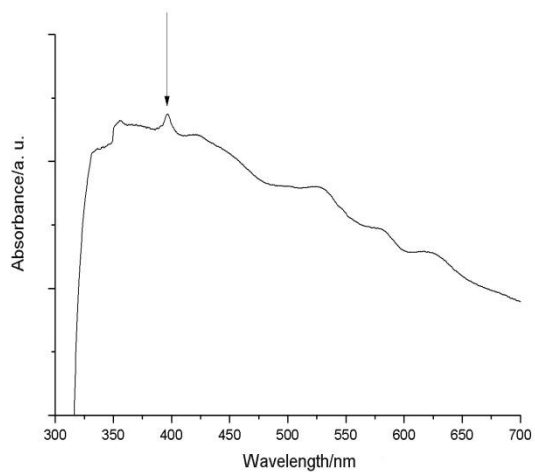


Fig. 18 UV/Vis spectrum of C₄mpyridBF₄ doped with Mn(NTf₂)₂.

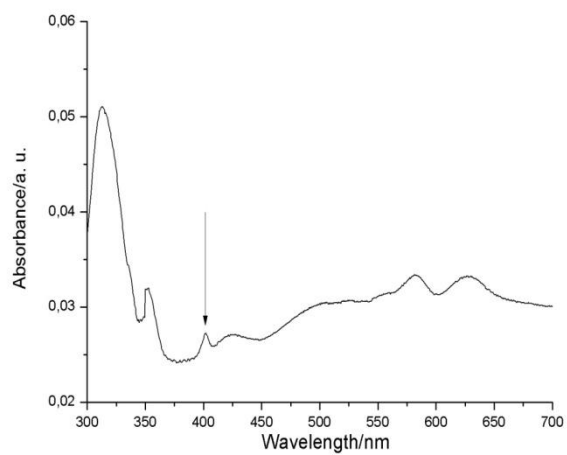


Fig. 19 UV/Vis spectrum of C₆mpyrNTf₂ doped with Mn(NTf₂)₂.

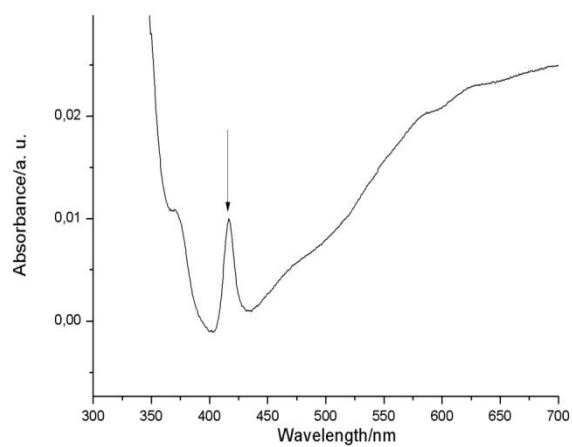


Fig. 20 UV/Vis spectrum of C₄mimDCA doped with Mn(NTf₂)₂.

9 Appendix D

9.1 EXAFS spectroscopy

The data were compiled and provided by C. Hardacre.

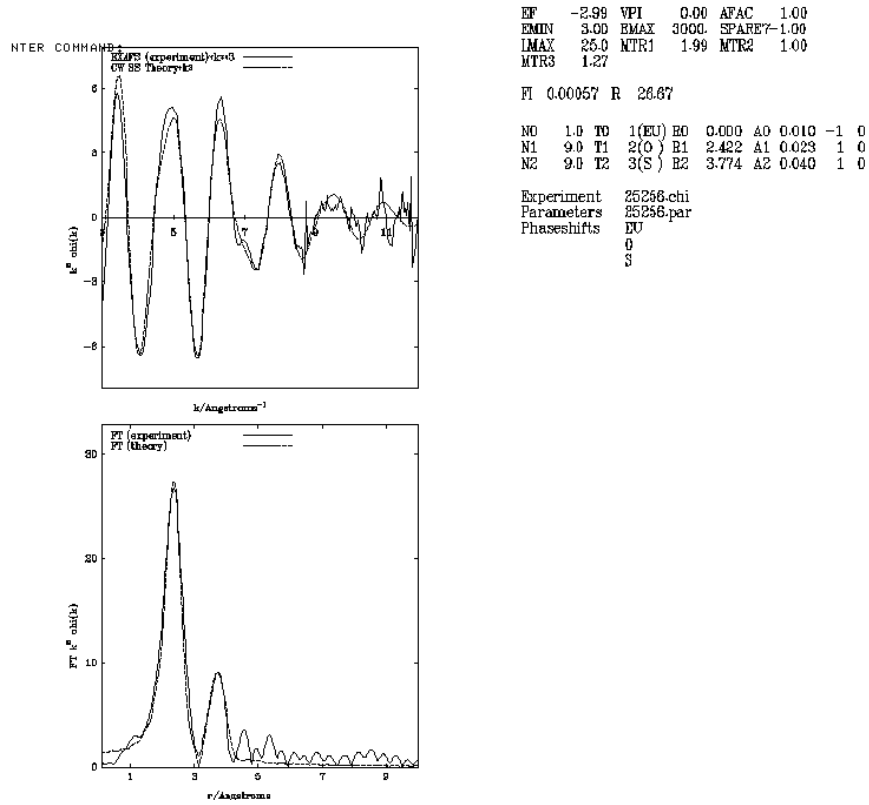


Fig. 1 EXAFS results (top) and FOURIER transformation (bottom) of solid $\text{Eu}(\text{NTf}_2)_3$.

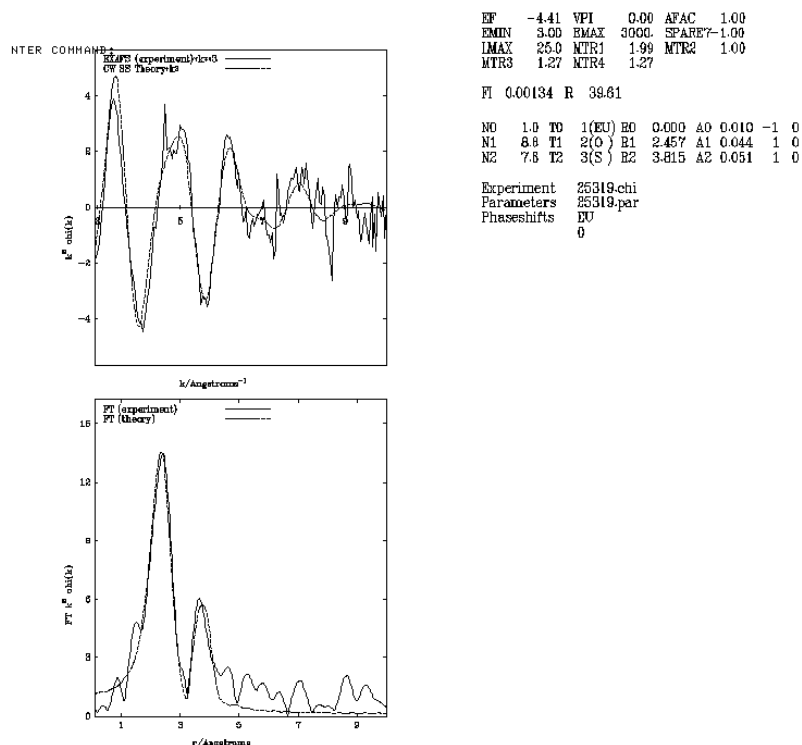


Fig. 2 EXAFS results (top) and FOURIER transformation (bottom) of $\text{Eu}(\text{NTf}_2)_3$ in $\text{C}_4\text{mimNTf}_2$.

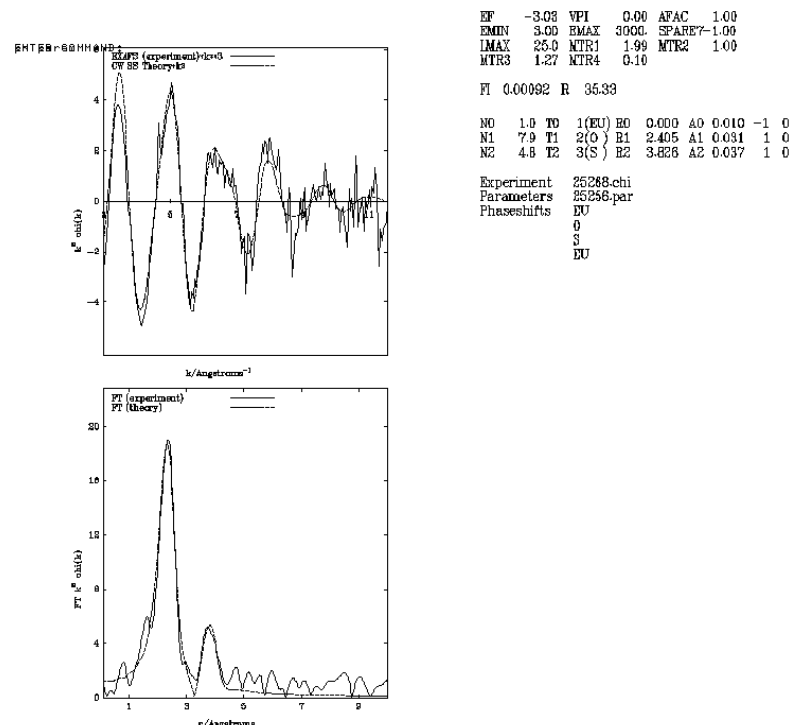


Fig. 3 EXAFS results (top) and FOURIER transformation (bottom) of $\text{Eu}(\text{NTf}_2)_3$ in C_2mimOTf .

Appendix

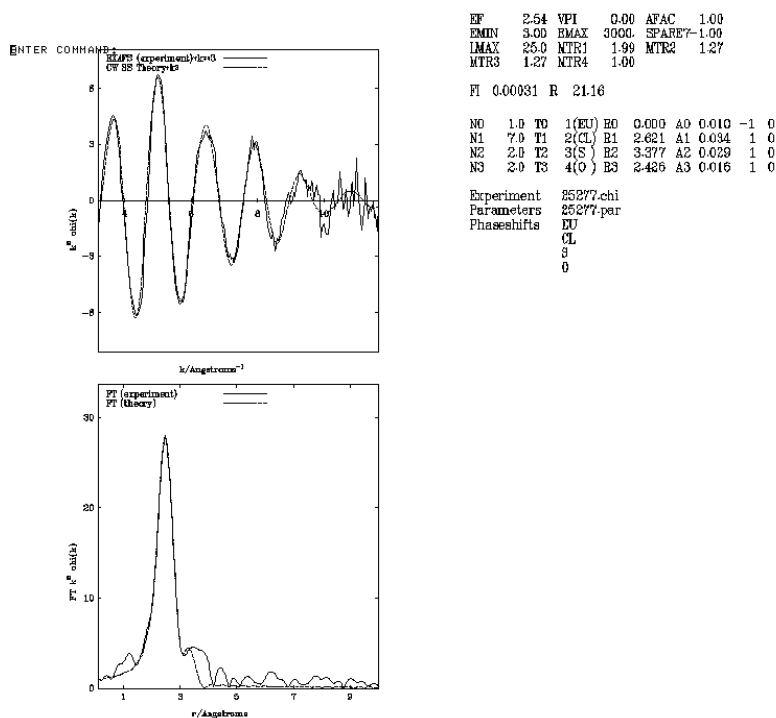


Fig. 4 EXAFS results (top) and FOURIER transformation (bottom) of $\text{Eu}(\text{NTf}_2)_3$ in C_4mimDCA .

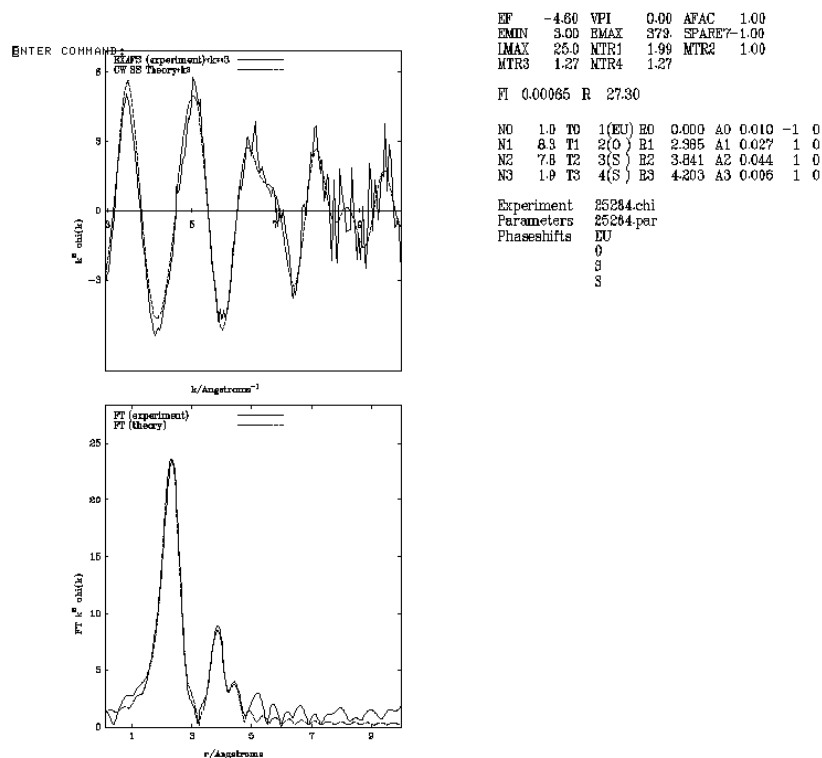


Fig. 5 EXAFS results (top) and FOURIER transformation (bottom) of $\text{Eu}(\text{NTf}_2)_3$ in C_4mimOTf .

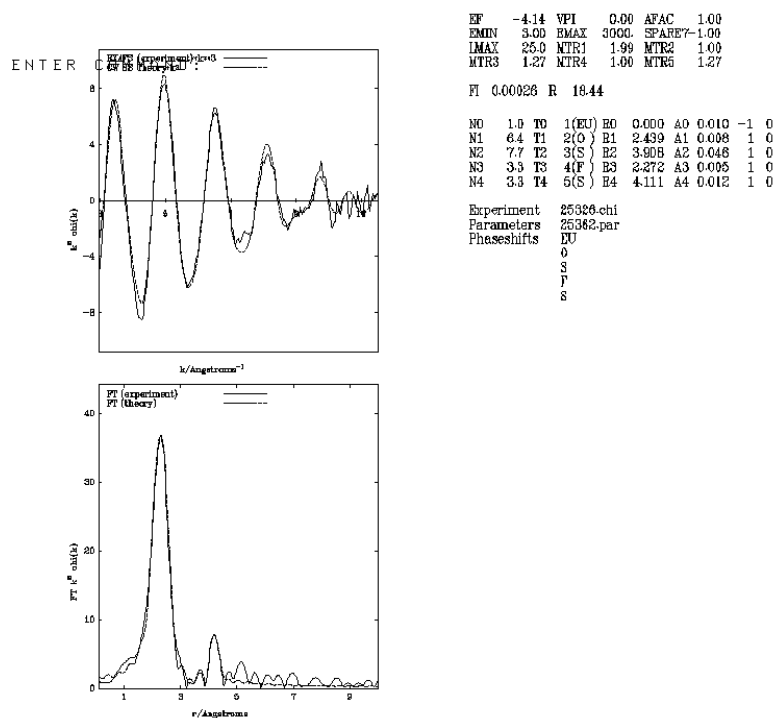


Fig. 6 EXAFS results (top) and FOURIER transformation (bottom) of Eu(NTf₂)₃ in C₄mimBF₄.

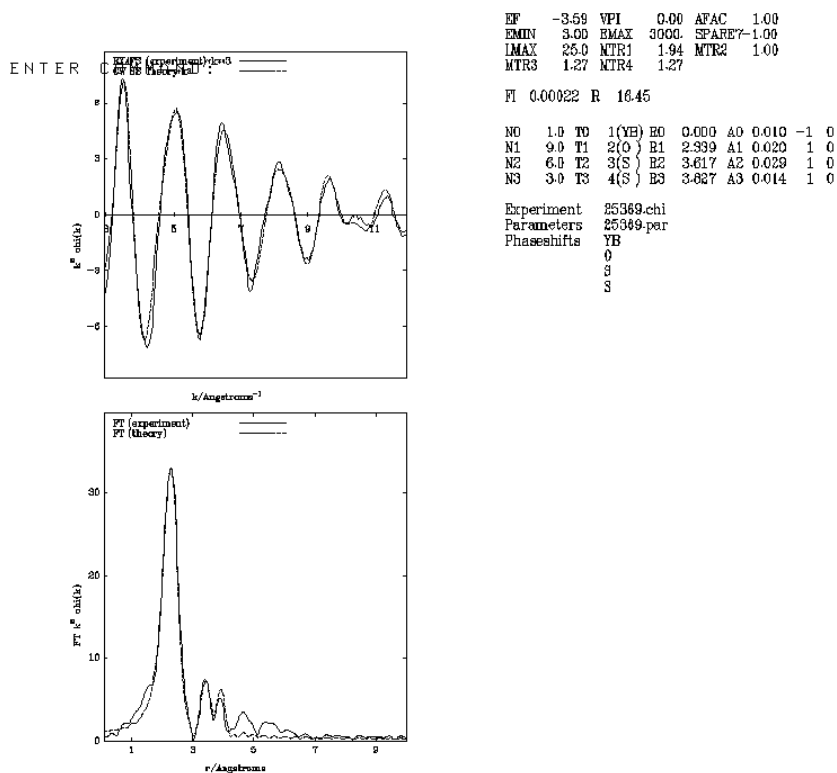


Fig. 7 EXAFS results (top) and FOURIER transformation (bottom) of solid Yb(NTf₂)₃.

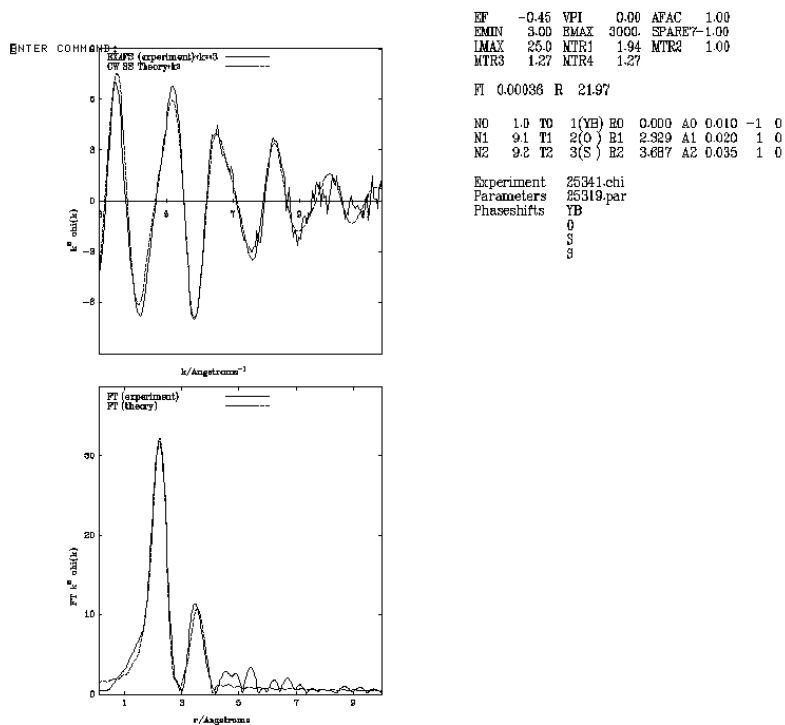


Fig. 8 EXAFS results (top) and FOURIER transformation (bottom) of Yb(NTf₂)₃ in C₄mimNTf₂.

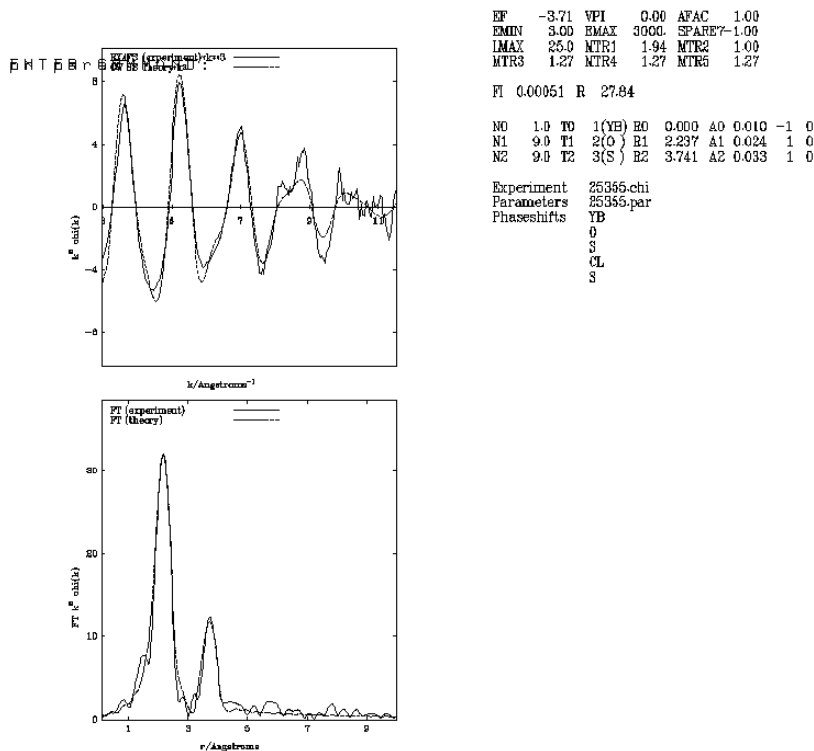


Fig. 9 EXAFS results (top) and FOURIER transformation (bottom) of Yb(NTf₂)₃ in C₂mimOTf.

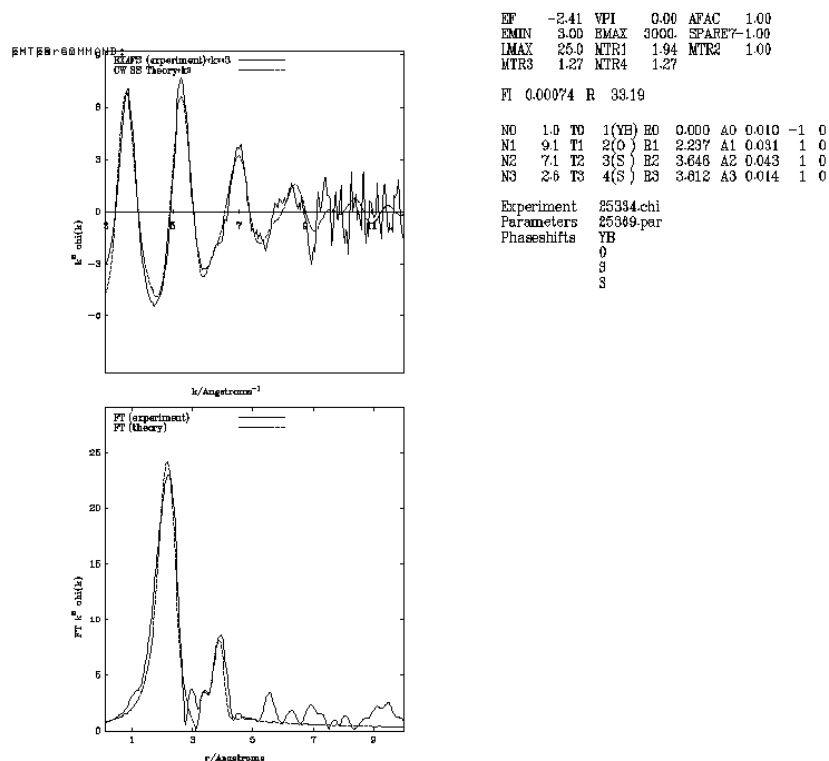


Fig. 10 EXAFS results (top) and FOURIER transformation (bottom) of Yb(NTf₂)₃ in C₄mimOTf.

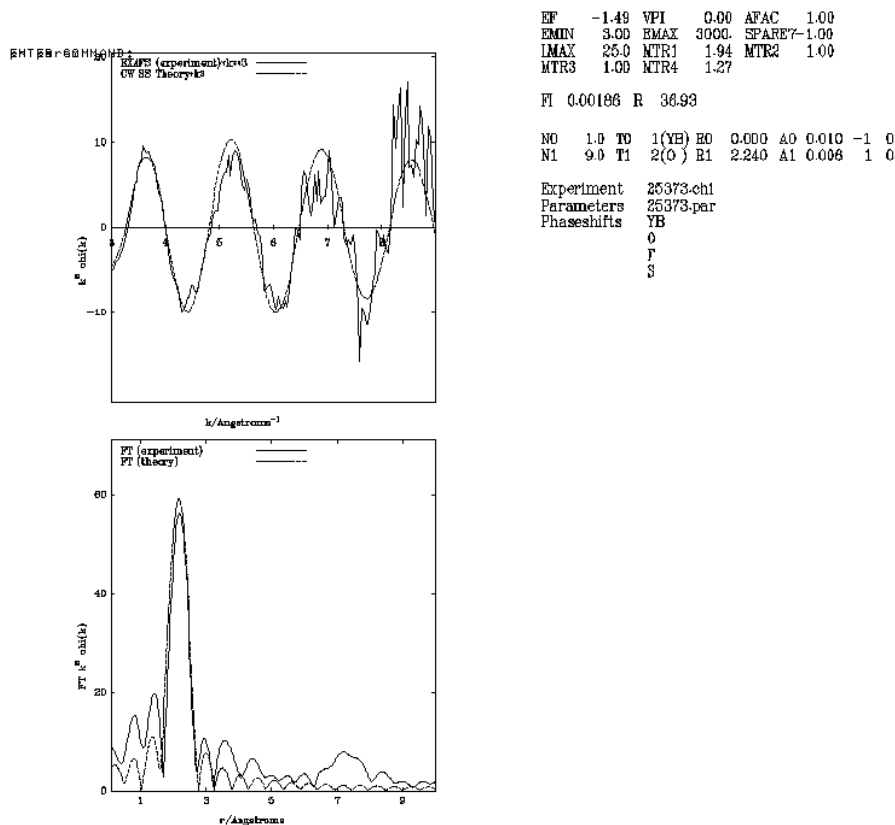


Fig. 11 EXAFS results (top) and FOURIER transformation (bottom) of Yb(NTf₂)₃ in C₆mimPF₆.

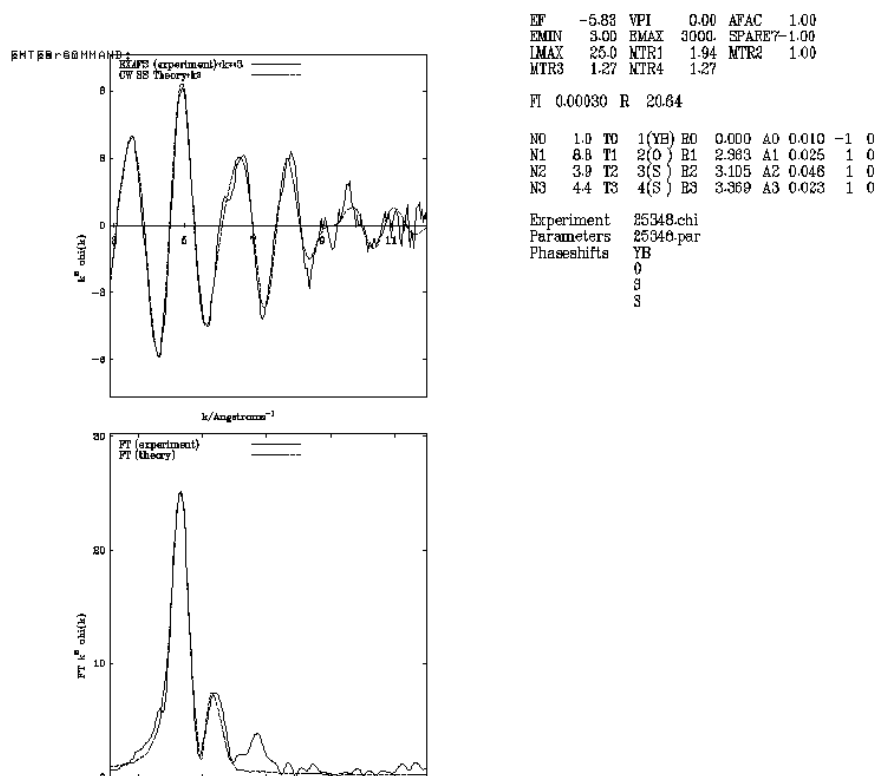


Fig. 12 EXAFS results (top) and FOURIER transformation (bottom) of Yb(NTf₂)₃ in C₄mimDCA.

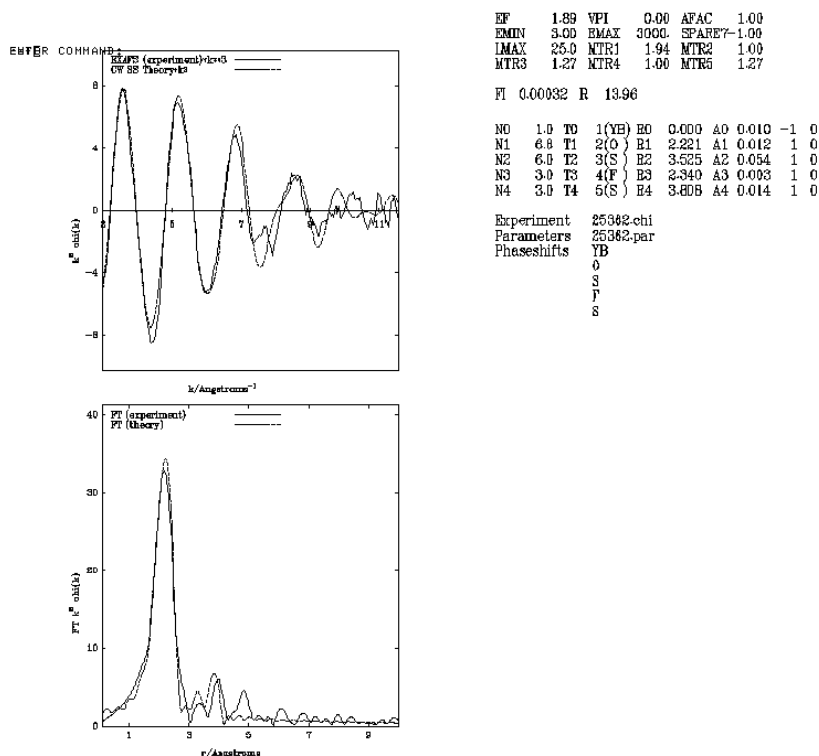


Fig. 13 EXAFS results (top) and FOURIER transformation (bottom) of Yb(NTf₂)₃ in C₄mimBF₄.

9.2 Cyclic voltammetry

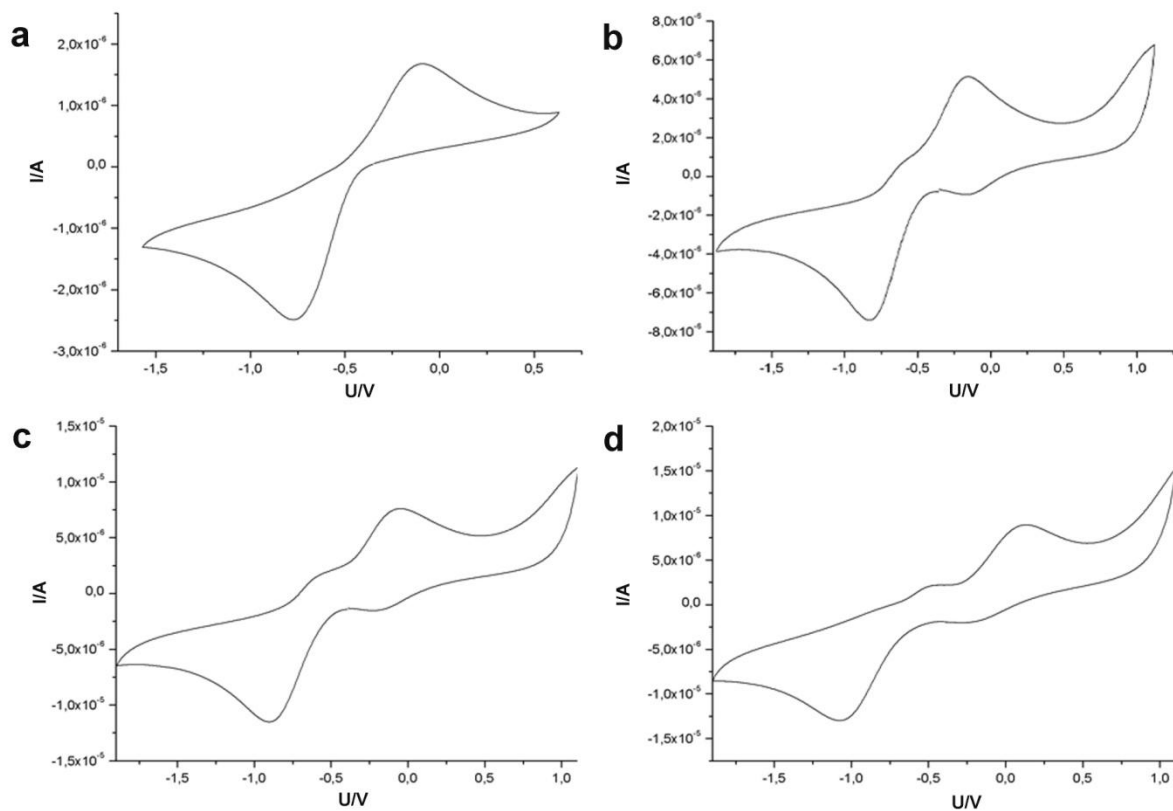


Fig. 14 Cyclic voltammograms of $\text{Eu}(\text{NTf}_2)_3$ in $\text{C}_4\text{mimNTf}_2$ vs. Fc/Fc^+ measured with different scan rates a) 10 mV/s, b) 50 mV/s, c) 100 mV/s and d) 200 mV/s.

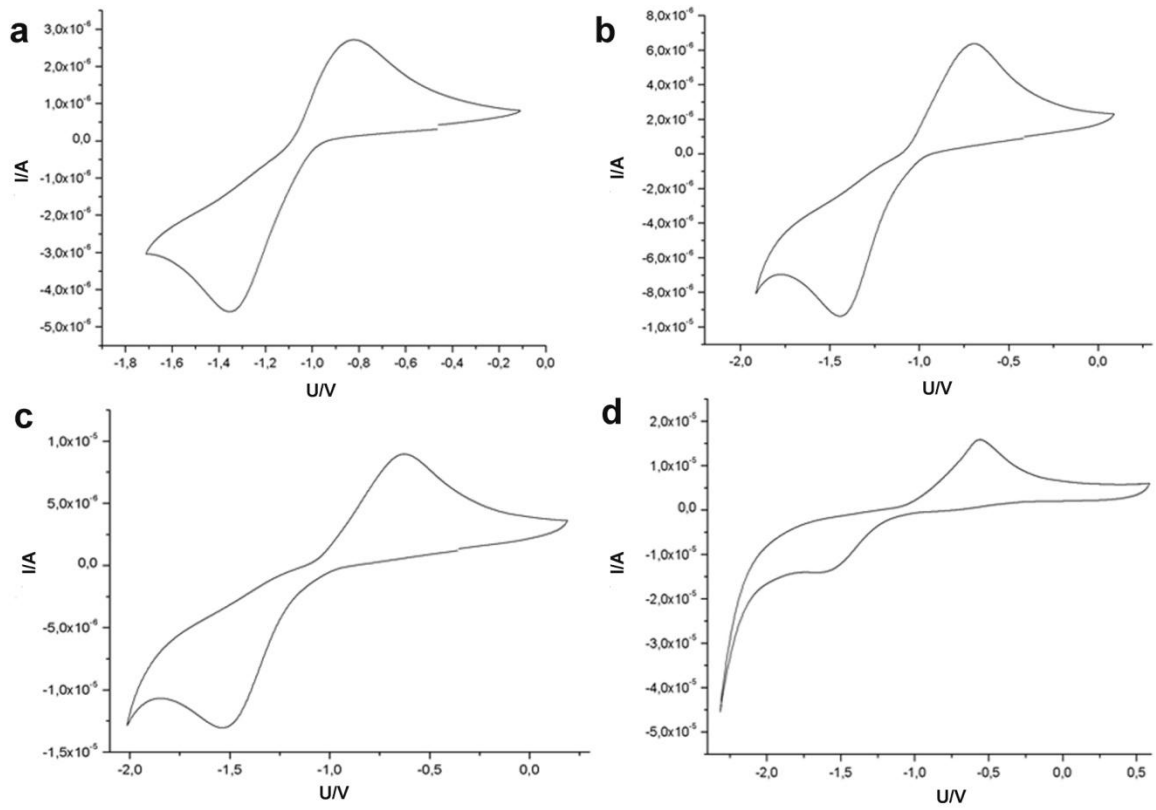


Fig. 15 Cyclic voltammograms of $\text{Eu}(\text{NTf}_2)_3$ in C_4mimDCA vs. Fc/Fc^+ measured with different scan rates a) 10 mV/s, b) 50 mV/s, c) 100 mV/s and d) 200 mV/s.

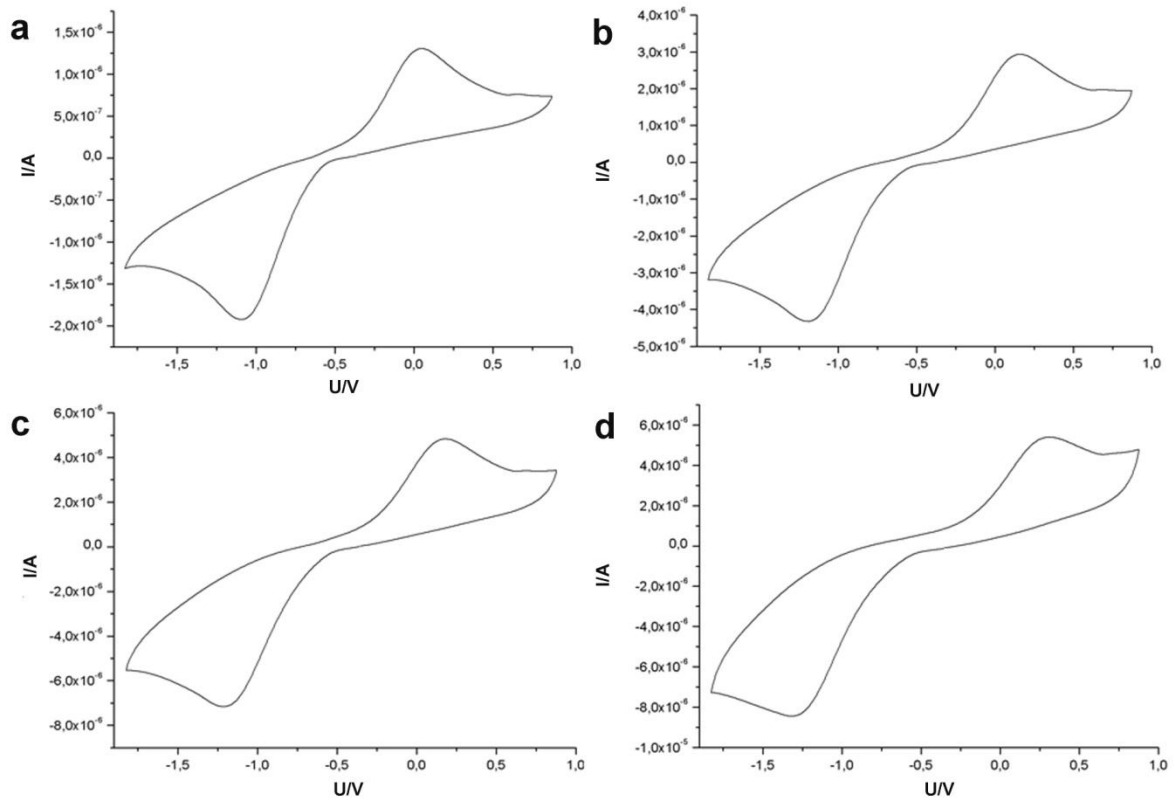


Fig. 16 Cyclic voltammograms of $\text{Eu}(\text{NTf}_2)_3$ in C_4mimOTf vs. Fc/Fc^+ measured with different scan rates a) 10 mV/s, b) 50 mV/s, c) 100 mV/s and d) 200 mV/s.

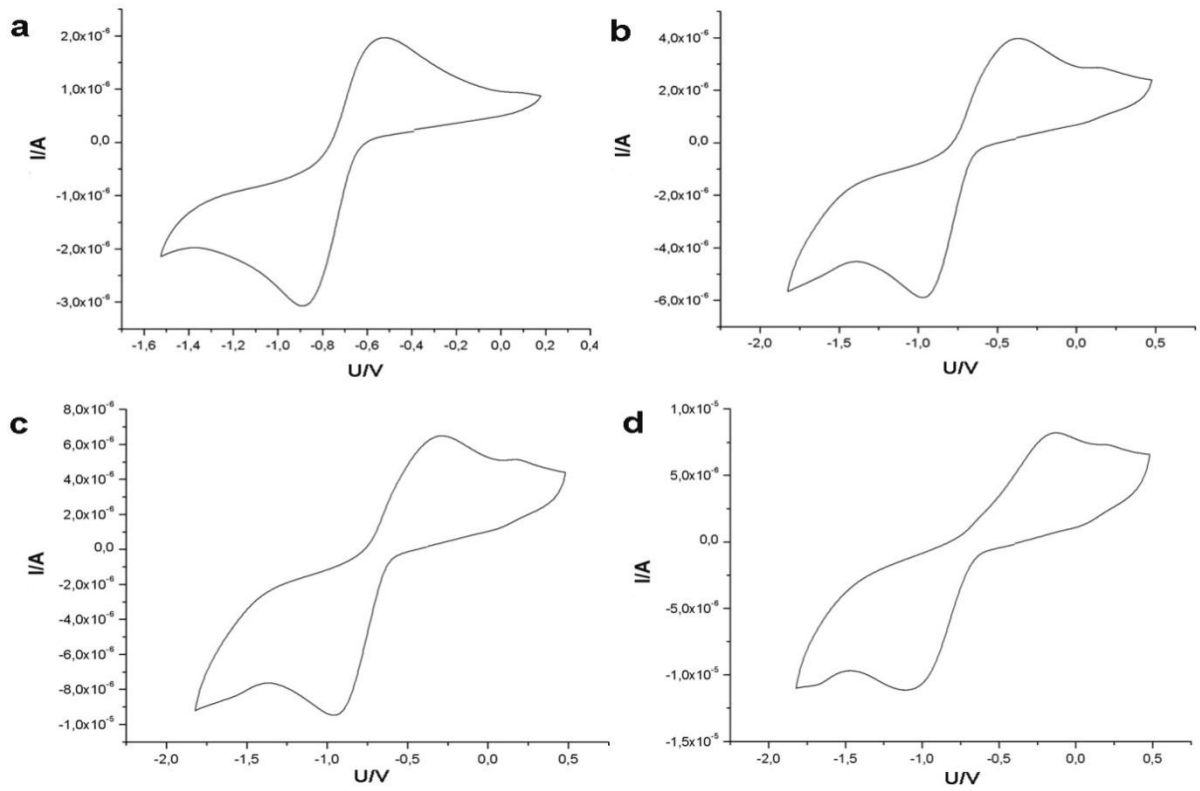


Fig. 17 Cyclic voltammograms of $\text{Eu}(\text{NTf}_2)_3$ in C_2mimOTf vs. Fc/Fc^+ measured with different scan rates a) 10 mV/s, b) 50 mV/s, c) 100 mV/s and d) 200 mV/s.

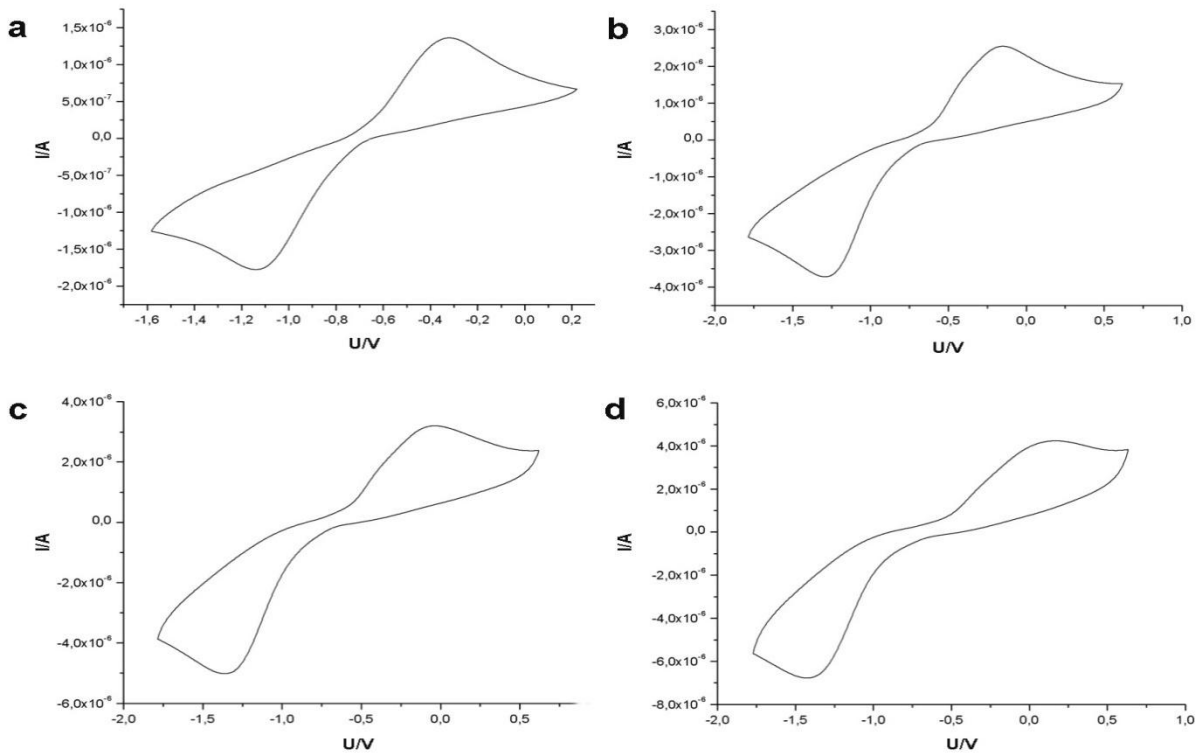


Fig. 18 Cyclic voltammograms of EuOTf_3 in $\text{C}_4\text{mpyrOTf}$ vs. Fc/Fc^+ measured with different scan rates a) 10 mV/s, b) 50 mV/s, c) 100 mV/s and d) 200 mV/s.

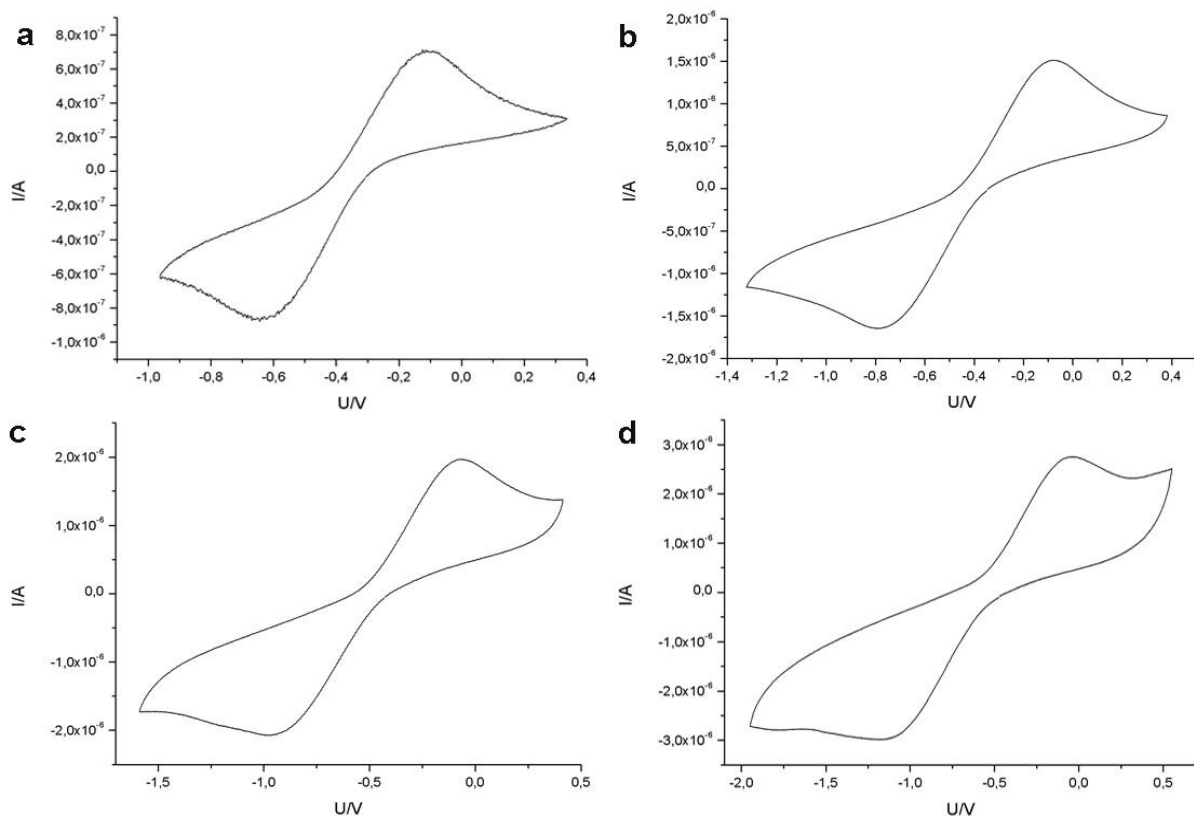


Fig. 19 Cyclic voltammograms of $\text{Eu}(\text{NTf}_2)_3$ in $\text{P}_{66614}\text{NTf}_2$ vs. Fc/Fc^+ measured with different scan rates a) 10 mV/s, b) 50 mV/s, c) 100 mV/s and d) 200 mV/s.

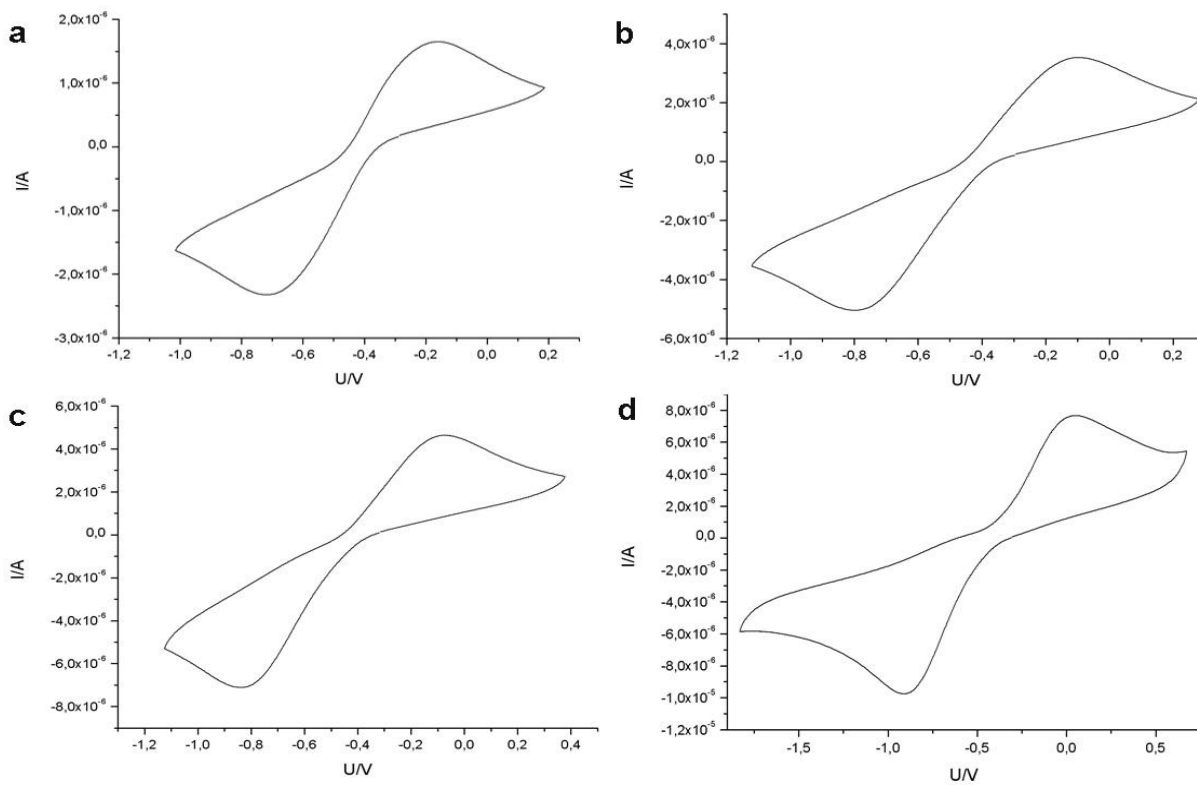


Fig. 20 Cyclic voltammograms of $\text{Eu}(\text{NTf}_2)_3$ in $\text{C}_4\text{mpyridNTf}_2$ vs. Fc/Fc^+ measured with different scan rates a) 10 mV/s, b) 50 mV/s, c) 100 mV/s and d) 200 mV/s.

Erklärung

Ich versichere, dass ich die von mir vorgelegte Dissertation selbstständig angefertigt, die benutzten Quellen und Hilfsmittel vollständig angegeben und die Stellen der Arbeit - einschließlich Tabellen, Karten und Abbildungen, die anderen Werken in Wortlaut oder dem Sinn nach entnommen sind, in jedem Einzelfall als Entlehnung kenntlich gemacht habe; dass diese Dissertation noch keiner anderen Fakultät oder Universität zur Prüfung vorgelegen hat; dass sie noch nicht veröffentlicht worden ist; dass ich eine solche Veröffentlichung vor Abschluss des Promotionsverfahrens nicht vornehmen werde.

Die Bestimmungen der geltenden Promotionsordnung sind mir bekannt. Die von mir vorgelegte Dissertation ist von Frau Prof. Dr. Anja-Verena Mudring betreut worden.

Köln, im Dezember 2009

Lebenslauf

Name Slawomir Pitula

Geburtstag 12.7.79

Geburtsort Bydgoszcz/Polen

Familienstand ledig

Promotion 08/07 – 02/10 Promotion Chemie

Diplom 06/07 Diplom-Chemiker

Vordiplom 08/04 Vordiplom Chemie

Studium 10/00 – 06/07 Chemiestudium

Wehrdienst 07/99 – 04/00 Pionierbatallion 2./320

Abitur 06/99 Hochschulreife

Gymnasium 08/90 – 06/99 Erftgymnasium Bergheim

Grundschule 08/86 – 07/90 Glasbläserbrunnen Bergheim
